LV-2007/075

Geothermal Projects in NE Iceland at

Krafla, Bjarnarflag, Gjástykki and Theistareykir

Assessment of geo-hazards affecting energy production and transmission systems emphasizing structural design criteria and mitigation of risk

Landsvirkjun

Landsvirkjun

Key page

LV report no.: LV-2007/075 Date: August 2007

Number of pages: 157 Copies: 100 Distribution: ☐ Open ☐ Limited until

Title: Geothermal Projects in NE Iceland at Krafla, Bjarnarflag, Gjástykki and Theistareykir. Assessment of geo-hazards affecting energy ...

Authors/Company: Axel Björnsson, Kristján Saemundsson, Freysteinn Sigmundsson, Páll Halldórsson, Ragnar Sigbjörnsson, Jónas Thór Snaebjörnsson

Project manager: Axel Björnsson

Prepared for: Theistareykir Ltd, Landsnet, Landsvirkjun Landsnet-07025

Co operators:

Abstract: The geo-hazards that may cause operational interruptions or damage to planned geothermal power plants and transmission lines are assessed and the likely impacts of hazardous events is determined. Time between major rifting episodes in the Krafla system is several 100s of years. The last eruption in Theistareykir occurred 2500 years ago. During the last centuries a major stress release has taken place in the area. Therefore, the probability of new rifting during the next 100-200 years is low. Probability of earthquakes with M > 5 close to the geothermal fields is low. However, earthquakes up to M = 6.5 within the Húsavík fault are considered. Risk is mitigated by locating structures at four different sites and outside the central active zone. It is extremely unlikely that all four sites will be affected simultaneously. Two separate transmission lines will be in use. The main findings of the probabilistic and deterministic hazard analysis are synthesized into suggested design provisions for earthquake action conforming to Eurocode 8.

Keywords: Geothermal Projects, Krafla, Bjarnarflag, Gjástykki, Theistareykir, geo-hazards, structural design criteria, mitigation of risk

ISBN no.:

ISSN no:

Axel Björnsson

Landsvirkjun's project manager's signature

Table of Contents

Executive Summary

Landsvirkjun, in cooperation with Theistareykir Ltd and Landsnet plans to build geothermal power plants at four geothermal sites within the volcanic zone in NE Iceland and associated transmission systems to supply power for an industrial site at Bakki near Húsavík. The proposed power plant sites are Krafla, Theistareykir, Gjástykki and Bjarnarflag. To facilitate the work, a group of experts was appointed in February 2007 to study the effects of geo-hazards within the Northern Volcanic Zone. The results of their investigations are presented herein.

The first objective of the present study is to assess the geo-hazards that may cause operational interruptions or damage to planned geothermal power plants in NE Iceland, transmission lines and sub-stations. The hazard assessment for the area of concern can be limited to three types of geo hazards. They are: volcanic activity, earthquakes and tectonic movements of land. The second objective is to determine the likely impacts of hazardous events in the area on the proposed power plants and the transmission systems, and to put forward measures to mitigate the risk through protective measures and location of structures, along with structural design recommendations based on a predefined probability of occurrence.

Time between major volcano-tectonic rifting episodes in the Krafla volcanic system is several 100s of years. The last episode, called the Krafla Fires, lasted 1975-1984. Another similar episode took place 250 years ago in the early 18th century. Before that, about 1000 years ago the area was volcanically active. The last eruption in the Theistareykir field occurred ~2500 years ago. Since then no tectonic movements have occurred in the eastern part of the field where the present drilling area is located and where the planned power plant will be built. During the 18th and 20th century rifting episodes a major stress release took place in the northern part of the Northern Volcanic Zone. Therefore, the probability of new rifting during the next 100-200 years is low. Dyke and sheet intrusions are more likely, but it should be noted that they are beneficial in the long term as they act as heat source for the geothermal systems. Associated fracturing can also facilitate flow of water in the crust.

Probability of earthquakes with $M > 5$ within or close to the geothermal fields is low. However, earthquakes up to $M = 6.5$ within the southern part of the Húsavík faults are considered in the present study, along with larger magnitude events in the transform zone of the coast.

Probabilistic seismic hazard analysis reveals low to moderate earthquake hazard for the proposed power plant sites. This result is obtained using conservative estimates for upper bounds of earthquake magnitudes. De-aggregation of the seismic hazard curves indicate that small to moderate sized near-fault earthquakes with short duration contribute most to the suggested design values for the study sites. In the case of long periodic structures a big distant earthquakes may be a contributing event. The results of the de-aggregation are used in deterministic hazard analysis resulting in simulated time series applicable for design considerations. The main findings of the probabilistic and deterministic hazard analysis are synthesized into suggested design provisions for earthquake action, including presentation of inelastic effects. The recommended design requirements conform to good engineering practice and leading design guidelines such as Eurocode 8.

Risk can be mitigated by locating structures outside the central zone of the fissure swarms. Risk is further mitigated and reliability of energy delivery increased by building four power plants at four different locations in the volcano-tectonic zone. Simultaneous eruptive activity and fracturing in all of the four considered geothermal fields at any time is highly unlikely. To further enhance the reliability of energy delivery, two separate transmission lines will be running from the power plants to the industrial lot. Each power line will be able to carry the total energy needed.

Samantekt

Landsvirkjun, Þeistareykir ehf og Landsnet undirbúa byggingu fjögurra jarðgufuvirkjana í gosbeltinu á Norðausturlandi og lagningu háspennulína frá virkjununum að iðnaðarsvæði á Bakka norðan Húsavíkur. Virkjunarstaðirnir eru Þeistareykir, Gjástykki, Krafla og Bjarnarflag. Í febrúar 2007 skipuðu fyrirtækin 6 sérfræðinga í vinnuhóp til þess að meta jarðvá fyrir virkjunarstaðina og línustæðin. Er það mat kynnt í þessari skýrslu.

Í fyrsta lagi var metin vá er gæti valdið truflun á rekstri eða skemmdum á virkjunum, spennuvirkjum og háspennulínum. Slík vá tengist einkum eldvirkni, jarðskjálftum, hreyfingu tengddri landreki og kvikusöfnun í jarðskorpunni. Í öðru lagi var reynt að meta líkleg áhrif slíkra viðburða á fyrirhugaðar virkjanir og flutningslínur og lagðar eru til aðgerðir til þess að draga úr áhættunni. Þær felast í varnaraðgerðum, ráðleggingum um staðsetningu mannvirkja og tillögum um hönnunarforsendur, sem byggðar eru á líkum á tíðni og stærð atburða sem vá stafar af.

Meiri háttar landreks- og eldgosahrinur verða í Kröflu sprungureininni á nokkur hundruð ára fresti. Síðasta hrina, sem nefnd er Kröflueldar, varð 1975-1984. Önnur svipuð hrina varð fyrir um 250 árum og þar áður var eldvirkni fyrir um 1000 árum. Síðasta gos varð á Þeistareykjum fyrir um það bil 2500 árum. Síðan þá hafa engar landhreyfingar átt sér stað á eystri hluta svæðisins þar sem núverandi borsvæði er og þar sem fyrirhugað er að reisa virkjun. Í eldgosahrinunum á 18. og 20. öld varð mikil gliðnun og spennuslökun í norðurhluta gosbeltisins á Norðausturlandi og þess vegna eru litlar líkur á nýrri stórri hrinu næstu 100-200 árin. Minni háttar innskot eða gangamyndun gæti átt sér stað en slíkt er til bóta þegar til lengri tíma er litið því innskot og gangar eru hitagjafar háhitasvæðanna. Meðfylgjandi myndun sprungna eykur einnig lekt jarðlaga sem er af hinu góða.

Litlar líkur eru á að jarðskjálftar stærri en 5 verði á eða í grennd jarðhitasvæðanna. Hins vegar er gert ráð fyrir að skjálftar með stærðina 6,5 geti orðið á suðausturhluta Húsavíkurmisgengisins.

Líkindafræðileg jarðskjálftagreining leiðir í ljós að jarðskjálftavá á fyrirhuguðum byggingarsvæðum orkuveranna er fremur lítil. Þessi niðurstaða er byggð á íhaldsömu mati á mestu stærð jarðskjálfta með upptök á nálægum upptakasvæðum. Enn fremur benda niðurstöðurnar til þess að nálægur lítill til meðalstór jarðskjálfti sem varir stutt valdi allajafna mestri áraun á virkjanasvæðunum. Undanskilin eru mannvirki með langan eiginsveiflutíma, svo sem mjög háreist mann-

virki, en fyrir þau er áraun af völdum fjarlægra stórra jarðskjálfta ráðandi. Meginniðurstöður rannsóknarinnar eru dregnar saman í heildstæða tillögu að hönnunarleiðbeiningum er varða jarðskjálftaáraun, hér með talin umfjöllun um ólínulega áraun svo og framsetning tímaraða sem er ætlað að líkja eftir hreyfingu yfirborðs jarðar í jarðskjálftum á byggingarsvæðunum. Þær hönnunarkröfur sem settar eru fram og mælt er með að verði lagðar til grundvallar við mannvirkjagerð á svæðinu eru í samræmi við góðar verkfræðiheðir og helstu hönnunarstaðla, svo sem Evrópustaðal nr. 8.

Unnt er að draga úr áhættu með því að staðsetja öll mannvirki á yfirborði utan virkustu miðju sprungureinanna. Einnig er dregið verulega úr áhættu og orkuframleiðsla gerð tryggari með því að dreifa fyrirhuguðum jarðgufuvirkjunum á fjögur jarðhitasvæði með nokkuð löngu millibili innan eldvirka beltisins. Það er einkar ólíklegt að öll fjögur jarðhitasvæðin yrðu fyrir áhrifum frá jarðhræringum, eldgosum eða jarðskjálftum á sama tíma. Lagðar verða tvær háspennulínur frá jarðgufustöðvunum að Bakka til að tryggja rekstraröryggi og getur hvor um sig flutt nægjanlega orku fyrir stóriðjuver.

1. Introduction

Axel Björnsson, University of Akureyri

1.1 Assumptions and objectives

1.1.1 Introduction

Landsvirkjun, in cooperation with Theistareykir Ltd. and Landsnet plans to build geothermal power plants at four sites in the volcanic zone in NE Iceland and transmission systems to an industrial site Bakki near Húsavík. For location see Figure 1.1. The geothermal sites are Krafla, Theistareykir, Gjástykki and Bjarnarflag. The goal is to produce 400 MWe. The first production phase of 200 MWe is expected to be finished in 2012 and the second production phase of 200 MWe in 2015. In February 2007 Landsvirkjun, Theistareykir Ltd. and Landsnet appointed a group of experts to study the effects of geo-hazards within the volcanic zone in NE-Iceland. The aim was to present a report in August 2007. In the beginning it was decided to base the study mainly on existing and available data. The first discussions lead to the conclusion that the hazard assessment for the area of concern could be limited to three types of natural hazards. They are: volcanic activity, earthquakes and tectonic movements of land.

1.1.2 Objectives

The first objective of the present study is to assess the geo-hazards that may cause operational interruptions or damage to planned geothermal power plants in NE Iceland, transmission lines and substations. The first step is to identify the type of hazard, location, frequency and the severity of the events. In the volcanic zone of NE Iceland there are three types of geo-hazards to be considered. They are:

- Volcanic activity with lava flows from nearby craters or fissures and freatic eruptions and ash fall from distant volcanoes in other parts of the country
- Earthquakes originating in the Tjörnes fracture zone as well as local earthquakes within the volcanic zone.
- Tectonic movements associated with the plate movements, rifting of the plates and intrusion of magma into the crust.

The second objective is to determine the likely impacts of hazardous events in the area on the proposed power plants and the transmission systems, and to propose measures to mitigate the risk through protective measures and location of structures, along with structural design recommendations based on a predefined probability of occurrence.

1.1.3 Layout

The present report consists of six chapters. The first chapter contains an introduction to the geological setting of Iceland with a special emphasis on the geology of the volcanic zone in NE Iceland. It also contains a brief description of a major rifting and volcano-tectonic episode which took place 1975-1989 in the northern volcanic zone. The second chapter deals with volcanic

hazard, both local eruptions as well as danger of ash-fall from distal volcanoes. It further studies in detail the proposed site location of power plants, substations and transmission lines with the aim of avoiding active faults and fissures. The third chapter presents hazards caused by tectonic activity, i.e. horizontal and vertical land movements associated with plate movements and magma accumulation in the earth crust. The fourth chapter deals with seismic activity both in the off-shore Tjörnes fracture zone and the volcanic zone on land. The fifth chapter deals with earthquake action in terms of engineering seismology, building on the previous chapters to develop structural design recommendations. The sixth chapter summarizes the essential parts of the work.

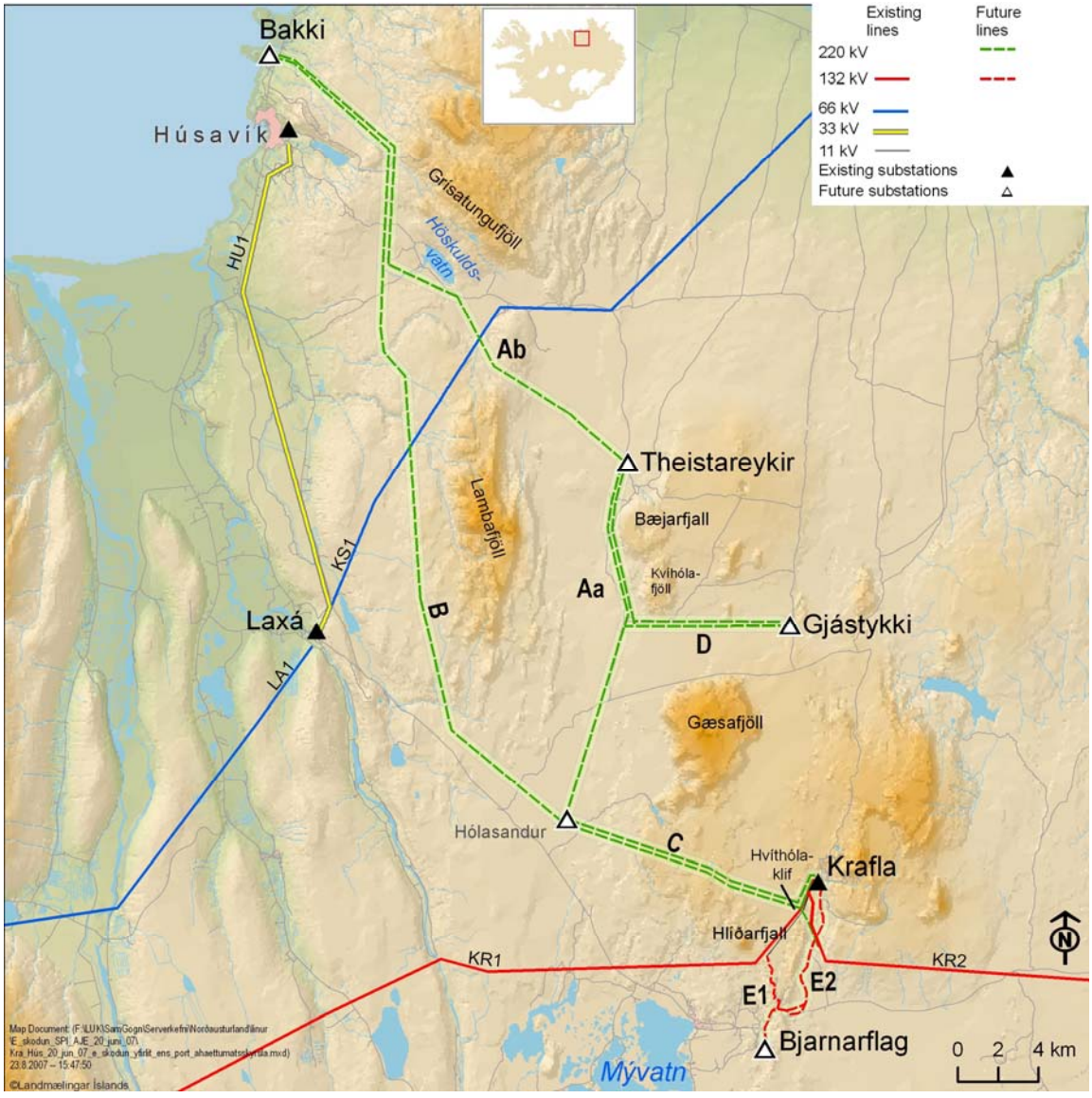

Figure 1.1 Location of the geothermal sites at Krafla, Theistareykir, Gjástykki and Bjarnarflag and the industrial lot at Bakki. Also shown are existing and future power lines (green lines).

1.1.4 Group of experts

The authors of this report are a group of geoscientists and engineers. Every group member has contributed to all chapters of the report and the manuscript has been discussed thoroughly by the whole group at various stages. Nevertheless each member has been the principal author of one chapter as indicated below. The group members are Dr. Kristján Saemundsson, chief geologist at the Iceland GeoSurvey (Chapter 2), Dr. Freysteinn Sigmundsson, geophysicist, Nordic Volcanological Center, University of Iceland (Chapter 3, with co-authors), Páll Halldórsson, seismologist, The Icelandic Meteorological Office (Chapter 4), Dr. Jónas Thór Snaebjörnsson, structural engineer, and Professor Ragnar Sigbjörnsson, both at the Earthquake Engineering Research Centre of the University of Iceland (Chapter 5) and Dr. Axel Björnsson, Professor in environmental sciences at the University of Akureyri (Chapter 1), chairman of the group and editor in chief of the report.

1.1.5 Use of Icelandic letters in names

Most Icelandic place names are written with Icelandic letters (Gjástykki and not Gjastykki). There are three exceptions for letters not existing in English. The Icelandic letter Þ, þ (pronounced like th in thunder) is replaced by Th and th. The letter ð (pronounced like th in although) is replaced by d. The letter æ is replaced by ae. Consequently the name of the geothermal field Þeistareykir is written as Theistareykir in the English text and the surname of one of the group member Sæmundsson is written Saemundsson.

1.2 The geological setting

Iceland is located at the intersection of the Mid-Atlantic ridge and the Greenland-Iceland-Faeroes ridge. The former lies on the diverging plate boundary of the American and the Eurasian plates. The spreading direction is N100°E. The Greenland-Iceland-Faeroes ridge is thought to be the trail of a mantle plume located beneath Iceland which has been active from the time of opening of the North-Atlantic some 50 Ma ago (Figure 1.2). The plume is now situated below central East-Iceland, within the eastern branch of the volcanic rift-zone which crosses Iceland from southwest to northeast. The existence of a mantle plume is supported by a seismic anomaly and by a major Bouguer gravity-low centred above the proposed plume. The mass deficit must presumably be sought in both the elastic crust and in the underlaying asthenosphere. An anomalously low P-wave velocity of 7.0-7.6 km/s and attenuation of S-waves has been observed in the mantle beneath Iceland, indicating partial melt. This anomalous mantle terminates abruptly near the insular shelf south of Iceland where normal oceanic crust and lithosphere is found.

The spreading rate near Iceland was first estimated to be about 1cm/y in each direction, based on magnetic anomalies to the north and south of Iceland (Figure 1.2). Repeated regional GPS measurements have delivered similar values as shown in Figure 1.3.

The axial rift zone crosses Iceland from the Reykjanes Peninsula where it connects with the Reykjanes Ridge (RR). Transform fault zones, the Tjörnes Fracture Zone (TFZ) in the northeast

and the South Iceland Seismic Zone in the south (SISZ), connect the presently active spreading zones with the submarine ridge segments (Figure 1.4).

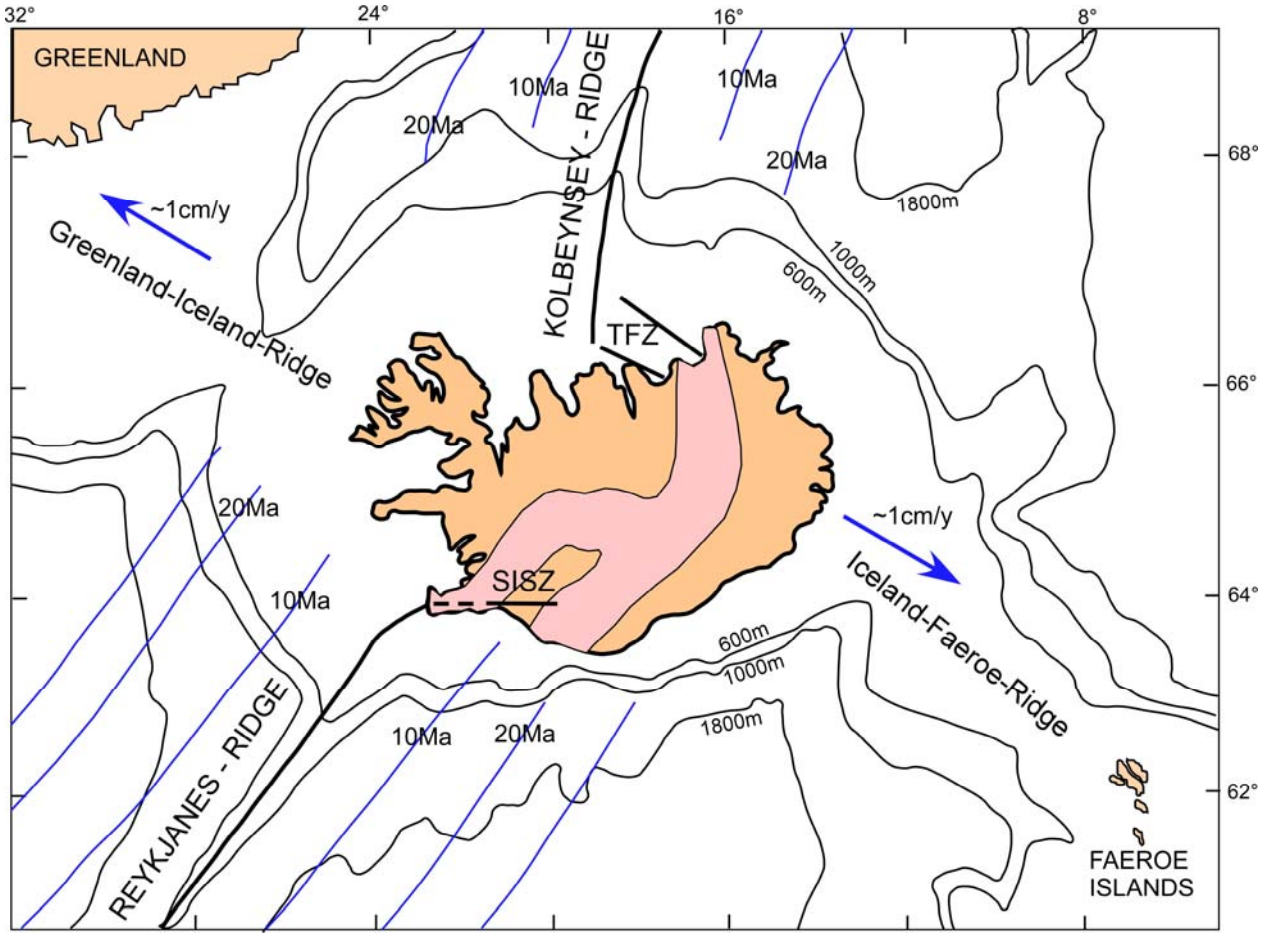

Figure 1.2 Iceland is an elevated plateau of volcanic basalt in the North Atlantic, situated at the junction between the Mid-Atlantic-Ridge (MAR) which characterizes the plate boundaries of the American and the Eurasian plate and the elevated Greenland–Iceland–Faeroes Ridge. The Reykjanes Ridge southwest of Iceland and the Kolbeinsey Ridge to the north are segments of the MAR. The spreading rate is around 1cm/y, indicated by blue arrows. Magnetic anomalies (blue lines) indicate increasing age in million years (Ma) of the ocean bottom with increasing distance from the rift axes. Also shown in red are the volcano-tectonic rift zones crossing Iceland from southwest to northeast. The South Iceland Seismic Zone (SISZ) in the south and the Tjörnes Fracture Zone (TFZ) in the north are transverse zones which connect the volcanic rift zones to the segments of the MAR.

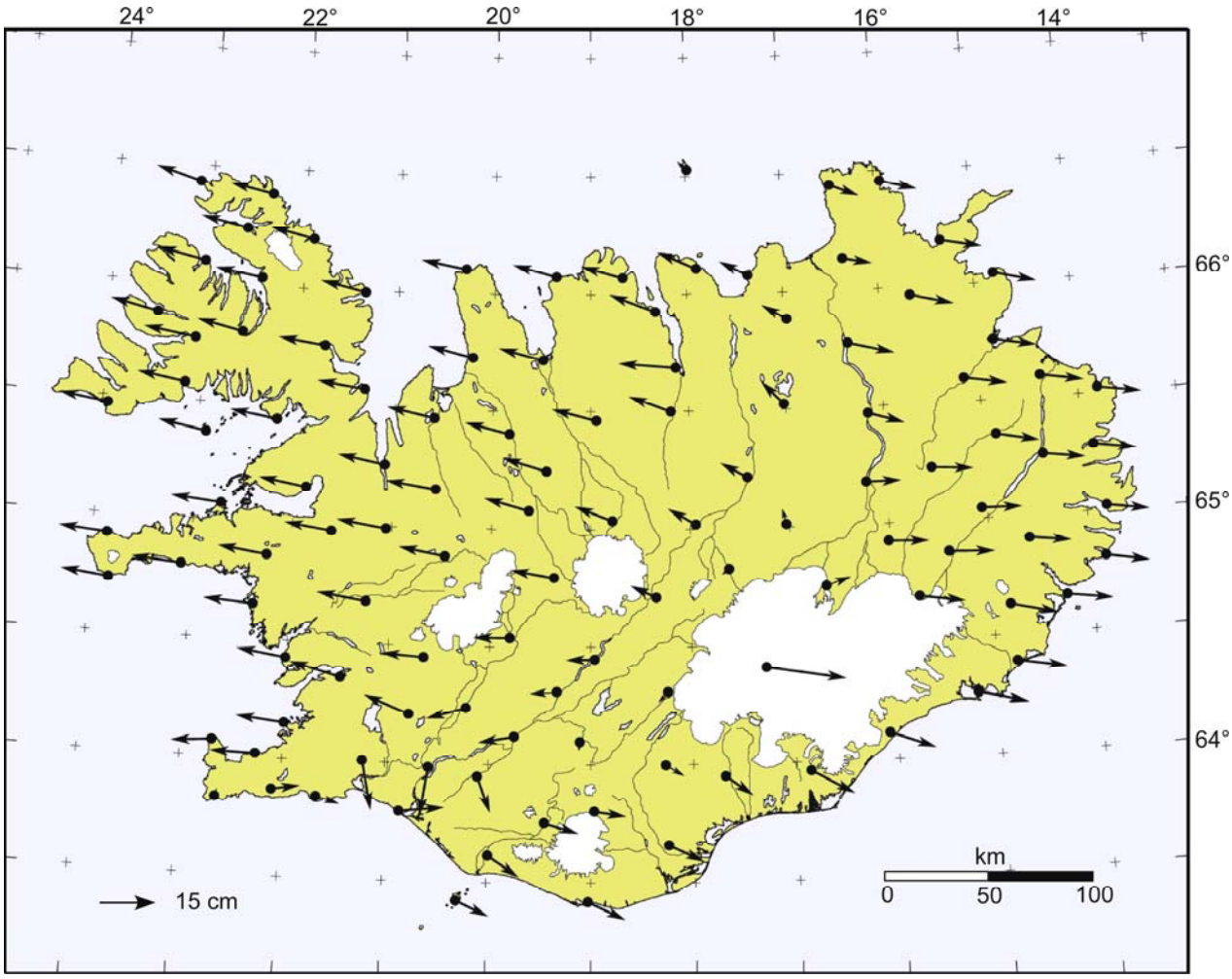

Figure 1.3 Plate movements from 1993 to 2004 in Iceland measured in GPS surveys. Regional north component of the movement has been removed. The center zone of the rift zones in north and east Iceland was kept fixed. Data provided by Landmaelingar Íslands (National Land Survey of Iceland, 2007).

Tectonic earthquakes are due to relative movements of the North American and Eurasian Plates. The biggest tectonic earthquakes in and around Iceland occur in the transverse zones in south (SISZ) and north Iceland (TFZ) and may reach at least magnitude seven. In the spreading volcanic zones magnitudes are smaller and usually do not exceed 5 (Figure 1.5) This is due to the fact that the elastic crust is presumably only 5-10 km thick in the volcanic rift zones and the temperature gradient is high. In the transform zones (TFZ and SISZ) the elastic crust is thicker, some 10-15km, and the temperature gradient lower. Volcanic earthquakes located in the vicinity of the major volcanoes usually do not exceed magnitudes 4-5. Small earthquakes, which occur quite frequently in high-temperature geothermal areas, usually do not exceed magnitude three.

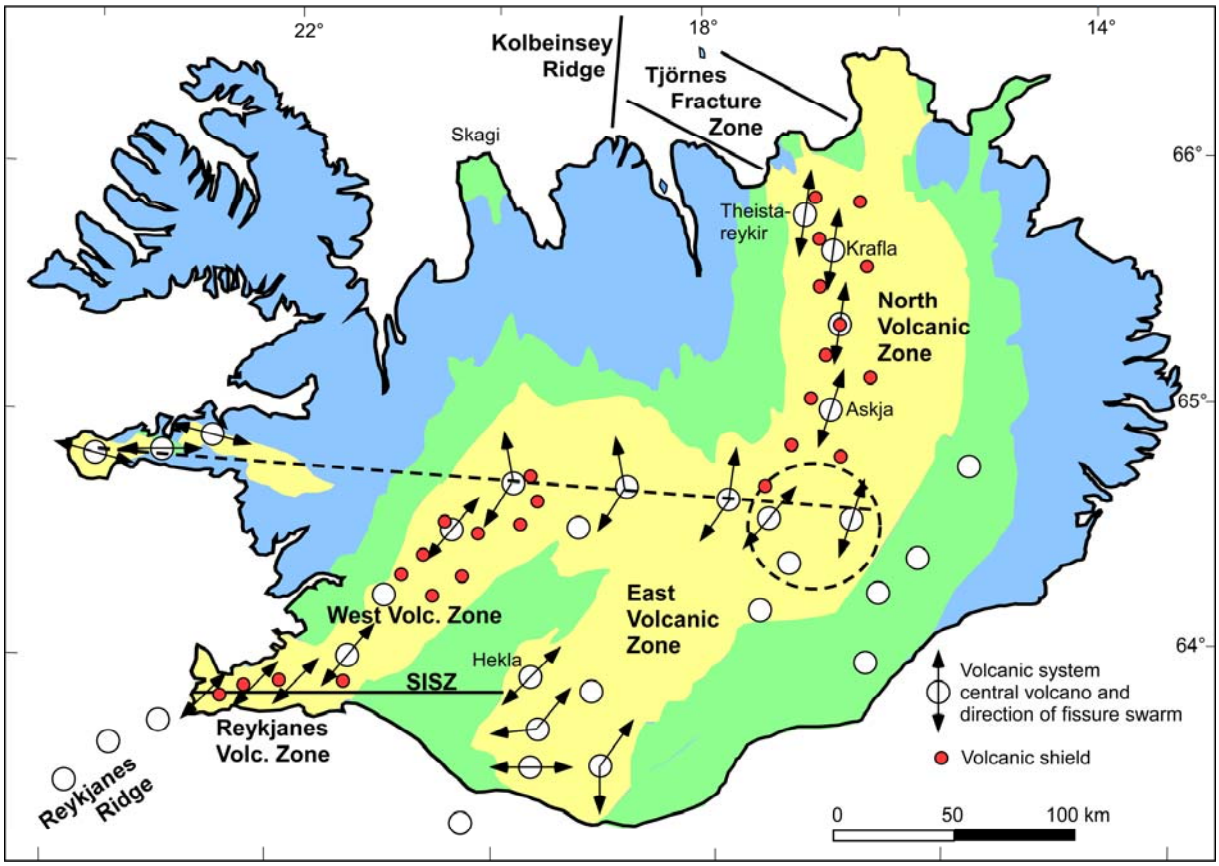

Figure 1.4 Simplified geological map of Iceland. The yellow area indicates the volcano-tectonic zone younger than 0.8 Ma. The green area shows bedrock 0.8-3.3 Ma old, and the blue area indicates Tertiary bedrock with age up to 16 Ma (Saemundsson, 1978). Open circles represent central volcanoes and direction of the associated fissure swarms (arrows). Filled red circles indicate large olivine-tholeiitic lava shields (not all shown). Heavy or dotted lines mark the transform faults and the dotted circle indicates the proposed location of the mantle plume beneath the island. SISZ is the south Iceland Seismic Zone. The map is modified from Saemundsson (1978). The geothermal areas assessed in this report, Krafla and Theistareykir, are marked in the NE volcanic zone.

1.3 The Volcano-tectonic rift zone in NE Iceland (NVZ)

The volcanic zones in Iceland are segmented into discrete volcanic systems. Most of them include a central volcano and a fissure swarm with proximal eruptive fissures and distal non-eruptive faults and ground fissures. The fissures extend far beyond the area of surface volcanism being the subsurface expression of dyke swarms (Saemundsson, 1974, 1977, 1978). Geothermal areas are an integral part of most of the central volcanoes. Sometimes subsidiary geothermal systems occur at volcanic foci on the fissure swarms, well away from the central volcanoes. The chemical compositions of lavas exhibit a wide range in most of the volcanic systems (Jakobsson, 1979). Acid volcanism is confined to the central volcanoes, rocks of intermediate composition occur around the center, but only basalt is erupted in the fissure swarms. These features indicate shallow magma chambers at some 3-10 km depth under the central volcanoes where the magma ascending from the mantle evolves.

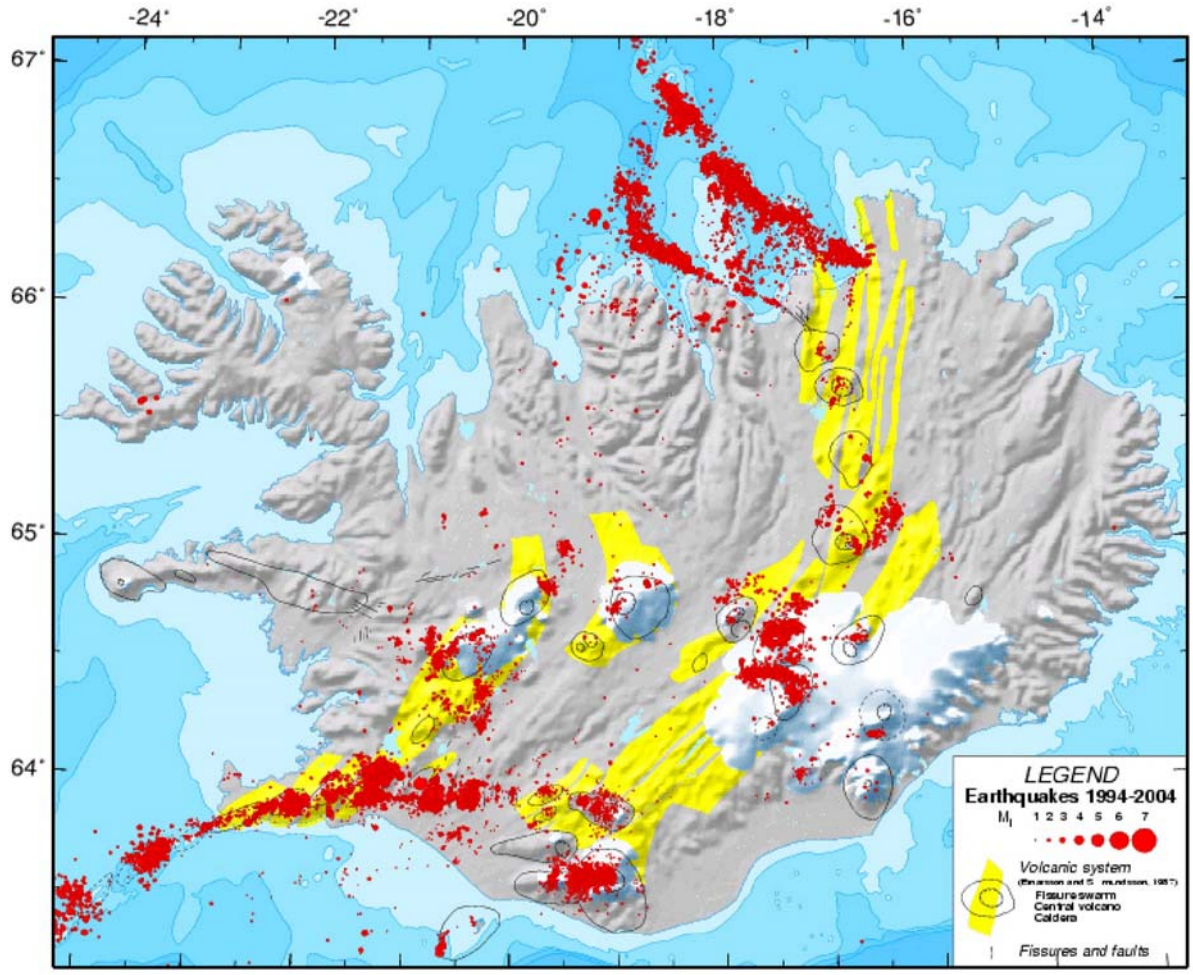

Figure 1.5 Spatial distribution of earthquakes in and around Iceland in the years 1994-2004. Red dots of different sizes indicate earthquakes of various magnitudes (Halldórsson, 2005). Also shown are fissure swarms, elongated yellow areas, and central volcanoes, circular areas, mapped by Saemundsson (1978).

A second major type of volcanoes is large monogenetic lava shields and table-mountains, composed of primitive olivine-tholeiites indicating a deeper mantle magma source. Some of the volcanic shields are composed of picrite, suggesting a still deeper source. The lava shields are only found in the West Volcanic Zone (WVZ) and North Volcanix Zone (NVZ) axial rift zones, and most of them were formed during the last part of the ice age and in a short time interval after the end of the ice age. The axial rift zones are flanked by Quaternary volcanic formations and, further to the east and west, by Tertiary flood basalts as shown in Figure 1.4 (Saemundsson, 1978, 1979; Johannesson and Saemundsson, 1998).

The axial rift zone in NE-Iceland contains 5 volcanic systems. The associated en-echelon fissure swarms are oriented N10°E. They derive their names from the intersected central volcanoes, all of which contain high temperature geothermal fields. They are, from west to east (Figure 1.6), the Theistareykir-, Krafla-, Fremrinámur-, Askja- and Kverkfjöll-fissure swarms (Saemundsson, 1974). See also Figure 1.7, which is an aerial view of the Krafla fissure swarm. The Theistareykir- and Fremrinámur central volcanoes have no developed calderas, which indicates absence

of shallow crustal magma chambers. In both these volcanic systems olivine-tholeiitic lava shields are more numerous than elsewhere in the axial rift zone.

The plate movements are oblique to the plate boundary and perpendicular to the individual fissure swarms in this area. This indicates that the fissure swarms in NE-Iceland are created mainly in the upper brittle crust, by tensile crack formation perpendicular to the axis of minimum compressive stress. The Krafla fissure swarm is characterized by open fissures, faults and nested grabens. Its total length is some 100 km and its width usually 4-10 km. The Krafla central volcano has a caldera, is characterized by a topographic high, and is situated just south of the longitudinal midpoint of the swarm. The northern end of the fissure swarms connects with the Tjörnes Fracture Zone (TFZ) in the bay Öxarfjördur (Saemundsson, 1991).

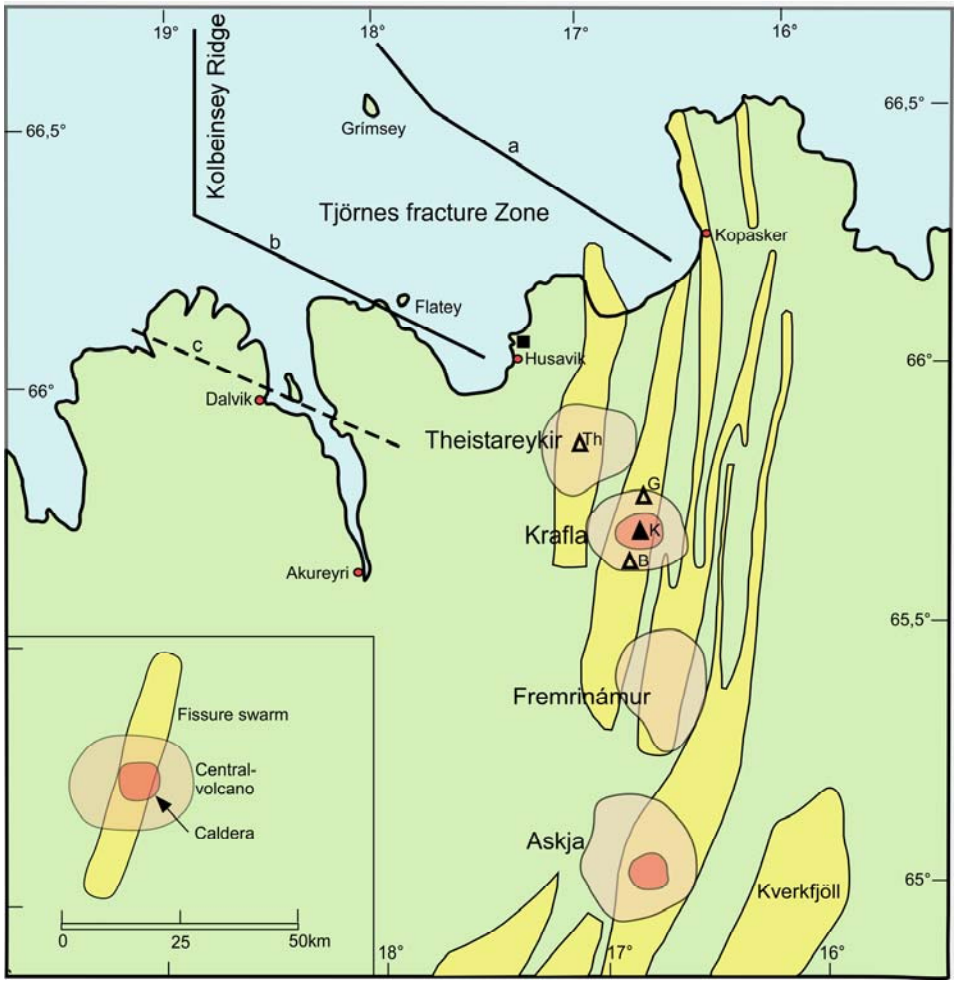

Figure 1.6 The volcanic zone in NE-Iceland is segmented into five major discrete volcanic systems. They include a central volcano characterized by topographic high (light red areas) and elongated fissure swarms (yellow areas) with proximal eruptive fissures and distal non-eruptive faults and tensional fissures (Saemundsson, 1974, 1978). The main seismic lineaments of the Tjörnes Fracture Zone are shown as massive or dotted lines: a) Kópasker–Grímsey fault, b) Húsavik-Flatey fault and c) Dalvík lineament. The location of the seismic lineaments is based on earthquake distribution in Figure 1.5. The Krafla power plant is marked with filled triangle K and the future power plants at Theistareykir, Gjástykki and Bjarnarflag with open triangles and Th, G and B respectively. The filled square, just north of the town Húsavík, shows the location of the industrial lot at Bakki.

Major volcano-tectonic activity is episodic in the axial rift zone in NE Iceland, occurring every 100-200 years. Each episode may last a few years. It is characterized by discrete short events of days or weeks. Only one fissure swarm is active at a time, only a part of a swarm may become active and widening and faulting varies along the swarm. Major seismic activity was reported in the Theistareykir fissure swarm in 1618, volcanism and tectonic activity occurred in the Askja fissure swarm from 1874-1875 and in the Krafla fissure swarm from 1724-1729. At that time the activity was mainly within and south of the Krafla caldera, in contrast to the most recent activity of 1975-1989 which was mostly within and to the north of it. For further details see Chapter 2, Section 2.1

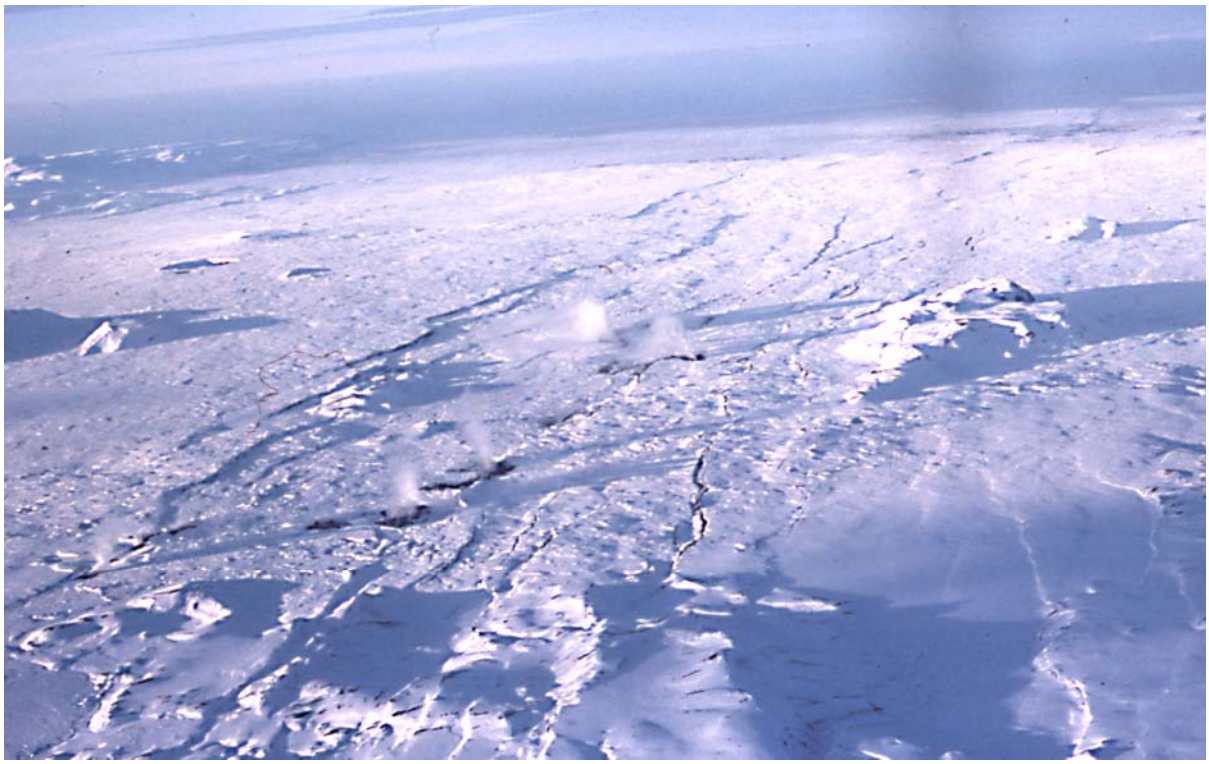

Figure 1.7 Aerial view to the north of the Krafla fissure swarm by Gjástykki some 10 km north of the caldera. The fissure swarm is about 5 km wide and some 80 km long. It is bounded by normal faults to the east and west. In between open tensional fissures are dominating. Several fumaroles and steam vents can be seen, that were reactivated during the initial phase of the Krafla Fires before the area was covered by lavas.

1.4 The crust in NE-Iceland

During the last three decades, two different models of the Icelandic crust and upper mantle have been presented. First, there is the classical thin crust model where the crust is thought to be about 10-15 km thick under the main rifting axes. This thin crust thickens with age to some 25-30 km beneath the older Tertiary areas in the west and east Iceland, where it connects to the thick crust of the Iceland-Faeroes ridge. According to this model the uppermost 10-15 km of the crust are mainly formed by dike intrusion and lava eruptions and continuous subsidence and mixing of magma in the rift zones (see e.g. Palmason, 1980; Hermance, 1981; Mayer et al., 1985; Gebrande

et al., 1980). Hence, this upper part of the crust is partly crust derived. The lower crust is created by up-flow of magma, intrusions and under-plating causing thickening of the crust with age. At the crust mantle boundary, there is a thin layer with low electrical resistivity which has been interpreted to be partially molten basalt which migrates from the mantle and creates the lower crust (Beblo and Björnsson, 1980). Second, there is the so-called thick-crust model, which is mainly based on recent seismic data and reinterpretation of old seismic data where a reflector can be seen at many spots beneath the seismic profiles at 20-40 km depth. The thick-crust model is primarily based on the assumption that these reflectors can be interpreted as the Moho boundary between anomalous thick oceanic crust and the anomalous low-velocity mantle below (see e.g. Bjarnason et al., 1993; Menke and Levin, 1994). Another explanation for the deep reflections could be melt patches in the mantle, which confirms with various recent petrogenetic studies on the origin of magmas beneath Iceland (Schiellerup, 1995; Maclennan, 2001; Breddam, 2002). For detailed discussion of both these crustal models see e.g. Björnsson et al. (2005) and references therein.

It is not relevant here to discuss further the difference between the two crustal models; the problem may be a matter of definition of terms like the words crust and Moho. On the other hand it is important to know the thickness of the elastic or rigid layer (elastic crust) beneath Iceland and to be able to estimate the viscosity of the asthenosphere below. Two different methods have been used to estimate the viscosity below the upper rigid crust (lithosphere). One method uses isostatic rebound measurements around the Vatnajökull glacier in SW Iceland (Sigmundsson, 1991; Sigmundsson and Einarsson, 1992; Pagli et al., 2007). The other method investigates stress redistribution following the major Krafla tectonic event which took place in NE-Iceland in 1975-1989 (Foulger et al., 1992; Heki et al., 1993; Hofton and Foulger, 1996a, 1996b). All these elasticity models dealing with Iceland make the simplifying assumption that the elastic layer has a constant thickness of ~10 km and that the underlying asthenosphere is homogenous. This is most likely not the case. It is more likely that the elastic layer thickens with age from the spreading axes, see Figure 1.8. Further the viscosity of the asthenosphere presumably decreases with increasing distance from the plate boundaries and the mantle plume. Buerger et al. (2002) have estimated the thickness of the lithosphere and the viscosity of the asthenosphere in southeast Iceland from gravity variations over one decade. They found the lithosphere to be 10-15 km thick, and the thickness of the asthenosphere to be about 170 km with a viscosity in the range of $0.3\text{-}1\cdot 10^{18}$ Pa s. Sjöberg et al. (2000) found the lithosphere to be 30 km thick in this area, and the asthenosphere to be about 100 km thick with a viscosity of $5\cdot 10^{18}$ Pa s. Kaban et al. (2002) on the other hand estimated the thickness of the rigid crust to be only about 6 km. It can be concluded from above mentioned work that the viscosity of the asthenosphere vary in the range of $0.3\text{-}30\cdot 10^{18}$ Pa s, which is exceptionally low on a global scale.

At the maximal earthquake focal depth, where it can be measured in Iceland, the temperature has been estimated to be about 600-800°C (Bjarnason et al., 1994, Foulger, 1995, Ágústsson and Flóvenz, 2005). Hence, the depth to the ~700°C iso-surface corresponds to the thickness of the elastic crust. If the surface temperature gradient, which has been measured in shallow drillholes outside geothermal areas (Saemundsson et al., 2003), can be extrapolated linearly down to 700°C the thickness of the elastic crust is known. Some studies indicate that the temperature gradient may decrease somewhat with depth (Ágústsson and Flóvenz, 2005) but other ongoing studies

made in the SISZ (Björnsson, 2007) indicate that the temperature gradient is, as a first order estimate, linear from the surface down to the 700°C iso-surface and even down to the good electrical conductor at 10-30 km depth where the temperature is thought to be 1100°C (Björnsson et al., 2005). Using both these data sets i.e. the surface temperature gradient and the depth to the conductor, we can estimate the thickness of the elastic crust in NE Iceland. It varies from ~ 5 km within the major evolved volcanic zone (NVZ) to some ~ 15 km in the old Tertiary areas (Figure 1.8).

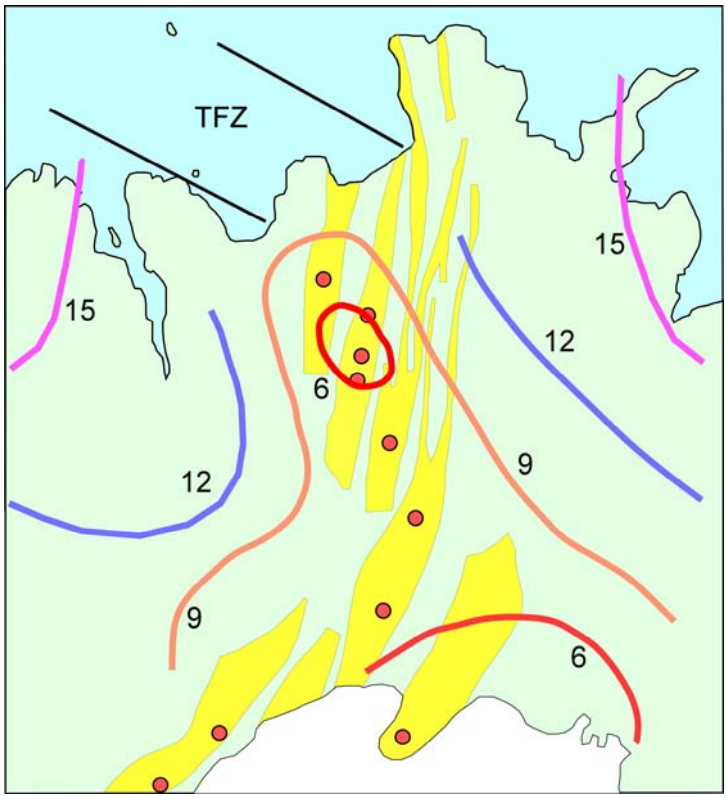

Figure 1.8 Estimated thickness of the brittle crust in NE Iceland. Numbers at the isolines indicate thickness in km. TFZ is the Tjörnes Fracture Zone. The bottom of the brittle crust (seismogenic layer) is assumed to be at 700°C. The depth estimate is based on surface temperature gradient data (Saemundsson et al., 2003) and the depth to a low-resistivity layer assumed to be at 1100°C (Björnsson et al., 2005). Red circles are high-temperature areas and the yellow zones are fissure swarms (Saemundsson, 1978).

It is interesting to note that the minimum thickness is found above the mantle plume and the Krafla area. The 9 km depth line shows an elongated anomaly trending NNW below the central volcanoes. This may delineate the plate boundaries at depth and their connection to the Húsavík Flatey Fault and the Kolbeinsey Ridge.

1.5 The Krafla Fires – a volcano-tectonic episode 1975 - 1989

1.5.1 Description of the volcano-tectonic episode

In 1975 a major rifting episode started in the Krafla fissure swarm. This rifting episode created a major threat to a geothermal power plant which was already under construction in the Krafla geothermal field, and to several deep production wells which had been drilled. Hence, the activity was monitored carefully. The scientific results have been described in detail in the literature (see e.g. Björnsson 1976, 1985; Björnsson et al., 1977, 1979; Einarsson, 1978; Einarsson and Brandsdóttir, 1980; Tryggvason, 1980, 1984; Einarsson, 1991; Saemundsson, 1991). The most important findings are summarized here because this episode is most likely an excellent and characteristic example of a rift episode likely to occur in some other volcanic centers in Iceland.

During the year 1975 some precursory symptoms occurred. Increased seismic activity was observed in the Krafla area on a seismometer in Akureyri some 100 km to the west of the area. During the years 1964 – 1974 the average number was only 4 earthquakes per year of magnitude >2. In March 1975 this number increased sudddenly to 4-6 earthquakes per month of the same magnitude and continued until December (Stefansson, 1976). In December 1975 a minor fissure eruption occurred near the hill Leirhnjúkur in the center of the caldera and major earthquake activity was observed in the fissure swarm, mainly to the north of the caldera. Fissures in the swarm widened up to some tens of cm. An extended dry tilt leveling survey made in March 1976 showed that the center of the caldera floor had subsided over 2 m. The subsidence bowl was centred close to the hill Leirhnjúkur and had a radius of some 10 km. A few weeks after this initial rifting event the land started to rise again. The speed was about 5 mm/day at the apex of the bowl. The second deflation and rifting event occurred in September 1976. This periodic inflation for weeks or months, interrupted with sudden subsidence-rifting events, continued for 9 years until 1984. This course of events was explained by the existence of a shallow magma chamber in the center of the caldera with a steady inflow of magma from below and periodic rifting and flow of magma into the fissure swarm. The shape and location of the inflation-/deflation bowl is shown in Figure 1.9. The center of the bowl was in a similar place during the whole rifting episode and is presumably located above the highest point of the shallow magma chamber.

Model calculations (Björnsson et al., 1979; Mogi, 1958) pointed to an upper crustal magma chamber at 3 km depth which received a continuous inflow from below, of 1-5 m^3/s of magma, from the beginning of the activity. The volcano inflated at a rate of a few mm/day for weeks or months, and increased earthquake activity was observed in the crust above the inflation center. This went on until the land elevation, the amount of magma, and the pressure in the magma chamber reached some critical values sufficient to initiate rifting of the fissure swarm. As the rifting propagated laterally outwards from the caldera, magma migrated along the fissures, forming a dike, and a nearly circular deflation bowl with a radius of about 10 km was created with a maximum deflation at the southeast end of the hill Leirhnjúkur. The earthquake activity ceased within the caldera as the land subsided but earthquake activity was observed in the fissure swarm and individual fissures widened up to tens of cm where the dikes were formed. The

earthquake activity and the widening of ground fissures propagated laterally along the fissure swarm with a speed of around 0.5 m/s (~2 km/h). These short active pulses, known as rifting or deflation events, usually lasted several hours, or at the most, a few days. The inflation periods usually lasted several months. Earthquake surveys done during the first inflation/deflation cycles delineated two regions of high S-wave attenuation. These were a few km in diameter and the top was at about 3 km depth. They were located to the east and west of the apex of the inflation-/deflation bowl, for location see Figure 2.2 in Chapter 2, Section 2.3.2 and were interpreted as the expression of a magma chamber (Einarsson, 1978).

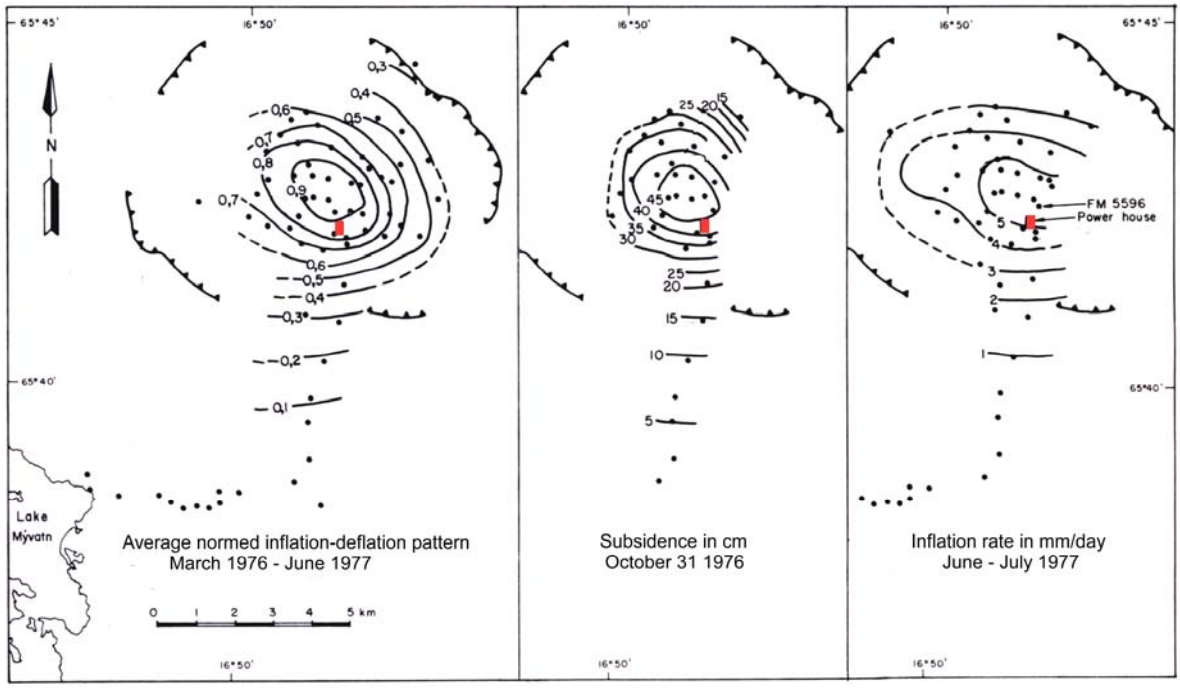

Figure 1.9 Inflation – deflation bowl with an apex at the SE end of the hill Leirhnjúkur near the center of the Krafla caldera and ~1 km NNE of the Krafla power house, shown as a red square. Average land elevation changes (left), one subsidence event (middle) and inflation rate during an inflation period (right) are shown. The center of the inflation-deflation bowl was nearly at the same place during the whole episode and presumably delineates the location of the top of the magma chamber. The two S-wave shadows, mapped by Einarsson (1979) are on the other hand located to the west and east of the center of the inflation bowl (see Fig. 2.2). Figure modified from Björnsson et al., (1979).

Figure 1.10 shows elevation changes during a 20 year period from 1975 to 1995, at a benchmark (FM 5596) about 0.8 km SSE of the center of the inflation/deflation bowl. A benchmark near the southern end of Lake Mývatn, 20 km away (FM6414), is used as a reference height. The elevation changes at the apex of the inflation-deflation bowl were about 10% higher. The vertical deflation at the center during a single rifting-deflation event varied from a few cm up to 2.3 m. A total of 24 rifting events occurred from 1975-1984. Some were very small with subsidence of less than 5 cm. Others were some tens of cm and up to 105 cm (Table 1.1). After the last major rifting event and the last volcanic eruption the land elevation continued to increase. In March 1989 the maximum height was reached at about 1.3 m higher than in 1975 before the activity started. The inflow of magma into the magma chamber at Krafla seems to have stopped abruptly and since then the land has been deflating at a slow rate. At the beginning the deflation was a few cm/y and

later measurements showed that the deflation was decaying exponentially. According to recent modelling work the deflation rate has reached a few mm/y (de Zeeuw-van Dalfsen et al., 2006).

Table 1.1 Rifting events during the Krafla rifting episode 1975-1984

Year	Subsidence period	Subsidence in	Rifting	Lava
	Start - End	FM-5596 (cm)	(North/South)	(km^2)
1975/6	20. Dec. - Feb.	203	N+S	0.036
-	29. Sep. - 04. Oct.	14	N	-
-	31. Oct. - 01. Nov.	57	N	-
1977	20. Jan. - 21. Jan.	29	N	-
-	01. Apr. - 02. Apr.	1	?	-
-	27. Apr. - 28. Apr.	77	S	0.001
-	08. Sep. - 10. Sep.	21	S	0.5
-	02. Nov.	3	N	-
1978	07. Jan. - 25. Feb.	105	N	-
-	10. Jul. - 13. Jul.	57	N	-
-	10. Nov. - 15. Nov.	64	N	-
1979	13. May. - 18. May	84	N	-
-	17. Sep.	1	?	-
-	02. Dec. - 08. Dec.	3	N?	-
1980	01. Feb. - 09. Feb.	10	S	-
-	16. Mar. - 17. Mar	38	N+S	1.3
-	20. Jun. - 25. Jun.	2	?	-
-	10. Jul. - 14. Jul.	40	N	5.3
-	01. Oct. - 02. Oct.	2	?	-
-	18. Oct. - 23. Oct.	30	N	11.5
-	24. Dec. - 28. Dec.	10	N	-
1981	30. Jan. - 04. Feb.	27	N	6.3
-	18. Nov. - 29. Nov.	50	N	17
1984	04. Sep. - 18. Sep.	55	N	24
1989	16. Mar.	Inflation stops	Deflation starts	
Total sum in	FM5596	9.83 m	Total area:	66 km^2
Total sum at	apex of inflation	10.81 m		
Inflation	1984 -1989	0.70 m		
Total volume	of inflation bowl	0.65 km^3	Volume lava:	~ 0.25km^3

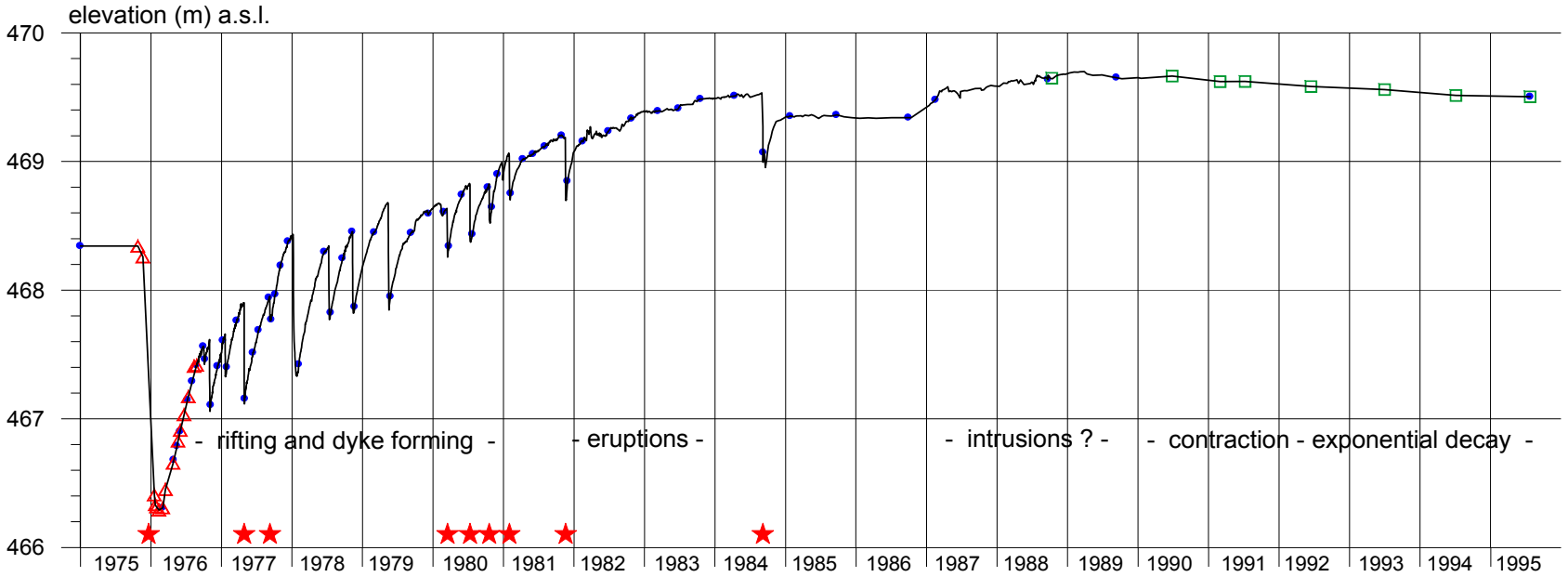

Figure 1.10 Land elevation changes during the Krafla fires at benchmark FM5596 0.8 km SSE of the apex of the inflation-deflation bowl. The first 9 years are characterized by continuous inflow of magma of about 1- 5 m^3/s into a shallow magma chamber at 3 km depth, and drainage of magma into the fissure swarm in short rifting events, releasing the pressure in the magma chamber. In 9 of 24 total rifting events magma came up to the surface, indicated by red stars. Most of the rifting took place during the first 5 years (1976-1980) when the magma was flowing into the fissure swarm. During the next 4 years (1981-1984) most of the magma came up to the surface. During the following 2 years1985-1986 the elevation was stable, which indicates that the inflow of magma had stopped. In 1987 the land started to rise again, indicating increasing pressure in the magma chamber or intrusions into the roots of the central volcano without rifting. In March 1989 the inflow of magma from below suddenly stopped and since then slow, exponentially decaying deflation has been observed. Blue dots are elevation values based on extensive dry tilt surveys with a distal reference point. Open triangles during the first year show elevation calculated from tilt measurements at the Krafla power house, and the open squares are based on tilt measurements at a station south of the power hose. The curve itself is calculated from daily tilt measurements within the power house. The smallest subsidence events (< 4cm) shown in Table 1.1 are too small to be seen in this diagram. Data from Björnsson and Eysteinsson (1998).

The elevation data fit very well to the simple model of Mogi (1958) assuming a varying pressure source at 3 km depth. The total sum of subsidence in all deflation/rifting events was 9.83 m as shown in Table 1.1. The total value for the center of the deflation/ inflation bowl is 10% higher or 10.8 m. Inflation from 1984 to 1989 vas about 0.7 m and, hence, the total sum is 11.5 m. If we assume that the surface volume changes associated with all the deflation events and the final inflation phase correspond to the amount of magma flowing into the magma chamber, an estimate of the total volume of magma is about 0.65 km^3. This can be taken as a rough estimate based on the theoretical relationship between volume of the surface bowl and magma increase in the chamber, considering the compressibility of the magma (Freysteinn Sigmundsson, pers. comm. and Chapter 3).

In nine instances the rifting events were accompanied by basaltic fissure eruptions. The first eruption occurred during the initial rifting phase in December 1975 and the last one in September 1984. Figure 1.11 shows typical fissure eruption in the Krafla area in September 1977.

It is difficult to estimate exactly the total volume of erupted lava. In some areas the thickness is less than 1 m, in other places many individual layers of lava have piled up to several meters in depth. The total volume has been estimated to be around 0.25 km^3 if treated as nonporous solid rock (Saemundsson, 1991). More than 70% of the total erupted lava during this episode erupted in the last three eruptions.

Figure 1.11 Fissure eruption in the Krafla area in September 1977. The fissure is about 800 m long. The magma erupted at the beginning of the Krafla eruptions has a low viscosity, contains high amount of gas and is flowing like water. Photo A. Björnsson.

During the rifting-deflation events one confined part of the inner zone of the fissure swarm widened and subsided, and the sides to the east and west were contracted and uplifted (Björnsson et al., 1979; Tryggvason, 1980; Einarsson and Brandsdottir, 1980). These activated sections of the fissure swarm were 5-25 km long during each event, and coincided with the area of maximum earthquake activity. See Figure 1.12 for location of the first activated segments. They are thought to demarcate the areas where shallow subsurface dike intrusion was occurring. During the first major rifting event from December 1975 to January 1976 the northernmost part of the fissure swarm, some 50-60 km north of the caldera, was activated. Major elevation changes and widening of fissures were observed in Kelduhverfi close to the coast. Earthquake activity was observed both in the fissure swarm as well as in the Grímsey-Kópasker segment of the Tjörnes Fracture Zone. Some of the subsidence events were small and no corresponding active area in the fissure swarm could be located. The total widening along the whole fissure swarm during 1975-1984 is shown in Figure 1.13.

Monitoring of micro-earthquakes during the rifting-deflation events clearly demonstrated that rifting was initiated within the caldera at the magma chamber, and propagated along the fissure swarm to the north or south (Einarsson and Brandsdóttir, 1979). Monitoring of changes in the width of surface fissures verified this. The horizontal migration velocity of propagating fissures and micro-earthquake activity along the swarm was close to 0.5 m/s (~ 2km/h) (Björnsson, 1976; Einarsson and Brandsdóttir, 1980). Figure 1.14 shows the spatial migration of earthquakes during one of the rifting events, from the caldera to the north along the fissure swarm.

An example of vertical land movements along a profile transecting the fissure swarm is depicted in Figure 1.15. The elevation changes across the Krafla fissure swarm near Bjarnarflag, some 10 km south of the caldera, are shown for several time intervals. Subsidence of up to 1 m occurred in the inner zone during rifting events and uplift of tens of cm on both sides to the west and east. The shore of the lake Mývatn was uplifted about 30 cm during this period, and a small island which had sunk below the water surface in the early part of the last century reappeared. This indicates a slow subsidence at the plate boundaries, along with widening, during quiet periods between rifting episodes.

Figure 1.16 shows clearly the vertical and horizontal land movements in January 1978 during rifting of the Krafla fissure swarm in Kelduhverfi, some 40 km north of the caldera. The center active part of the fissure swarm is 5-6 km wide in this area and subsided up to 1 m and widened up to 2.5 m. The flanks on both sides to the east and west are contracted and uplifted. The total contraction on the flanks was about 1.4 m so the net widening between both ends of the profile was about 1.1 m (Björnsson, 1980). The measured profile is not a straight line and not quite perpendicular to the rift zone, hence, the numbers are not precise. Still higher numbers were observed during the initial rifting of December 1975 to February 1976, as can be seen from Figure 1.13.

Figure 1.17 shows variations in the width of individual fissures in the caldera during inflation-deflation periods and in the fissure swarm during rifting.

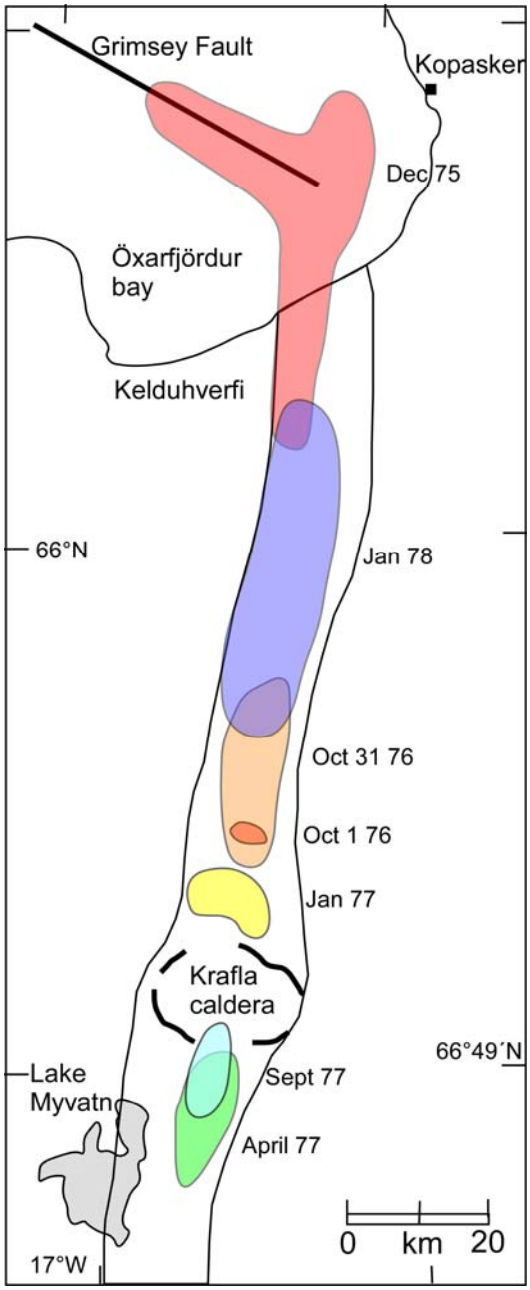

Figure 1.12 Activated areas of the Krafla fissure swarm from 1975 to 1978. Only one section is activated during each subsidence / rifting event. Redrawn from Einarsson and Bransdsdóttir (1980), who delineated the active areas by locating earthquake epicenters. Mapping of ground fissures delivered in some instances a more detailed picture, for example during the initial rifting phase in December 1975 where the whole central part of the fissure swarm was activated (Sigurdsson, 1977; 1980), and not only the western part as indicated by the earthquake locations.

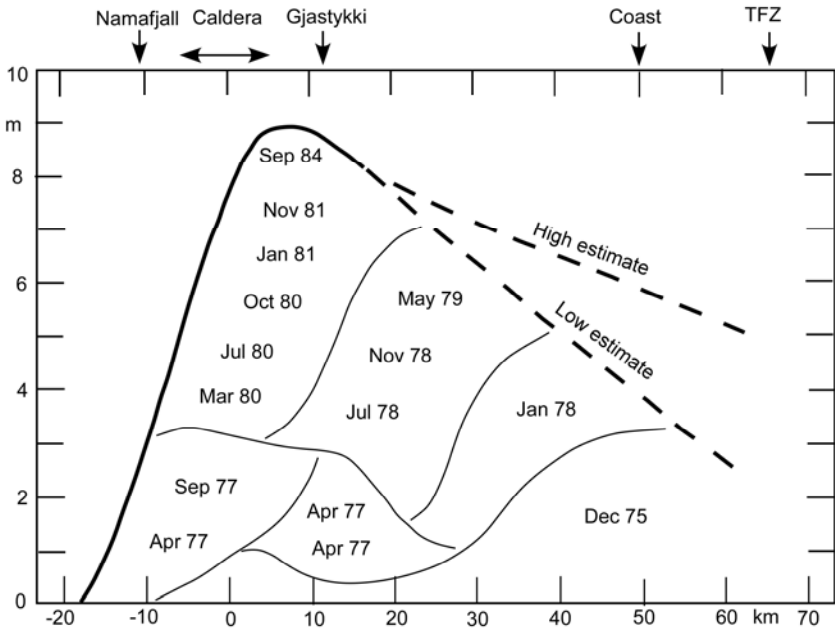

Figure 1.13 Total accumulated widening along the Krafla fissure swarm during the 1975-1984 volcanic episode. The maximum extension of 9 m took place close to the northern rim of the caldera. Redrawn from Tryggvason (1984). Additional data for September 1984 from E.Tryggvason and F. Sigmundsson.

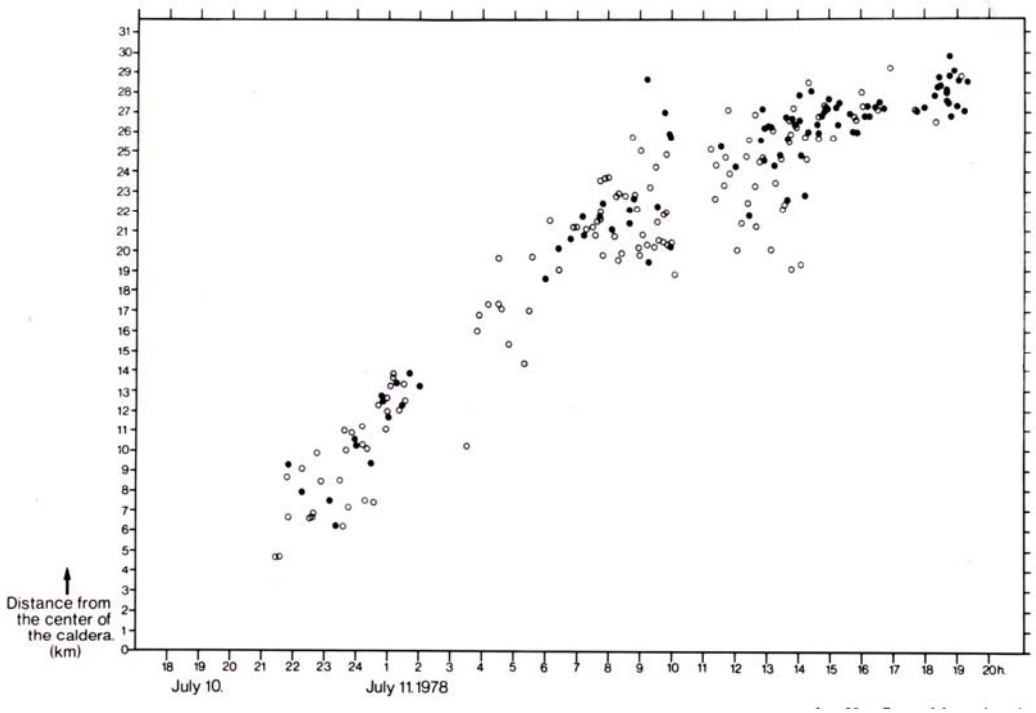

Figure 1.14 Horizontal migration of earthquakes with time from the Krafla caldera to the north along the fissure swarm during a subsidence-rifting event in July 1978. The horizontal distance is measured from the center of the caldera. In the Snagi area some 10 km north of the caldera most of the earthquakes were at 2-4 km depth, but one occurred at 7 km and another at 14 km depth. The highest magnitude was around 4 but the majority of the earthquakes had a magnitude between 2.5 and 3.5. The b-value was 1.7 ± 0.2. Figure from Einarsson and Brandsdóttir (1980)

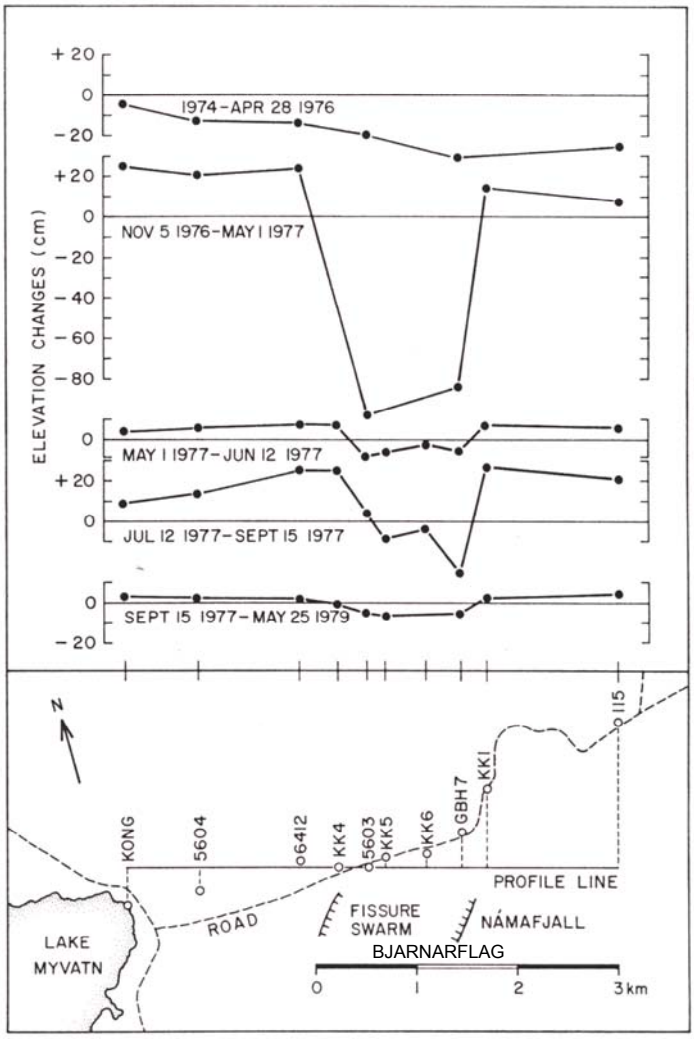

Figure 1.15 Vertical movements across the Krafla fissure swarm at Bjarnarflag /Námafjall some 10 km south of the center of the caldera. The first profile (1974-1976) shows subsidence along the whole profile which might be part of the initial subsidence bowl, as well as regional pre-rifting subsidence. The second profile includes the rifting event of April 27.-28. 1977, as the magma was flowing to the south. The center part of the fissure swarm subsided about 80 cm and the flanks to the east and west were uplifted some 20 cm. The fourth profile includes the rifting event of 8.-10. September 1977 when the magma was also flowing to the south and some 6.5 $m^3$of scoria were erupted through one of the geothermal wells in Bjarnarflag. The last profile (1977-1979) shows some subsidence in the center part and uplift of the flanks. Figure from Björnsson et al. (1979).

In addition to these local observations, some regional geodetic measurements were made in the area in order to investigate land deformation over longer periods. They demonstrate that horizontal and vertical land movements occurred out to at least 50 km east and west of the axial rift zone. Möller and Ritter (1980) and Möller et al. (1982) made extensive high precision geodetic distance measurements in a triangulation network crossing the axial rift zone in NE-Iceland. They found up to 8 m of extension in the center of the Krafla fissure swarm during the

period 1971 to 1980, and contraction on the sides. Kanngieser (1983) measured elevation changes on a 140 km long E-W profile crossing the active zone near Bjarnarflag. Comparison of measurements made in 1975 and 1980 shows that a regional uplift of up to some 0.6 m occurred, centered on the Krafla fissure swarm, see Figure 1.18. The half width of the bell-shaped, uplifted zone was some 20 km.

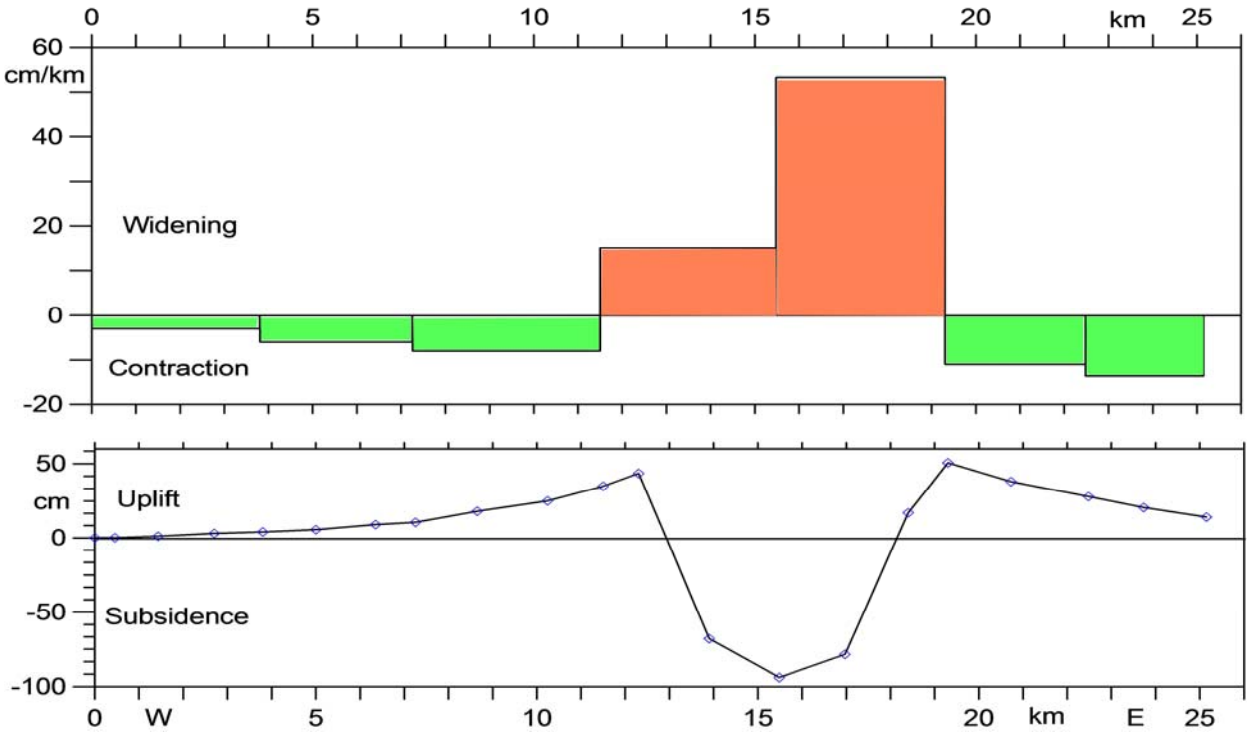

Figure 1.16 Widening and elevation changes across the Krafla fissure swarm in Kelduhverfi, some 40 km north of the caldera, during a rifting event in January 1978. Figure redrawn from Sigurdsson (1980).

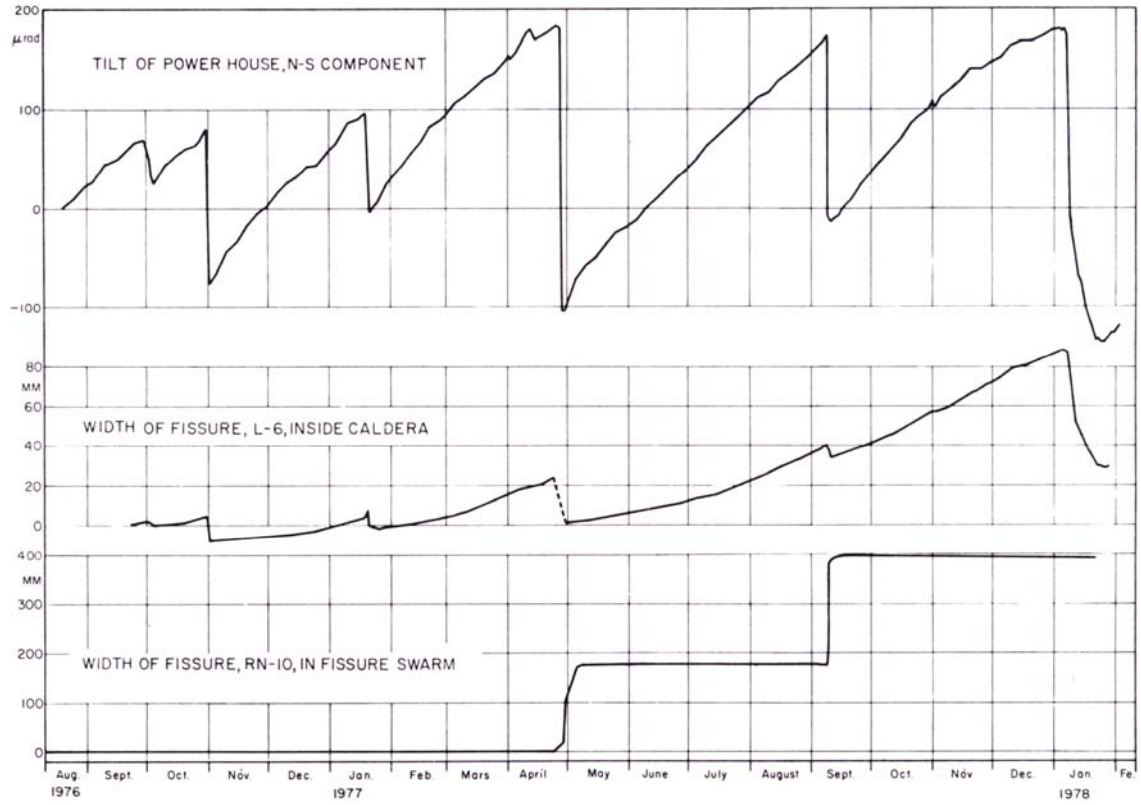

Figure 1.17 The upper part shows the tilt variations of the power house (in micro-radians) caused by land elevation changes, for the period August 1976 to January 1978. The middle part shows variation in width of a fissure located close to the apex of the inflation-deflation bowl. The fissure width correlates with the elevation (tilt). The lower part shows the width of a fissure in the central fissure swarm at Bjarnarflag, south of the caldera. The width is nearly constant except during two rifting deflation-events when the magma moved to the south, i.e. in April and September 1977. The widening of the fissure is around 20 cm in both cases. Figure from Björnsson et al., (1979).

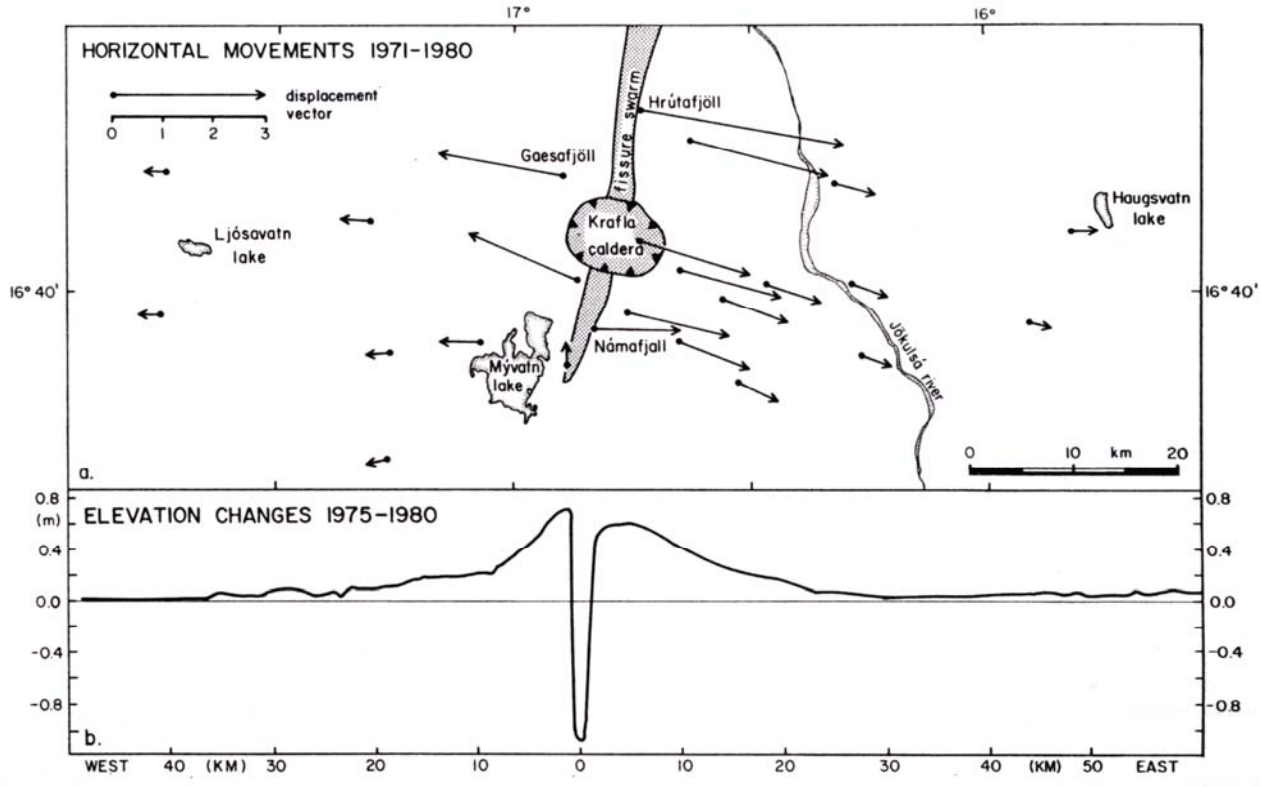

Figure 1.18 The upper part shows horizontal movements from 1971 to 1980 in the Krafla area. The measurements were made by Möller et al. (1982) in co-operation with Orkustofnun. Horizontal widening of up to 8 m was observed across the active fissure swarm but contraction of the flanks. The lower part shows elevation changes from 1975 to 1980 on an E-W profile crossing the Krafla fissure swarm by Bjarnarflag. The measurements were made by Kanngieser (1983) in co-operation with Orkustofnun. Here the elevation data have been projected onto latitude 16°40´. The flank zones of the fissure swarm were uplifted around 0.6 m and uplift was observed out to a distance of 30 km from the rift zone. Figure from Björnsson (1985).

1.5.2 Influence on man made structures and on the exploitation of geothermal systems

The first rifting episode of 1975 triggered a 6.2 magnitude earthquake in the bay of Öxarfjördur, 65 km NNE of Krafla at the intersection of the Krafla fissure swarm with the Tjörnes Fracture Zone (TFZ). This earthquake caused considerable damage in the village Kópasker which is some 10 km from the epicenter. Earthquakes in the fissure swarm were much smaller with a magnitude up to only 4. These earthquakes did not cause any direct damage due to acceleration. Comparing the small magnitude of the earthquakes within the caldera and in the fissure swarm to the major tectonic movements on faults and fissures demonstrates that the major part of the tectonic movements has taken place aseismically. This is explained by a thin elastic crust and its high temperature.

At the geothermal site in Bjarnarflag, 10 km south of Krafla, all buildings and other pre-1975 surface construction was sited within the central zone of the fissure swarm, which rifted and subsided during the Krafla fires. Buildings survived, though partly damaged, but storage ponds

for diatomite were destroyed due to opening of ground fissures. Four of six boreholes were also destroyed, either disrupted by faults or more likely plugged by lava. One borehole erupted about 6.5 m^3 of basaltic scoria (some 2500 kg) (Björnsson and Sigurdsson, 1978), but cleaned itself and produced steam for 25 years after that. New boreholes were drilled less than 100 m east of the activated fault zone, in the area which was uplifted and contracted during the rifting episode. They have produced without interruption for 25 years now.

Surface construction at Krafla was not affected by ground fissuring as it is located about 1 km east of the central rift zone affected by fault movement. On the other hand, cleaning of one borehole at Krafla showed that it had been plugged by an intrusive sheet.

It may sound strange, but ground tilting and regional uplift or subsidence, even up to more than one meter, did not cause major problems at Krafla, neither during the construction phase nor during operation of the power plant. The reason is that the inflation-deflation bowl had a radius of more than 10 km. Whole buildings, pipelines and other construction as well as the crust itself were moving up or down as a whole block. The maximum tilting of the power house was on the order of 300 μrad (microradians) during the larger subsidence events, which did not affect any part of the machinery of the plant. Earthquakes and seismic tremors did not affect routine operations (Birkir Fanndal, pers. comm.).

On the other hand the volcano-tectonic activity had a major impact on the geothermal systems, mainly in Krafla. A part of the Krafla geothermal system closest to the magma chamber was contaminated by high fluxes of volcanic gases, mainly CO_2 (over 90%) but also SO_2 and HCl, causing acidification of the reservoir water to a pH below 2 (Ármannsson et al., 1989). This caused corrosion and dissolution of iron casings and well heads, and leaching of heavy metals from the reservoir rocks. In one case a blow-out occurred, which sealed itself with scaling within a few months. Another nearby well was closed within three weeks of discharge by high temperature scale like iron-silicate, magnetite and anhydrite (Kristmannsdóttir and Swantesson, 1978; Kristmannsdóttir, 1984). Discharge of black-coloured water due to fine grained precipitates of iron sulfide was observed in several wells further away from the magma chamber. The magma chamber in the roots of the Krafla field and intrusions into the geothermal system may explain the fluxes of magmatic gas into the Krafla geothermal system. The Bjarnarflag field was not affected seriously by gas influx. Both fields were intruded by dykes or sheets cutting off or plugging boreholes.

The amount of non-condensable gas (CO_2) in the geothermal fluid increased from less than 1% to peak values of about 6% in some of the production boreholes during the initial rifting and dyking stage of the Krafla Fires (Figure 1.19). The part of the Krafla geothermal reservoir which was affected by gas contamination became non-exploitable for several years. The gas content gradually approached the initial value after the eruptive phase began. It was not until 1994 that the total gas concentration from all producing wells reached values lower than 1-2% and the reservoir again became fully exploitable.

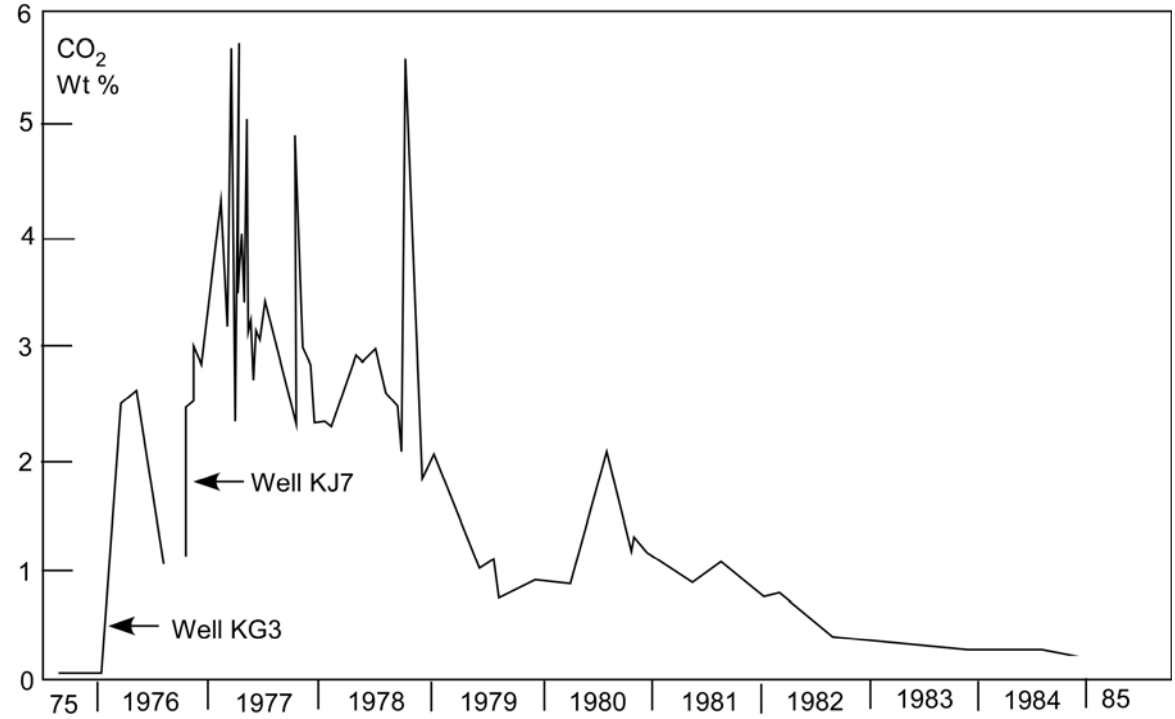

Figure 1.19 Variation in CO_2 content in two geothermal wells at Krafla from 1975 to 1984, measured in weight % of the total flow. Redrawn from Ármannsson et al. (1989).

1.6 The rifting mechanism in the volcanic zone in NE-Iceland

The total amount of magma which flowed from below into the magma chamber at Krafla has been estimated to be around 0.65 km^3. The erupted lava was only some 0.25 km^3 if treated as solid rock. Thus the intruded magma has a volume of about 0.4 km^3. This demonstrates that crustal accretion during the Krafla rifting episode was mainly by dike injection.

The total widening across the central active part of the Krafla fissure swarm may be estimated from Figure 1.13 to be around 0.5 10^6 m^2 (increase in surface area). Dividing this number into the estimated volume of intruded magma the average height of the dikes formed is estimated to be less than 1 km and, hence, confined to the upper part of the crust. These calculations are close to estimates of dike height made by Einarsson and Brandsdottir (1980) and by Tryggvason (1984) for single rifting events. Gudmundsson (1983), however, has estimated dike height in eroded dike swarms in eastern Iceland to be much greater, some 10 km. Model calculations using tilt and horizontal displacements during the last eruption in Krafla in 1984 leads to 7 km depth of the formed dyke (Árnadóttir et al., 1998; see also Chapter 3 Figure 3.3b). These depths, 7-10 km, are comparable to the crustal thickness in the axial rift zone according to the thin-crust model. The contribution to crustal widening by normal faulting is assumed to be negligible for this

calculation since fault planes are generally close to vertical in the Krafla area, and movements on them were small compared to the horizontal extension of several meters.

It is most likely that dikes which are formed close to the magma chamber are fed horizontally by lateral movements of magma along a propagating fissure (Björnsson et al., 1977, Björnsson, 1985). This conclusion is based on observed migrations of earthquake hypocenters during rifting events (Einarsson and Brandsdottir, 1980), and the close time-correlation between subsidence rate in the caldera and activity in the fissure swarm. The dikes so formed may be confined to the upper elastic part of the crust which is about 4-6 km according to seismogenic depth (Einarsson, 1978). On the other hand, the dike-forming mechanism at larger distances from the caldera may be different and follow the classical model of dikes formed by magma ascending vertically in fissures. Thayer et al. (1981) discussed the possibility that magma could flow vertically from the sub-crustal semi-fluid layer. During the major rifting episode at Krafla, an 80 km long segment of the plate boundary in NE-Iceland was activated. The elastic crust in this area is 6-16 km thick and it seems likely that sudden rifting in the elastic uppermost few km may change the stress field in the lower viscous crust and rifting then propagates down to the base of the viscous crust. This is supported by observation of deep earthquakes during rifting events (Einarsson and Brandsdóttir, 1980). The close correlation between subsidence in the caldera and distant activity in the fissure swarm could then be due to hydrostatic connection along the low resistivity semi-fluid layer.

Rifting of the crust down to the partially molten layer facilitates magma movements, both vertically and horizontally. The mixing of magmas from different depths and hence of different chemical compositions would thus be expected. Grönvold (1984) has found that magma erupted north of the caldera rim is more primitive in composition than magma erupted within the caldera. An explanation for this could be that magma is drawn from different depths within a layered magma chamber. It is also possible, and even more likely, that the evolved magma is drawn from the shallow upper crustal magma chamber within the caldera and the primitive magma is drawn directly from the base of the crust. Petrogenetic studies by Maclennan et al. (2001) show that magma is generated over a broad depth range beneath the Northeast Volcanic Zone in Iceland.

Most of the micro-earthquakes in the Krafla area occur in the uppermost 4-5 km of the crust which indicates elasticity in this upper part of the crust. Deeper earthquakes down to 14 km are also observed (Einarsson and Brandsdottir, 1980). Below the seismogenic limit the crust is visco-elastic. However, it does not necessarily follow that fissuring and magma transport is confined to the uppermost 4-6 km. Visco-elastic material behaves like a fluid over long time intervals and stress is released by creep. Over short periods of time, i.e. on the time scale of minutes or hour, however, the material may behave elastically and transmit seismic waves without noticeable attenuation (Sanford and Einarsson, 1982). Rifting, which occurs on the time scale of a few hours or days, probably takes place largely aseismically in the lower part of the crust. This is supported by the fact that only small seismic energy release accompanies the major horizontal and vertical land movements observed.

The rifting episode of Krafla can be explained by a gradual build-up of local tensional stress over a period of centuries in a narrow zone of the crust near the plate boundary as a result of slow retreat of the plates (Figure 1.20). The build-up of strain in the axial zone results in gradual crustal thinning and subsidence. Tension is then suddenly released in a rifting episode, accompanied by the intrusion of magma into fissures in the crust. Magma may have previously

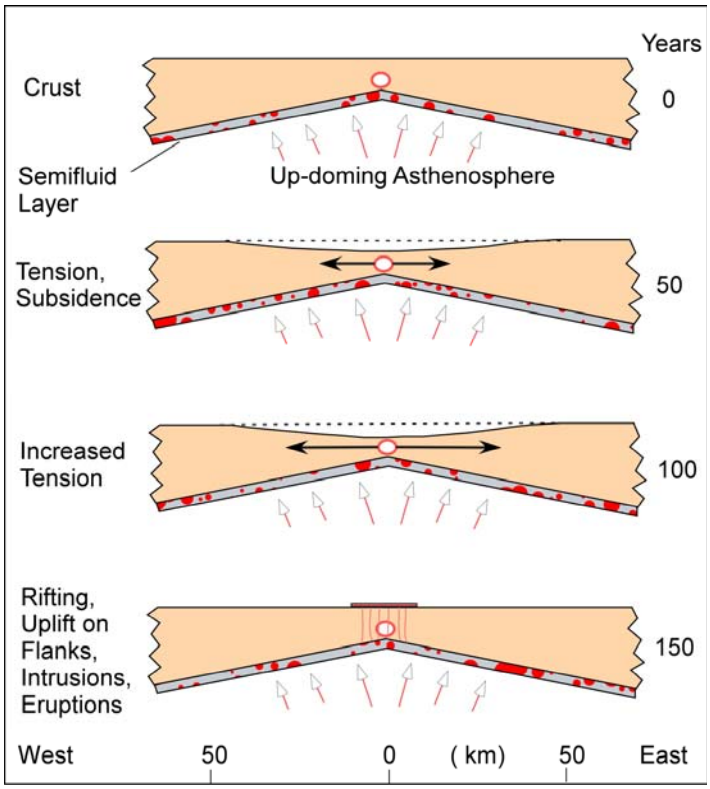

Figure 1.20 A simplified model of episodic rifting in NE Iceland. Tension is gradually built up in the axial rift zone and is released every few 100 years in a rifting episode. Redrawn from Björnsson (1985).

accumulated in a confined magma chamber which forms a weak point within the crust, where rifting is initiated. Magma migrating from the semi-molten layer or from a magma chamber through pre-existing or newly created joints and cracks in the lower crust increases the pore pressure and lowers the failure stress (Shaw, 1980). Magma infiltration is hence capable of initiating a rifting episode. The amount of available mobile magma is very likely one of the most important factors that control the periodicity of both rifting episodes and individual rifting-deflation events within a rifting episode. Other important parameters are tension at the plate boundary, the shear strength of the lower part of the crust, the tensile strength of the upper elastic crust and, possibly, pressure in the magma chamber. The strength of the upper crust must depend heavily on crustal thickness and the existence of upper crustal magma chambers. A magma chamber is, according to this, not a requisite for the rifting process. However, a volcanic system containing a magma chamber in the roots of its central volcano should rift more frequently than a system without one. It is possible that magma chambers develop preferentially in volcanic

systems underlain by thin crust and that rifting episodes occur at much longer time intervals, or some thousands of years, in volcanic systems that do not have magma chambers (Björnsson, 1985).

When rifting occurs in one fissure swarm elastic rebound causes land to rise and east-west contraction takes place in the crust on both sides. Elastic rebound in the adjacent crust releases tension in nearby en-echelon arranged fissure swarms, preventing them from rifting simultaneously. The main activity during the Krafla Fires rifting episode was probably mostly confined to the northern half of the Krafla swarm because tension in the southern part had been released during the active rifting episode in the Askja swarm during the period 1874 - 1875.

2. Volcanic hazards

Kristján Sæmundsson, Iceland GeoSurvey

2.1 Introduction

The following chapter describes the main characteristics of the geothermal areas and their setting within the structural framework of the North Volcanic Zone (NVZ). It summarizes the volcanic and volcano-tectonic hazards relating to borefield and power plant locations. Also considered are transmission lines and substations as regards hazards from proximal as well as distal events. The assessment is based on pre-existing knowledge of events which have occurred within or close to the areas concerned.

2.2 High temperature geothermal areas of the NVZ in relation to active volcanic systems

Volcanism in Iceland occurs in discrete volcanic systems (Saemundsson 1978). In the spreading zone these are more than 100 km long, about 3–10 km broad and arranged en echelon (Figure 2.1). A central volcano marks the core from which a prominent system of ground fissures fans out. The fissures extend far beyond the area of surface volcanism being the subsurface expression of dyke swarms. The geothermal areas are an integral part of the central volcanoes. Sometimes subsidiary geothermal systems occur at volcanic foci on the fissure swarms, well away from the central volcanoes.

Volcanic activity and rifting occurs episodically. Each episode may last a few years. It is punctuated by discrete short volcanotectonic events of days or weeks. During an episode the fissure swarms are not activated across their entire width. Rather, fault movement affects only a part of them and faulting varies along their length. Three volcanotectonic episodes have occurred and are documented in the northern part of the NVZ in the last 300 years, two of them involved the Krafla system. The Askja fissure swarm was also active in this period at least as far north as the latitude of Krafla. Theistareykir may have experienced a non-volcanic rifting episode in 1618 AD. Two episodes involved hydrovolcanic eruptions of rhyolitic pumice and hydrothermal steam (Krafla 1724 and Askja 1875). Before 1724 we have to look back 400 years to the early 14th century (1332?) for an eruption in the NVZ north of Askja.

Four volcanic systems run parallel and partly overlap in the northern part of the NVZ (Figure 2.1). The central part of two of them, Theistareykir and Fremrinámur, is covered by 2500-3000 year old lavas. These have not been affected significantly by later faulting contrary to lavas of similar age in the fissure swarm of Krafla. It is clear from this evidence though that the Krafla system was the main focus of eruptions and fault movement in the northern NVZ north of Askja during this period of time, i.e. for the last 3000 years.

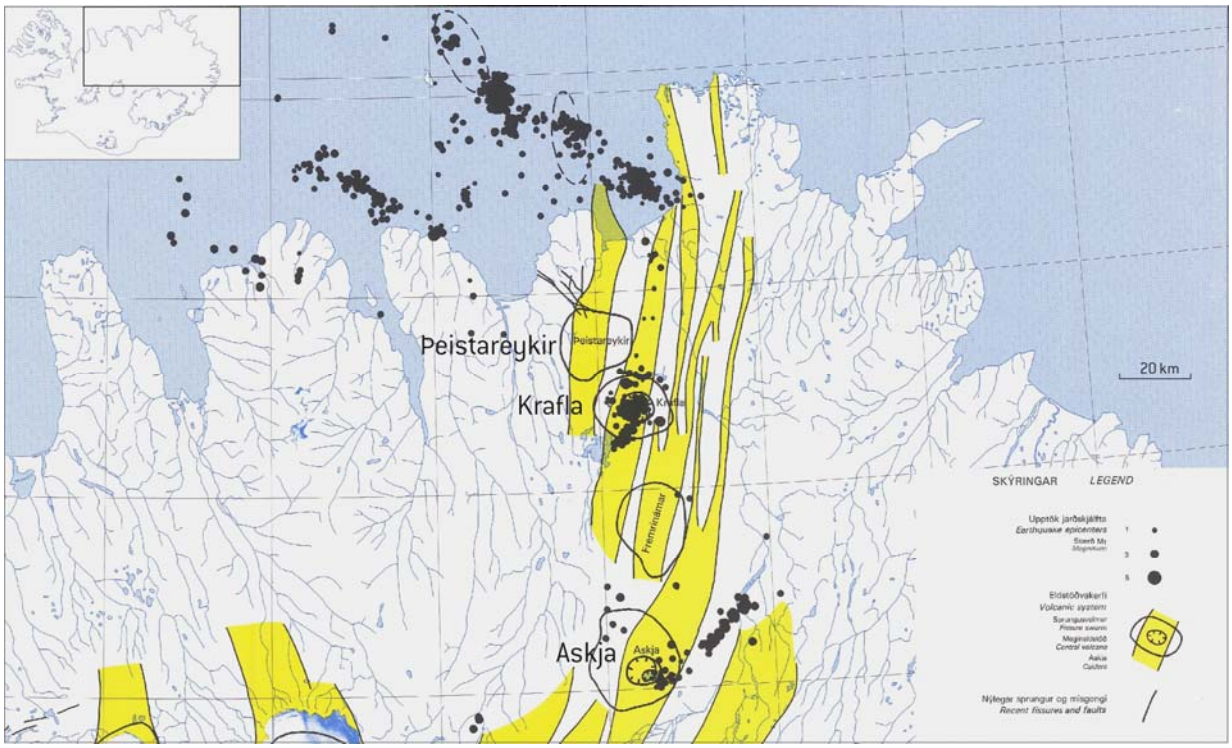

Figure 2.1 The Northern Volcanic Zone (NVZ) is segmented into discrete volcanic systems. They include a central volcano and a fissure swarm with proximal eruptive fissures and distal non-eruptive faults and ground fissures. The two northernmost systems, those of Theistareykir and Krafla, host geothermal reservoirs to be harnessed, three of which are already exploited or proven. Dots show earthquake epicenters of magnitude 1-5 over a 4 years period (1982-1985). Map by Einarsson and Saemundsson (1987).

Volcanic and tectonic unrest in the NVZ is documented since 1618. The activity has been of varying types: 1) Volcanic eruptions associated with rifting of entire or a large part of fissure swarms (Krafla 1724-1729-1746, 1975-1984, Askja 1874-1875), 2) Volcanic eruptions limited to calderas without rifting of the fissure swarms (Askja 1920-1930, 1961), 3) Rifting of parts of fissure swarms associated with transtensional slip of the Tjörnes Fracture Zone (TFZ) (western Theistareykir system 1885 and probably also 1618). Inversely, rifting of a fissure swarm has triggered slip in the TFZ (Öxarfjördur 1976). The first and third types of unrest will be discussed in detail as these are of prime concern for the geothermal areas to be harnessed. Volcanic episodes without rifting such as at Askja are the main type of eruptive behavior at some of Iceland´s most active volcanoes such as Grímsvötn and Katla, but also Krafla during a period of high volcanic production in early postglacial time. They seem to thrive on intermittent inflow and short residendce time of magma in their respective magma chambers. As regards future volcanotectonic episodes the northern part of the NVZ can be regarded as having been reset in 1975-1984 (Krafla fires) with regard to stress build up. Similarly the southern part was reset in 1874-1875 (Askja fires).

Table 2.1 Volcanotectonic and tectonic episodes of the NVZ since 1600

Year	Northern part	Southern part
1618	Western Theistareykir at intersection with TFZ – non-volcanic rifting episode lasted ~3 months	
1724-1729	Krafla, Bjarnarflag – full scale episode	
1746	Krafla, minor eruption and ground fissuring	
1874-1875		Askja – full scale episode, fissure eruption on parallel swarm east of Krafla system
1885	Western Theistareykir at intersection with TFZ – earthquake, ground fissuring	
1920-1930		Askja eruptions restricted to central volcano
1961		Askja eruption restricted to central volcano
1975-1984	Krafla, Bjarnarflag, Gjástykki - full scale episode	

Note: *Full scale episode means a fissure eruption and rifting of the major part of a volcanic system. Several medium size earthquakes (M 6-7) occur per century in the TFZ. One is included in Table 2.1 as the epicenter lay in the area of its intersection with the NVZ.*

2.3 Main characteristics of geothermal areas proposed for power production

Three geothermal areas, harnessed or proven suitable for harnessing are considered for power production. These are Theistareykir, Krafla and Bjarnarflag. All have been drilled and power stations have been in operation in the latter two for decades. The Theistareykir geothermal field is located in the central area of the Theistareykir volcanic system. Krafla and Bjarnarflag are both located in the Krafla volcanic system, the former is nested within an 8x10 km diameter caldera in the center of the Krafla central volcano. The other, at Bjarnarflag, is located 7 km to the south in an area of high volcanic production on the fissure swarm. One other field, Gjástykki, has been suggested as a potential production area. It is 10-12 km north of Krafla in the same volcanic system. Surface exploration is as yet inconclusive regarding its potential and drilling has not been carried out. For location see Figure 1.1.

2.3.1 Theistareykir

General features and type of postglacial volcanism

During postglacial time volcanic eruptions of the Theistareykir volcanic system have been of the lava shield type only, producing olivine tholeiite and minor picrite. The eruptions produced pahoehoe flows, mostly from single vents. Several such eruptions took place in early postglacial time, 14–10.000 years ago, following the retreat of the Weichselian ice sheet from the area. Volcanism of this type was particularly intense in Iceland during this period of glacial rebound (Sigvaldason, 2002). Only one later eruption has occurred in the area. It produced Theistareykja-hraun, also of the lava shield type, about 2500 years ago.

Geothermal manifestations

Geothermal activity at Theistareykir is characterized by mud pools and fumaroles with abundant deposition of sulphur. The main activity is at 320-520 m a.s.l. on the northslope and north of Mt. Baejarfjall. Cold, altered ground extends north from the active, area, clearly fault controlled as are the fumaroles. The size of the geothermal area from such surface manifestations is 7-8 km². Steam emanations from ground fissures south and north of these as well as ground water wells drilled there indicate hot off-flow. See map 2.2 in pocket.

Faults and tension gashes

The early postglacial shield lavas of the Theistareykir area are extensively broken up by normal faults and tension gashes. This applies in particular to the western part of the active geothermal field, west of Tjarnarás (see map 2.1 in pocket). The eastern part of it between Tjarnarás and Ketilfjall is much less faulted. However, from mapping of fumaroles in this area and faults on the plateau of Baejarfjall immediately to the south a connection clearly stands out. The central part of the Theistareykir fissure swarm west of Tjarnarás is covered by 2500 year old lava which has not been affected by later faulting except in the NW at the intersection with the TFZ.

Historically documented tectonic events

There is one possible rifting event on historical record. It occurred in l618. Earthquakes were felt over a period of a few months. Ground fissuring is only reported to have occurred in the inhabited area at eastern Tjörnes. The Askja episode of 1873-1875 was heralded by two earthquakes estimated >M6 in the sea NW of Húsavík in 1872. Another ~M6 earthquake closed the episode in 1885. Its epicenter was at the intersection of the TFZ with the NVZ at eastern Tjörnes with right lateral movement and ground fissuring.

Slides and mud flows

Mt. Baejarfjall, 200 m high, consists of pillow lava which has spread out evenly in all directions from a centrally located crater. Its northern slope is strongly altered by fumarolic activity which is most intense around the traces of three faults or fault zones. There, clayey slip mounds have piled up on the lower slopes. None have travelled far but mud flows have contributed to the thick overburden on the lava at the foot of the hill. Well THG-1 is located on such ground with 14 m of clayey debris overlying the early postglacial lava. Sliding is most likely to occur during rifting episodes as these are accompanied by earthquake activity, although of low magnitude. The slide mounds are unstable, with creep and minor slips occurring at other times as well.

2.3.2 Krafla, Bjarnarflag and Gjástykki

These three geothermal fields are closely related being located on the Krafla volcanic system (Figures 2.2-2.4) and connected by a common NNE-SSW trending fissure swarm. Volcanic activity is primarily fissure eruptions of tholeiite. They produce shelly pahoehoe flows from fire fountaining, followed by lava flows and sometimes a final stage of tube fed pahoehoe flows. The various lava types are erupted at different eruption rates and may last from hours (shelly pahoehoe) to months (tube fed pahoehoe) (Table 2.2).

Table 2.2 Main phases and characteristics of Krafla type fissure eruptions.

	Initial phase	Main phase	Final phase
Duration	hour or hours	days-weeks	weeks to months
Lava type	shelly pahoehoe	aa lava	tube fed pahoehoe
Distance travelled	< 1 km	several km	several km
Crater type	long fissure	single or few vents	single vent
Eruption style	curtain of fire	fire fountaining	lava lake at vent
Production rate	very high 100 - several 100 m^3/s	high >10-100m^3/s	low < 10 m^3/s
Flow rate	very fast	fast to slow	slow
Type of flow	spread aerially	tend to be channelled	spread as flow units

***Note:** Lavas of the initial phase are very gas-rich. Where ponded, bathtub marks indicate that they deflated to about half the original thickness.

The eruption history of the Krafla volcanic system for the past 3000 years is shown in Tables 2.3 and 2.4. (Saemundsson 1991). There have been six eruptions in the system in this period. Three occurred between 2000 and 3000 years ago, the other three in historical time, after ~870 AD.

Four eruptions were common to both Krafla and Bjarnarflag and two were common to all three geothermal areas. From 3000 to about 8000 years ago only one eruption occurred in the western part of the Krafla caldera. In early postglacial time several fissure eruptions occurred at Krafla and Bjarnarflag.

Table 2.3 Eruptions of Krafla volcanic system since 3000 y BP: Area, fissure system and number of events.

	Area of lava			Length of eruptive fissure	Number of eruptive events
	Krafla	**Gjástykki**	**Bjarnarflag**		
Krafla fires 1975-1984	20 km²	15 km²	0	11 km	9
Mývatn fires 1724-1929 (1746)	33 km²	0	0.25 km²	13 km	5
Daleldar ~900 AD	5 km²	0	5.5 km²	12 km	?
Hólseldar 2 ~2000 y BP	>10 km²	0	0	7 km	4?
Hólseldar 1 ~2300 y BP	>10 km²	0	0	7 km	?
Hverfellseldar ~2900 y BP	~40 km²	~20 km²	~10 km²	25 km	?

Hólseldar 2 erupted at about the same time as a crater row SE of Lake Mývatn which produced about 220 km² of lava. The lava of Hólseldar and that of the SE-crater row are petrologically different, suggesting that the fissures tapped two magma sources. Other examples are known in Iceland where single fissures cut two volcanic systems causing volcanic eruptions in both, different in type and petrology.

The lava flows of Krafla are compound, being formed during several eruptive events which were separated in time by a few months or years. The Daleldar and Hólseldar flows are among the smallest by area (~10 km²) of the Krafla system. One flow is smaller, about 1 km². This is the only one erupted during a ~5000 years "quiet period" when the western branch of the Krafla fissure swarm was tectonically active between ~8000-~3000 y BP (Saemundsson 1991).

Geological evidence from parallel volcanic systems shows that the Krafla volcanic system has been the main spreading zone in the northern part of the NVZ for the past 3000 years. It is the only volcanic system where the course of events during a volcano-tectonic episode has been observed by scientists. A detailed description is given in the introduction, covering its various aspects.

Krafla

Main geological features

Krafla is a mature shield type central volcano with a caldera, an interglacial acidic welded tuff sheet, concentric eruption fissures and rhyolite extrusions. The oldest exposed rocks are about 300,000 year old. The associated fissure swarm is divided into two subswarms from Krafla southwards with the activity shifting alternatively for long periods of time (thousands of years) between the two. Geothermal exploitation and planning has so far concentrated about the eastern part of the eastern subswarm (Figure 2.2).

The geothermal area is at about 500-600 m altitude with Mt Krafla rising to over 800 m east and north of it. The lower slopes of Krafla on the south are draped over by clayey debris from a hydrothermal eruption in 1724.

The Krafla geothermal area has the most varied types of volcanic activity. Basaltic fissure eruptions are the main type of volcanism. Other noteworthy features are four rows of large diameter (over 300 m) explosion craters, two of them Holocene. Both erupted mixed basalt scoria -rhyolite pumice, but developed into hydrothermal eruptions. The youngest, Víti, erupted in 1724. Purely hydrothermal explosion craters of smaller diameter (<100 m) also occur. Rhyolitic fissure eruptions occured, in late Weichselian time, dated to about 20,000 years.

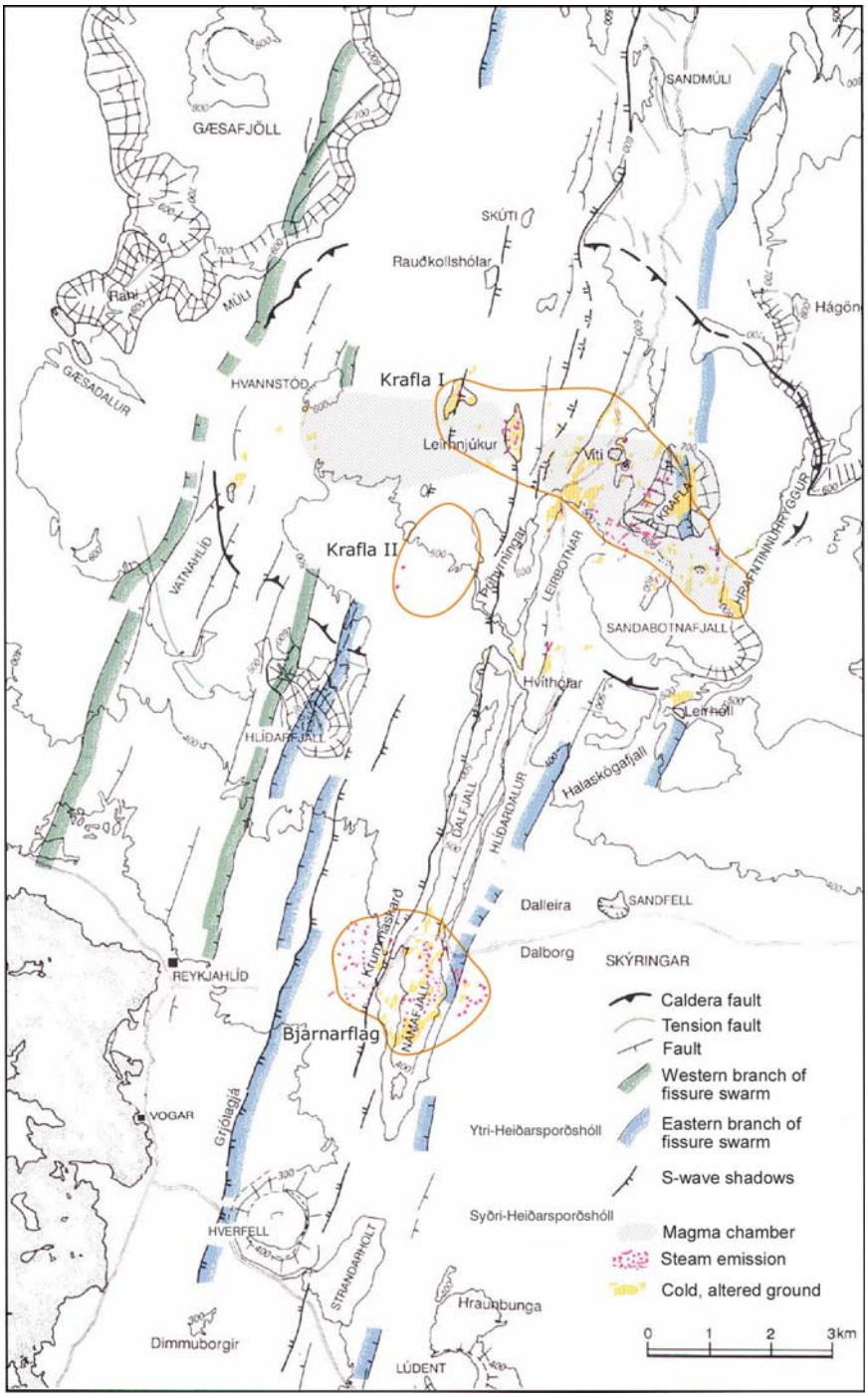

Figure 2.2 Central part of the Krafla volcanic system showing the caldera and the fissure swarm which traverses it. An inner segment of the fissure swarm was active during the last two volcanic episodes of 1724–1729 and 1975–1984. The geothermal areas of Krafla and Bjarnarflag are shown. Krafla has a magma chamber (S-wave shadow, Einarsson, 1978) at 3-7 km depth. Map from Saemundsson 1991.

Geothermal manifestations

Geothermal activity is mainly concentrated on the western and southern slopes of Mt. Krafla and at Leirhnjúkur in the center of the caldera. The activity is mainly in the form of mud pools and fumaroles with minor sulphur deposition. Much of it is fault controlled but some of the larger fumaroles are associated with explosion craters. At Leirhnjúkur in the center of the caldera the fumaroles and mud pools follow the trace of closely spaced eruptive fissures, among them the two youngest ones which erupted during the Mývatn and Krafla fires 280 and 30 years ago. Fumarolic activity increased significantly there during both volcanic episodes. Minor surface manifestations occur at the southeast margin of the caldera. See map 2.3 in pocket. Exploitation is limited to the west and south slopes of Mt. Krafla and the south caldera margin. Leirhnjúkur has been excluded from exploitation due to environmental aspects.

Fissure eruptions of the last three millennia

Volcanic activity of the last active phase of the eastern subswarm began about 2900 years ago after a quiet period of about 5000 years. Three fissure eruptions occurred in the fault bounded center of the rift zone at Leirhnjúkur extending from there to the north and south. Another three fissure eruptions occurred east of the main rift zone east and west of Mt. Krafla, nearer to the area of present day exploitation. The eruptions are unevenly distributed in time (Table 2.4). The two last ones included several eruptive events, lasting intermittently for 5 years (excluding a single event following 17 years after the main episode) and 9 years. Individual events lasted a few hours to several weeks. They are referred to as events and are grouped into eruptive episodes (fires = eldar in Icelandic).

Table 2.4 Eruptions of Krafla volcanic system since 3000 y BP. Type of explosive volcanic activity besides lava emission**.**

Year	Krafla	Bjarnarflag	Gjástykki
1975-1984	X	borehole erupted	X
1724-1729 (1746)	X+P hydrothermal	X	
About 900 AD	X	X	
About 2000 y BP	X+ hydrothermal		
About 2300 y BP	X+ hydrothermal		
About 2900 y BP	X	X+ phreatovolcanic	X

Note: X stands for lava flows and P for mixed rhyolite pumice-basalt scoria eruptions. The eruption of 1746 was a minor one with mud and scoria thrown out in the Leirhnjúkur area. Faults were also reported to have opened and thus this event may be regarded as a final phase of the Mývatn fires.

Explosive eruptions

Three of six eruptive episodes affected the geothermal system causing hydrothermal rock-mud eruptions from the geothermal reservoir and mixed volcanic-hydrothermal eruptions. Most were of minor explosivity with fall-out of mud traceable only a few hundred meters from the craters. The largest occurred at the outset of the Mývatn fires (1724). It produced a small amount of mixed basaltic scoria and rhyolitic pumice but developed into a hydrothermally driven mud eruption which lasted half a day. The mud was blown south. Its thickness at the Krafla power house is about 10 cm and 2–3 cm at the main road east of Bjarnarflag, 7 km to the south (Figure 2.3). The thickness of the layer in the Krafla borefield was from 0,1-3 m (Figure 2.3). The phreatovolcanic eruption of 2900 years ago caused fall-out of ash at Krafla which is about 7 cm thick in the soil around there.

Faulting at Krafla

Most active faults of the eastern fissure swarm of Krafla pass west of the production area. Being normal type growth faults the throws vary relative to the age of the affected lavas. Large scale faulting during the Krafla fires occurred towards Leirhnjúkur. A NW-SE trending normal fault was reactivated though on the south slope of Mt Krafla and fumaroles became active on it. Large normal faults trend from SSW to NNE towards the production area west of Mt Krafla with displacements of over 100 m in the pre caldera Krafla shield. They separate between the shoulder of the fissure swarm to the east and its graben structure to the west, however, with minor if any throws during the Holocene.

Gas flux during Krafla fires

A hitherto unknown kind of hazard turned up during the Krafla fires as the western part of the geothermal reservoir was fluxed by volcanic gases, rendering it unexploitable for years. The gas increase and its effects are treated in Chapter 1.5, Section 1.5.

Bjarnarflag

Main geologic features

Bjarnarflag is a shallow, fault bounded depression at 320 m altitude which forms the westernmost part of the larger Námafjall geothermal area. This is about 4 km² in size, rich in sulphuric fumaroles, mud pools and steaming ground. Crater rows characterize the southern part of the geothermal area whereas terraces of glacial outwash bound it to the north. Mt. Námafjall (470 m) is part of a NNE-SSW trending, subglacially formed ridge system, composed mainly of pillow lava. The geothermal area is dissected by the eastern fissure swarm of Krafla which is about 5 km broad with prominent faults, however, they are smoothed out somewhat in the strongly altered and clayey ground at Námafjall. Bjarnarflag west of the ridge is covered by lavas of different ages and bounded by crater rows in the west and south. See map 2.4 in pocket.

Geothermal manifestations

Geothermal activity at Bjarnarflag is mainly fumaroles which are conspicuously lined up along faults and the 1728 crater row. The thermal activity increased markedly in 1977 during two successive rifting events. These were caused by lateral magma flow from the Krafla magma chamber as is manifest by a volcanic eruption up through a 1100 m deep borehole. Steam emanations from groundwater in the lavas to the south and west of Bjarnarflag mark hot outflow from the geothermal area. It emerges in open faults and as tepid springs at the shore of Lake Mývatn. Their temperature increased markedly following the 1977 Krafla fires events, but has dwindled since.

Crater rows younger than 3000 years

Three fissure eruptions have occurred at Bjarnarflag during the last 3000 years. A large phreatic eruption occurred at the outset of the first of those 2900 years ago. This was due to the access of lake- and groundwater to the lava conduit allowing for efficient steam explosions. The ash layer from that eruption is about 7 cm thick at Krafla and over 1 m at Bjarnarflag. The last eruption occurred in 1728 during the Mývatn fires. The volcanic fissure cuts across Bjarnarflag and a pahoehoe flow spread over the floor of the depression.

Faulting at Bjarnarflag

The central part of the eastern Krafla fissure swarm transects Bjarnarflag. It is bounded by a single 5 m fault in the west and two of a similar combined throw in the east. Fault displacement was limited to this strip during the Krafla and Mývatn fires. Fault displacement during the 1977 events affected every tectonic fissure in the area between the boarder faults. It totalled about 2 m across the zone and subsidence was on the order of 1 m. See Figures 1.15 and 1.17 (Björnsson et al., 1979; Tryggvason 1984). Six boreholes were located along one of the eastern boarder faults. A subsurface dyke intrusion intercepted four of them. Three were clogged. One erupted but remained productive for the next 25 years. No gas fluxes apart from a minor increase in methane were associated with the magma intrusions into the geothermal reservoir at Bjarnarflag.

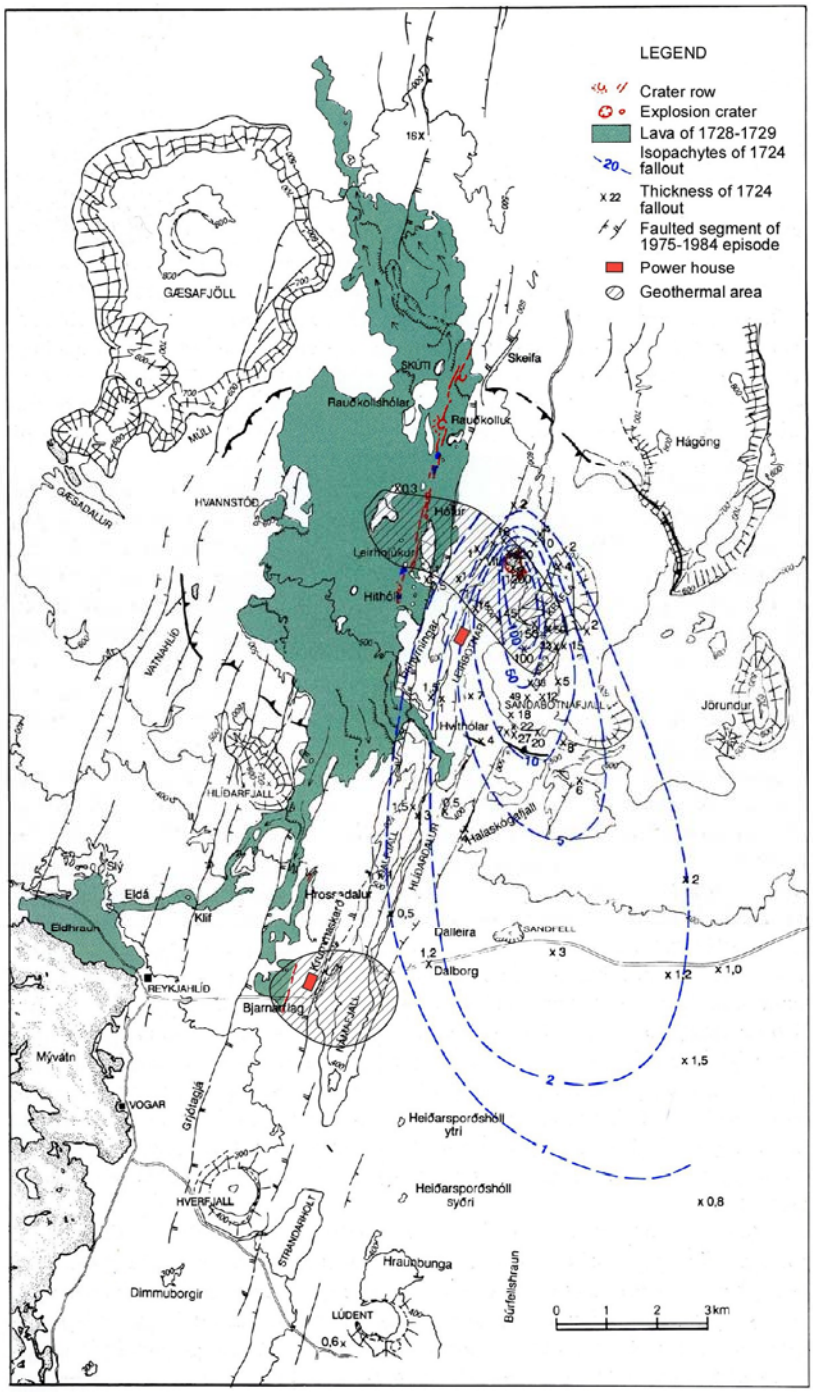

Figure 2.3 Spread of hydrovolcanic mud erupted at Krafla in 1724 and basaltic lava of 1728–1729. The mud eruption started as a mixed rhyolite/basalt volcanic eruption which developed into a hydrovolcanic eruption due to ingression and explosive boiling of geothermal water. It lasted half a day. Two years of intermittent rifting events and another two years of also intermittent fissure eruptions followed. Map from Saemundsson 1991.

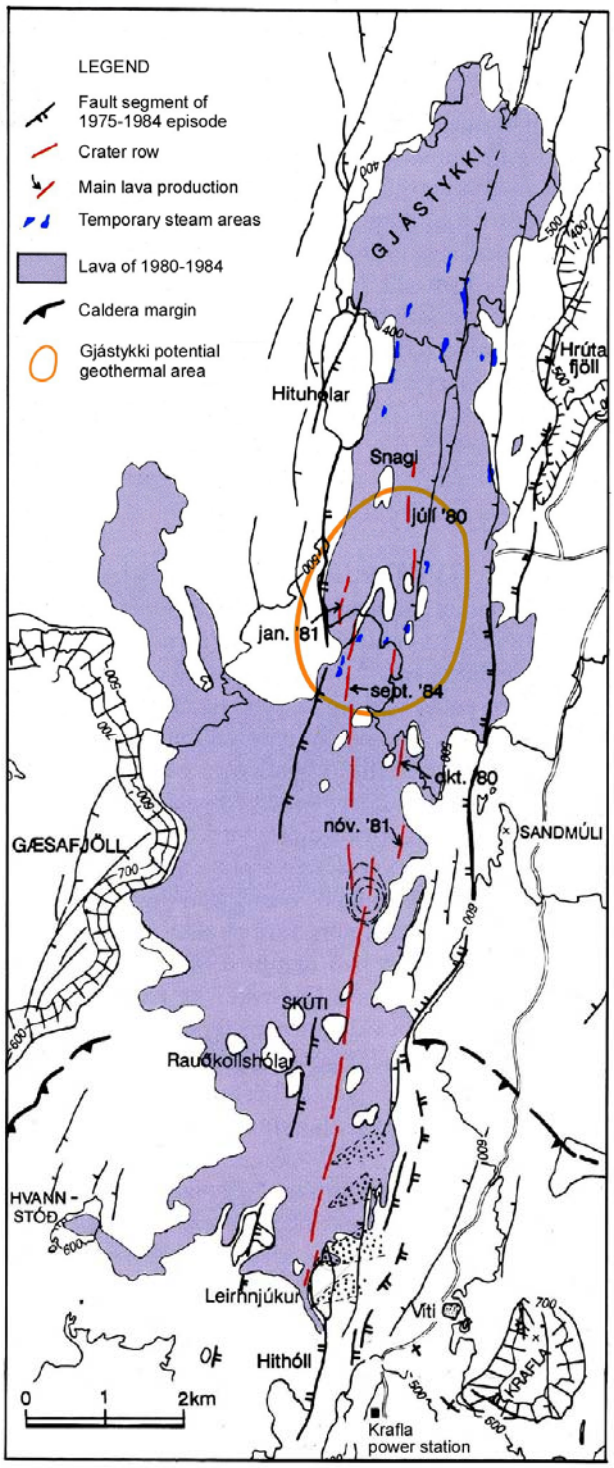

Figure 2.4 The Krafla volcano-tectonic episode of 1975–1984 produced basaltic lava about 35 km^2 in area. The eruptive phase of 1980–1984, which included five eruptive events that lasted 5–14 days each, was preceded by 5 years of intermittent rifting events. The main lava producing craters were in Gjástykki, well north of the Krafla caldera. Southern Gjástykki is being explored for geothermal utilization. Map from Saemundsson (1991).

Gjástykki

General features

The Gjástykki field is located on the Krafla fissure swarm 9 km north of Krafla at an elevation of about 500 m a.s.l. It is located near the apex of an extensive, early postglacial lava shield. The Krafla fissure swarm transects the center of the shield and later lavas have almost buried the shield crater. See geologic and geothermal map 2.5 in pocket.

Young fissure eruptions

Two basaltic fissure eruptions have occurred in the Gjástykki geothermal area. The older occurred about 2900 years ago and the younger during the Krafla fires 20-30 years ago. The area is heavily broken up by faults and tension gashes which have formed incrementally over a period of about 12000 years since eruption of the shield lava. The fault bounded, central, depression of Gjástykki was overflowed by lava during both fissure eruptions.

Faulting of Gjástykki

Gjástykki is a 4 km broad, densely faulted strip of land. It is a graben structure with marginal step faults of up to 40 m throw and numerous tension gashes across the graben floor. The spacing of faults or fault bundles is commonly on the order of 100-200 m. Postglacial craters and thermal manifestations occur in the structurally lowest part of the graben near to its west margin. Faults and fissures on the floor of the graben were smoothed out by lavas of the Krafla fires. Their location is known from mapping and air photos from before that eruption.

Transient nature of surface geothermal manifestations

Gjástykki is much inferior to Bjarnarflag as regards surface geothermal manifestations. The activity there is of a transient nature, blooming during volcano-tectonic crises and fading off during quiet intervals. During the Krafla fires maximum widening of the fissure swarm of about 9 m occurred at Gjástykki during 8 out of 20 rifting events with a corresponding accumulation of intrusions underneath.

Subsurface geothermal characteristics

Gas chemistry of a fumarole which has persisted for more than 25 years gives a reservoir temperature of ~260°C. A resistivity survey indicates that a subsurface temperature of more than 240°C has been reached over a 4 km² area at 500 m depth below surface, centered in the area of the fumaroles. If the area proves to be suitable for exploitation, boreholes will be drilled within or sidetracked towards this zone of latest rifting.

2.4 Concluding remarks and future prospects for the NVZ geothermal areas

2.4.1 Future prospects of volcano-tectonic activity at Theistareykir

Theistareykir is divided in two parts as regards faulting. The Tjarnarás fault separates between areas of meter scale faults and open fissures to the west and barely visible faults and higher ground in the same early postglacial lava to the east. Fault movement after the youngest shield lava of Theistareykjahraun (2500 years old) has been restricted to its westernmost outliers. The eastern part is suitable and fairly safe as a building site. This part is also best suited as a borefield from the point of view of drilling and reservoir characteristics. Theistareykjahraun is one of only two lava shields in Iceland younger than 3000 years. Its volume was 1-2 km³ a good deal of which would have flowed down into pre-existing several meters wide ground fissures at its base. Renewed volcanic activity of the Theistareykir system in the near future must be considered very unlikely in view of the distribution of eruptions in time and rare occurrences of late Holocene shields in Iceland. The possibility of a recurrent dyke injection underneath the western or central part of the fissure swarm is more likely in the distant future (Table 2.1). The high density of the olivine tholeiite magma of the Theistareykir system (and lava shields in general) is probably the main reason for preventing it from reaching the surface during rifting episodes (Walker, 1989).

2.4.2 Future prospects for Krafla

From the minimum recurrence intervals of earlier episodes of about 250 years (Table 2.1), and the fact that it takes time to build up sufficient tensional stress for a new episode, the Krafla system is considered comparatively safe for utilization during this century at least. Inter rifting volcanic eruptions due to overpressure in Kraflas magma chamber are not known to have occurred since early Postglacial time. The production area and power station of Krafla are located east of the main activity of the fissure swarm.

2.4.3 Future prospects for Bjarnarflag

Most surface constructions planned for future development of Bjarnarflag will be on relatively safe ground, east of the zone that rifted in the 18th and 20th centuries. Boreholes, however, are planned both in this area and partly sidetracked into the rifted segment to the west.

2.4.4 Future prospects for Gjástykki

The prospect area of Gjástykki reaches on to the margins of the central depression with its fresh lava cover and zone of most recent rifting (Figure 2.4). A power house could be built on the western flank outside it, in an area where faults and ground fissures are clearly visible. They can thus be avoided as building sites, and in case of pipelines appropriate measures can be taken where faults need to be crossed. Faults, now hidden by lava of the Krafla fires, are traceable on air photographs and maps from before 1980.

2.4.5 General conclusion regarding future activity

It is concluded from the above that a rifting episode can be expected perhaps once a century in the northern part of the NVZ, accompanied by a volcanic eruption in the case of the Krafla and Askja systems but less likely so as regards the Theistareykir volcanic system. However, from Figure 1.13, strain release during the Krafla fires might need over 200 years of stress accumulation of an 80 km segment to prepare for renewed activity of a similar scale to occur in the NVZ at latitude corresponding to Bjarnarflag in the south and Theistareykir in the north. It should be noted that dyke and sheet intrusions are beneficial to the geothermal system in the long run. They form a dense complex at 1–3 km depth and act as a heat source which maintains and drives the circulation of the geothermal system.

2.5 Siting of surface constructions and boreholes with regard to protective measures against volcanic or volcano-tectonic hazards

In harnessing the high temperature geothermal areas under discussion it is difficult to select perfectly safe ground. A prime issue from an engineering point of view is definition of a production area suitable for steam production in terms of temperature and permeability. Conditions for waste water disposal/reinjection must be considered as well as availability of fresh water. Thus care must be taken to select solid ground for surface constructions where geological conditions and engineering aspects fit best. This applies in particular to power generation buildings but also to well sites and pipes. Faults and ground fissures are avoided as regards buildings and drill sites. Pipelines must inevitably cross some. For reinjection the margins of the geothermal reservoir need to be defined. Other factors which have to be considered include definition of areas which are least likely to be inundated by lava. This may seem problematic, but a rift related fissure eruption would be expected to follow the trace of the next episode before, given a short repose period, with lava flows controlled by topography. Other types of volcanic activity would be expected to occur in the same general area as the earlier ones.

At Theistareykir the three optimal situations happen to co-incide i.e. suitable production area, low fault dencity, and least likely exposure to flow of lava. This also applies to Krafla as all surface constructions are planned east of the part of the fissure swarm that was activated during the 18th and 20th century volcano-tectonic episodes. It should be noted that the Krafla power station was built close to a 1000 years old crater row (Daleldar) on solid ground west of an area thickly covered by fall-out and partly redeposited clayey debris. At Bjarnarflag all surface constructions erected up to 1975 were sited within the zone which was rifted during those episodes. Most of them were damaged. For future development of Bjarnarflag surface constructions will be on relatively safe ground, east of the zone that rifted in the 18th and 20th centuries. Boreholes, however, are planned both in this area and side tracked into the rifted segment to the west. At Gjástykki surface constructions will be at the west margin of the the fissure swarm and well west of the segment which was affected by rifting during the Krafla Fires. Drill sites are planned in the west of the rift, both on the graben floor and on its western shoulder. Due regard can and will be given to the location of faults and fissures as these are clearly visible on the surface.

Power transmission lines as designed will cross fissure swarms and the Húsavík faults as do the existing ones (Figure 1.1). During the Krafla episode a transmission line which crosses the Bjarnarflag area (KR1) was stretched due to about 2 m dilatation of ground fissures. Substations are in all cases planned in areas where faults occur. At Krafla, Gjástykki and Bjarnarflag they are well away from the recently activated fissures. A substation planned at Þeistareykir will be located in an area where faults have not been activated for the past 2500 years. The Hólasandur substation will be located on the southern limb of the Þeistareykir fissure swarm in an area of interglacial basalts covered by moraine and outwash. Faults which occur there, despite being draped over by the morainic material, have a clear topographic expression. Minor faults or tension gashes are not visible. Trenching would be needed to detect and avoid them. The substations are as save as can be against lava flows in otherwise volcanic areas.

The location of the future power lines is outlined below with regard to faults and lava flows (Figure 1.1). Power line E1 between Bjarnarflag and Krafla will lie partly along the recently reactivated part of the Krafla fissure swarm. In the south and north it will lie parallel and east of it. Also E2 will be entirely east of that part of the Krafla fissure swarm which was affected during the Krafla fires. The eastern half of power lines C from Krafla west towards substation Hólasandur will cross the Krafla fissure swarm and come to be partly on lavas erupted during the 18th century Mývatn fires. A 2 km broad strip within it was activated during the Krafla fires, the dilatation amounting to about 6 m. Power line B will cross normal faults of the Þeistareykir swarm in an area of interglacial basalts and glacial outwash in the south and the Húsavík-Faults in the north. Line D from Gjástykki west will cross a few minor tension cracks in early postglacial lavas between the two fissure swarms of Krafla and Þeistareykir. Line Aa will cross faults of the Þeistareykir swarm at an acute angle, half of it in an area of Pleistocene basalts and half in early postglacial lavas. Line D will continue almost parallel with the faults north to Þeistareykir substation. Power line Ab from Þeistareykir towards NE will cross the Þeistareykir fissure swarm at about 45° angle to Höskuldsvatn, almost all of it on postglacial lavas. From there the line will run parallel with B to north of the Húsavík faults. The Húsavík faults are transtensional with a right lateral and a normal down to the SW components. West of Höskuldsvatn the B1 power lines cross in a northerly direction several NW-SE trending faults at an angle of about 45°. They belong to this transtensional fault system.

There is little concern that the two fissure swarms will experience a new rifting episode in near future, i.e. next 100 or even 200 years because the northern part of the NVZ may be regarded as having been “reset” with regard to stress accumulation during the Krafla fires. For the Krafla swarm this is concluded from the large strain release that occurred. The Theistareykir fissure swarm is not considered to be of much concern either as there is no indication of it having been activated during the past 2500 years except in the northwest, at the intersection with the TFZ. There the stress field is different and transform faulting interacts with rifting of the fissure swarm. A marked decrease in microearthquake activity on the Húsavík faults following the Krafla fires may indicate the same kind of “reset” for them or that they became locked.

In Table 2.5 the hazards envisaged for the three geothermal areas are listed. It should be noted that none of those are imminent but might be expected after some 200 years. If any of the three geothermal or rather volcanic systems will be the scene of the next volcano-tectonic episode it is most likely that it will follow the same path as the previous ones as regards fissure segments activated. This is concluded from the short time elapsed since the last episodes. If delayed by centuries it is more likely that a new segment breaks up.

Table 2.5 Possible hazards for geothermal power plants in NE-Iceland.

	Hydrovolcanic eruptions	Lava flow	Fault movements	Dyking	Gas fluxing
Theistareykir, effects on					
geothermal system	no	negligible	X	X	?
boreholes	no	negligible	X	X	?
well heads and pipes	no	negligible	?	X	?
power house	no	no	no	no	no
transmission lines	no	X	X	no	no
Krafla, effects on					
geothermal system	X	negligible	X	X	X
boreholes	X	negligible	X	X	X
wellheads and pipes	X	negligible	no	no	no
power house	X	negligible	no	no	no
transmission lines	X	X	X	no	no
Bjarnarflag, effects on					
geothermal system	no	negligible	X	X	no
boreholes	no	X	X	X	no
wellheads and pipes	no	X	no	no	no
power house	no	negligible	no	no	no
transmission lines	no	X	X	no	no

Note: X marks possible hazard. no means not endangered. Hydrovolcanic includes hydrothermally driven eruptions.

2.6 Ground movements and hazards caused by man

2.6.1 Ground sagging

Production of fluid from a geothermal reservoir causes drawdown of its groundwater level. This may cause compaction of the drained rock series and sagging of the ground. The largest sag observed so far in Iceland is at Svartsengi in SW-Iceland amounting to to maximally 28 cm (Ingvar Thór, pers. comm.). The corresponding ground tilt there is less than that observed at the Krafla power house from alternating inflation and deflation of the Krafla magma chamber. This is not considered as hazardous.

2.6.2 Pressure increase of shallow steam zone

A corollary of drawdown in a boiling reservoir is the development or thickening of a shallow steam zone. The volume increase from water to steam under conditions such as prevail at shallow depth may be on the order of 50 fold with a corresponding pressure increase. This is manifest by increased steam flow from hot ground and fumaroles and locally also by new steam emanations from fissures. Such conditions may result in steam explosions if fissures open up. No such have occurred so far in Iceland. The obvious practice in Iceland to avoid disastrous consequences is to drill and exploit the steam zone. Krafla, and to a lesser degree Bjarnarflag, show signs of drawdown.

2.6.3 Blowout

Blowouts may occur during drilling if casing is not sufficient to hold against reservoir temperature and pressure in a situation of inside well flow. The last blowouts in Iceland occurred 30 and 40 years ago at Krafla and Bjarnarflag. Both were soon brought under control.

2.7 Hazard from distal events

Hazard from distal volcanic events is considered below for the power plants, transmission lines and substations. Knowledge of the type of eruptions, their frequency, magnitude and location is essential. Some experience has accumulated over the past decades regarding the effects of plinian and phreatomagmatic ash fall-out on electric installations throughout the country. The geothermal areas of the northern NVZ are out of reach of catastrophic floods due to volcanic melting of glacier ice.

2.7.1 Ash fall-out

Volcanic hazard from distal events involves ash fall-out from volcanoes in Central and South Iceland. Four of them erupt frequently: Katla, Grímsvötn, Bárdarbunga and Hekla. The three first are glacier covered and produce basaltic ash due to phreatomagmatic eruptions. The eruptions of these may last for days or weeks with continuous ash production, however, most vigorous at the beginning. The fourth, Hekla, starts with a dacitic to rhyolitic plinian phase of short duration.

Katla in South Iceland has erupted on average twice a century during the last millenium (Larsen, 2000). The volcano is ice-covered and the eruptions are phreatomagmatic. Ash layers from Katla in the soil of Northeast Iceland are generally only a few mm thick. Katla eruptions may last several weeks with some ash production all the time.

Grímsvötn and Bárdarbunga volcanoes taken together erupt 10–20 times a century. They are located in the ice sheet of northwestern Vatnajökull, hence their eruptions are phreatomagmatic. The ashes are common in the soil of Northeast Iceland (Figure 2.5) among them are two prominent historic ash layers that were erupted in 1477 and 1717 AD. The former is 3–5 cm thick in soils between Krafla and Theistareykir. Another two fell about 1300-1400 years ago. Their thickness is about 1 cm in the area. So far no disturbances of the electric network are on record due to eruptions of those volcanoes. There have been 3 of them since 1996.

Hekla eruptions start with a plinian phase of rarely rhyolitic but usually dacitic to andesitic pumice and ash. This volcano has erupted regularly every 10 years since 1970. In one case (1980) ash from the plinian phase affected transmission lines in North Iceland as fine, wet ash was plastered on to isolators and needed to be washed off (Figure 2.6). Large plinian type rhyolite eruptions of Hekla have occurred after long repose periods (Thórarinsson, 1971). Ash layers from the two largest ones are prominent in soils in Northeast Iceland. Their thickness is in the range of 3–5 cm in the area of Krafla and Theistareykir. They are marked as H3 and H4 in Fig. 2.5). They occurred 4500 and 3100 years ago. The last ones of this type occurred in the 12th century (1104 and 1158). Similar magnitude eruptions are most unlikely to occur as a repose period of several centuries would be required to generate a volume of acid magma comparable to that which caused the previous ones.

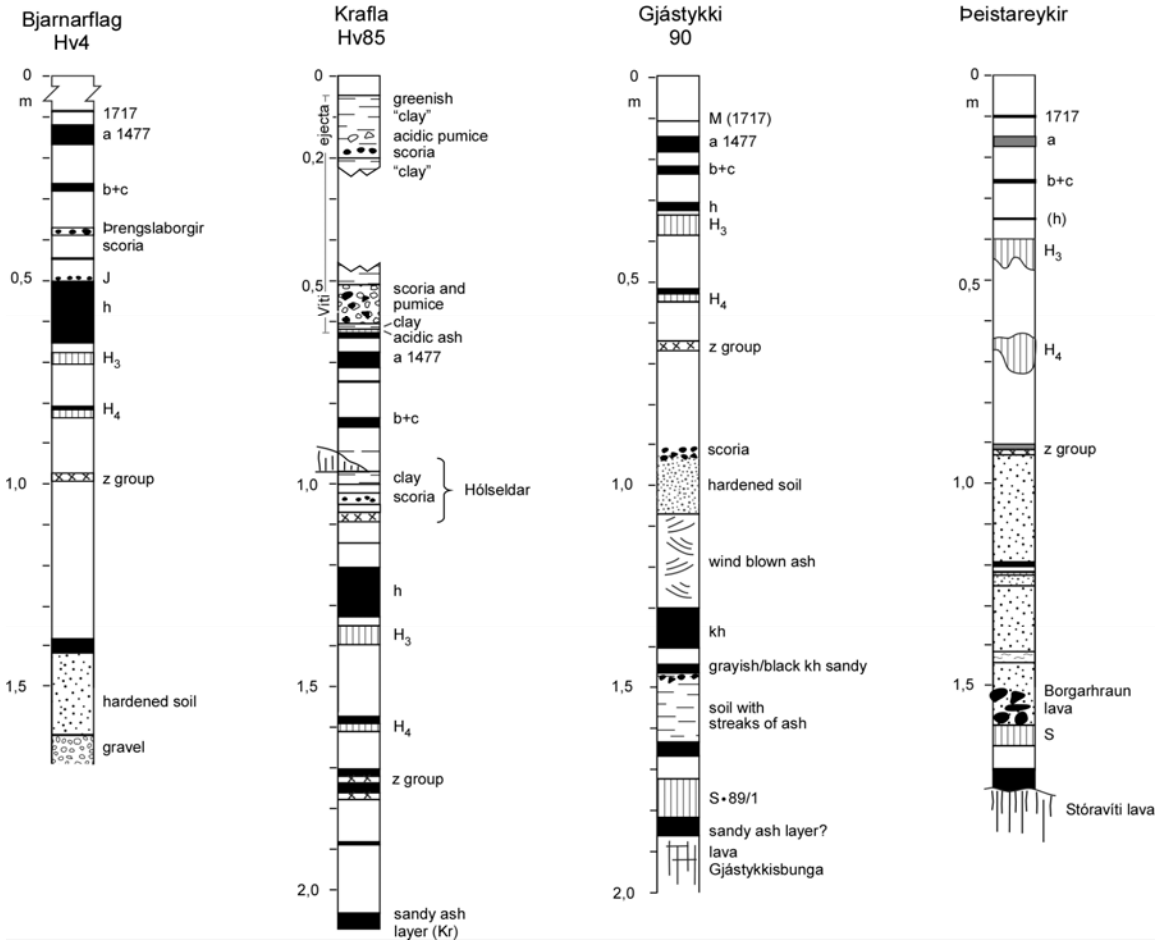

Figure 2.5 Soil sections from the area between Bjarnarflag and Húsavík. Whitish ashes, H3 (3100 years old) and H4 (4500 years old), provide straigarphic markers. The age and provenance of the more prominent ashes has been determined by C-14 and by their chemical composition which is characteristic for each volcano. Fall-out of basaltic ash was relatively frequent during the first millenia of the postglacial, i.e. during the time of and following glacier melting. Ages are given for the most prominent ash layers. The year of fall-out is given for two historical ashes.

Other volcanoes have had paroxysmal plinian eruptions in the not very distant past. Askja is one of them. It had a plinian type eruption in 1875. This eruption lasted a few hours. It produced acid pumice and ash which was blown to the east. The thickness of the pumice at a distance comparable to Krafla and Theistareykir was about 5 cm taking the axis of maximum thickness as a reference.

Öraefajökull had a plinian eruption in the 14th century. It produced rhyolitic pumice which was carried towards southeast. The magnitude of this eruption was similar as that of Askja 1875.

Torfajökull in South-Central Iceland had plinian rhyolitic eruptions about 2000 years ago and late in the 9th century. Both were less explosive than those of Askja and Öraefajökull. The light ash of the former which was blown to the northeast is barely recognizable in soils of the Mývatn area.

The second was preceded by a phreatomagmatic eruption, the basaltic ash of which was blown northeast and is found locally in the Mývatn area a few mm thick.

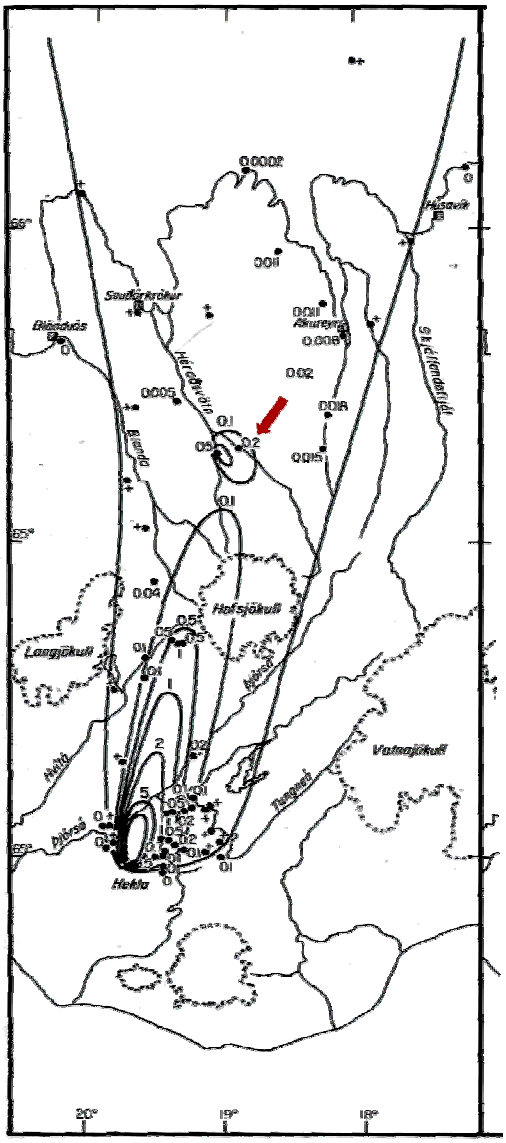

Figure 2.6 Isopach map of the 1991 Hekla ash fresh fallen. Thickness is in cm. The arrow points at the area affected by shortcuts. Figure from Larsen et al. (1992).

Ash fall-out from these volcanoes is not likely to interrupt power generation in the geothermal fields. Transmission lines (isolators) are more likely to suffer disturbance as temporary shortcuts may occur under unfavourable and a not very frequent weather conditions (wind from south carrying rain). Substations would not be affected as these will be under cover. One case of shortcuts in a rural district is known to have occurred in North Iceland at a distance of 150-200 km from Hekla.

3. Assessment of crustal movements and related hazards

Freysteinn Sigmundsson[(1)], Erik Sturkell[(1)], Rikke Pedersen[(1)], Thóra Árnadóttir[(1)], Halldór Geirsson[(2)], Páll Einarsson[(3)].

(1) Nordic Volcanological Center, Institute of Earth Sciences, University of Iceland
(2) Icelandic Meteorological Office
(3) Institute of Earth Sciences, University of Iceland

3.1 Crustal structure and rheology of the Northern Volcanic Zone

Volcanic and seismic processes are dependent on subsurface structure and material properties where they occur. Understanding these processes requires knowledge about the environment where these processes take place, the crust/mantle structure and rheology.

The oceanic crust-mantle boundary marks the transition from peridotitic mantle to gabbroic lower crust, with the bulk of crustal material being formed by material melted and transported from the mantle. For Iceland, the models of crustal structure have changed in recent decades. Results of seismic and magnetotelluric measurements in the 1970s were interpreted in terms of a thin crust, underlain by anomalous mantle with high melt concentrations. This model has about 10-15 km thick relatively hot crust under parts of the volcanic zones, thickening away from these zones, underlain by anomalous mantle with about 10% partial melt. This model seemed at that time to be consistent with various types of data, including seismic shear-wave profiles collected across Iceland (e.g. Gebrande et al., 1980), extrapolation of near-surface temperature gradients, and results of magnetotelluric measurements clearly showing a high electrical conductivity zone (e.g., Beblo and Björnsson, 1980). No seismic reflection from a Mohorovicic discontinuity (Moho) at the crust-mantle boundary was inferred. Extensive seismic surveys in the last decade of the twentieth century revealed a different picture. Seismic data indicate a thick cold crust under Iceland, with crustal thickness increasing from ~15 km in the coastal areas towards ~40 km under central Iceland, with clear seismic reflections interpreted to originate from the Moho. A summary is given by Sigmundsson (2006a). The variable crustal thickness calls for variable activity in the Icelandic mantle plume, and/or flow of the lower crust that can modify the topography of the crust/mantle boundary. The earlier seismic data can be reconciled with the thick crust model (Menke et al., 1996). There is little contrast in density between crust and mantle, and the large crustal thickness in Iceland is consistent with high melt production in a mantle plume under Iceland. A detailed study has in particular revealed the seismic structure at Krafla (Figure 3.1).

A.

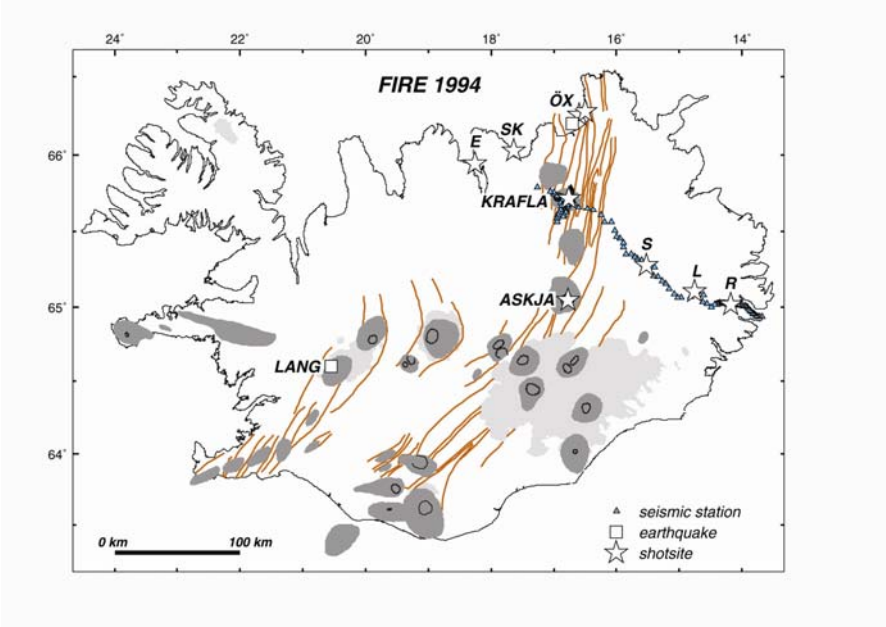

B.

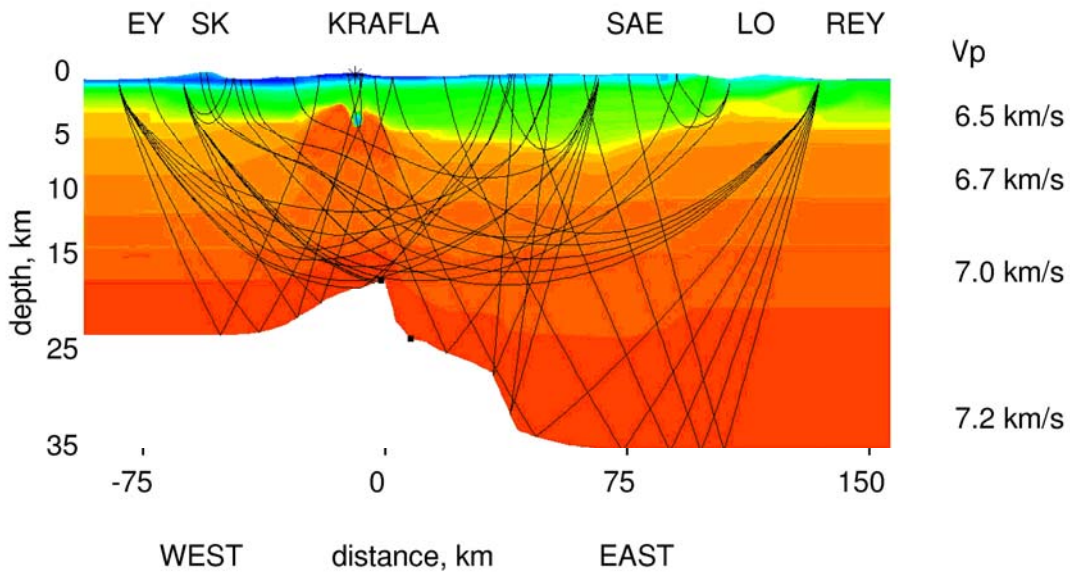

Figure 3.1 Seismic study of the Northern Volcanic Zone and the Krafla central volcano. (A) The seismic array of the FIRE 1994 project. (B) P-wave velocity cross section along the profile with a low-velocity anomaly under Krafla interpreted as a magma chamber. Modified from Brandsdóttir et al. (1997). Courtesy of Brandsdóttir.

Various types of evidence suggest that only the uppermost fraction of the crust behaves in an elastic manner over long time scales, with associated brittle failure if deviatoric stress exceed critical limit (e.g., Sigmundsson, 2006a, b). This elastic behaviour over long time scales appears to characterize the uppermost 5-10 km of the crust. At greater depth ductile deformation domin-

ates (Figure 3.2), although brittle failure can as well occur in this layer, in particular if strain rates are high (e.g., magma intrusion).

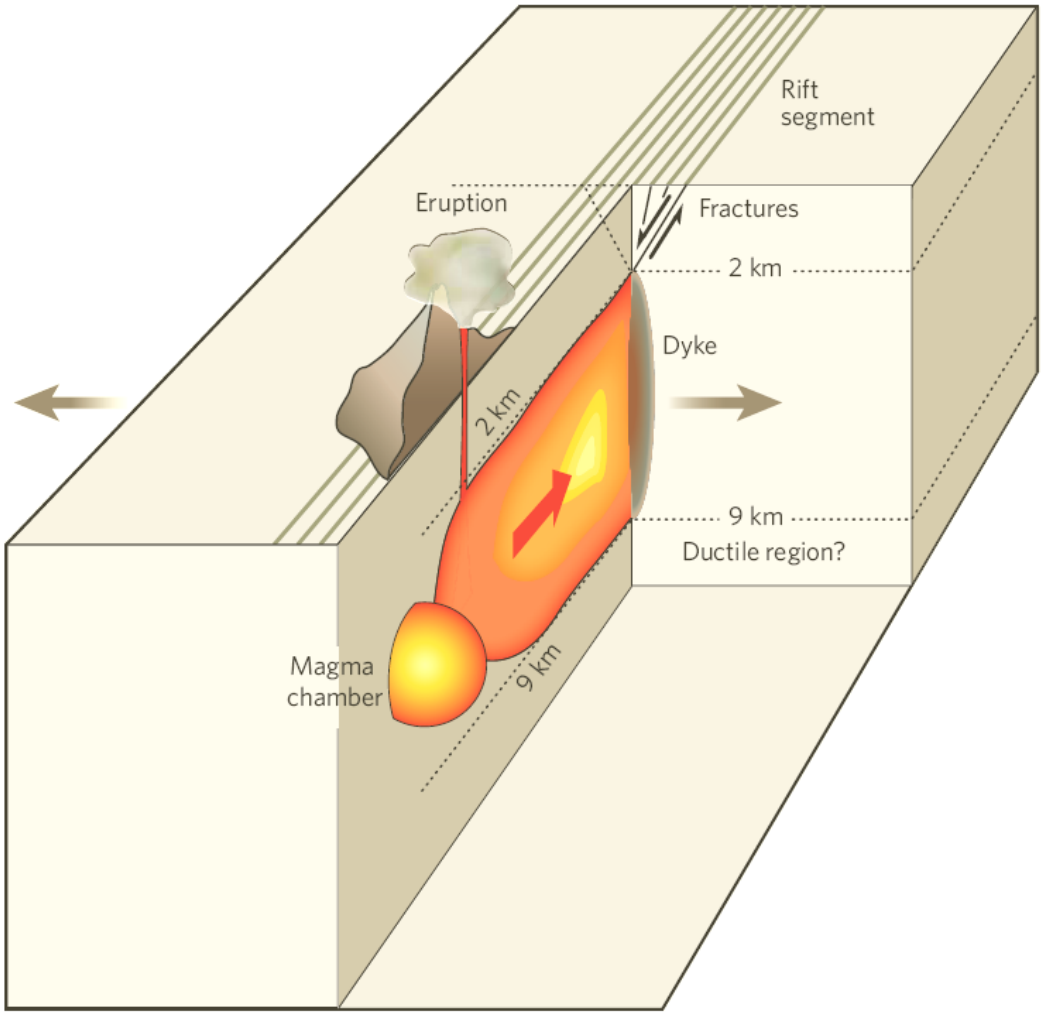

Figure 3.2 Schematic rheological structure of the oceanic crust and a riting event dominated by magna intrusion. The uppermost 5-10 km of the crust behave in an elastic manner over long time scales, but at greater depth viscoelastic effects are important and stresses relax in a ductile manner. Reproduced from Sigmundsson (2006b) with permission of Nature, London.

3.2 Causes of crustal movements: Plate spreading effects and pressure sources

The Northern Volcanic Zone in Iceland (NVZ) and its geothermal areas are continuously being deformed due to their location on the boundary between the North-American and Eurasian plates. The style of deformation in the area is known from various types of crustal deformation measure-

ments, including electronic distance measurements (EDM), tilt observations, GPS geodesy, and interferometic analysis of synthetic aperture radar images acquired by the satellites (ImSAR).

The Krafla rifting episode, 1975-1984, was followed by inflation of a shallow magma chamber until 1989 (see Chapter 1, Section 1.5). At that time, gradual subsidence began above the magma chamber and has continued to date, at a decreasing rate. Subsidence due to pressure decrease in a shallow magma chamber is not the only source of deformation at Krafla as other deformation processes occur at geothermal fields, together with plate spreading. In addition, deep-seated pressure increase appears to take place, with its centre about 12 km north of the location of the shallow magma chamber. This pressure increase has been interpreted as accumulation of magma near the crust-mantle boundary at ~21 km depth (de Zeeuw-van Dalfsen et al., 2004). At this depth, viscoelastic rheology is dominant. The relative strength of deformation sources in the Krafla area has varied with time. New results from a leveling survey and GPS measurements in 2005 allow an updated view on the deformation field. Deformation rates spanning 2000-2005 are the lowest recorded in the 30 years history of geodetic studies at the volcano. The rate of subsidence 2000–2005 is less than 0.2 cm/y whereas it was about 5 cm/y in 1989–1992. Currently, the highest rate of subsidence at Krafla takes place in the Leirbotnar area and there it appears to be dominated by geothermal exploitation (Sturkell et al., submitted).

3.3 Co-rifting deformation

Rifting episodes are considered the primary geological hazard along the spreading plate boundary in North Iceland. Observations from the Krafla rifting episode 1975-1984 demonstrate what can be expected in a future rifting episode along the plate boundary. The events are described in details in Chapter 1, Section 1.5. Following a quiet period along the plate boundary, a period of years may be expected with series of eruptions and dike injections, associated with inflow /outflow of magma to/from a shallow magma chamber playing a central role. The widening of the crust in a rifting episode is expected to be on the scale of a meter or meters. Widening of the Krafla fissure swarm during the 1975-1984 rifting episode was very variable, with a maximum of up to 9 meters. The average widening was about 5 meters along a 80 km long segment. With average plate movements across the plate boundary on the order of 2 cm per year, the inferred average widening during the Krafla rifting episode corresponds therefore to about 250 years of plate movements. North of the Krafla caldera where inferred widening was more than 8 meters, the widening corresponds to more than 400 years of plate movements.

The onset of a new rifting episode along the plate boundary is expected to depend on a complex interplay of tectonic stress accumulation and inflow of magma towards shallow levels in the crust, *e.g*. recharging of a magma chamber. The exact timing of such magma recharging in the crust is difficult to predict (see Section 3.7). The geologic knowledge presented in chapter 2 gives, however, some guidance. It is clear that time between rifting episodes associated with eruptive activity is very irregular. For the last three thousand years, six rifting episodes

associated with volcanic activity are known in the Krafla volcanic system (Table 2.3). However, in the preceding period from 3000 to 8000 years ago, only one eruption is known at Krafla. During that time period, crustal spreading may have been accommodated by dike injections, without eruptive activity. Rifting episodes may thus occur without eruptions. In general, magma is inferred to be denser than the topmost (about 0-3 km) part of the crust and may thus in many circumstances favour being emplaced as intrusion if magmatic overpressure is not large. For Theistareykir, the only known rifting episode in historical time is a possible event in 1618, happening without an eruption (see Chapter 2, Section 2.3.1). For an order of magnitude probability of a new rifting episode associated with eruptive activity in the Krafla system, one can consider the history of rifting episodes at Krafla as presented in Table 2.2.

The estimated intervals between onsets of new rifting episodes with eruptions at Krafla are about 251, 824, 950, 300 and 600 years (years BP correspond to years prior to 1950). The average interval between onset times is 585 years and the standard deviation is 309 years, reflecting a wide range in the length of intervals between rifting events. This time series can be treated with statistical methods, but probabilistic estimates of a renewed activity at Krafla within a certain time period will depend on a number of assumptions. Treating the onset times as a homogeneous Poisson's process corresponding to random instants of time (e.g., Ross, 2003) is one approach, but that is likely to be an oversimplification of the real situation. A more complicated probabilistic model may be warranted, considering that a new rifting episode appears less likely in decades following a recently finished episode as presently at Krafla. If probability of renewed activity is to be considered in general, then activity without eruptions (and not be reported in Table 2.2 for Krafla), such as dike injection at depth and fracturing at the surface without eruptions, needs to be considered. Such activity is unknown, but existence of "missing events" in the time series for activity at Krafla would lead to shorter intervals between events than indicated in the time series based on Table 2.2. For the Theistareykir system, only one eruption is known in the last 9000 years (after the end of the extensive early postglacial volcanism). The probability of renewed activity at Theistareykir is accordingly considered to be an order of magnitude less than for Krafla.

The behaviour of a future rifting episode at Krafla may be expected to be similar as that of the 1975-1984 Krafla rifting episode. It is expected to consist of a series of events, with each event being associated with rapid outflow of magma from a magma chamber and into the rift zone, where the magma will either be emplaced as dikes or erupted to the surface. In the case of rifting in Krafla or Theistareykir volcanic systems, the stress conditions may be such that limited dike widening may presently be possible in these systems. Considering the short interval since the last diking event of the Krafla Fires in 1984 and the spreading rate of about 2 cm/y, the expected "space" created by gradual stretching across the plate boundary for new dikes in the crust is severely limited. Events like those characteristic for the later half of the Krafla Fires, with limited dike lengths and effusive lava eruptions, would be expected, with most magma being emplaced on the surface rather than in dikes. Deformation during individual diking event might thus resemble what occurred in 1984 at Krafla (Figures 3.3a and 3.3b). Alternatively, magma may be emplaced as intrusions in the deeper parts of the crust.

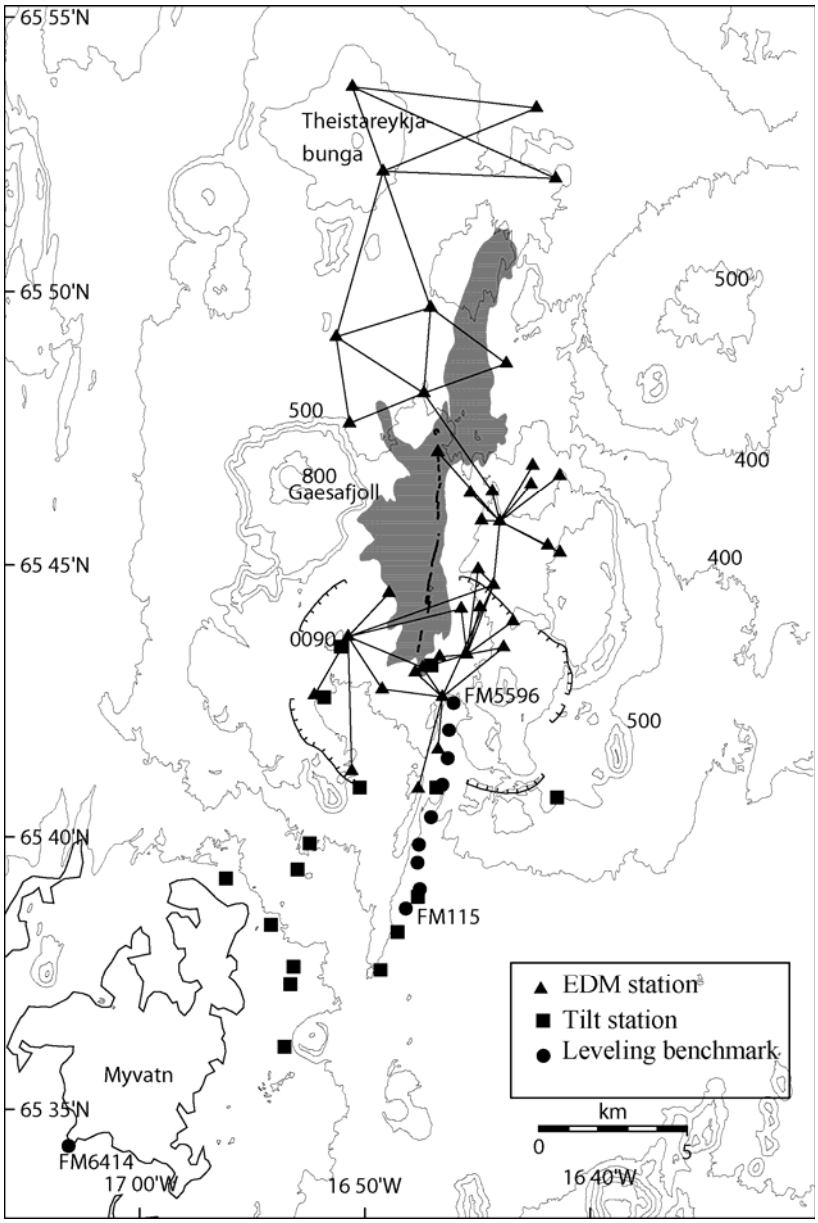

Figure 3.3a Geodetic network used to constrain deformation during the 1984 eruption of Krafla volcano consisting of electromagnetic distance measurements (EDM) stations, optical levelling tilt stations, and levelling bench marks. Shading shows the extent of a lava flow formed in 1984, with the broken line on top outlining the eruptive fissure.

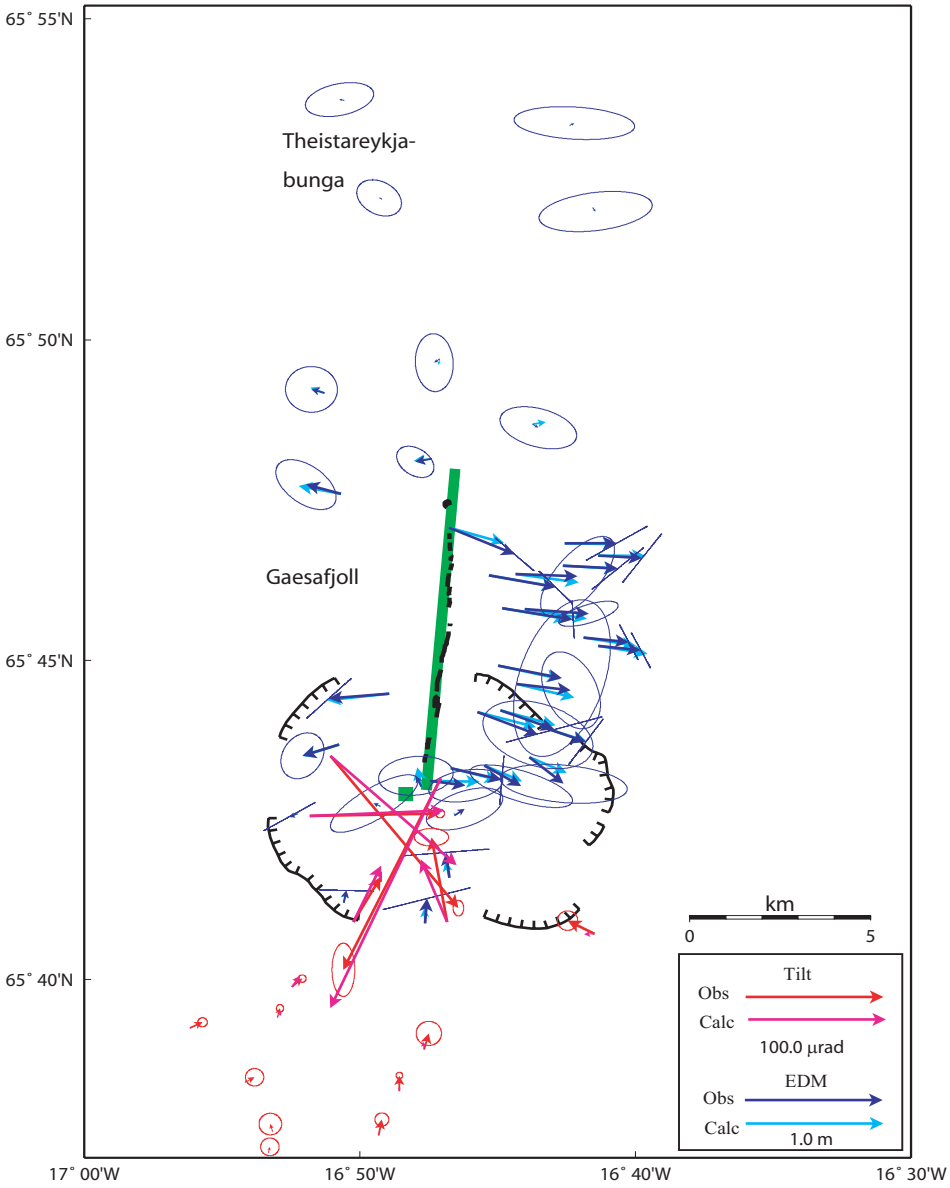

Figure 3.3b Observed and model tilt and horizontal displacements (inferred from EDM) associated with the 1984 Krafla eruption. Eruptive fissure and extent of the modelled dike are indicated by broken and thick shaded line, respectively. Inversion of the geodedetic data gives a model dike extending to 7 km dept. Green rectangle denotes the location of a Mogi pressure source, located at 3 km depth. After Árnadóttir et al. (1998). Copyright by the American Geophysical Union.

Fracturing in new rifting episode would be expected to occur in a narrow zone directly above dikes emplaced in the crust, in a similar manner as in the 1975-1984 rifting episode (Figure 3.4). A narrow strip of land above the dikes is most affected. Zones of extensive recent fracturing should be avoided as sites of buildings and other infrastructure when possible, as these may be the sites of next diking events as well as past ones.

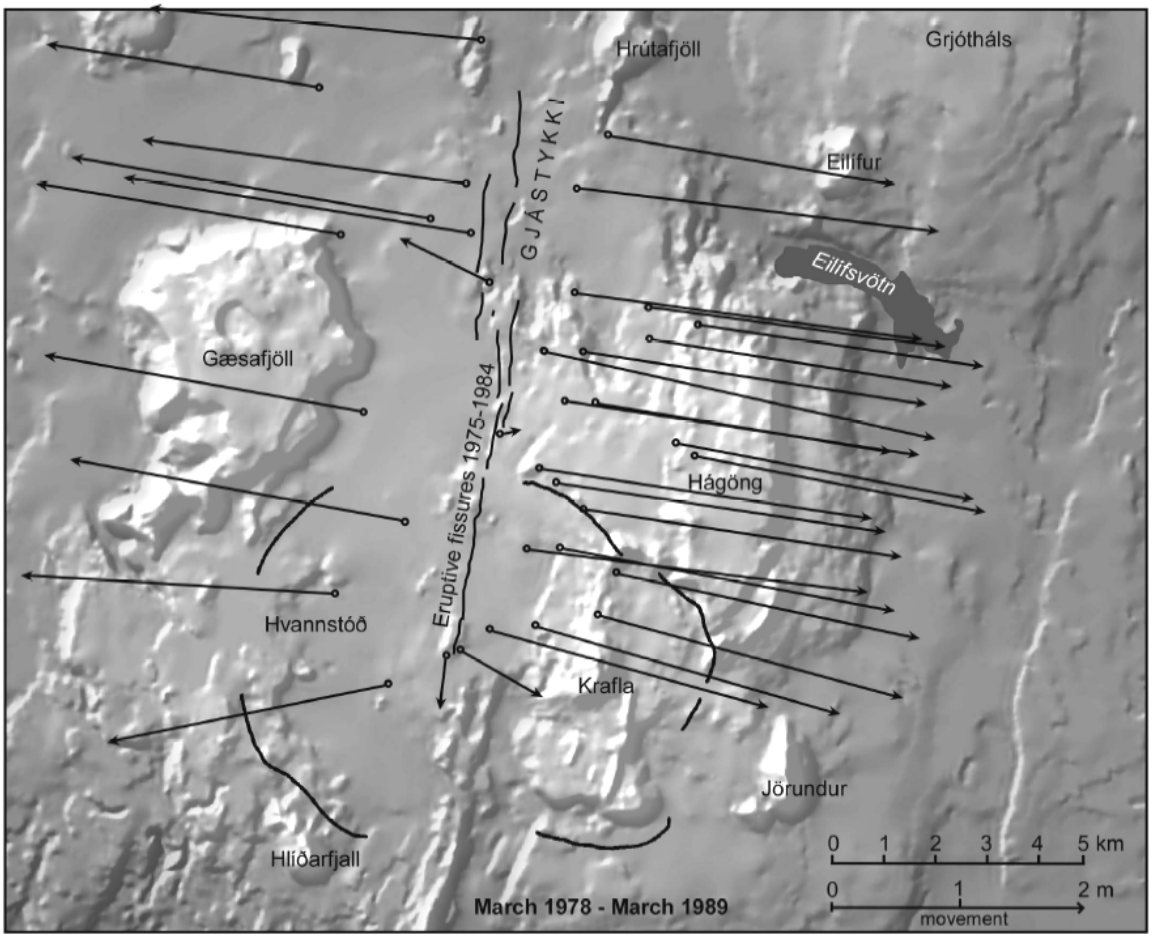

Figure 3.4 Map view of horizontal displacements in the Krafla area March 1978 – March 1989, based on electronic distance measurements. Reproduced from Tryggvason (1994) and Sigmundsson (2006a). The main deformation occurs along the central axis of the Krafla fissure swarm, with large cumulative horizontal displacements on both sides of the dike complex emplaced.

3.4 Post-rifting deformation

Rifting episodes appear to be followed by a time period of higher than average crustal displacements, and stress changes, as the crust readjusts to the previous rifting events. Hazards related to plate movements during such "post-rifting" periods include eventual fracture movements and seismicity in response to rates of deformation higher than in the inter-rifting period that follows (but much smaller deformation than during rifting episodes). Hazard evaluation should consider the style of deformation during such periods, and if the post-rifting deformation period after the Krafla Fires is finished.

GPS-measurements in North Iceland in 1987, 1990 and later, after the termination of the Krafla Fires, revealed a higher than average extension rate across the plate boundary. Average extension

rates in the period 1987-1990 across the Northern Volcanic Zone were as high as 5.6 cm/y, three times the average spreading rate (Foulger et al., 1992; Jahn, 1992). In the 1987-1990 period, horizontal displacements increased away from the rift axis and reached a maximum at a distance of about 25-50 km from the spreading axis. At larger distances, the displacement rates decreased again. Measurements in 1992, 1993 and 1995 revealed decaying extension rates compared to the 1987-1990 period (e.g., Völksen, 2000; Völksen and Seeber, 1998), with rates approaching the long-term average. The observed rate in the 1993-1995 was 2.1 cm/y.

Various models for post-rifting deformation behaviour have been presented. Common to these models is the consideration of an Earth model with ductile rheology under an elastic uppermost layer. The ductile rheology leads to time-dependent transient response following a dike injection. An overview of these models is given by Sigmundsson (2006a). The simplest model for a post-rifting deformation assumes a simple viscous behaviour (Newtonian rheology) under an elastic plate. A simple cross-sectional model consists of a dike injected into a thin elastic layer overlying a Newtonian viscous layer (Figure 3.5). Such a model can broadly mimic the pattern of deformation observed in north Iceland after the Krafla Fires and the model is as well useful to understand the overall plate boundary deformation cycle (see Section 3.7).

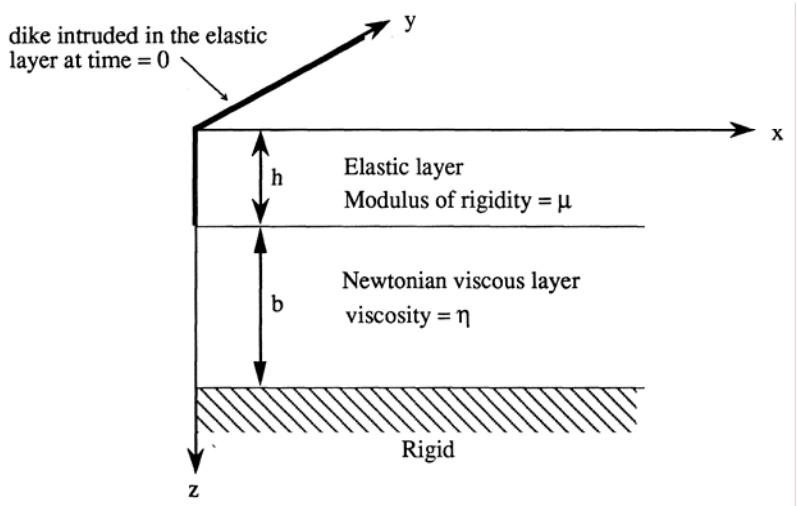

Figure 3.5 Spreading plate boundary – model for post-rifting deformation.

A dike, injected at time $t = 0$, extends through the thickness of the elastic layer. The model assumes the elastic layer is thin and conditions of plane strain exist within it. The horizontal displacement within the plate, $u(x,t)$, is in that case only a function of time and distance, x, from the dike. The horizontal velocity is $\partial u/\partial t$. The underlying viscous layer, with thickness b and dynamic viscosity η, rests on a rigid surface. Velocity gradients within the layer amount to approximately $(1/b)\partial u/\partial t$. Following from the basic definition of dynamic viscosity, the force or traction exerted by the viscous layer on the base of the elastic layer is $-(\eta/b)\partial u/\partial t$. This traction is balanced by elastic forces within the plate. Consideration of force balance, the relation between

stress and strain, and material properties (e.g., Foulger et al., 1992; Heki et al., 1993; Sigmundsson, 2006a) leads to the following equation of motion:

$$\frac{\partial u}{\partial t} = \kappa \frac{\partial^2 u}{\partial x^2} \tag{3.1}$$

κ is equal to:

$$\kappa = \frac{Mhb}{\eta} \tag{3.2}$$

where M is an elastic modulus and h is the thickness of the elastic layer. Equation 3.3 is the diffusion equation and in this context the diffusivity term, κ, is termed stress diffusivity. For a dike of half-width U_0 intruded into the elastic layer at time t = 0, the resulting horizontal displacement field is:

$$u(x,t) = U_0 \mathrm{erfc} \frac{x}{2\sqrt{\kappa t}} \tag{3.3}$$

where erfc is the complementary error function. The horizontal velocity field is:

$$\frac{\partial u(x,t)}{\partial t} = \frac{U_0}{t\sqrt{\pi}} \frac{x}{2\sqrt{\kappa t}} e^{-x^2/4\kappa t} \tag{3.4}$$

The above model predicts displacements and velocities of a similar type as observed in north Iceland after the Krafla rifting episode.

High rate of displacements dominate during a period after dike injection because of stress interaction; stresses built up in the viscous layer during the diking event relax and drive excess displacements away from the dike axis. A velocity pulse diffuses away from the plate boundary, in a characteristic pattern determined by the stress diffusivity. The fit of GPS-derived displacements in 1987-1990 with this one-dimensional model suggest a stress diffusivity of 1.1 m^2/s (Foulger et al., 1992). Interpreatation of GPS-data collected in 1992 with the same model provides a similar conclusion for the stress diffusivity (Foulger et al., 1994). The above analysis demonstrates well the nature of post-rifting displacement and its temporal variations. However, it depends on a number of simplifying assumptions. In reality, the finite length of dikes and associated lack of opening off their ends will limit the amount of deformation. An extension of the above model, considering the finite length of dikes, gives a map view of the horizontal deformation field. Such a model by Heki et al. (1993) provides an improved fit to the observations and gives a stress diffusivity of 10 m^2/s, an order of magnitude higher than application of the cross-sectional model. Applying this model to the Krafla data assuming h = 8-30 km and b = 5-10 km, Heki et al. (1993) estimate the underlying viscosity to be $0.3 - 2 \times 10^{18}$ Pa s.

In summary, modelling shows that observed displacements in the period 1987-1995 can be explained as a response to transient post-rifting stress relaxation following the 1975-1984 Krafla

rifting episode. Higher extension rates across the boundary in the period after the rifting events originate from interaction of a ductile lower crust under an elastic brittle uppermost crust. Judging from the present-day horizontal displacement field (see also Section 3.5), it appears that the crustal stress due to the 1975-1984 diking events has presently relaxed. It appears that the post-rifting deformation period is over, and there are no indications of elevated horizontal plate motion taking place across the plate boundary.

3.5 Inter-rifting plate movements

The time between rifting episodes is mostly characterized by extension across the plate boundary at a steady rate. This "inter-rifting" period follows the post-rifting period of enhanced deformation rates, and it continues until a next rifting episode occurs. Deformation takes place due to plate movements, but also due to magma movements and processes in geothermal areas. Deformation directly related to plate movements is first considered, and in the following chapter we evaluate deformation due to magmatic and geothermal processes that may take place during the inter-rifting period.

Gradual stretching occurs presently across the plate boundary in North Iceland and the main associated hazard is the associated build-up of stress. Geodetic measurements show how and where stretching takes place, and they give an indication of the rate of stress increase along the plate boundary. The areas of stress accumulation gradually build up potential for future activity along the plate boundary, as the accumulated stress in these areas will be released in future activity along the plate boundary.

Continuous GPS-measurements in Iceland show that plate motions outside a plate boundary zone in Iceland are steady (Geirsson et al., 2006), with minor modulation e.g. due to snow loading in Iceland (e.g., Grapenthin et al., 2006). The size and direction of plate movements agree with global plate boundary models (Figures 3.6 and 3.7). The best-constrained global plate motion model based on geologic evidence is the NUVEL-1A model (DeMetz et al., 1994). According to the NUVEL-1A model, the full spreading velocity in central Iceland (64.5°N, 18°W) is 18.3 mm/yr in direction N105°E. Plate motion models can also be derived from geodetic data. A model based on space geodetic data from 1993-2000, primarily observations from continuous GPS stations distributed around the globe, was inferred by Sella et al. (2002). Their REVEL model gives plate motion as Euler poles of rotation and angular velocities, in the same manner as plate motion models based on geologic evidence. The model incorporates only GPS data from stable plate interiors when determining angular velocities. GPS stations at or close to plate boundaries, such as in Iceland, are excluded. This model gives a full spreading rate in central Iceland as 19.7 mm/yr in a direction N103°E. The agreement with the NUVEL-1A model is good despite the fact that the NUVEL-1A model corresponds to average motion in the last 3 Myr, whereas the REVEL model describes plate motion in the 1993-2000 period.

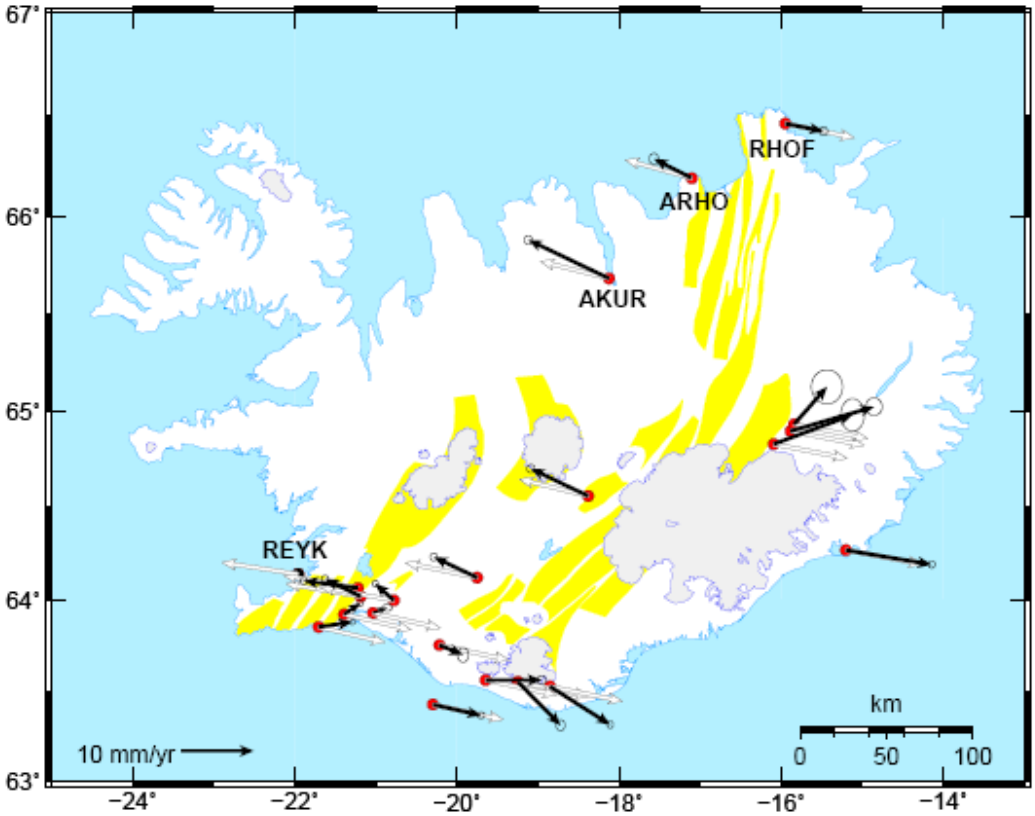

Figure 3.6 Horizontal crustal displacements inferred from continuous GPS-measurements in Northern Iceland (Geirsson et al., 2006 and later work). Black arrows are observations, the inferred velocity vectors relative to a stationary plate boundary. The white arrows are predictions of the REVEL plate motion model. See also http://www.vedur.is. Data from stations indicated by name (RHOF, ARHO, AKUR, REYK) displayed in Figure 3.7.

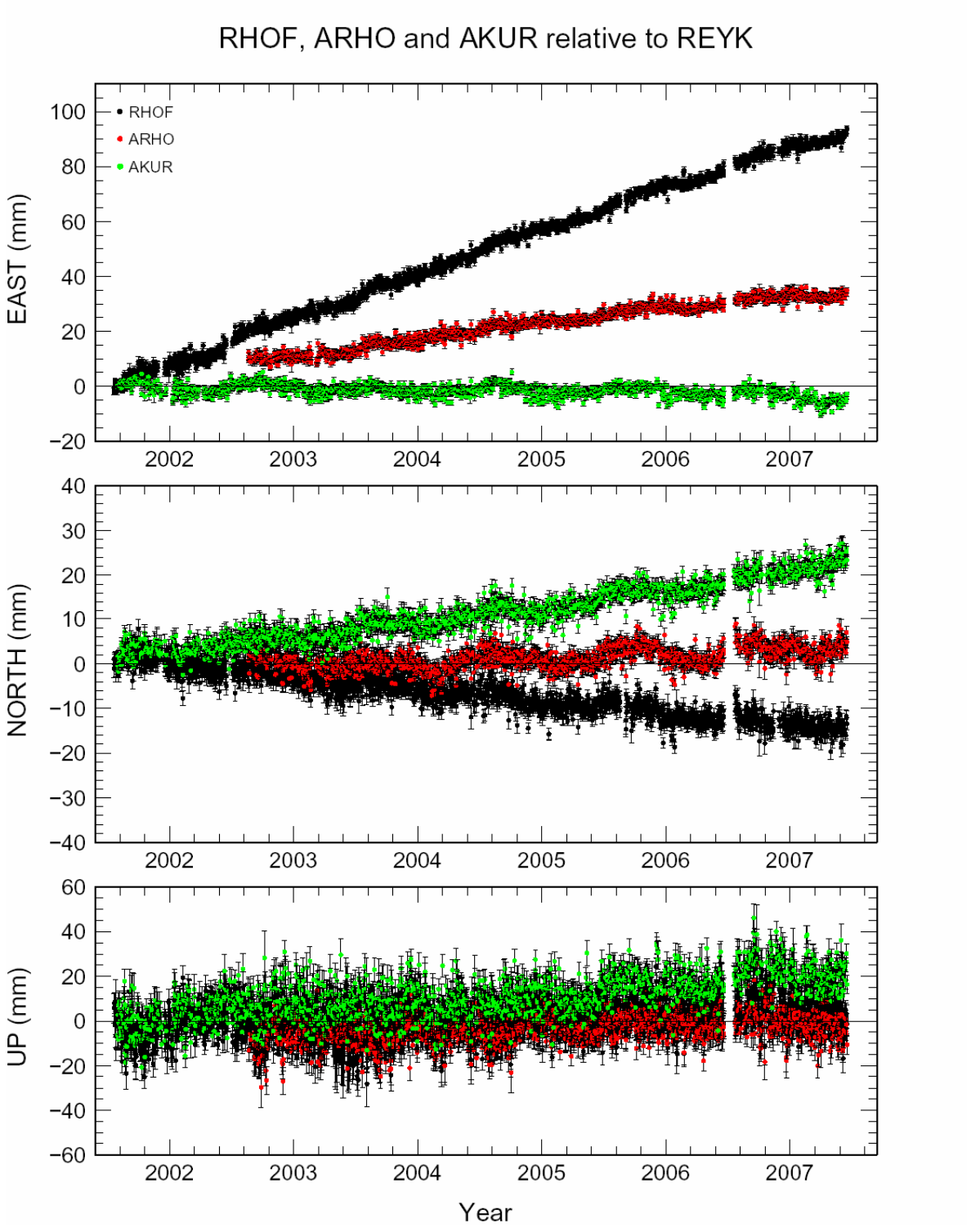

Figure 3.7 GPS time series at selected sites relative to the REYK reference station (Geirsson et al., 2006 and later work). See Figure 3.6 for locations of the RHOF, ARHO and AKUR sites

The plate movements are also revealed by other GPS-measurements in Northern Iceland. These include the ISNET GPS surveys in 1993-2004 (Geirsson et al., 2006) (Figure 3.8).

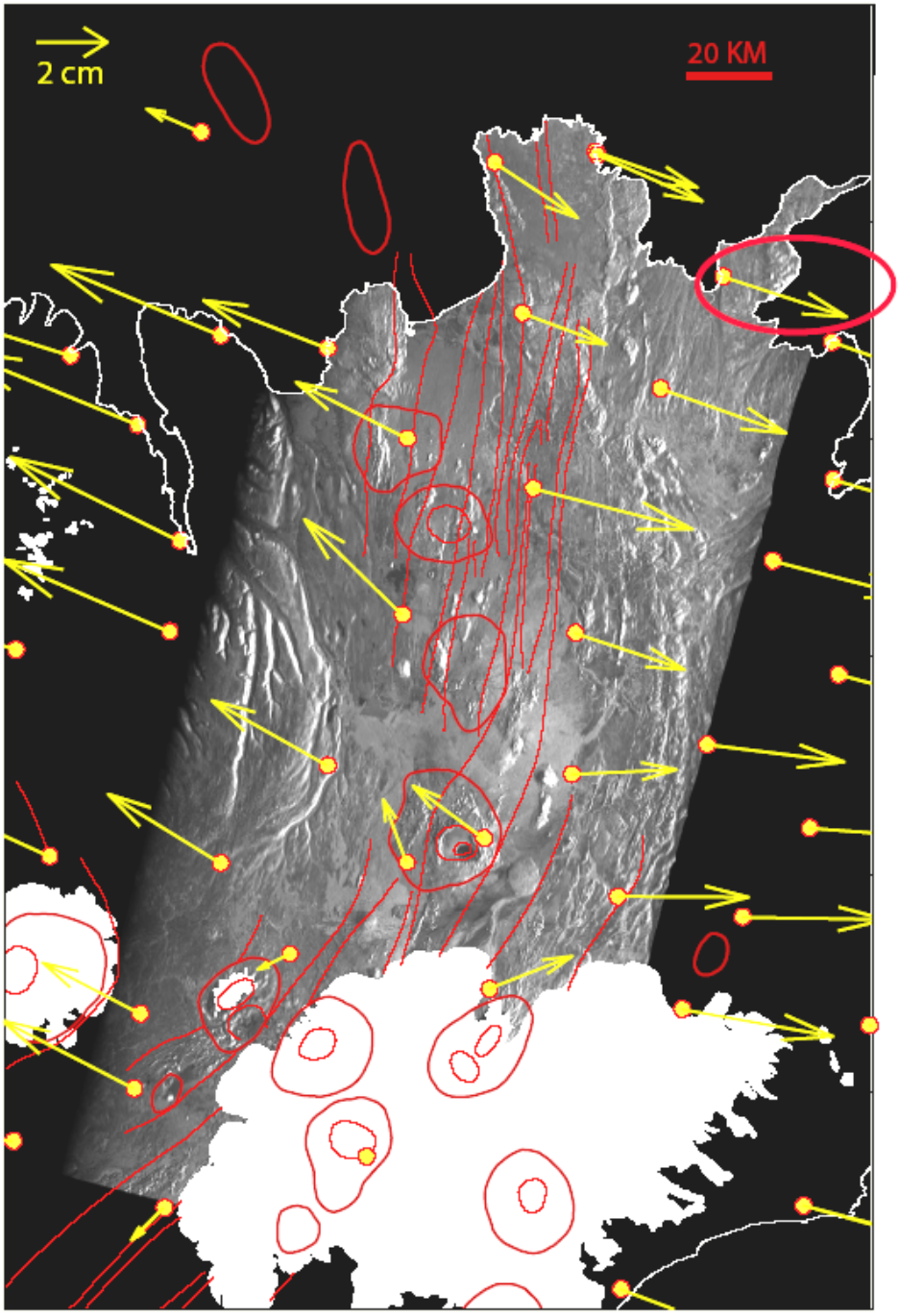

Figure 3.8 Regional average plate velocities 1993-2004 in northern Iceland (ISNET suveys by the Land Survey of Iceland – data processing Thóra Árnadóttir). The results are displayed in a reference system relative to a stationary plate boundary.

A study by Jouanne et al. (2006) reveals the strain accumulation in more details. When plate movements in the 1999-2002 period are displayed relative to the stable Eurasian plate (Figure 3.9), then stations on the other site of the plate boundary move to the west at a velocity approaching the full spreading rate of close to 2 cm/y. More stretching occurs across the Krafla fissure swarm than across the Theistareykir fissure swarm, suggesting that Krafla may continue to be the site of activity along the plate boundary in the future, as in the past.

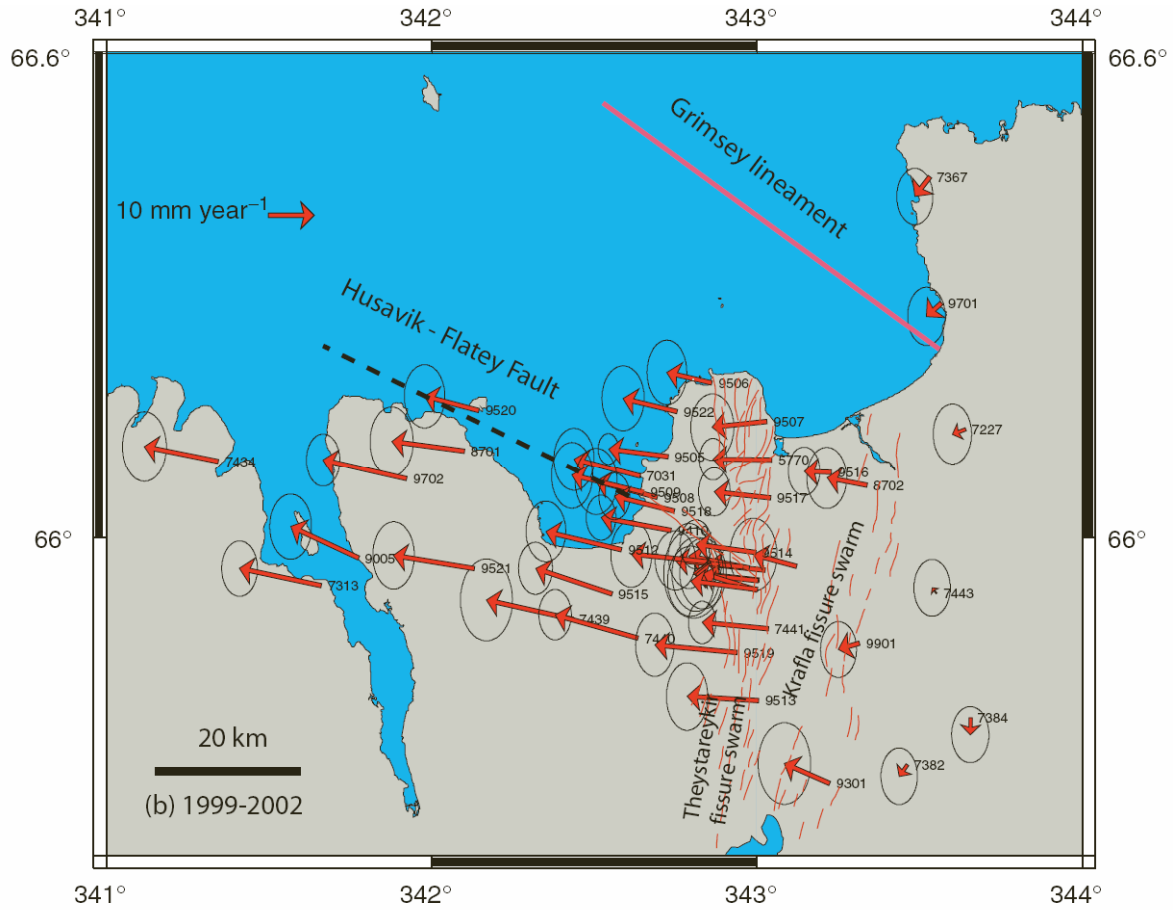

Figure 3.9 Regional crustal velocities 1999-2002 at the rift-transform junction in N-Iceland displayed relative to stable Eurasian plate. After Jouanne et al., (2006).

The level of tectonic stress increase along the plate boundary can be inferred from the geodetic measurements. If displacements only take place perpendicular to the rift zone axis, then we have the conditions of plane-strain. Furthermore, if we assume the brittle upper crust that is being stretched behaves as an incompressible elastic plate, the stretching will be balanced by thinning of that plate. Conservation of volume requires the horizontal and vertical strain to be equal. Under these assumptions, the relation between horizontal strain, ε_{xx}, and tectonic stress, $\Delta\sigma_{xx}$, perpendicular to the rift is (e.g., Jaeger et al., 2007):

$$\Delta\sigma_{xx} \approx 2(\lambda + \mu)\varepsilon_{xx} \tag{3.5}$$

where λ and μ are the Lamé moduli for the elastic plate. If we take $\lambda = \mu = 30$ GPa then we have $\Delta\sigma_{xx} \approx$ (120 GPa) ε_{xx}. If a full spreading rate of 2 cm/yr is taking place across a plate boundary zone of 20 – 60 km width, then the average strain accumulation is 0.3 - 1 μstrain/y. This will cause tectonic stress build-up of about 0.04 – 0.12 MPa /y.

This stress will be released in future activity, but in a way depending on a complex interaction with magma movements (see Sections 3.6 and 3.7). More stretching across the Krafla volcanic system than the Theistareykir system facilitates magma generation and magma up-flow under Krafla rather than the Theistareykir system.

3.6 Evolution of magmatic and geothermal pressure sources in the crust

The inter-rifting deformation is characterized not only by the plate movements discussed in the preceding chapter, but also local deformation due to magmatic and geothermal processes in the crust. Detailed geodetic studies have revealed these processes. Utilization of geothermal areas is known to cause pressure changes in them, and eventual deformation. Measurements and interpretation of the resulting deformation can reveal the processes taking place in geothermal areas. Deformation due to such process can proceed at rate of millimetres or centimetres per year. Although such processes may be important for the use of the geothermal fields, it is not considered a main hazard. One of the best observed sites of subsidence induced by geothermal exploitation in Iceland is in Svartsengi (geothermal area where the Blue lagoon is located). Deformation due to the exploitation has been constrained by a variety of techniques, including satellite radar interferometry (e.g., Vadon and Sigmundsson, 1997).

The main hazard from magmatic and geothermal processes, in addition to rifting episodes, is occurrence of an eruption or injection without significant rifting (individual eruptions between rifting episodes, not associated with significant regional crustal widening along the plate boundary). Frequency of such eruptions without rifting episodes varies at Iceland's central volcanoes. In the Northern Volcanic Zone, they are most frequent at the Askja volcano, as discussed in Chapter 2, but not known in the Krafla volcanic system.

Geodetic measurements can identify areas of persistent deformation, and these areas may be more susceptible to future activity than other areas. Geodetic measurements that constrain local deformation processes include interferometric analysis of synthetic aperture radar images, as well as resurveying of local geodetic networks (Figure 3.10).

Two sites of persistent local deformation, continuing for decades, are known in the Northern Volcanic Zone; in the Krafla caldera and the Askja caldera (see e.g. overview by Sigmundsson, 2006a). The persistent deformation is interpreted as the response to processes taking place in shallow magma chambers in these locations. At Krafla volcano various geodetic studies consistently point to a similar location for the shallow magma chamber (Figure 3.11 and Figure 1.8).

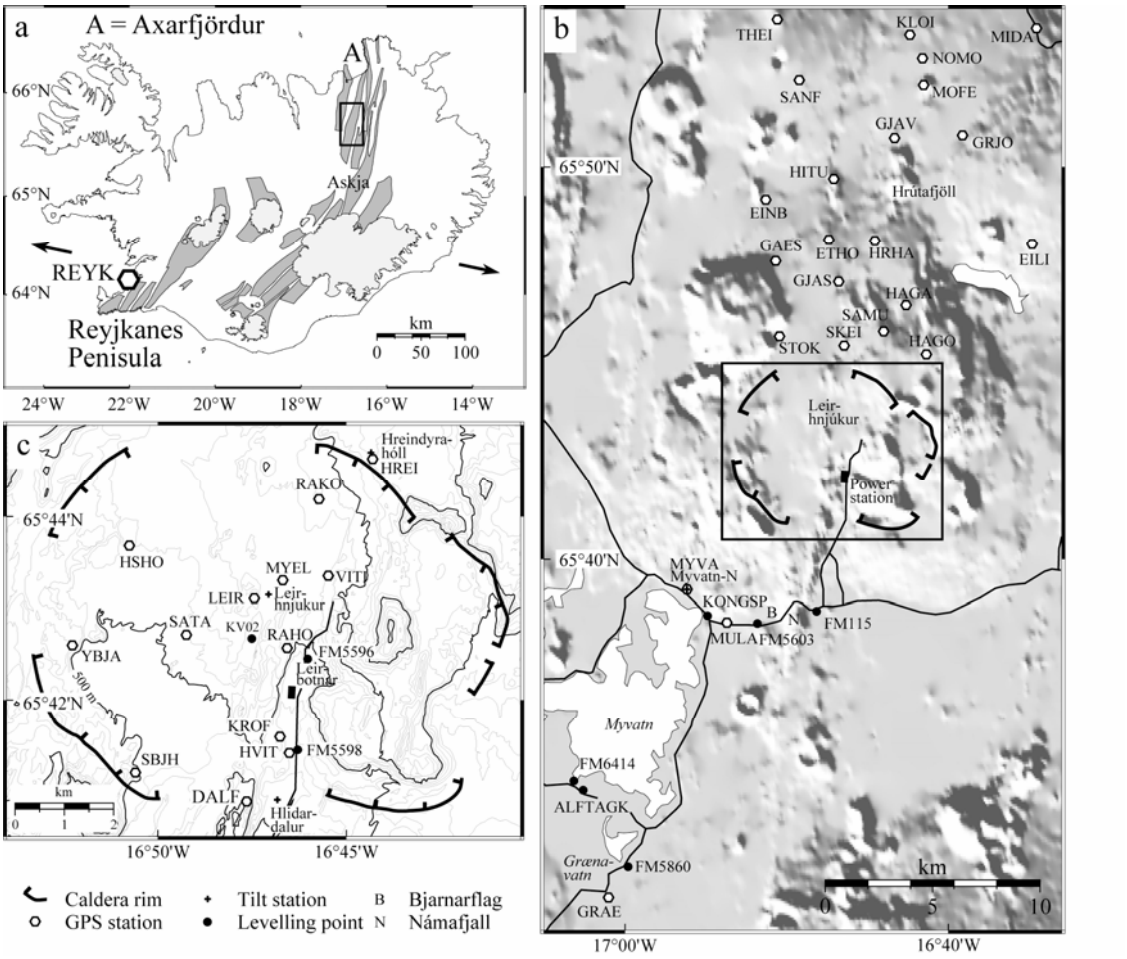

Figure 3.10 Local GPS and tilt network at Krafla from Sturkell et al. (submitted).

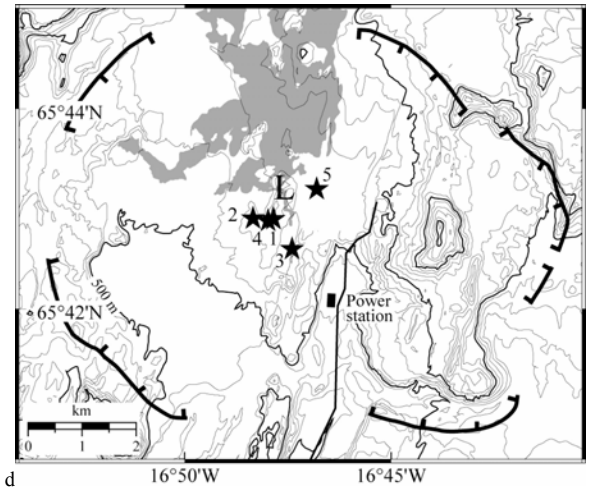

Figure 3.11 The shallow magma chamber at Krafla – Stars indicate inferred locations of Mogi sources from different studies. After Sturkell et al. (submitted).

Deformation in the Krafla caldera following the Krafla rifting episode 1975-1984 is not steady in time. After 1989, the area has been subsiding but at a variable rate. Furthermore, the spatial character of the subsidence has changed. Repeated levelling surveys demonstrate clearly the evolution and change in style of deformation due to processes in the shallow magma chamber (Figure 3.12).

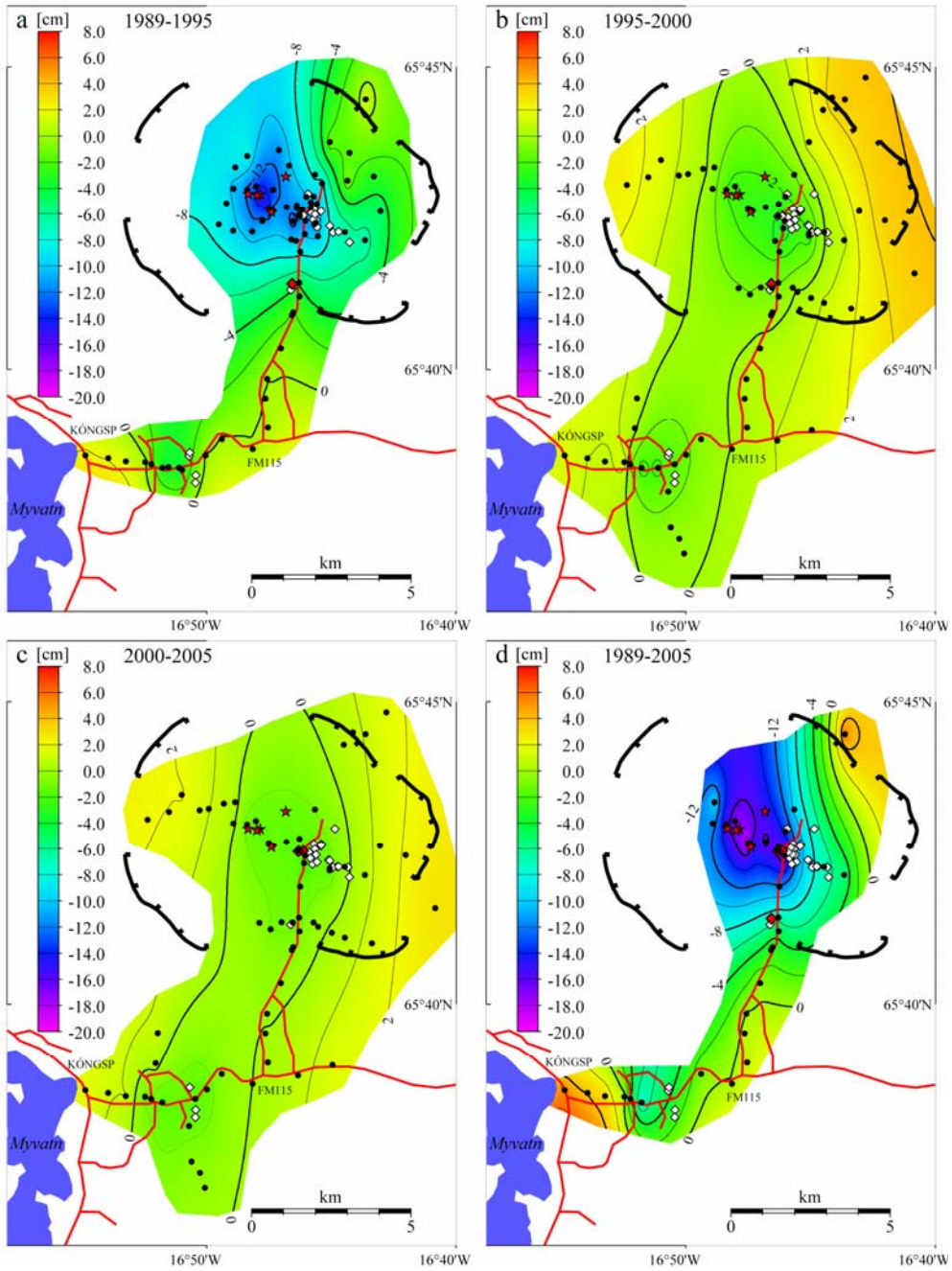

Figure 3.12 Vertical displacements inferred from levelling in the Krafla area 1989-2005. a) Vertical changes 1989-2005, b) vertical changes 1995-2000, c) vertical changes 2000-2005, and d) vertical changes 1989-2005. After Sturkell et al. (submitted).

The rate of subsidence has decayed to less than 3 mm/yr at present times, and it is inferred that pressure reduction in the Krafla geothermal area has taken over as the dominant local deformation process.

An additional deformation signal indicative of deep pressure increase under Gjástykki requires particular consideration. This signal is best detected in an InSAR study of Krafla (Figures. 3.13a, 3.13b and 3.14). InSAR studies rely on interferometric analysis of synthetic aperture radar images acquired by radar satellites (ERS and ENVISAT satellites have been the most used in Iceland). Resulting interferograms show the inferred change in range from ground to satellite, with an accuracy of about 10 mm (e.g., Massonnet and Sigmundsson, 2000). The satellite has an incidence angle relative to the vertical (23° in the case of ERS), and as a consequence the inferred change in range depends on a combination of vertical and horizontal displacements.

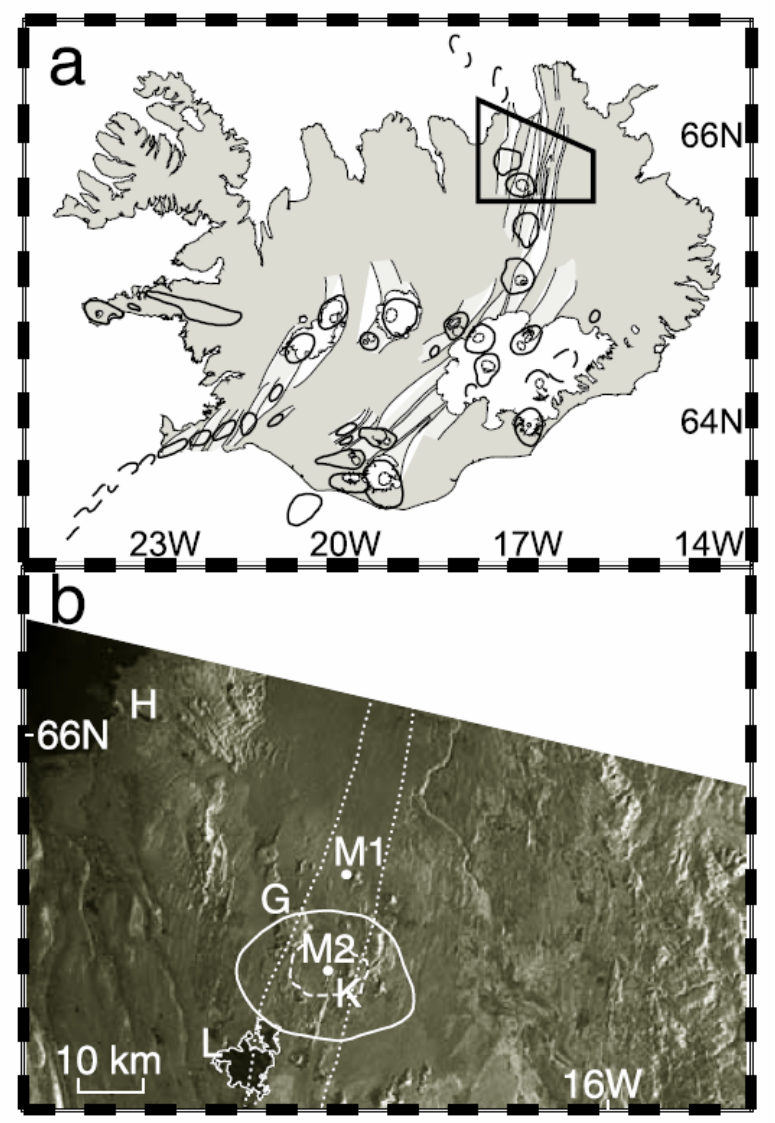

Figure 3.13a Location of an InSAR study of the Krafla area showing the town of Húsavík (H), Lake Mývatn (L), the Krafla fissure swarm (dotted), the outline of the Krafla caldera central volcano (solid white line), and the Krafla caldera (white dashed line). M_2 and M_1 inidcate the location of the Krafla magma chamber and the site of deep pressure increase in Gjástykki respectively. Reproduced from de Zeeuw-van Dalfsen et al., (2004).

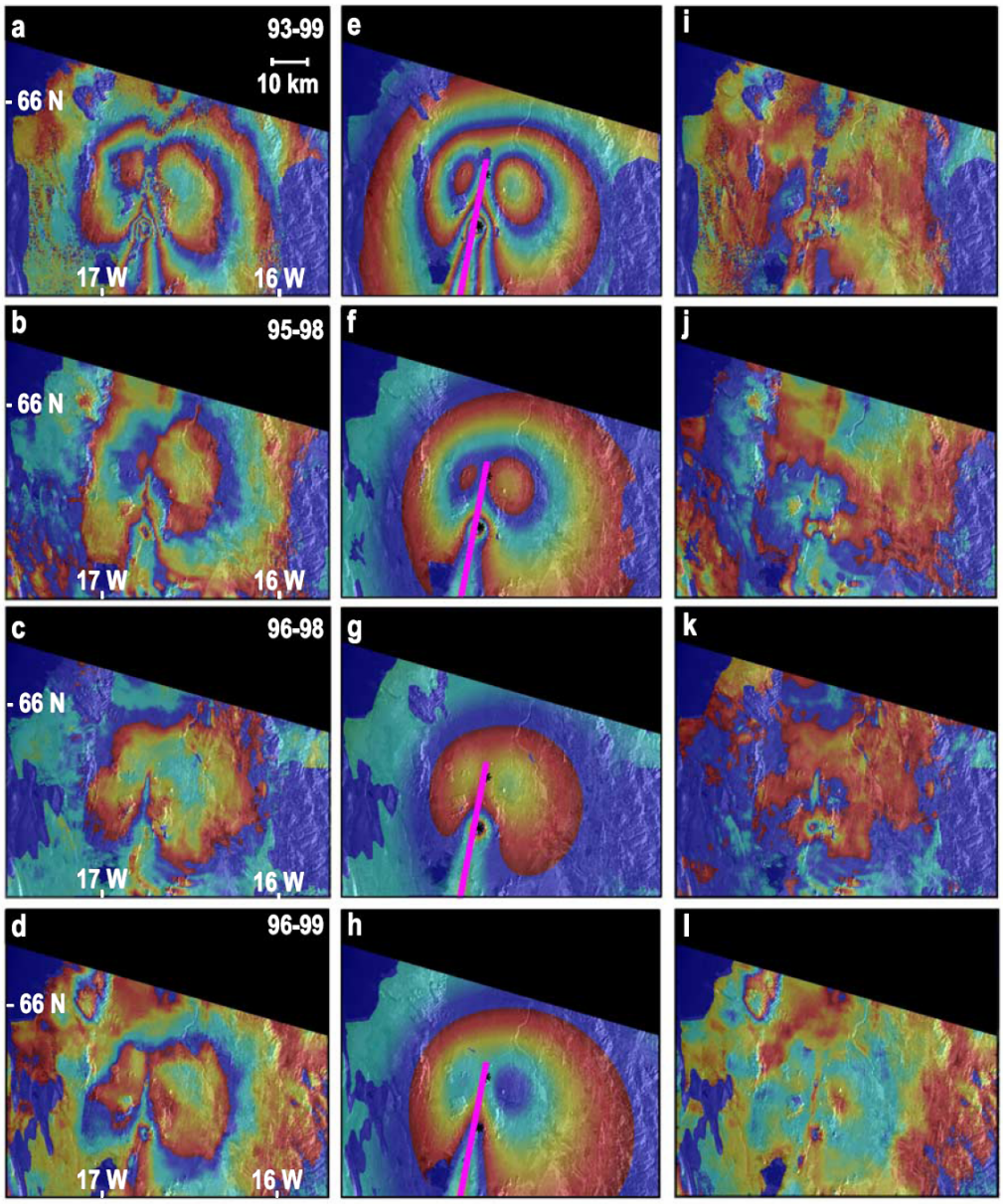

Figure 3.13b InSAR study of Krafla area. Interferograms (left column), models (center column), and residuals (right column). Each full color cycle (fringe) corresponds to a change in range from ground to satellite of 28 mm. See text for discussion. Reproduced from de Zeeuw-van Dalfsen et al., (2004).

The regional InSAR study of Krafla reveals inflation over a broad area centred on Gjástykki. In the 1992-1999 period the rate of uplift averages to about 10 mm per year at its maximum, over a ~50 km wide area. The signal is consistently seen in a number of interferograms. The signal can be attributed to pressure increase at about 21 km depth in the crust. The signal from the deep pressure source can be further studied with additional interferograms. Interferograms based on data from the ENVISAT satellite reveal that pressure appears to increase steadily in the deep source. A comparison of two time periods, 1993-1995 and 2003-3005 reveals that although

deformation due to the shallow magma chamber mostly disappears, then the signal from the deep source is similar (Figure 3.14). A steady rate of pressure increase in the deep source is suggested.

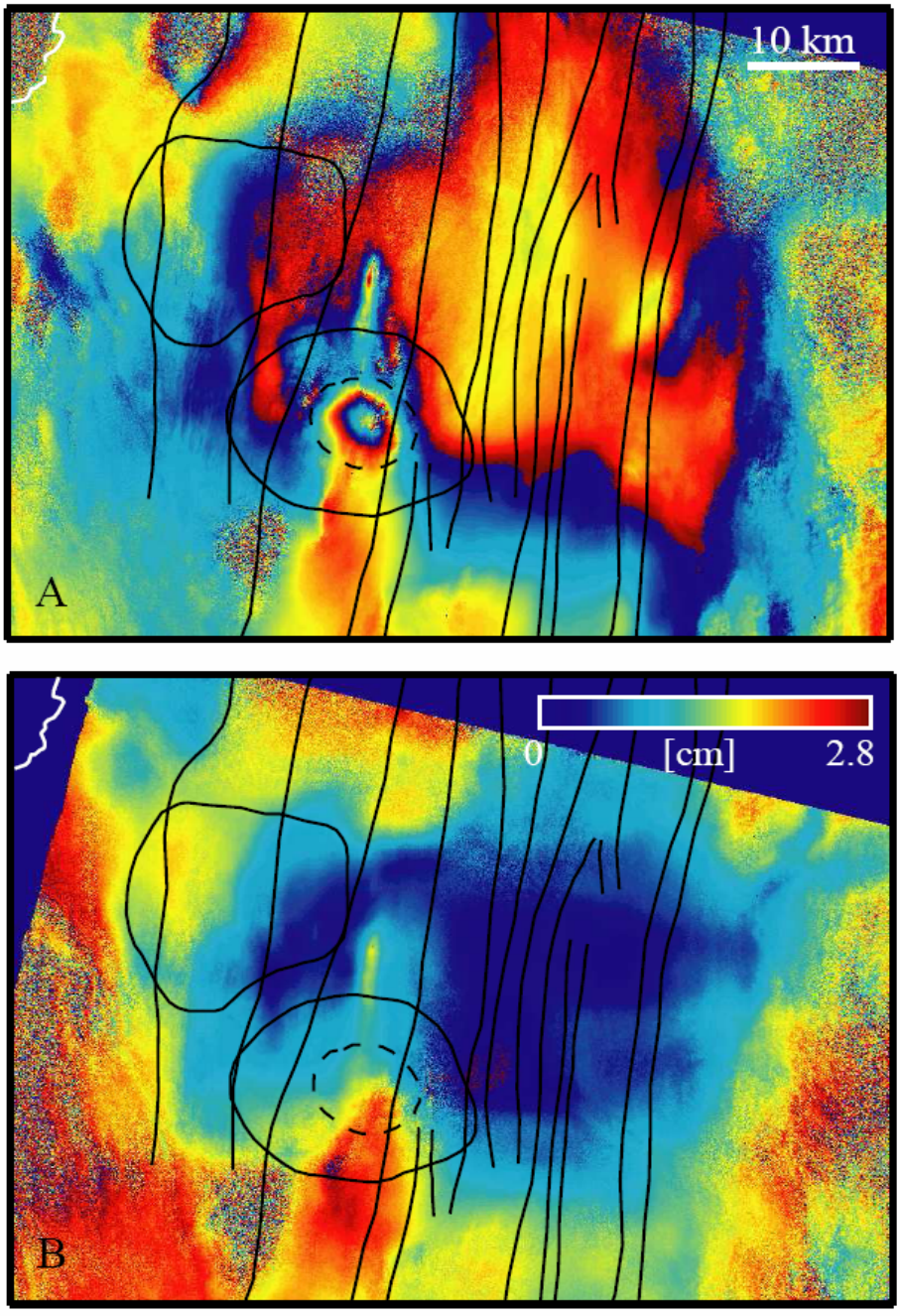

Figure 3.14 Interferometric data covering the Northern Volcanic Zone. Black lines outline the fissure swarms in the area, circular outlines show the location of central volcanoes and the black stippled outline shows the location of the Krafla caldera. A) ERS data spanning 1993-1995. B) ENVISAT data spanning 2003-2005. Subsidence above shallow magma chamber has declined but deep inflation under Gjástykki continues. After Pedersen et al. (2007).

The deep seated pressure increase under Gjástykki has been interpreted as magma accumulation near the crust-mantle boundary at about 21 km depth (de Zeeuw-van Dalfsen *et al*. 2004). An alternate suggestion is that it may relate to post-rifting deformation processes, but no model has yet been produced that can explain GPS and InSAR derived present deformation in the area as a post-rifting response. In particular the even rate of deformation over long time period is difficult to reconcile with post-rifting process, that otherwise appear to be completed in the Krafla area. The favoured explanation for the deep pressure increased is considered to be magma accumulation. Simple model for that process appears to satisfactorily explain the observations (Figure 3.13a). Magma at this depth may be expected to be primitive basalt. The pressure source may signify an ongoing intrusion in the lower crust, forming a lower crustal gabbro as a part of the generation of the oceanic crust.

Continuous crustal movements can be expected at Krafla in coming decades even if deformation rates in the last few years are low. Krafla is a restless caldera, movements up and down can occur without eruptions. That is characteristic for many calderas world-wide.

3.7 Tectonic-magmatic interplay: The plate spreading deformation cycle and magmatic systems

Some main aspects of the plate spreading deformation cycle have been outlined in the previous sections of this chapter. In general, displacement field at spreading plate boundaries can be regarded as the sum of deformation associated with the latest rifting episode, superimposed on background movement, being the summed contributions of all prior episodes. When strain accumulation (associated with stretching) has reached a critical limit the plate boundary will fail and rifting occurs. The critical limit is, however, highly variable and depends strongly on availability of magma. Therefore, intervals between rifting episodes are not regular.

If no magma is present at shallow depth along the plate boundary, then normal faulting will relieve the stresses. In that case, the critical deviatoric stress is the one needed to cause normal faulting. For example, to initiate slip of a normal fault at 5 km depth may require deviatoric stresses on the order of 65 MPa, according to the Anderson theory of faulting (e.g., Turcotte and Schubert, 2002). If magma is in contact with stretched brittle crust, then diking events will relieve the stress by tensile failure and accommodate the spreading. The rupture criterion for tensile failure (e.g., Pinel and Jaupart, 2003) is that the magnitude of the deviatoric stress must exceed a certain threshold value, which is the tensile strength of the crust, T_s. The criteria can be written as

$$\Delta\sigma_3 < -T_s \tag{3.6}$$

where $\Delta\sigma_3$ is the deviatoric minimum compressive stress (minimum compressive stress minus lithostatic stress). The tensile strength of the crust in Iceland is not well known, but analysis of hydro-fracturing measurements in the uppermost 600 m of a drillhole at Reydarfjördur, eastern Iceland have revealed it to be 1-6 MPa (Haimson and Rummel, 1982).

In absence of tectonic stress, magma chambers may fail because of stresses created by pressure inside them. This has to be considered as well. For a two-dimensional magma source such as a pressurized pipe in an infinite medium, the hoop stress (tensile stress on the pipe walls) is constant along the walls of the pipe and is equal to the overpressure in the pipe. In this case, and for a pressurized pipe of small radius in an elastic half-space, the eruption criteria will be

$$\Delta P_c \rightarrow T_s \tag{3.7}$$

The critical overpressure needed for failure, ΔP_c, equals the tensile strength. In general, the geometry of magma sources will cause deviations from this simple relationship. Hoop stresses on the walls of a magma chamber will be modified by the finite dimensions of the source, and also by the presence of a volcanic edifice above the source. Stress concentration around magma bodies has to be considered. A general form of the failure criteria includes an amplification factor, *k*, such that the criterion becomes

$$k\Delta P_c \rightarrow T_s \tag{3.8}$$

In reality, the stress concentration needs to be evaluated for three-dimensional sources. For example, the hoop stress at the boundary of a sphere in an infinite elastic half-space is equal to half the overpressure in the source, corresponding to $k = 0.5$ (McTigue, 1987).

In Iceland, both of two factors above contribute to the failure condition, the regional accumulation of tectonic stress, and pressure increase in magmatic sources. By considering both the effects expressed by equation 3.6 and 3.8, the condition for rifting is (*e.g.*, Jaeger et al., 2007):

$$\Delta\sigma_3 - k\Delta P_c = -T_s \tag{3.9}$$

As a consequence, inflow of magma towards shallow depths may be a precursor to many rifting events where tensional stress may have previously built up to high levels. A modest volume of magma flowing into a rift zone can therefore cause rifting, long before the strain could be accommodated by normal faulting. Although magma may be generated in the mantle at a relatively steady rate under normal conditions, its transport towards shallow levels may be highly irregular and episodic, depending on the transport mechanism. This may be a primary factor causing irregular intervals between rifting events.

3.8 Rift-transform interaction and regional stress: Influence of the Krafla volcanic system on stress along the Húsavík-Flatey fault system

A diking event compresses crustal volumes adjacent to the intruded dike. Cumulative horizontal displacement over regional scale show how horizontal displacement decays away from the dikes intruded during the Krafla rifting episode. Stresses are significantly modified in this crustal volume, with increased compressional stress. Such effect can modulate seismic activity. Increased compressional stress may clamp faults and reduce seismicity from levels prior to rifting. Seismic activity on the easternmost part of the Húsavík-Flatey fault may be affected by this process in relation to rifting in the Krafla volcanic system. Chapter 4.2 documents how the easternmost part of the fault had nine earthquakes of magnitude 4 or larger in the period 1927-1973. The last of these events occurred shortly prior to the onset of the Krafla rifting episode, but none have been recorded since. As plate movements gradually restore stresses towards the pre-rifting levels, seismic activity on the easternmost part of the Húsavík-Flatey fault may eventually increase again towards the level existing prior to the Krafla rifting episode. The known earthquake history is considered in the seismic hazard estimate presented in Chapter 5.

3.9 Incorporation of crustal deformation results into hazards estimates

Volcanic hazards can be quantified in different ways. A study of the eruption history and past events of a dormant volcano gives an estimate of the long-term probability of renewed activity. Such estimates are often hampered by limited knowledge. Frequently, only few events are used to estimate statistical distribution of repose periods in a volcanic area. Such probabilistic estimates can be "upgraded" into time-dependent hazard estimates if information is available about ongoing tectonic and magmatic activity in an area. A detailed understanding of volcano dynamics is needed to fully understand the hazards involved. The style of crustal deformation in a volcanic area inferred from repeated geodetic measurements can be incorporated into such hazard estimates. The role of geodetic measurements is at least two fold: (i) identification of areas and amount of significant tectonic strain accumulation and (ii) identification of areas of magma movements and accumulation within the crust.

Gradual stretching across the divergent plate boundary in northern Iceland causes strain accumulation of about 0.3 - 1 μstrain/yr. The associated tectonic stress build-up is on the order of 0.04 – 0.12 MPa /yr. When strain accumulation has reached a critical limit the plate boundary fails and rifting occurs. The critical limit is highly variable and depends strongly on availability of magma. If no magma is present at shallow depth along the plate boundary, then normal faulting will relieve the stresses. In that case, the critical deviatoric stress is the one determining when normal faulting occurs. Initiation of slip of a normal fault at 5 km depth may require deviatoric stresses on the order of 65 MPa. If magma is in contact with stretched brittle crust, then diking events will relieve the stress and accommodate spreading. The condition for rifting is then a deviatoric stress that exceeds the tensile strength of the crust, inferred to be about 6 MPa in Iceland, or an order of

magnitude smaller than if no magma is present. Inflow of magma towards shallow depths within the rift zone may therefore be a precursor to major rifting events along the plate boundary. An order of magnitude longer time is needed to accumulate sufficient stress to cause large scale faulting in a magma starved system.

The rifting events at Krafla 1975-1984 and subsequent volcano inflation until 1989 have been followed by no eruptive activity in the area. No known magma accumulation is taking place at a shallow depth in the crust, but magma accumulation near the crust-mantle boundary has been suggested (alternatively that signal may relate to post-rifting adjustment). Geodetic measurements indicate a relatively uniform strain accumulation along the length of the plate boundary in north Iceland and suggest that Askja segment adjacent to Krafla should be considered as the likely location of renewed activity. However, future location of magma accumulation at shallow depth will determine the site of the next eruptive or intrusive activity in the Northern Volcanic Zone. Early detection of such renewed magma accumulation at shallow crustal depth, put in context with previous pattern of magma movements in a volcanic area, is therefore a key in updating long-term probabilistic volcanic hazard estimates. Much longer time series of crustal deformation observations are needed in the area to fully understand the hazards throughout the full plate boundary deformation cycle.

4. Assessment of earthquake hazard

Páll Halldórsson, The Icelandic Meteorological Office

Earthquakes in northeast Iceland occur mainly within the Tjörnes Fracture Zone. Since 1994, seismicity in this region has been monitored by the SIL seismic network. Earthquakes cluster on two northwest trending lineaments (Figures 4.1 and 4.2) named the Grímsey-Kópasker lineament and the Húsavík-Flatey fault (HFF), which extends northward to the Kolbeinsey Ridge.

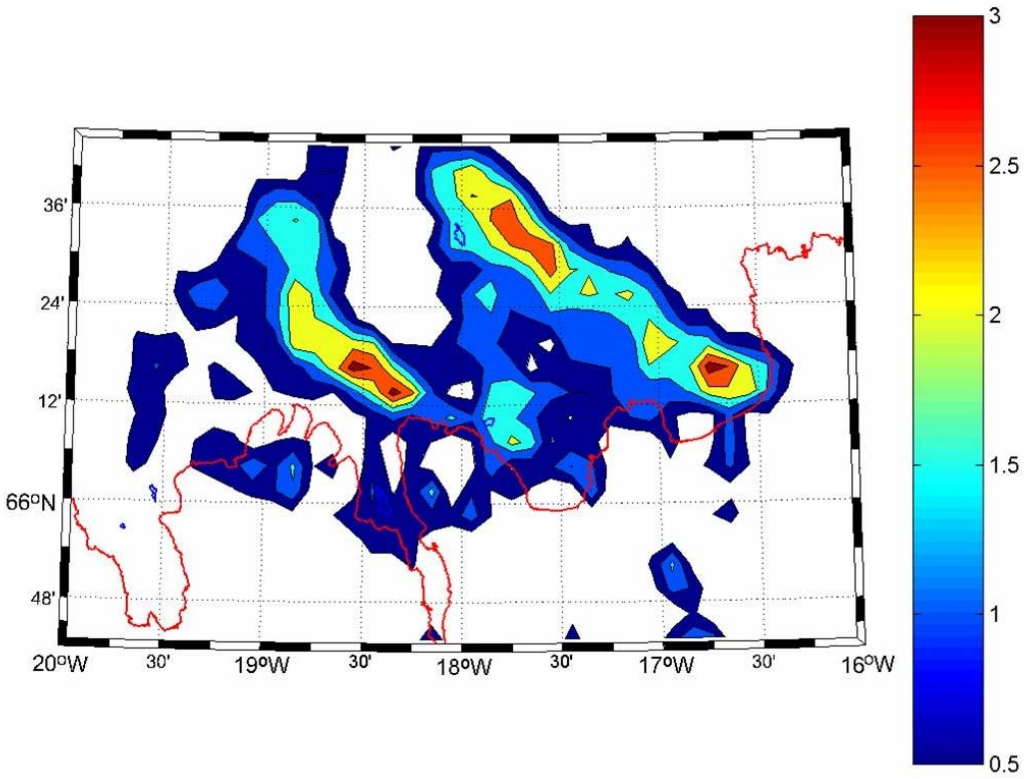

Figure 4.1 Logarithm of the number of earthquakes since 1994, having a magnitude ≥ 1.5 on the Richter scale. Number of earthquakes is counted in confined 25 km^2 areas.

Earthquakes also cluster at Tröllaskagi, located between Fjót and Dalvík, suggesting the presence of a third lineament (Figure 1.6). Historically, all large earthquakes in the Tjörnes fracture zone have occurred on these lineaments. Additionally, increased seismicity on the Grímsey-Kópasker lineament is, apparently, connected to rifting episodes in Iceland's northern volcanic zone.

4.1 Historical earthquakes in northern Iceland and their proximity to power plants

Figure 4.2 shows the distribution of large earthquakes (M ≥ 6) in northern Iceland. The events include pre-1900 estimates of earthquake size and location, together with measured earthquakes. Major earthquakes are sourced both on and off the coast of the Tjörnes fracture zone. Historically, the exact size and location of offshore earthquakes is uncertain because of the difficulty of using intensity-based estimates.

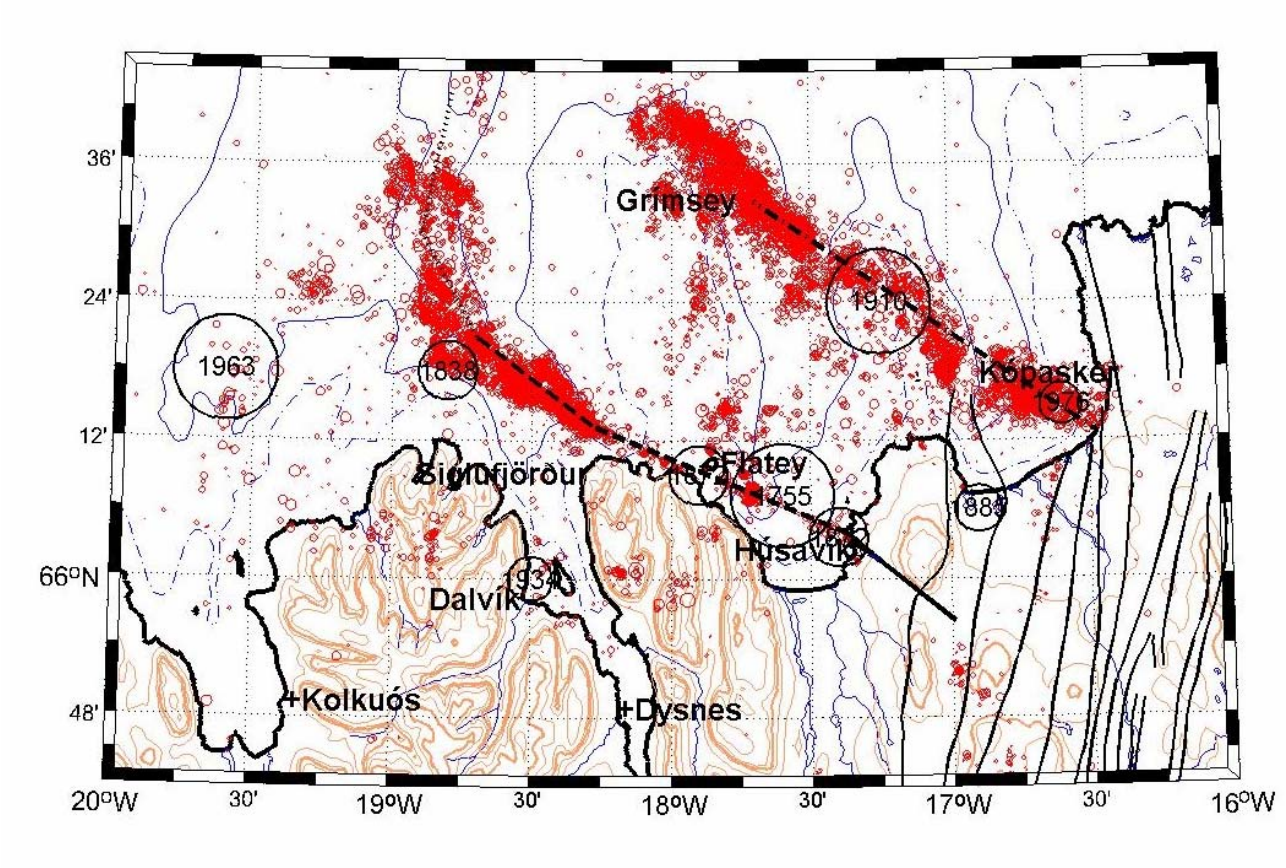

Figure 4. 2 Historical earthquakes (M ≥ 6) since 1700 and earthquakes ≥ 1.5 since 1994.

The following Table 4.1 summarises the proximity to and effects of large, historic earthquakes that have occurred near to the sites of the power plants. Data on earthquake intensities and ground acceleration are included, alongside felt intensity values, where available.

Tafla 4.1

			Theistareykir		Gjástykki			Krafla			Bjarnarflag			
Year	M	Dist	Int	Acc	Dist	Int	Acc	Dist	Int	Acc	Dist	Int	Felt Int	Acc
		[km]	[MM]	[%g]	[km]	[MM]	[%g]	[km]	[MM]	[%g]	[km]	[MM]	[MM]	[%g]
1755	7	40	7	7	50	6½	5	60	6½	4	65	6½	≤ 4	3
1838	6.5	95	5	1	105	5	1	115	4½	1	115	4½		1
1872	6.5	30	6½	6	40	6	4	50	6	3	55	6		3
1872	6.5	50	6	3	60	6	2	70	5½	2	75	5½		2
1885	6	25	6	5	35	6	3	45	5½	2	50	5½		2
1910	7.1	75	6	3	85	6	2	95	5½	2	100	5½	5	2
1934	6.25	70	5	1	80	5	1	85	5	1	85	5		1
1963	7	130	5	1	140	5	1	145	5	1	145	4½	4	1
1976	6.2	45	6	2	50	6	2	60	5½	1	70	5	4	1
NN	6.5	15	7	18	25	7	8	35	6½	5	40	6		4

The table shows that, where felt intensities are known, the values are lower than calculated, conforming with the assumption of higher attenuation rates in the eastern volcanic zone than in Iceland in general; the same can also be assumed for predicted and actual ground acceleration. The effect of a possible earthquake on the eastern part of the HFF – identified as 'NN' – is shown in the table. The earthquake's loci is at Höskuldsvatn.

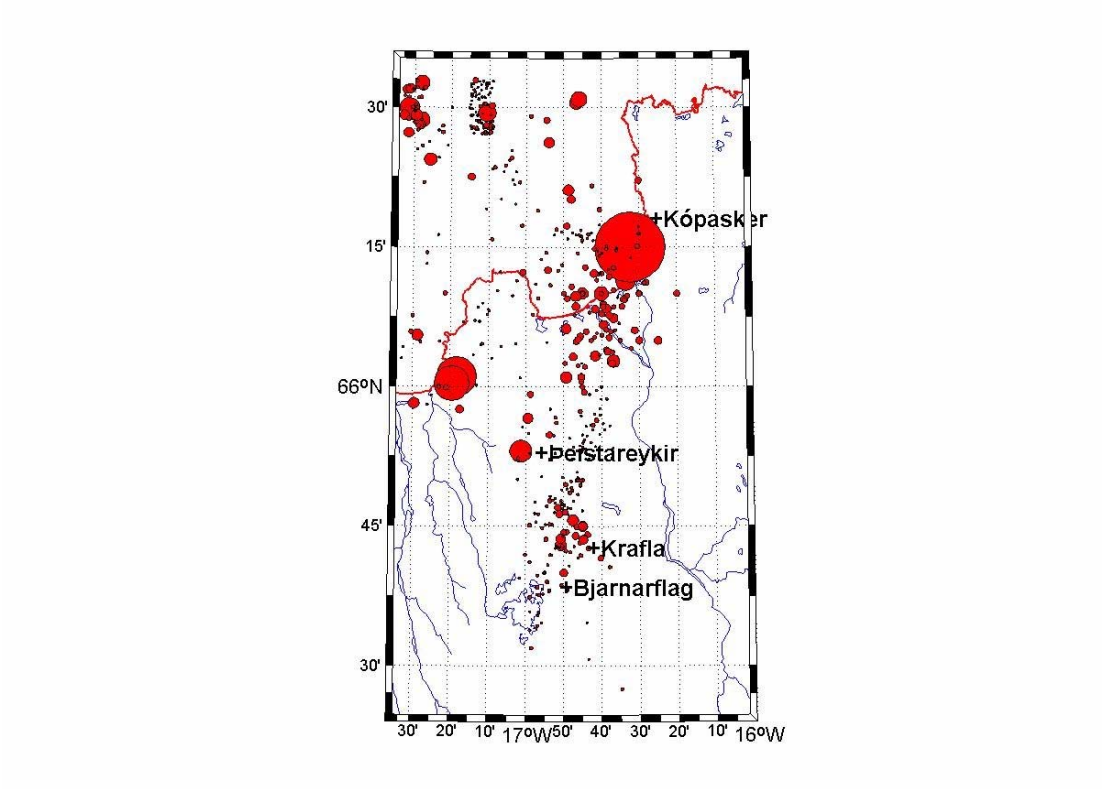

Figure 4.3 Measured earthquakes ($M \geq 3$) in the region from 1930 to 2000.

The 1976 Kópasker earthquake was associated with the Krafla rifting episode, which spanned 1975 to 1989. The seismic moment of the 1976 earthquake was equal to the total moment of the subsequent earthquake swarms between Axarfjördur and Krafla (Ragnar Stefánsson, pers. comm.). Two other earthquakes in Axarfjördur are known, one in 1618, the other in 1885. There is no evidence of volcanic activity at the Gjástykki Krafla area at the same time.

4.2 Activity on the Húsavík-Flatey Fault

Seismic hazards in the region are due primarily to large earthquakes on the Húsavík-Flatey fault (HFF). This northwest-striking system of faults adjoins the Theistareykir fissure swarm in the east and the Kolbeinsey Ridge in the west. Before 1755, only one damaging earthquake is known on the HFF. It occurred in 1260 and is described in medieval annals from the region as a "great earthquake in Flatey".

In 1755 an earthquake took place on the HFF, with an epicentre somewhere between Flatey and Húsavík. Its magnitude has been estimated at 7 on the Richter scale, and the intensity of the earthquake in Húsavík could have exceeded VIII on the Modified Mercalli scale. These estimations are based on felt intensities. Note that the 1755 event represents the highest calculated intensity in the previous table. At Theistareykir, the intensity of the 1755 earthquake would have been ~7, with a corresponding ground acceleration of 7% g.

The next sequence of earthquakes on the HFF began in 1867 with an earthquake that possibly originated near to Höskuldsvatn lake, east of Húsavík. The magnitude of this earthquake has been estimated at 5.5 – 6 on the Richter scale. In 1872 two large earthquakes occurred in the Skjálfandaflói bay. Both earthquakes were approximated at magnitude 6.5 on the Richter scale – the first sourced just north of Húsavík and the second close to Flatey. Both earthquakes caused widespread damage in Húsavík and the surrounding area. The intensity of the first event in the Húsavík area is thought to have exceeded VIII on the Mercalli scale (Halldórsson, 2005).

Since 1927, 9 earthquakes ≥ 4 on the Richter scale have been detected within the HFF region. They are as follows:

1927 M = 4.1 Location; Reykjaheidi
1940 M = 4.5 Location uncertain; possibly west of Theistareykir, intensity in Húsavík III
1940 M = 5.2 Location uncertain; possibly west of Theistareykir, intensity in Húsavík VI
1944 M = 5.6 Location near Húsavík, intensity there VI
1944 M = 5.7 Location near Húsavík, intensity there VI
1944 M = 4.6 Location near Húsavík, intensity there VI
1958 M = 4.6 Location between Húsavík and Flatey
1972 M = 4.3 Location near Húsavík, intensity there IV
1973 M = 4.0 Location near Húsavík, intensity there IV

Since 1872 no major earthquake has occurred on the HFF, however, a notable earthquake sequence persisted in the region from 1940 to 1944, with the largest earthquake measuring M 5.6 on the Richter scale. The first two events were sourced from the eastern part of the fault, but their location is considered inaccurate. Since 1973 no earthquakes exceeding magnitude 4 have occurred on the fault. Figures 4.1 and 4.4 also reveals low seismicity on the eastern part of the fault since 1994.

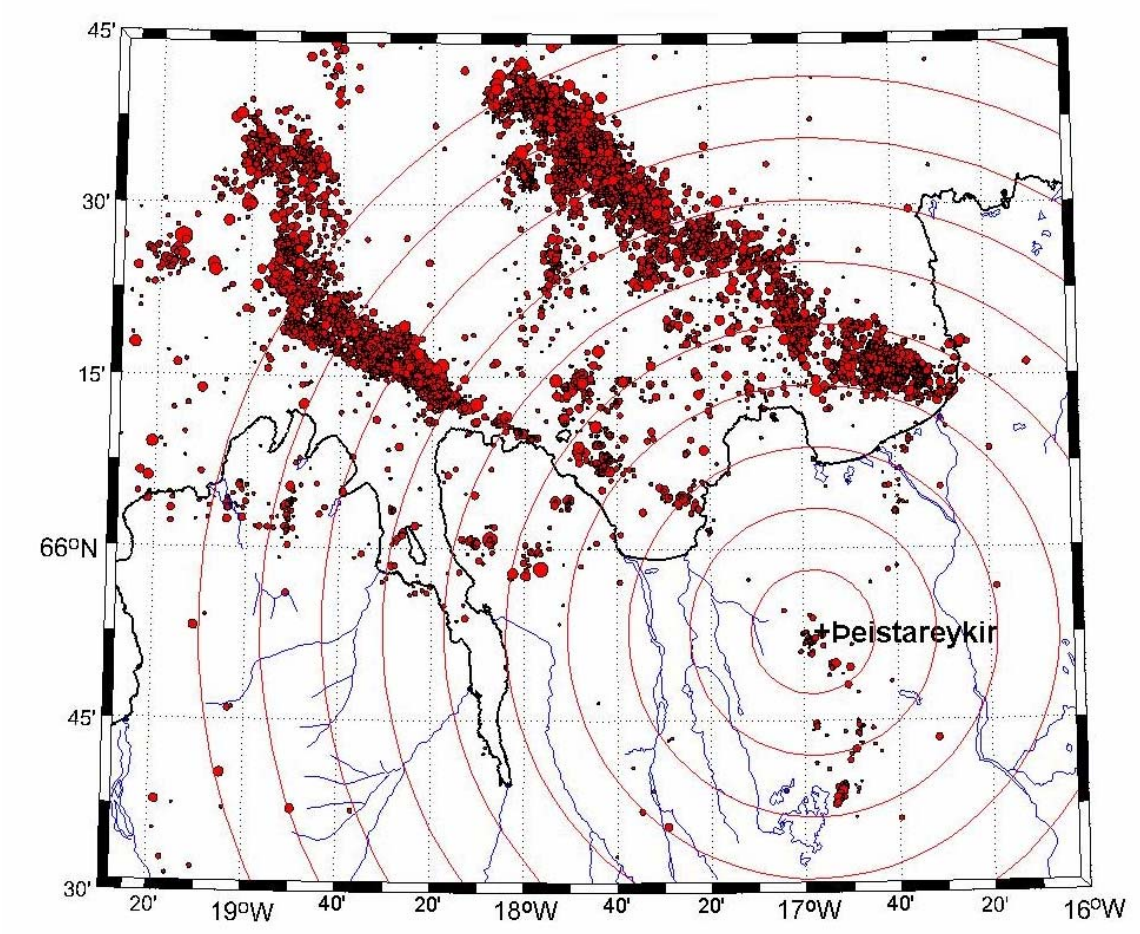

Figure 4.4 Activity since 1994, M ≥ 1.5. The concentric circles show the distance to Theistareykir at 10 km intervals.

From 1999 a continuous GPS system (CGPS) has been operated in the Tjörnes Fracture Zone (TFZ). Its purpose is to monitor crustal movements and to provide more detailed insight into the controls on seismic activity in Iceland. Between 2001 and 2006 the CGPS measurements show a steady ESE drift of Raufarhofn relative to Akureyri by 18 mm a year, but at Tjörnes the drift rate is only 8 mm per year relative to Akureyri. This indicates that 60% of the present drift is occurring across the Grímsey fault and 40% across the Dalvík and Húsavík – Flatey faults (Geirsson et al., 2006). It is not known whether this drift is occurring as aseismic slip on the faults or whether stress is accumulating on locked faults. Given that the present-day seismicity

does not indicate aseismic slip, 10 additional CGPS stations were installed in the Tjörnes fracture zone in September 2006 to help elucidate whether the HFF fault system is locked or not.

It is also possible that, following the 1975 – 1989 rifting episode in the Krafla area, aseismic movements on the HFF might have released accumulated stresses in the region. However this view is in contrast to the 1724 – 1746 Mývatnseldar rifting episode, which was followed 9 years later by a major earthquake (M ≈ 7) on the HFF.

Assuming that the HFF is locked and the accumulated moment can be estimated, the moment rate is:

$$\frac{\Delta M_o}{\Delta t} = \mu A \nu$$

Where A is the rupture area, for the whole fault (assumed as 10 x 100 = 1000 km^2), rigidity μ = 30 GPa and drift rate ν = 8 mm per year. Then the rate of moment accumulation is 2.4 x 10^{17} Nm per year. Therefore, the accumulated moment since 1872 is 3.1 x 10^{19} Nm. If this energy were released in one earthquake, the corresponding moment magnitude (M_w) would be 6.9 and the Ms would be the same if the stress drop is 3 MPa.

As mentioned earlier, the HFF boarders the Theistareykir fissure swarm. It is plausible to assume a future earthquake magnitude of 6.5 in the eastern part of the fault with an epicentre near to Höskuldsvatn. Table 4.1 summarises the effects of a 6.5 earthquake at the power plants sites.

4.3 Expected earthquake activity in the vicinity of power plants and sub-stations

Figure 4.4 shows the surroundings of the study region and the seismicity levels in the period 1990 to 2005. The minimum magnitude of completeness is 1.2. During the last 15 years it is clear that low levels of seismicity have persisted at the power plant sites.

The b-value is the relation between earthquake size and the frequency of occurrence, which is represented by:

$$\log N = a - bM$$

where N is the number of earthquakes ≥ M. The maximum likelihood estimate of b is

$$b = 0.4343/(M_m - M_{min}) \pm 1.96b/\sqrt{n} \text{ - for 95\% confidence}$$

were M_m is mean magnitude for all events with magnitudes above or equal M_{min}, and n is the number of events (Aki, 1965). The error assessment is based on the assumption of no uncertainty

in M_m. Figure 4.5 shows the number of measured earthquakes since 1930. The location of these events is shown in Figure 4.6.

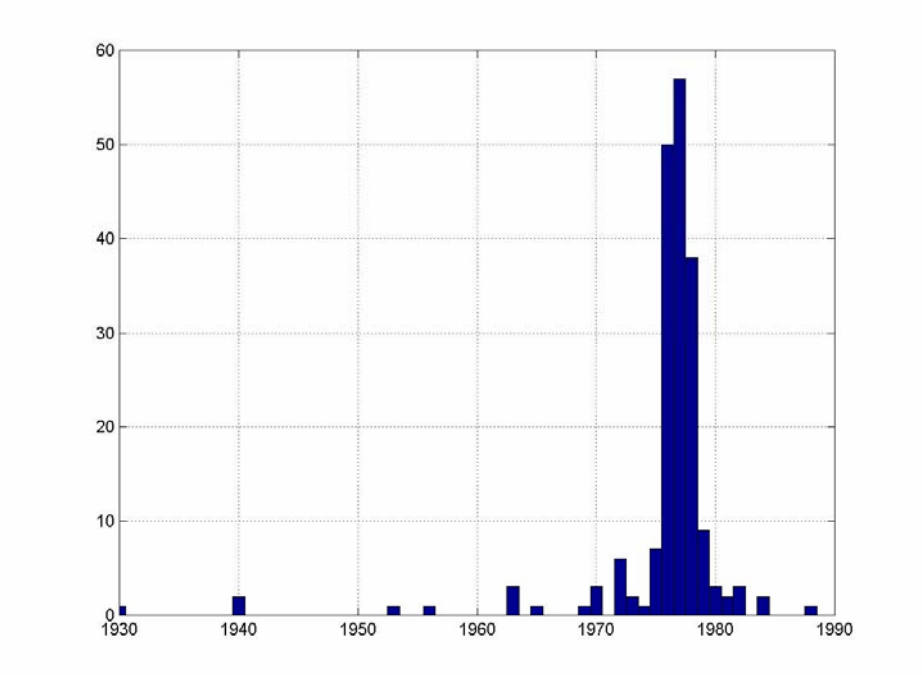

Figure 4.5 Number of measured earthquakes in the area shown in Figure 4.6.

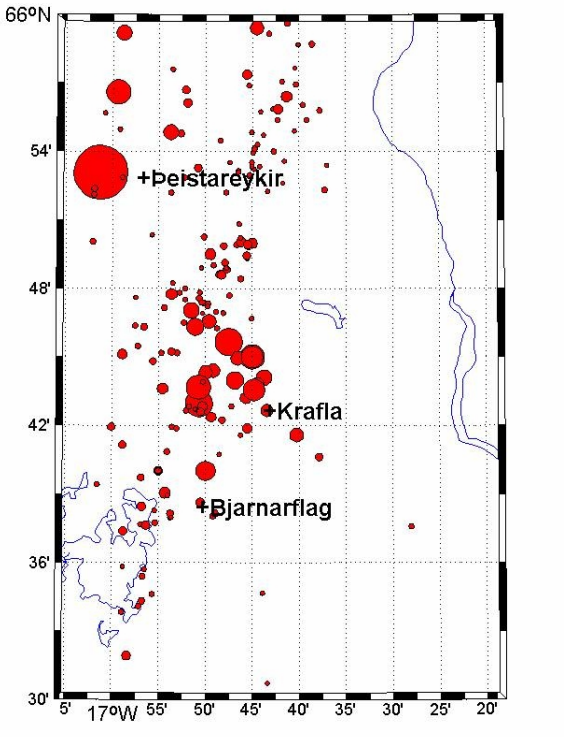

Figure 4.6 Measured events (M ≥ 3) since 1930.

The largest event (M = 5.2) was located just west of Theistareykir on 12 January 1940. As mentioned before, the location of this event is inaccurate and its foci could be in Skjálfandaflói. For the interval 1940 – 1963, 20 earthquakes ≥ 3 are known to have occurred in the region. The detection level for earthquakes in the area before 1964 was above 4.5, meaning that an accurate b-value for this period cannot be derived.

In the period 1964 to 1973, 97 events ≥ 2 were detected in the area. The maximum magnitude was 4.1 and the mean magnitude 2.49. Consequently, b = 0.89 ± 0.18 (Figure 4.7).

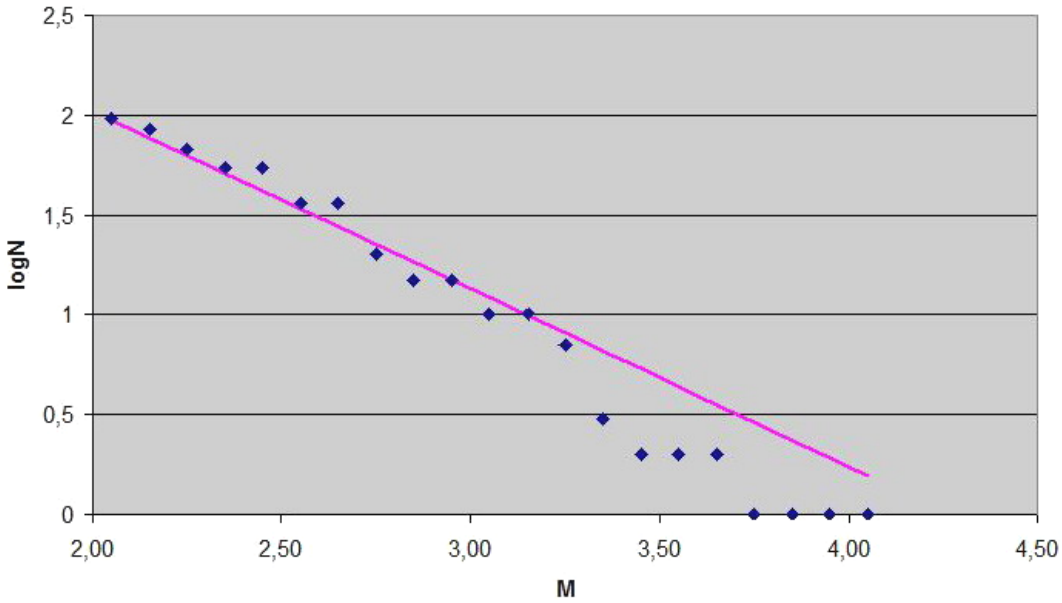

Figure 4.7 Frequency versus magnitude for the period 1964 to 1973, M ≥ 2.

In March 1974, increased seismicity was observed in the area and, in December 1974, the Krafla fires began. During the rifting episode an additional seismic network was operated in the area. Homogenous data exist to magnitude 3 during the rifting period (Figure 4.8).

The largest earthquake had a magnitude of 4.6 and it occurred on 16 January 1976. This event belongs to the aftershock sequence of the Kópasker earthquake that happened on 13 January 1976. From 1975 to 1990, 172 earthquakes with M ≥ 3.0 were observed in the area. The mean magnitude was 3.37, giving a b-value of 1.17 ± 0.17. Note that the b-value is significantly higher in the period 1975 to 1990 than in the previous period (Figure 4.9).

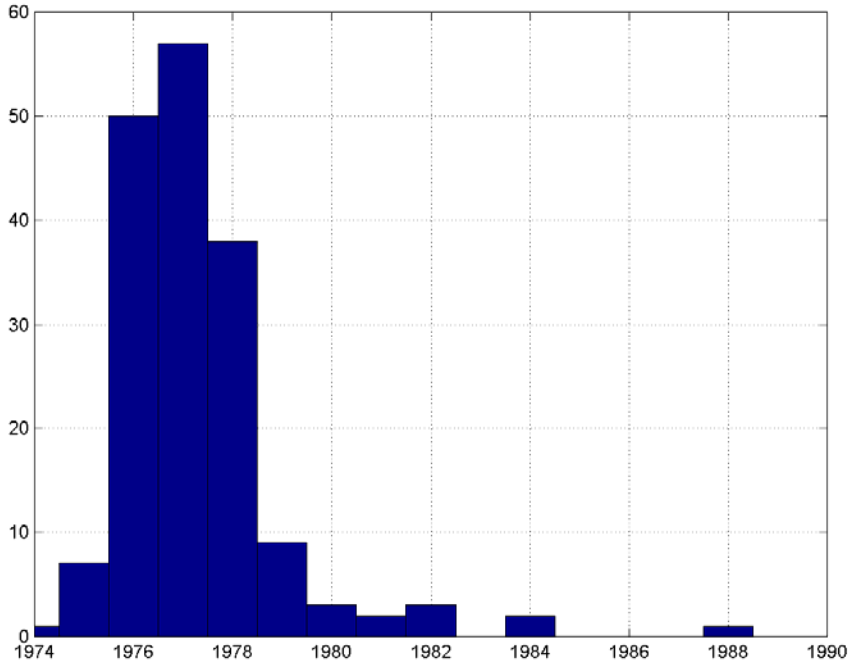

Figure 4.8 Number of events (M > 3) 1974-1990.

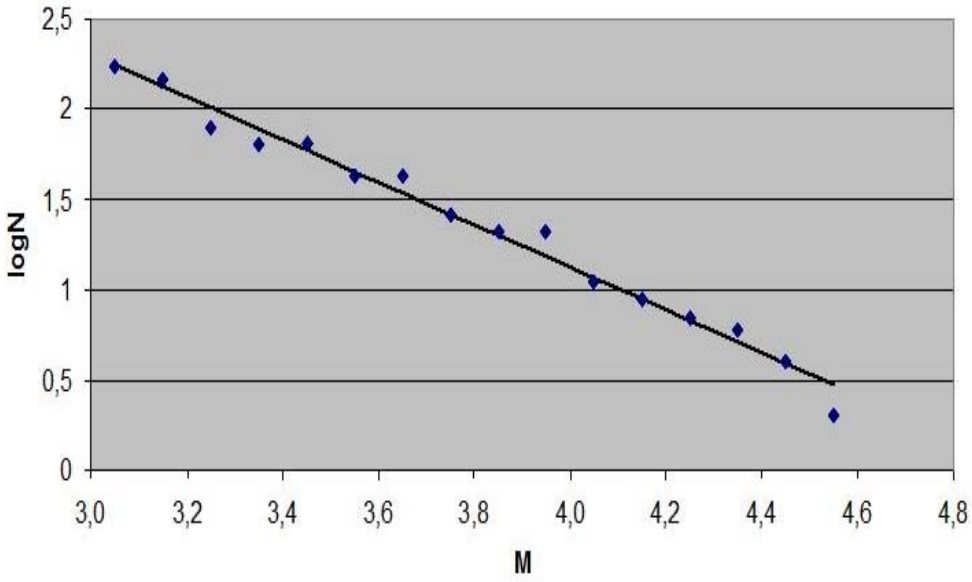

Figure 4.9 Frequency versus magnitude for the period 1974 to 1990, M ≥ 3.0.

In northern Iceland, the SIL seismic monitoring system has been in operation since 1994 (Stefánsson et al., 1993). During this period, seismic activity within the region has remained low, with the largest earthquake registering 2.6 on the Richter scale. A complete catalogue exists for earthquakes exceeding magnitude 1.2.

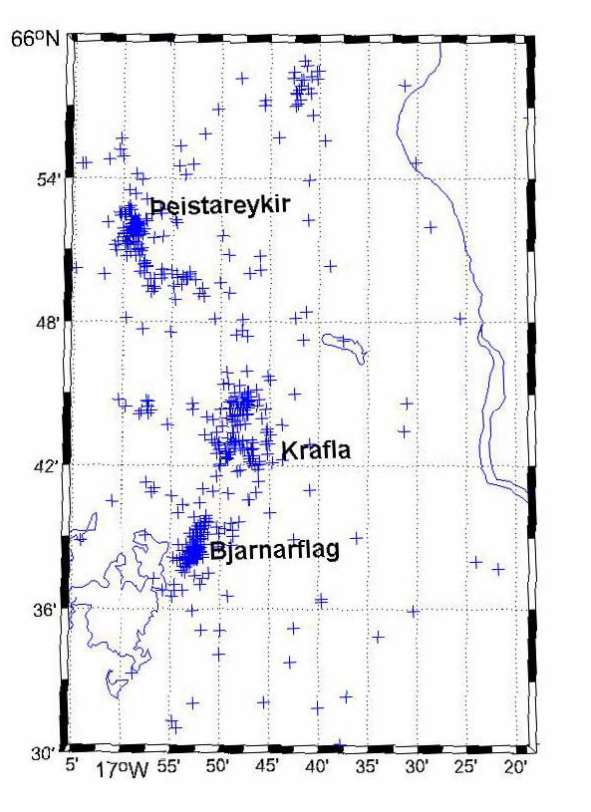

Figure 4.10 Locations of events ≥ 1.2 since 1994.

Within the period of the SIL seismic network, 116 events with a magnitude above 1.2 have been detected in the area, yielding a b-value of 1.21 ± 0.22.

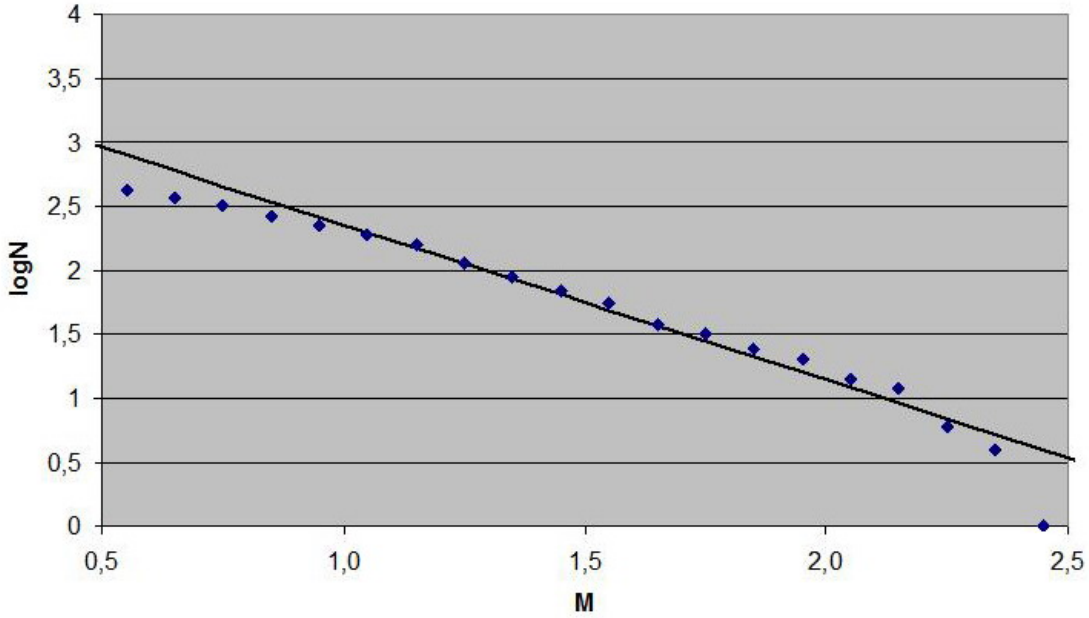

Figure 4.11 Frequency versus magnitude for the period 1994 to 2006, M ≥ 1.2.

Earthquakes hazards are commonly estimated using b-values. It is based on the assumption that the value is stable. However, many studies have demonstrated variations in the b-value over time. And in the area around the vicinity of the possible power plants, we have observed a significant change between the periods before and after 1975, from b ≈ 0.9 ± 0.2 to b ≈ 1.2 ± 0.2. A plausible explanation for high b-values is a weak crust that is incapable of sustaining high strain and heterogeneous stresses. The lower b-value before the last rifting episode indicates that the crust has stabilized during the 200 years since the 1724 – 1746 rifting episode.

Therefore, in the following decades, a b-value of 1.0 is a conservative value for hazard estimation in the area. Consequently, the probability of a magnitude 5 earthquake is considered to be low.

5. Earthquake Action

Jónas Thór Snaebjörnsson and Ragnar Sigbjörnsson
Earthquake Engineering Research Centre, University of Iceland

5.1 Engineering Analysis of Seismic Hazard

5.1.1 Introduction

The objective of an earthquake engineering hazard analysis is to quantify the magnitude and effects of ground motion due to earthquakes. The ground motion can be described by the intensity of the earthquake, displacement, velocity or acceleration of the seismic wave at the site. Seismic hazard is determined by the following three factors:

- The temporal and spatial distribution of the regional seismicity
- The attenuation of seismic waves radiating from an earthquake source
- The effects of the shallow geology in the distortion of the seismic motion

The hazard can be estimated using deterministic or probabilistic methods. In the first method known as deterministic hazard analysis (DSHA), ground motion is estimated from a given set of seismological parameters, such as earthquake magnitude and the distance from the earthquake rupture zone to the site of interest. On the other hand, probabilistic hazard analysis (PSHA) entails assessing the probability of exceeding a prescribed level of ground motion, for example peak ground acceleration (PGA), at a site during a specific time interval, such as 50 years. The analysis must incorporate the inherent uncertainty of the magnitude, location and time of occurrence of future earthquakes as well as the attenuation of seismic waves as they propagate from all the defined sources to the site.

The following sections will discuss the above-mentioned elements of engineering seismic hazard analysis. A short review of the seismic sources involved and the applied earthquake catalogue is given in section 5.1 along with a discussion of Icelandic attenuation characteristics. Models for estimating earthquake motion are briefly discussed in section 5.2 and the regression models applied in this study introduced. The fundamentals of the probabilistic seismic hazard analysis are presented in section 5.3. The corresponding design specifications suggested are given in section 5.5, along with comments emphasising the importance of a conceptual design approach.

5.1.2 Overview of structures and the related hazard

In general, the overall seismic performance of power generating stations has been good. In Iceland, however, it should be noted that such facilities have had limited exposure. One of the most common disturbances in the operation of generating stations has been due to switchyard

and substation damage that has forced them offline and getting them back online has sometimes been a delayed process.

The following main components of a geothermal power plant system are all, to some extent vulnerable to earthquake effects and ground movement:

- Production wells
- Pipe lines (insulated steel pipes ~1 m in diameter)
- Steam separators (~ 10 m high, ~500 m^2)
- Cooling towers (~15 m high, 1000 m^2)
- Power houses (access and control halls, turbine halls made of concrete shear walls and/or steel frames, ~10 m high)
- Substations
- Transmission/power lines

Krafla power station, which has now been in operation for about 30 years, is a good example of a geothermal power plant, such as those currently being planned. Figures 5.1, 5.2 and 5.3 show the structures present at the Krafla site as well as their arrangement.

Figure 5.1 Krafla geothermal power station.

Production wells (boreholes)

The availability of geothermal energy is commonly linked to fracture zones caused by earthquake or volcanic activity. It stands to reason that production wells may be affected by ground movements. Partial collapse that may block the wells is a possibility. However, seismic action is not known to have damaged production wells in Iceland severely, except on one occasion when a fracture passed through a well in Bjarnarflag in the Krafla fires. However, volcanic action did damage wells located inside the central graben during the Krafla fires (see Chapter 1).

Temporary disturbance in production is known to happen after seismic events, mainly due to pressure changes within the rock mass that may cause water levels to rise or fall, especially in low temperature geothermal areas. These disturbances are usually reversed in few weeks or months, but in general, increased fracturing and opening of old fractures appear to improve geothermal activity in the long run. It is worth noting that only one production well was permanently damage during the South Iceland earthquakes in June 2000.

Figure 5.2 Krafla geothermal power station, turbine hall.

Pipelines

Seismic consideration should be given to all pipe installations. However, the cost of implementation and system maintenance should be compared against consequences of system failure.

Pipelines are affected by differential motion due to wave propagation and permanent ground deformation, e.g. induced by lateral spread, settlement and fault rupture.

In Iceland, pipelines have been damaged in earthquakes but mainly those that are buried, and especially those made of asbestos or concrete. Pipelines typical for geothermal areas in Iceland have not been damaged, but have also not been severely tested.

Pipeline performance in earthquakes is a function of the pipe material and the properties joints as well as the earthquake action. The key pipeline performance parameters are: *ruggedness* of the material (strength, ductility); *resistance to bending failure* of the pipe body; *joint flexibility* ensuring the pipes ability to extend, compress or bend around a joint; and *joint restraint* making the pipe-joint system hold together in extension.

A variety of methods are available to mitigate seismic damage to pipelines. These include:

- Avoiding or rerouting pipes around areas particularly susceptible to damaging ground movements
- Various methods to isolate the pipeline from ground movements or reduce the effects of ground movement
- High strength and/or high ductility materials for the pipelines themselves
- The use of joints with enhanced expansion/contraction or rotation capability
- Include bends in the pipeline at regular intervals to increase its overall flexibility

Buildings (steam separators, cooling towers, power houses)

The steam separator station, the cooling towers and the power house can be categorised as building type structures. They will cover a considerable area (500-1000 m^2) and will generally have a height in the range 10 to 15 m. They are susceptible to earthquake actions in the same way as every building would be and should be appropriately designed to account for seismic excitation. These structures will have a load bearing system of either reinforced concrete shear walls or steel frames. Their vulnerability will vary depending, not the least, on appendages such as pipelines, power cables, towers, chimneys etc. Similarly, building halls with tall walls, which offer limited possibilities of lateral support, such as the turbine halls, are often susceptible to lateral force effects caused by earthquake motion and require careful design.

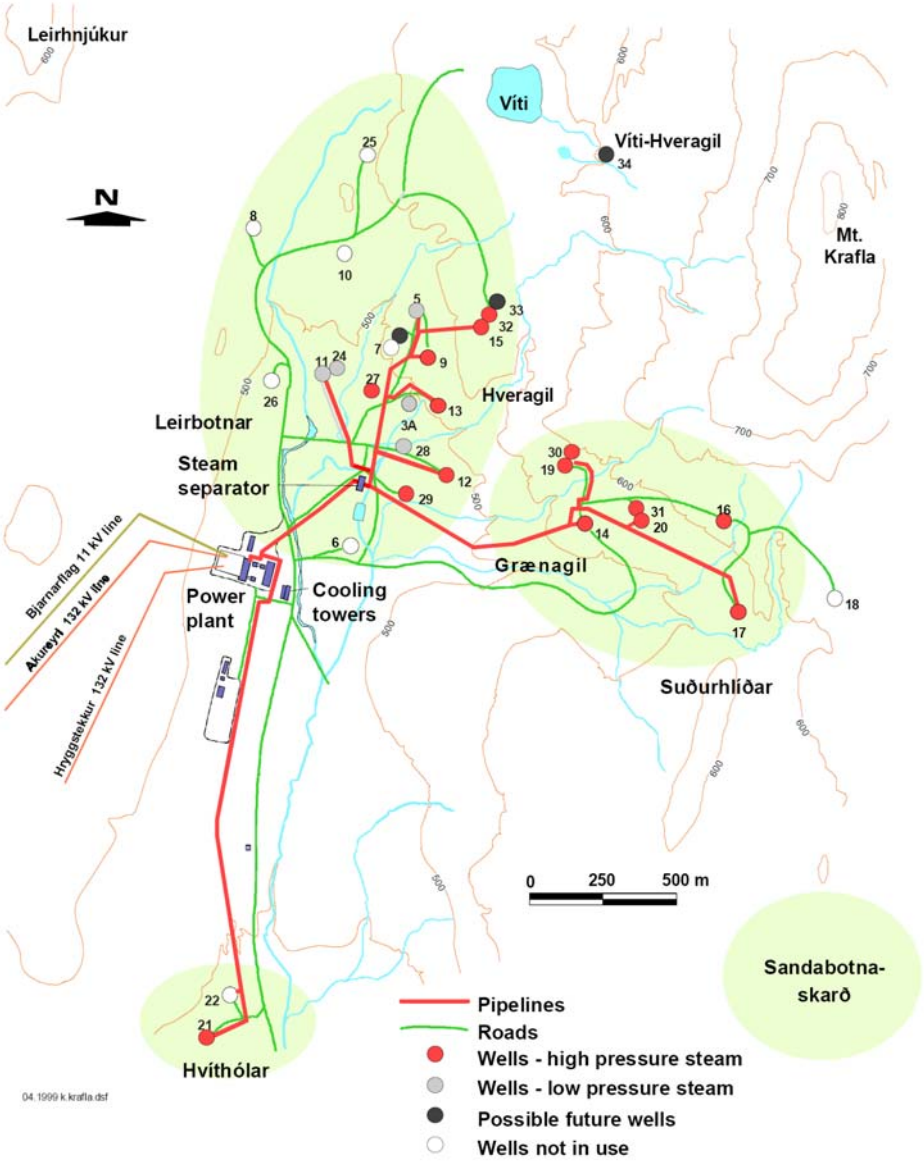

Figure 5.3 Schematic map of the Krafla geothermal power plant and the surrounding area.

Substations

Damage to porcelain elements of high-voltage substation equipment has been a recurring problem in earthquakes worldwide. It can often be attributed to equipment vulnerability and lack of slack in conductors connecting the equipment, which is often aggravated by flexible equipment supports that allow large relative displacements. Damage to transformers and related equipment is also common, often due to insufficient anchorage. There is, in general, a difference in equipment vulnerability depending on the operating voltage. Generally, the higher the operating voltage, the more vulnerable is the equipment.

In Iceland substation damage, has not been a problem so far, most likely because no substation has yet been tested by severe earthquake excitation.

It should be noted in this context, that the proposed substations will be indoor facilities. Indoor facilities generally have better seismic resistance than outdoor facilities and the equipment will be protected from the adverse impact of the environment.

Transmission lines

Transmission lines have, historically, been resilient to earthquake damage. Their main vulnerability seems to be foundation failure of transmission towers or the loss of a tower due to landslides. It appears that the low natural frequencies of the lines decouple their mass from the high energy content of earthquakes. Furthermore, their design loads for wind, ice and longitudinal load combinations ensures adequate reserve strength for earthquakes. However, in the 1999 Chi-Chi Taiwan earthquake, many transmission towers were damaged (Lee and Hsieh 2002), mainly due to ground failures and landslides, causing long-term blackouts in Taipei, which otherwise experienced minor damage.

The South Iceland Earthquakes in June 2000 caused some damage to transmission lines in the epicentral area. In all cases that damage was primarily related to towers located on soft ground. Damage of towers in the Burfellslina 1 transmission line was related to differential settlements of foundation on soft soil. Damage in Burfellslina 2 and 3 transmission lines was in all cases due to loss of tension in the supporting cables. It should be noted, that these damages did not cause disruption in power supply.

5.1.3 Selection of earthquake design criteria

For power plant structures and other industrial or lifeline-type installations it is important to ensure undisturbed operation during common design events, whereas that may not be economically feasible for extreme events. Therefore, it is generally recommended that the following levels of earthquake action should be considered in the design process, i.e. an Operating Base Earthquake for no damage and undisturbed plant operation, a Maximum Design Earthquake for life safety and limited damage and a Maximum Credible Earthquake for collapse prevention checking. These actions are defined as follows:

- ***The Operating Base Earthquake*** (OBE) is defined as an earthquake that can reasonably be expected to occur within the service life of the project, that is, within a 50% probability of exceedance during service life. This corresponds to a return period of 144 years for a project with a service life of 100 years and a return period of 95 years for a project service life of 50 years. The associated performance requirement is that the project functions with little or no damage and without interruption of function. The purpose of the OBE is to protect against economic losses from damage or loss of service. Therefore, based on economic considerations an alternative return period for the OBE may be chosen.

- ***The Maximum Design Earthquake*** (MDE) is defined as the maximum level of ground motion for which a structure is designed or evaluated. The associated performance requirement is that the project performs without catastrophic failure although significant damage or economic loss may be tolerated.

- ***The Maximum Credible Earthquake*** (MCE) is defined as the greatest earthquake that can reasonably be expected to be generated by a specific source on the basis of geological evidence.

For critical structures, especially in low seismicity zones, it is sometimes required that the MDE be set equal to the MCE. Structures are considered critical if their failure during or following an earthquake could result in loss of life. However, generally the MDE is selected as a less severe event than the MCE, which provides for an economical design meeting specified safety standards. The MDE is chosen based upon an appropriate probability of exceedance of ground motions during the design life of the structure, such as 10% probability of exceedance in 50 to 100 years. This corresponds to a return period of 475 and 950 years, for a project with a service life of 50 and 100 years, respectively.

5.1.4 Hazard modelling

The North Iceland Seismic Zone is a broad region of faulting and seismic activity, which connects the submarine Kolbeinsey Ridge and the volcanic zone in North Iceland at the bay Öxarfjörður. The seismic character of the zone is complex and cannot be associated with a single fault or clearly identified plate boundary. However, based on the geological and geophysical findings displayed by the figures in Chapters 1 through 4, it seems reasonable to associate the seismicity with few hypothetical lines, visualised as seismic delineations. Three parallel WNW trending lines represent the Tjörnes Fracture Zone, and four lines trending NNE represent the main fissure swarms of the Northern Volcanic Zone. These hypothetical lines are drawn on top of the fissure swarms in Figure 5.4.

The first of the WNW trending lines, counting from north-east, is the Grímsey seismic delineation that runs slightly north of the Grímsey island and joins the Krafla fissure swarm in Axarfjördur. There is not a clear trace in the topography. Instead, the surface structure is characterized by northerly-trending troughs and ridges. In some respect this resembles the structure in the South Iceland Seismic Zone where the epicentral belt lacks clear surface manifestation in terms of a single fault.

The second WNW trending seismic delineation runs from Höskuldsvatn, past Húsavík, across Flatey and north of Eyjafjördur. The 1872 magnitude 6½ earthquake originated within this delineation. It caused widespread damage in Húsavík, Flatey and Flateyjardalur.

The third inferred WNW trending seismic delineation runs from Eyjafjördur near Dalvík and to the inlet of Skagafjördur. A magnitude 7 earthquake occurred in the Skagafjördur inlet on this

third delineation in 1963. As is the case with most historic earthquakes in the North Iceland Seismic Zone, the epicentre was off the coast in the ocean and the land intensity therefore low to moderate. The earthquake caused alarm and some damage in the nearby town of Saudárkrókur.

The first NNW trending fissure swarm, from west to east, runs through the geothermal area of Theistareykir. The second NNW trending fissure swarm is linked to the Krafla central volcano and runs through the geothermal areas of Krafla, Gjástykki and Bjarnarflag. The third NNW trending fissure swarm runs through the geothermal area at Fremri Námar and the fourth NNW trending fissure swarm is linked to the Askja central volcano. This last seismic delineation is unlikely to have significant influences on the hazard at the four plant sites studied, but is included for the sake of completeness.

The characterisation of seismic sources involves quantification of three basic parameters:

- Geometry and location of the source (or fault), (where do earthquakes occur?)
- Rate of earthquake recurrence (how often do earthquakes occur?)
- Maximum magnitude (how big can we expect theses earthquakes to be?)

Earthquake catalogues are the fundamental database used to determine where, how often and how big earthquakes are likely to be. Unfortunately the related statistics are generally based on geologically short catalogues. Therefore, the information from seismic monitoring, historic records, geodetic monitoring, and geological records are combined to characterise seismic sources. These data, when available, are used in a physical interpretation of seismic source zones. Because different interpretations of the input data are possible, large uncertainties are often associated with source characterisation.

A Parametric Earthquake Catalogue for Iceland has been compiled by Ambraseys and Sigbjörnsson (2000) using public domain teleseismic data. The study area is defined as the area between the latitudes 62°N and 68°N and the longitudes 12°W and 26°W. The time period spanned by the catalogue is one century, i.e. from 1896 to 1996. The selection of the starting year for the catalogue was based on the fact that the first earthquake in Iceland for which there is available instrumental data was the destructive 1896 South Iceland earthquake. The magnitude scale applied is the surface-wave magnitude scale. The total number of events in the compiled catalogue is 422, including 276 events with a recalculated surface-wave magnitude.

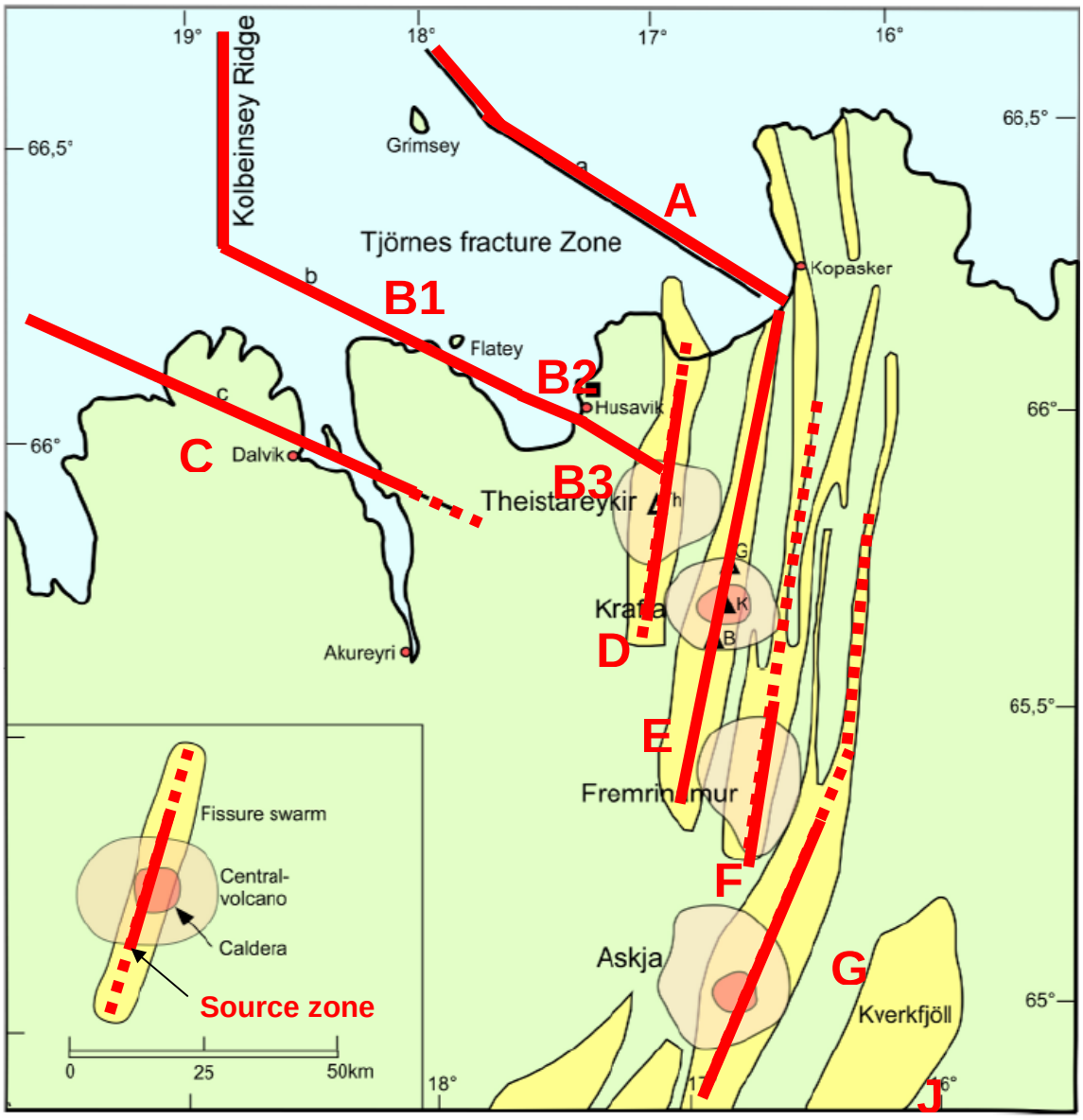

Figure 5.4 The seismic source zones and lineaments applied in probabilistic seismic hazard analysis. This figure is based on Figure 1.5 in Section 1.3 and the figures in Section 4. The solid red lines indicate seismic source zones producing earthquakes with magnitude greater than or equal to 4 and the dotted lines refer to source zones where event magnitude does not exceed 4. Legend: **A** – The Grímsey Island lineament, M_{max} = 7.3; **B** – The Flatey Island lineament: B1 – strike-slip earthquakes, M_{max} = 7.3, B2 – strike-slip faulting earthquakes, M_{max} = 7.3, B3 – oblique faulting earthquakes, M_{max} = 6.5; **C** – The Dalvík lineament, strike-slip earthquakes, M_{max} = 7.3; **D** – The Krafla zone, normal faulting earthquakes, M_{max} = 5.5; **E** – The Theistareykir zone, normal faulting earthquakes, M_{max} = 5.5; **F** – The Fremri-Námur zone, normal faulting earthquakes, M_{max} = 5.5; **G** – The Askja zone, normal faulting earthquakes, M_{max} = 5.5; **J** – Kverkfjöll Mountain zone.

The geographical distribution of earthquakes is shown in Figure 5.5, including all events. The circles denote earthquake epicentres applying an extended colour code as well as the size of the circles to visualise the earthquake magnitude.

The catalogue can be regarded as complete during the whole period for events with magnitudes roughly exceeding magnitude 4½, which is normally considered satisfactory for engineering hazard assessment. Furthermore, the catalogue seems to cover the main earthquake areas fairly well.

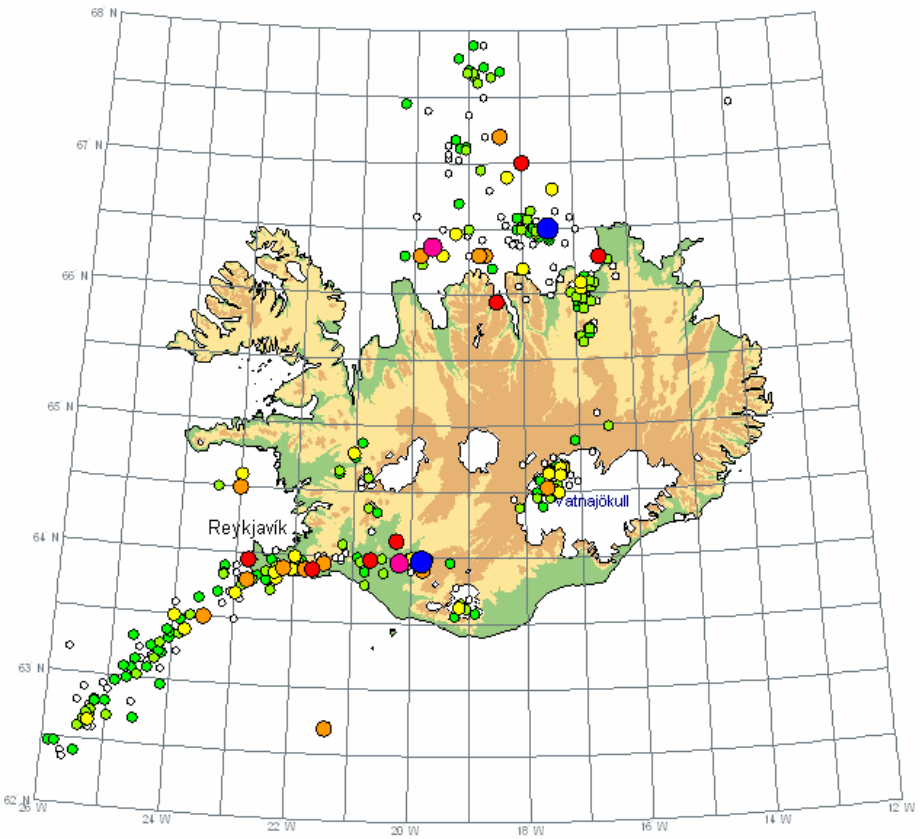

Figure 5.5 **Spatial distribution of earthquake epicentres in the Parametric Earthquake Catalogue for Iceland for the period 1896 to 1996 (Ambraseys and Sigbjörnsson, 2000). The following colour code is used: blue – $M_W \in [7.0; 7.5]$; purple – $M_W \in [6.5; 7.0]$; red – $M_W \in [6.0; 6.5]$; orange – $M_W \in [5.5; 6.0]$; yellow – $M_W \in [5.0; 5.5]$; yellow-green – $M_W \in [4.5; 5.5]$; green – $M_W \in [4.0; 4.5]$; white – $M_W \in [3.0; 4.0]$ or undefined.**

The activity of each source zone is described by frequency-magnitude occurrence relationship. The rate of recurrence of earthquakes on a seismic source is assumed to follow the Gutenberg-Richter relation. To characterise each source zone, the following parameters are evaluated:

- M_{max} and M_{min}, the upper and lower bound magnitude, related to the tectonic setting, geometry, and type of the seismic source
- The Gutenberg-Richter earthquake recurrence parameter (b-value)
- The activity rate, a_n, i.e. the number of event within a given reference period having magnitudes equal to or greater than M_{min} on the source
- The average hypocentral depth
- Style-of-faulting

It is clear that the presented parametric earthquake catalogue contains different types of earthquakes occurring within the study area. For instance, it is obvious that the catalogue contains earthquakes related to volcanic activity as well as earthquakes of more direct tectonic origin from at least three fault zones.

The assumed upper bound of magnitude is taken as 7.3 for Zone A, B1, B2 and C in accordance with the estimation for Iceland as a whole (Ambraseys and Sigbjörnsson, 2000). The style-of-faulting for these zones is assumed as strike-slip. The b-values for these zones are taken as equal to 0.7 which is in fair accordance with available data. The assumed average upper bound of magnitude for Zones D, E, F, G and J is taken equal to 5.5, which conforms to available data. The b-values are in all cases taken equal to 1, which is in fair accordance with Chapter 4. The seismic activity in these zones is assumed to be dominated by normal faulting earthquakes. The Zone B3 is of special interest in this study. Unfortunately, this is an area where reliable seismic information is not available. Tentatively, the upper bound of magnitude is taken as 6.5 and the b-value equal to 0.7. The style of faulting is taken as oblique. The lower bound of the magnitudes considered in the hazard analysis is in all cases equal to 4. The activity rate is an uncertain parameter assessed tentatively for each zone in such a way that the overall number of earthquakes fit the available data. The earthquakes are in all cases characterised as shallow. The depth parameter is based on statistical analysis and the results applied as overall values for the identified zones (see Section 5.2.2).

A secondary type of conceivable ground motion in the vicinity of the proposed power plant sites are volcanic tremors. Volcanic tremor is a sustained seismic motion which is observed at active volcanoes during either quiescent or eruptive stages. It is a continuous rhythmic ground vibration of low amplitude, generated by magma moving underground. This type of motion is not known to have damaging effects on structures and is therefore not considered further herein.

5.1.5 Ground motion estimiation modelling

Estimates of expected ground motion at a given distance-to-fault induced by an earthquake of a given magnitude are the second basic element of earthquake hazard assessments. These estimates are usually equations, referred to as ground motion estimation equations or attenuation relationships. They express the expected ground motion as a function of source-to-site distance for a given magnitude (and occasionally other variables, such as style of faulting and site conditions). Ground motion estimation relationships may be determined in two different ways: empirically, using previously recorded ground motions; and theoretically, using seismological models, which account for the source, site and path effects. However, there is an overlap in these approaches, since empirical approaches fit the data to a functional form suggested by theory and theoretical approaches often use empirical data to determine the key parameters.

The ground motion at a given site depends on the earthquake source, the seismic wave path and the site response. Earthquake source signifies the earthquake magnitude, the depth and the focal mechanism, the wave propagation depends mainly on material properties of the wave path as well

as the length of the wave path from source-to-site. The site response deals with the local geology commonly in terms of simplified site classification, e.g. hard rock, firm soil, etc., where the ranking is usually expressed in terms of shear wave velocity at shallow depth. Hazard values calculated for rock/stiff soil sites (the most common site classifications in Iceland) are lower than hazard values calculated for soft soil sites.

Earthquake effects attenuate rather rapidly in Iceland. This is a well-established property of Icelandic earthquakes and is believed to be related to the geological properties of the Icelandic crust and the characteristics of Icelandic earthquakes. The crust is relatively young in geological terms, heterogeneous and cracked. This results in higher anelastic attenuation than found in continental crust. The largest earthquakes in Iceland originating in the North and South Iceland fracture zones are characterised as shallow strike-slip earthquakes with a vertical fault plane rupturing to the surface for moderate sized events. In a narrow near source zone the peak ground acceleration (PGA) is roughly constant for a given event. For a magnitude 6½ event the size of this near source zone is limited to an area stretching 5 to 6 km from the surface trace of the causative fault. In the intermediate field the attenuation is faster than in the far field, where it is found to be inversely proportional to the source distance. For the above-mentioned moderate sized event the horizontal PGA has attenuated down to approximately 15% g at a 15 km distance from the surface trace of the causative fault (Sigbjörnsson and Ólafsson, 2004). This scenario is presented here as an approximation to the seismic events in the vicinity of the proposed power plant at Theistareykir.

5.2 Earthquake strong-motion estimation models

The term ‘strong-motion estimation model’ refers both to the ground motion estimation model mentioned above as well as to an earthquake response spectrum estimation model. They can be used to obtain characteristic quantities like peak ground acceleration and response spectrum acceleration. The methods and models outlined in this chapter are the basis for the probabilistic seismic analysis presented in the following section.

The ground motion estimation models, often referred to as attenuation models or attenuation laws, are used to obtain values for quantities used to describe the ground motion at a given site induced by earthquakes in a surrounding seismogenic region. These models can be divided into two main classes. Firstly, there are theoretical models, which are derived using the basic principles of mechanics. Secondly, there are models derived using regression analysis, which in principle consist of fitting an optimal model to a predefined strong-motion data set.

Strong-motion estimation models derived by regression analysis are more common in engineering applications than the theoretical models. A comprehensive overview of the available range of regression type models has been given by Douglas (2003). The reliability of these models depends heavily on the data set applied to derive the model parameters although the functional form is also an important factor.

5.2.1 Theoretical models

Theoretical models are derived using the basic principles of mechanics. There are several different modelling strategies in use, but primarily the modelling approaches can be divided into two categories, i.e. *point source models* and *finite source models*.

The point source model used in the present study is based on the Brune model for seismic shear waves. It was derived by considering the effective stress needed to accelerate the sides of a circular causative fault on which a stress pulse was applied instantaneously (Brune, 1970, 1971). It is commonly used to obtain fault dimensions from spectra of shear waves for small to moderate sized earthquakes (Udias, 1999). The model describes near- and far-field displacement-time functions as well as spectra and includes the effect of fractional stress drop.

The stochastic simulation technique for seismic motion (Boore, 2003) is based on a theoretical spectrum of point source and propagation process. In spite of the success of this method it is also well-known that the point source model has its limitations. The effect of large finite source, including rupture propagation, directivity and source receiver geometry, can profoundly influence the amplitude, frequency and duration of ground motion. A common approach to model these effects is to subdivide the fault into smaller parts, each of which is then treated as a point source (Hartzell, 1978). The ground motion at the observation point is obtained by summing the contribution over all sub-parts of the fault. A basic assumption in the implementation of this approach concerns the manner in which point sources and the effect of propagation are defined (Papageorgiou, 2003).

In view of the seismicity at the study sites, a near-field event large enough to display directivity or fling-step effects is unlikely. Furthermore, considering the uncertainty associated with the available modelling procedures it was not considered feasible to include these effects directly in the ground motion modelling for the study sites in question.

5.2.2 Regression models

In a resent study Ambraseys et al. (2005) derived a new set of regression models for both horizontal and vertical strong motion, which fulfil as far as possible the required model criteria and in addition account for the different faulting mechanism. The applied data is from the ISESD data bank (http://www.ISESD.hi.is, Ambraseys et al. 2002), which is one of the best available sources for strong ground motion data. The data bank contains data from over 12 countries in Europe and the Middle East. Data from the Icelandic Strong-Motion Network is a considerable part of the available data, especially for strike-slip source mechanism. Hence, the seismic environment in Iceland should be fairly well reflected in the Ambraseys strong-motion model.

In the models introduced by Ambraseys et al. (2005) the peak ground acceleration, *PGA*, and response spectrum, S_a, are expressed respectively, as follows:

$$PGA = f_G\left(M_w, d, site\,condition, style\,of\,faulting\right)$$
$$S_a = f_R\left(T_n, M_w, d, site\,condition, style\,of\,faulting\right)$$

Here, d is the distance from site to source, M_w is moment magnitude and T_n is the undamped natural frequency of the structure.

The functional form adopted in the study of Ambraseys et al. (2005) is given as:

$$\log_{10}\left(y\right) = a_1 + a_2 M_w + (a_3 + a_4 M_w)\log_{10}\sqrt{d^2 + a_5^2} + a_6 S_S + a_7 S_A + a_8 F_N + a_9 F_T + a_{10} F_O \qquad (5.1)$$

Here the following notation is used:

$a_1 \ldots a_{10}$ are regression coefficients derived using the data set outlined above,
M_w is moment magnitude (≥ 5)
d is source to site distance in km
$S_S = 1$ for soft soil sites and 0 otherwise
$S_A = 1$ for stiff soil sites and 0 otherwise
$F_N = 1$ for normal faulting earthquakes and 0 otherwise
$F_T = 1$ for thrust earthquakes and 0 otherwise
$F_O = 1$ for odd faulting earthquakes and 0 otherwise.

This general form is used both for the peak ground acceleration and the response spectral ordinate for both horizontal and vertical motion. Two different sets of regression coefficients are used to represent each component of acceleration. For the spectral ordinates, one set of parameters is derived for each set of undamped natural periods and critical damping ratios.

It should be noted that no data from western North America is used by Ambraseys et al. (2005) in their derivation of the regression model equations. That decision was, in part, based on the finding of Douglas (2003) that ground motions in Europe and Californian data seem to be different and that this difference is statistically significant. However, when the model was compared with data from the Parkfield earthquake (September 28, 2004) it was found to fit the data reasonably well, thus indicating that the differences in ground motions in western North America and Europe are perhaps not as significant as suggested in the above-mentioned study by Douglas (Ambraseys et al. 2005)

Earlier studies, where available regression models have been applied to Icelandic data have indicated slower attenuation than is characteristic for the Icelandic data (Ólafsson and Sigbjörnsson, 1999). This is also seen to be the case when the Ambraseys et al. (2005) model is compared to data from the June 2000 earthquakes, as well as a theoretical model discussed in Sigbjörnsson and Ólafsson (2004). Similar results are obtained for the response spectrum (Snaebjörnsson et al. 2004). However, a better fit is obtained for the more flexible structures (see Figure 5.6) than for the stiffer ones. A more thorough discussion of the bias can be found in Ambraseys et al. (2005).

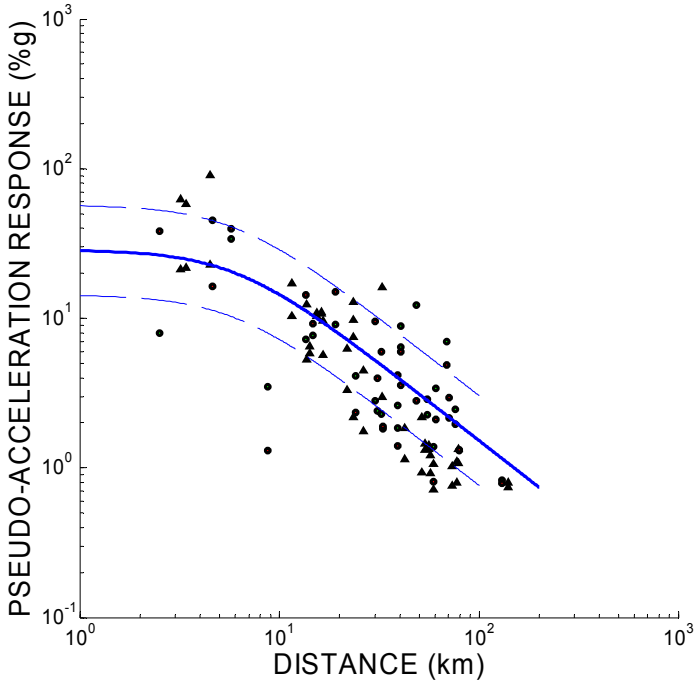

Figure 5.6 Attenuation of linear elastic spectral acceleration response. Comparison of strong-motion estimation models to data. Undamped natural period is 1.0 s and the critical damping ratio is 5%. The blue curve represents the Ambraseys et al. (2005) model and the blue dashed curves represent ± one standard deviation. The circles and triangles represent data from the South Iceland earthquakes on 17 and 21 June 2000.

5.2.3 Duration of ground shaking

The duration of strong shaking is one of the quantities needed in engineering analysis and earthquake resistant design of structures. An estimate of duration is required as an input into probabilistic analysis and therefore needed in connection with the methods discussed in the following chapter of spatial variability as well as for Monte Carlo simulation of time series. Furthermore, the damaging effects of an earthquake are strongly related to the duration of strong shaking. This is especially the case for deterioration of reinforced structural concrete as repeated cycles of seismic action leads to repeated cracking of the concrete and yielding in the reinforcement steel resulting in strength degradation and low cycle fatigue. Duration of strong shaking also plays an important role regarding operational reliability of equipment during earthquakes.

There are several definitions of duration. The most common are bracketed, uniform and significant durations, both absolute and relative. They need to be calculated with user-specified limits, which make direct comparison often difficult. The definitions of the most common ones are given in Ambraseys et al. (2004).

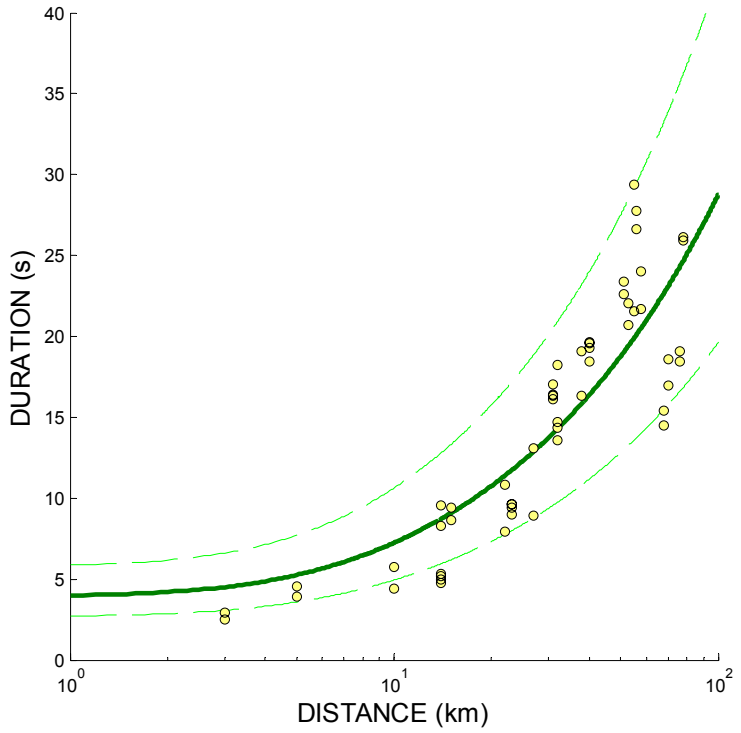

Figure 5.7 Relative significant duration of shallow strike-slip earthquakes. The duration values obtained for the June 2000 South Iceland Earthquakes compared to suggested duration model (solid line). The dashed lines represent the model ± one standard deviation of full dataset.

In cases when duration is used in connection with quantities like peak ground acceleration to model seismic action it is common to use the relative duration measures. In this assessment of duration, the relative significant duration has been applied, which is defined as the time interval between two separate fixed threshold values that are exceeded by the normalised Arias intensity. The relative significant duration appears to represent the S-phase of ground shaking in the near and intermediate fault area reasonably well, but in most cases in our study areas it is the S-waves that create the dominating horizontal seismic action on structures. Hence, it is also found that the relative significant duration of vertical motion tends to be greater than the horizontal motion. The reason is that the P-waves contribute relatively more to the vertical component than the horizontal component of acceleration.

The model suggested for the relative significant duration is given as follows:

$$\log_{10}(duration) = b_1 + b_2 M_w + b_3 \log_{10}\left(\sqrt{d^2 + b_4^2}\right) \tag{5.2}$$

Here, b_1 … b_4 are regression coefficients derived using regression analysis and appropriate data set, M_w is moment magnitude, d is source-to-site distance.

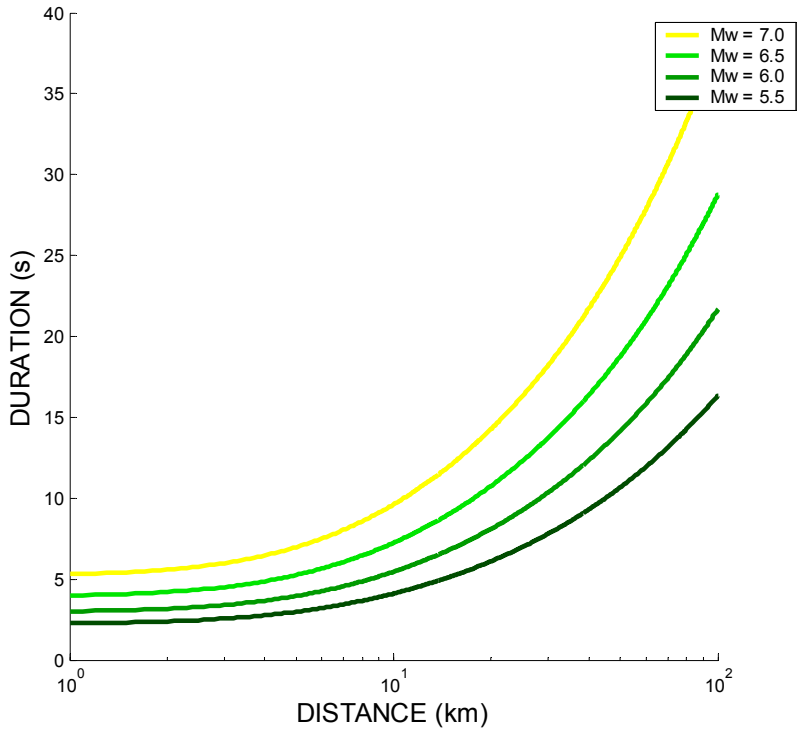

Figure 5.8 Relative significant duration of shallow strike-slip earthquakes with near vertical fault plane. Suggested model representing duration as a function of distance to surface trace of causative fault for different magnitude values.

Applying data from the ISESD databank (Ambraseys et al. 2002), obtained in shallow strike-slip earthquakes from Armenia, Greece, Iceland, Italy, Slovenia and Turkey, the following parameters were obtained: b_1 = -1.3877; b_2 = 0.2451; b_3 = 0.6280; and b_4 = 4.50. The residual error is approximately normal distributed with standard deviation equal to 0.166 (log-scale). These parameters refer to distance in km and duration in s. The resulting curve is shown in Figure 5.7 for magnitude 6.5 earthquake along with data from the South Iceland earthquakes on 17 and 21 June 2000. Here a logarithmic scale is used for the distance to emphasise the near fault area. The dashed lines indicated ± one standard error as obtained from the whole dataset applied. Visually the fit of the model to these data appears reasonable even though the model tends to give longer duration for distances shorter than 10 km than the duration reflected by the data points.

Finally, Figure 5.8 gives the relative significant duration as a function of distance to surface trace of the causative fault for different earthquake magnitude values. It is seen that the relative significant duration in the near fault area is not expected to exceed 10 s on average. However, it is also seen that the uncertainties reflected in the standard error can increase this value significantly. It is found that this increase is almost 50% if one standard deviation is added to the values reflected in the curves of Figure 5.7.

5.2.4 Spatial variation of wave motion

Observations from closely-spaced strong-motion arrays have shown that earthquake ground accelerograms measured at different locations within the dimensions of large scale engineered structures are significantly different. Modifications of common engineering methods have subsequently been developed to include the effect of incoherent ground motion. Furthermore, in current and upcoming code provisions, i.e. Eurocode 8, these effects are addressed, however, without the sufficient detailing needed for practical applications in engineering design (Eurocode 8, 2003). The current engineering practice assumes routinely:

- Excitations at all support points are the same; or
- Excitations are different by only a wave propagation time delay, i.e., excitations at all locations are assumed to be fully *coherent*.

The first approximation, (a), is a good one for structures with small horizontal dimensions at the structure-ground interface. The second approximation, (b), is valid for horizontal structures with large dimensions. However, this approach is oversimplified as the incoherence in ground motion is missing, which may lead to incorrect or inaccurate results.

An improved model should include all main effects governing the spatial structure of strong ground motion. These can be summarised as follows:

- ***Wave passage effect****:* The wave passage effects result from seismic waves arriving at different times at different stations.
- ***Incoherence effect****:* The incoherence effects result in loss in coherence of the wave motion. They are due to differences in the manner of superposition of waves (a) arriving from an extended finite source, and (b) wave scattering by irregularities and inhomogeneities along the wave path and at the site.
- ***Local site effect****:* Differences in local soil conditions at each station may alter the amplitude and frequency content of the bedrock motions significantly.

Based on these simplified observations, if local site effects are neglected, spatial variability of strong ground motion can be modelled as a locally homogeneous and stationary random field with cross-spectral density given as:

$$S_{rs}(f, d_{rs}) = S_r(f) coh_{rs}(f, d_{rs}) \exp(i\phi_{rs}(f, d_{rs})) \tag{5.3}$$

Here, f is frequency, d_{rs} is the separation distance between the observation points referred to by the indices r and s, S_r is the auto-spectral density, coh_{rs} is the coherence spectrum and ϕ_{rs} is the phase spectrum. The wave passage effects are furnished in the phase spectrum, whereas the coherence spectrum accounts for incoherence, i.e. loss in coherence visualised by coherence values that are less than one.

Coherence

The horizontal incoherence of ground motion has been studied using selected records from shallow strike-slip earthquakes obtained at rock sites in events with magnitude about 6.5. The records were obtained from the ISESD databank (Ambraseys et al. 2002 and 2004) from sites in Iceland, the South Iceland Lowland and in Turkey near the North Anatolian Fault.

The estimates of the coherence were computed from the strong-motion phase of acceleration containing 90% of the wave energy. The spectral estimates were obtained using Welch's averaged periodogram method. Before carrying out the computations the horizontal components of the records were transformed into principal coordinates

The loss in coherence increases, on average, with increasing frequency and increasing separation distance, which is in accordance with results reported in the literature. It was found that an empirical coherence model of the following type, commonly referred to in the literature, does not fit very well to the applied dataset:

$$coh_{rs}(f, d_{rs}) = \exp(-a_1 f)\exp(-a_2 d_{rs}) \tag{5.4}$$

Here f is frequency in Hz, d_{rs} is the separation distance between the observation points in m, a_1 and a_2 are parameters determined using linear regression analysis. An extension of the above model is the following simplified exponential type model:

$$coh_{rs}(f, d_{rs}) = \exp\left(-a_1 f^{a_3}\right)\exp\left(-a_2 d_{rs}^{a_4}\right) \tag{5.5}$$

where f is frequency in Hz as above, d_{rs} is the separation distance between the observation points in m and a_1 ... a_4 are parameters determined using non-linear regression analysis. It should be noted that values of the parameters a_1 ... a_4 depend on the units used for the frequency and distance. The following values were obtained using non-linear least-squares data fitting:

$$a = [\, a_1 \;\; a_2 \;\; a_3 \;\; a_4 \,] = [\, 3.6462\cdot10^{-3} \;\; 0.4890\cdot10^{-6} \;\; 1.85 \;\; 2.85 \,]$$

The fitted coherence model of Eq.(5.5) is displayed in Figure 5.9 and in Figure 5.10 the model is expressed as a function of frequency in Hz and separation distance in m. In spite of some theoretical shortcomings this model is found to be a reasonable approximation that fits the selected data better than the other available models tested. The presented model is especially applicable for moderate sized strike-slip earthquakes.

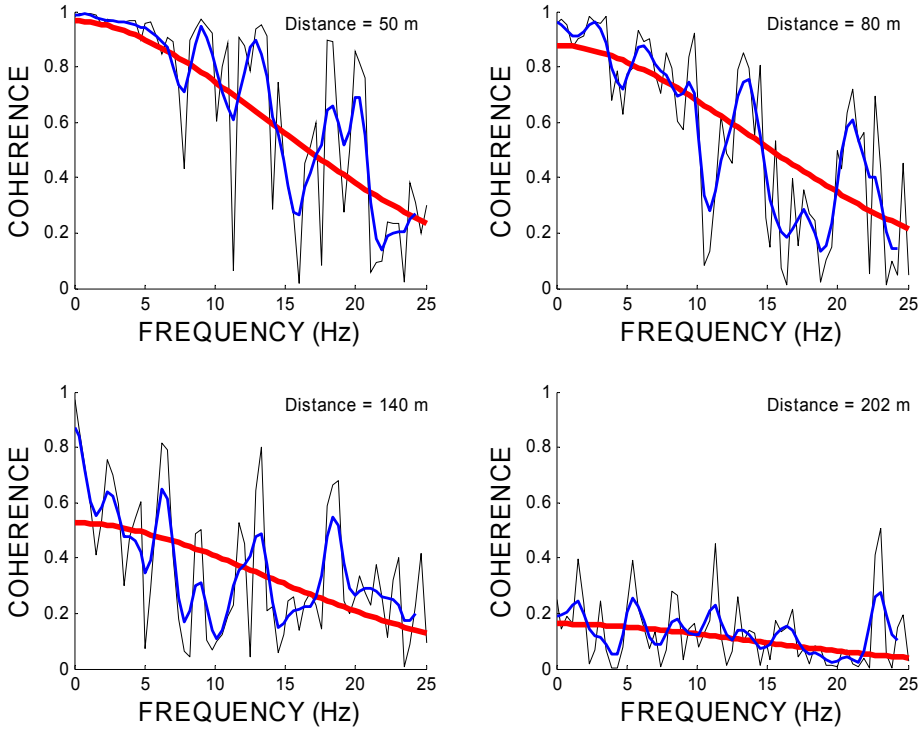

Figure 5.9 Horizontal coherence spectra. The black and blue curves are estimates derived from measurements and the red curves represent the suggested model using Eq. (5.5).

Phase

A commonly used model for the phase spectrum is to take it proportional to the gross propagation time delay reflecting the wave passage effects. Using this approach, the following simplified model for the phase spectrum is suggested:

$$\phi_{rs}(f, d_{rs}) = -2\pi \frac{V}{|V|^2} d_{rs} \tag{5.6}$$

Here, V denotes the gross apparent velocity vector and d_{rs} is the separation between observation points. The velocity vector should be transformed into principal coordinates before applying this equation with the coherence model outlined above.

The above presented models are useful in response calculations of horizontal structures, especially if linear statistical models apply. For non-linear response cases the above models have found application in the simulation of time series. However, if time series are needed, then completely different approaches can be adopted. These approaches are based on finite source models, i.e. the specific barrier model, and Green's function modelling of the spatial structure of the long periodic motion (Halldórsson and Papageorgio, 2005). It is worth noting that in such an approach it is usually necessary to use information on spatial incoherency to model the high frequency content of the simulated time series.

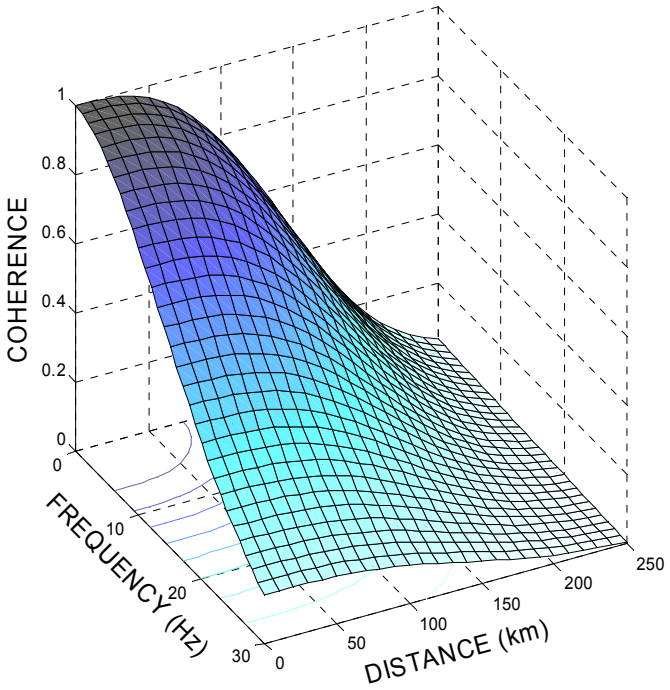

Figure 5.10 Simplified exponential model for horizontal coherence spectrum expressed as a function of frequency in Hz and separation distance in m. The model is given in Eq.(5.5) with the following parameters: $a = [\ a_1\ \ a_2\ \ a_3\ \ a_4\ ] = [\ 3.6462 \cdot 10^{-3}\ \ 0.4890 \cdot 10^{-6}\ \ 1.85\ \ 2.85\ ]$. It is worth noting that the parameters are dimensionally dependent.

5.3 Probabilistic seismic hazard analysis

5.3.1 Introduction (methodology)

The term *seismic hazard* refers to potentially damaging phenomena associated with earthquake threats. In general it is used to describe the phenomena qualitatively by setting up possible scenarios and spelling out potential effects. On the other hand, when the intentions are to express quantitatively the likelihood, frequency or probability of occurrence of specified effects at a particular site in a given region the term is commonly referred to as *probabilistic seismic hazard* and the quantitative methodology used named probabilistic seismic hazard analysis (PSHA). The theoretical foundation of the analysis is based on the framework of structural reliability and safety (Melchers, 1999). Contemporary probabilistic seismic hazard methodology is commonly based on the work of Cornell (1968) and McGuire (1995). The same methodology applies also to the development of structural design criteria expressed in terms of *uniform hazard spectra* to be used in performance-based codified design.

The purpose of this chapter is to outline the applied methodology and present the obtained computational results put forward as hazard curves and uniform hazard spectrum for the study site. The methodology applied herein follows the main trend in probabilistic seismic hazard

analysis as presented by Tenhaus and Campbell (2003) and McGuire (2004). Application to the Icelandic seismic environment are discussed in Sólnes, Sigbjörnsson and Elíasson (2004) and Snaebjörnsson, Sigbjörnsson and Ólafsson (2006). The analysis incorporates the inherent uncertainty of the size and location of future earthquakes, as well as the attenuation of seismic waves as they propagate from all possible sources in the seismic zones to the study site. For this purpose probabilistic modelling is required for:

- The magnitude (see Section 5.1.4)
- The epicentre (see Section 5.1.4) and distance to earthquake source
- The strong ground motion estimation relations (see Section 5.2)

To facilitate the probabilistic analysis generating synthetic earthquake catalogue using the Monte Carlo technique augments the existing parametric earthquake catalogue. An example of a simulated catalogue is displayed in Figure 5.11 representing a period of 200 years. In this context is worth emphasizing that the lower bound of magnitude is taken as 4 based on structural engineering considerations. Therefore, the number of earthquakes in the Northern Volcanic Zone is considerably smaller than the number of events within the three seismic lineaments defining the Tjörnes Fracture Zone.

The earthquake hazard curves are derived from the synthetic earthquake catalogue applying the strong-motion estimation model described in Section 5.2.2 and order statistics. Even though the simulation is carried out for a big catalogue, i.e. a catalogue covering a very long time period, the hazard curves show some random deviation from the expected smooth curve. This is dealt with by repeating the simulation of the hazard curve several times and then take the average value. This approach gives consistent results for the hazard values considered, even after 50 simulations based on a synthetic earthquake catalogue covering time period of 200 centuries.

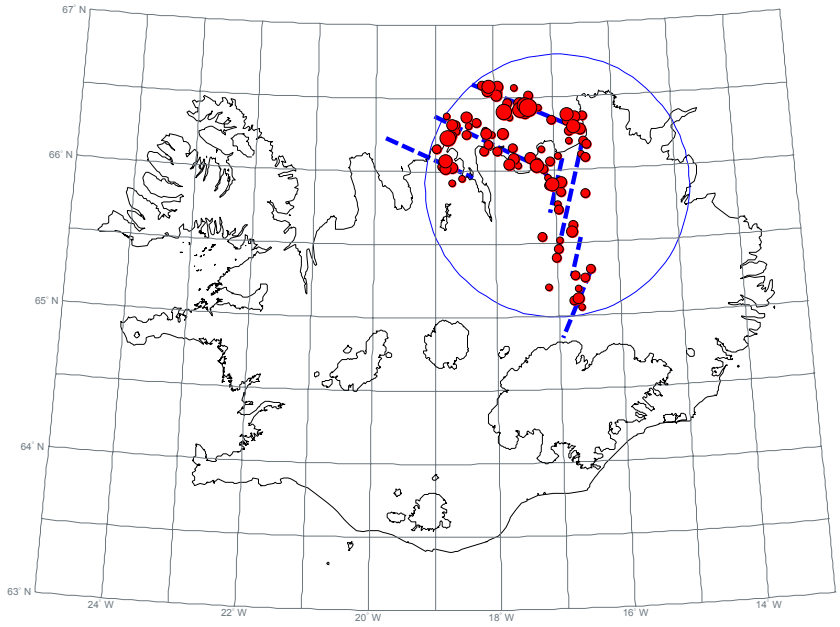

Figure 5.11 An example of simulated parametric earthquake catalogue for North Iceland. Seismicity is associated with dashed lines (blue) visualising the hypothetical seismic delineations and fissure swarms. The time period is 200 years and the radius of the study area is 100 km with the centre at Theistareykir. The magnitude range is between 4 and 7.3, where the upper bound is source zone dependent.

5.3.2 Hazard curves for peak ground motion

The methods and models outlined have been used to derive earthquake hazard curves for peak ground acceleration at the four selected study sites, i.e. Theistareykir, Gjástykki, Krafla and Bjarnarflag, which are all located within the fissure swarms in the Northern Volcanic Zone. The results are displayed in Figure 5.12(a) and (b) as well as Tables 5.1 and 5.2 for selected hazard values. Both horizontal and vertical acceleration components are considered. In Figure 5.12 the industrial lot at Bakki near Húsavik has been included as a reference value characteristic for moderate to large earthquakes originating on the Flatey-Húsavík seismic delineation. It is seen that the peak ground acceleration at the four study sites, which are located within the Northern Volcanic Zone, are significantly lower than at the Bakki lot, which is close to the Flatey seismic delineation. This variability in earthquake action is further demonstrated in Figure 5.13, which gives an indication of the distribution of horizontal peak ground acceleration (PGA) from the Bakki industrial lot in the north to the Bjarnarflag site in the south for a return period of 475 years. This has for instance bearings on the design of overhead transmission lines going from the power plants in the south to the Bakki site in the north (see Figure 1.1).

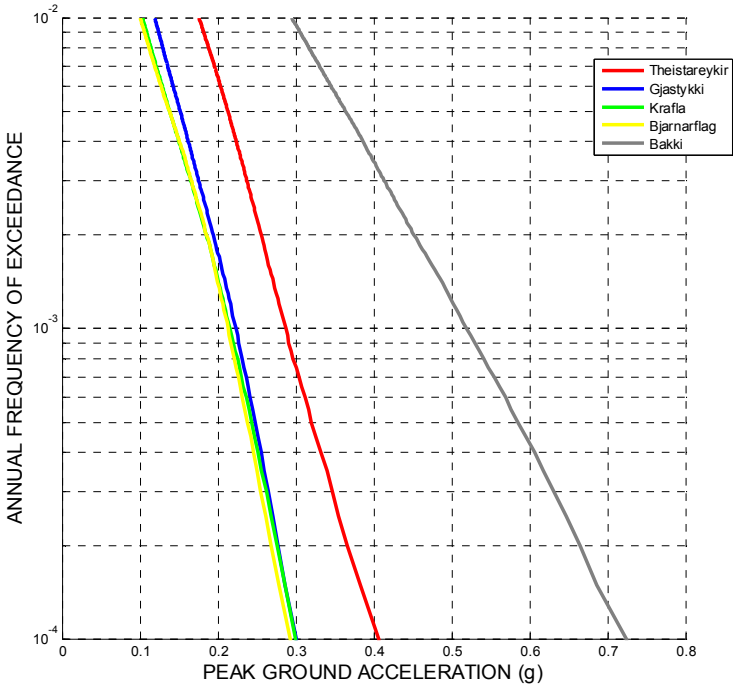

(a)

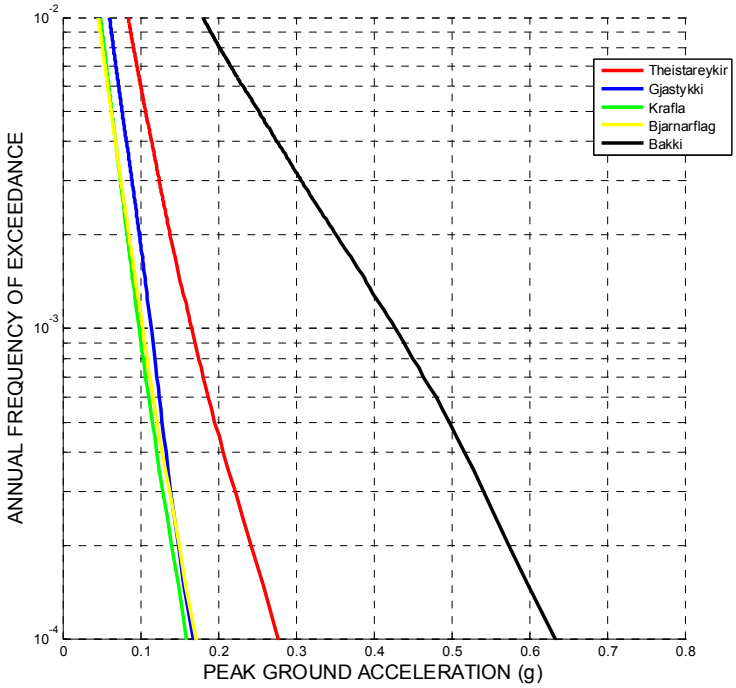

(b)

Figure 5.12 Peak ground acceleration (PGA) for the study sites based on synthetic parametric earthquake catalogue and assuming rock site conditions. (a) Horizontal component, (b) Vertical component. The hazard curve for the industrial lot at Bakki near Húsavík has been added to give a reference to a site close to the Flatey seismic delineation.

Table 5.1 Horizontal peak ground acceleration (*PGA*) derived from the hazard curves.

Reference	*Mean return period* (year)	*Annual probability of exceedance*	*Probability of exceedance in 50 years*	*Simulated horizontal PGA* (g)			
				Theista-reykir	*Gjástykki*	*Krafla*	*Bjarnar-flag*
OBE	95	1.05%	40.9%	0.17	0.12	0.10	0.10
EUROCODE 8	475	0.21%	10.0%	0.25	0.19	0.18	0.18
	1,000	0.10%	4.88%	0.29	0.22	0.21	0.21
MCE	3,000	0.033%	1.65%	0.34	0.26	0.26	0.25

Table 5.2 Vertical peak ground acceleration (*PGA*) derived from the hazard curves.

Reference	*Mean return period* (year)	*Annual probability of exceedance*	*Probability of exceedance in 50 years*	*Simulated horizontal PGA* (g)			
				Theista-reykir	*Gjástykki*	*Krafla*	*Bjarnar-flag*
OBE	95	1.05%	40.9%	0.08	0.06	0.05	0.04
EUROCODE 8	475	0.21%	10.0%	0.14	0.10	0.08	0.08
	1,000	0.10%	4.88%	0.17	0.11	0.10	0.10
MCE	3,000	0.033%	1.65%	0.22	0.14	0.13	0.13

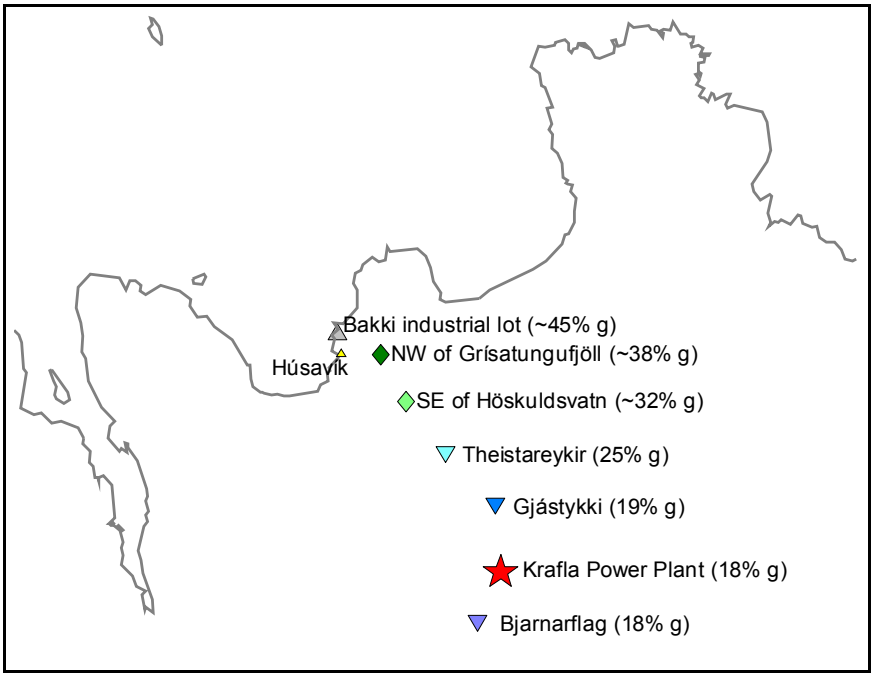

Figure 5.13 Distribution of horizontal peak ground acceleration (PGA) from the Bakki industrial lot in the north to the Bjarnarflag site in the south. The values are based on synthetic parametric earthquake catalogue, assuming rock site conditions and return period of 475 years.

For the three sites, Gjástykki, Krafla and Bjarnarflag, situated within the region of the Krafla central volcano fissure swarm the obtained peak ground acceleration can be treated as being equal for practical purposes. The Theistareykir site, on the other hand, yields significantly higher PGA values, resulting from the proximity to the Flatey-Húsavík delineation and the conservative model values adopted (see Section 5.1.4).

It can be seen by inspecting Tables 5.1 and 5.2 that the ratio between the vertical and the horizontal component is in the order 0.5 for study sites within the Northern Volcanic Zone, while for the Bakki site it is more than 0.8 for the longer mean return periods included. This reflects the different nature of the area considered. On the one hand the volcanic fissure swarms produce small normal faulting events and on the other hand strike-slip earthquakes of magnitude 7 originate on the Flatey-Húsavík delineation.

5.3.4 Uniform hazard spectrum for linear elastic response

The uniform hazard spectrum is derived in a similar manner as the above presented peak ground acceleration values in Tables 5.1 and 5.2. The starting point is a synthetic parametric earthquake catalogue. In general it enhances the accuracy of the estimation if more than one catalogue is applied. Then the hazard curves for the spectral ordinates are derived using the strong-motion estimation models presented in Section 5.2.2. The uniform hazard spectra are then obtained from the hazard curves covering undamped natural periods logarithmically spaced in the range 0.05 to 2.0 s. In all cases the critical damping ratio is taken to equal to 5% of the critical value. The results are shown in Figure 5.14 for the horizontal and vertical action for the sites at Theistareykir, Gjástykki and Krafla.

To facilitate the comparison of the uniform hazard spectra with standardise codified spectra a normalisation is performed using the peak ground acceleration as a reference value. This process gives the seismic coefficient curves presented in Figure 5.15 below.

It can be seen that the variation of the normalised spectra (seismic coefficient) for the different mean return period is not very great, especially not for the vertical action. This supports the commonly accepted simplification to adopt only one curve to describe the normalised spectrum. This approach is discussed further in section 5.5.

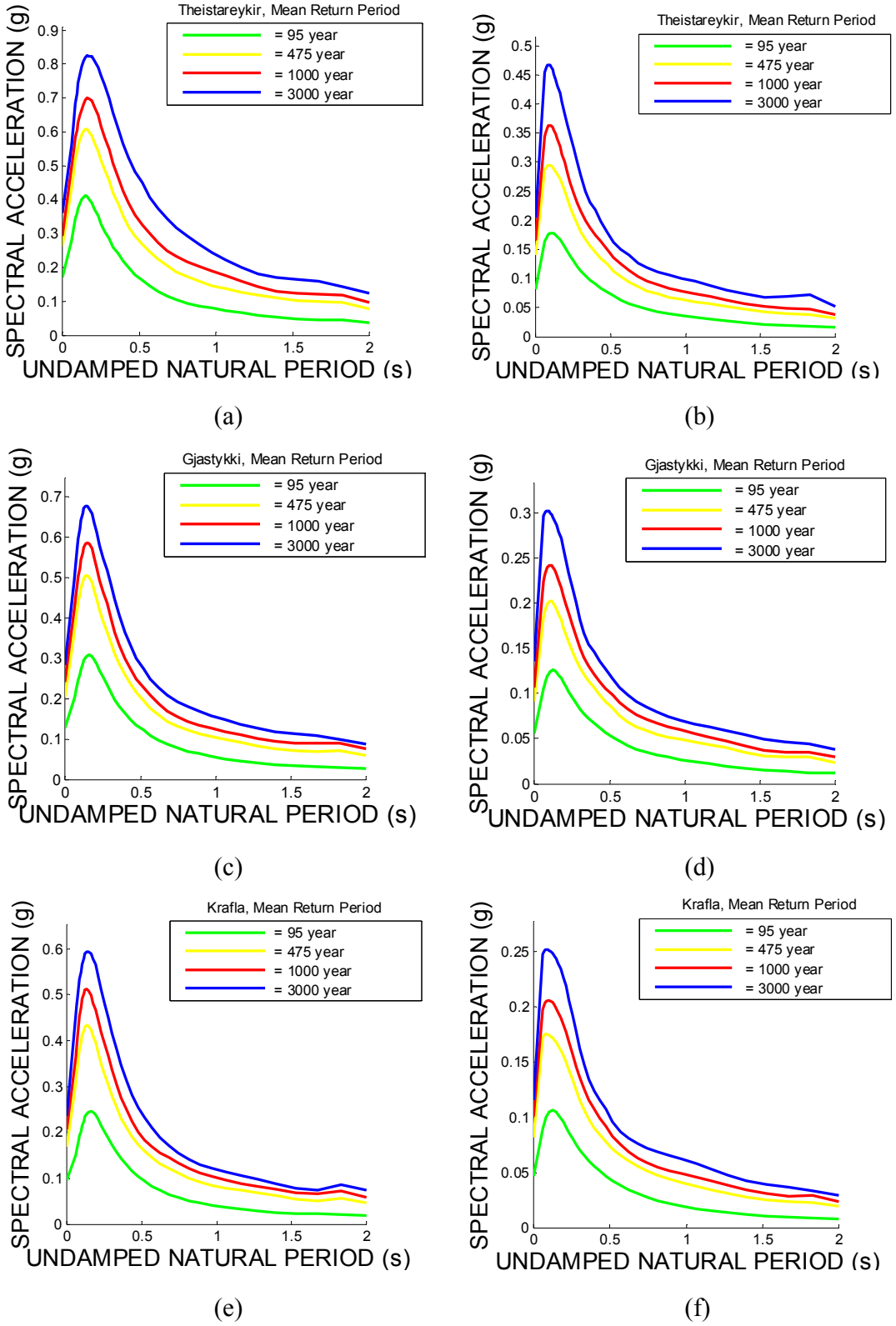

Figure 5.14 Horizontal (a,c,e) and vertical (b,d,f) earthquake response spectra for linear elastic systems under uniform hazard. Critical damping ratio is equal to 5%. Site conditions are rock.

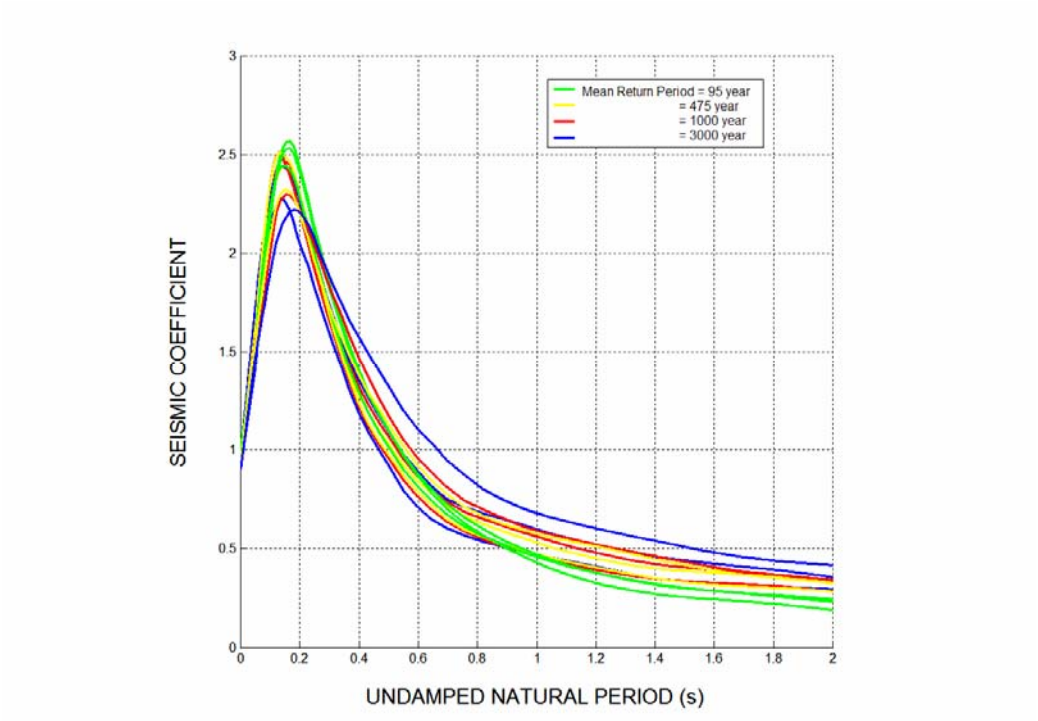

(a)

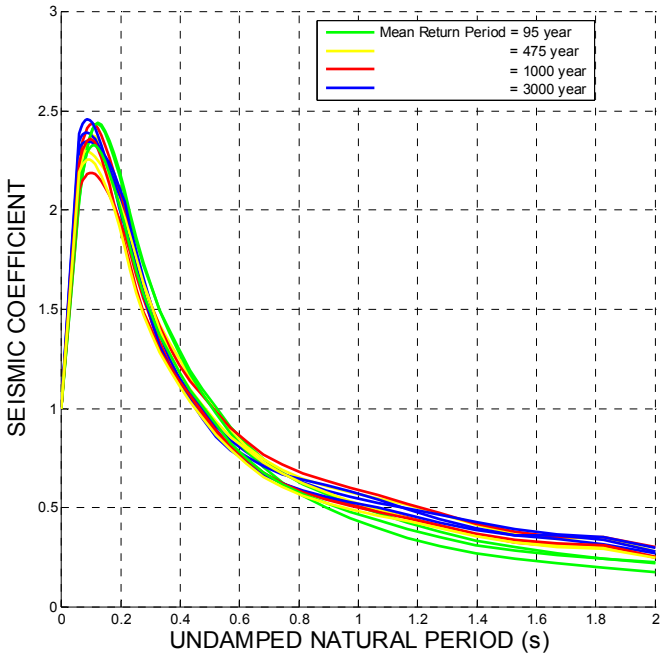

(b)

Figure 5.15 Normalised earthquake response spectra for linear elastic systems under uniform hazard. Critical damping ratio is equal to 5%. Site conditions are rock. (a) Horizontal action, (b) vertical action.

5.3.4 De-aggregation of strong motion

The de-aggregation of the hazard curves for strong-motion at the study sites indicates the following main trends.

For the Theistareykir site, the event contributing most to the 475 year horizontal peak ground acceleration is a moderate sized earthquake with small epicentral distance. The same applies to the horizontal spectral acceleration for structures with short natural periods. On the other hand, for structures with long natural periods a moderate sized to big earthquake with epicentres on the Flatey-Húsavík delineation start to dominate. The event contributing most to the 475 year vertical peak ground acceleration and response spectral acceleration is a moderate sized local earthquake.

For the sites at the Krafla fissure swarms, the event contributing most to the 475 year peak ground acceleration is a small to moderate sized local event with small epicentral distance. The same event also contributes most to the 475 year spectral acceleration for short periodic structures, whilst a big distant event dominates the response of long periodic structural systems. The vertical peak ground acceleration as well as spectral ordinates is influenced most by small to moderate sized local events.

These results give an indication regarding the selection of earthquake scenarios to be used in the generation of synthetic time series required for the so-called deterministic analysis.

5.4 Deterministic seismic hazard analysis

The term ‘deterministic seismic hazard analysis’ refers to the methods used to obtain strong-motion information for engineering design. The information is derived from predefined deterministic earthquake scenarios specified in terms of seismological parameters like earthquake magnitude, distance from the causative earthquake fault to the site of interest as well as style of faulting and site conditions. The strong-motion estimation models provide the tools required for such an analysis. The purpose is to generate synthetic acceleration series and the derived response spectra for selected earthquake scenarios. Special emphases are placed on strong-motion induced by events corresponding to available information on faults and general geology of the study area.

5.4.1 Earthquake scenarios

To be able to assign a probability level to the earthquake scenarios selected for design purposes they should be based on the de-aggregation discussed above. Further support can also be found using credible geological information on faults and fractures in the area. This leads to the following scenarios corresponding roughly to the event corresponding most to the 475 year peak ground acceleration and spectral acceleration for structural systems with short natural period:

- The Theistareykir site: magnitude 6 event with short epicentral distance.

- The Bjarnarflag, Krafla and Gjástykki sites: magnitude 5 to 5¼ event with short epicentral distance.

The maximum credible earthquakes for these sites are approaching the upper bound defined in Section 5.1.4 (see Figure 5.4).

5.4.2 Fault rupture effects on surface motion

The fault rupture induced by moderate sized earthquakes may result in a low frequency pulse at sites in the direction of the causative fault. This effect can be significant as seen in the South Iceland earthquakes in 2000. The result is a broad peak in the response spectrum in the natural period range 1.0 to 1.5 s. For structural systems with periods in this range this effect should be considered (see section 5.4.3 on simulation of time series) For small earthquakes (magnitude 5.5 or less) this is usually of no concern as the ruptured fault surface is not large enough to create a significant difference in the arrival times of the radiating seismic waves (i.e. the fling effect).

5.4.3 Time series of strong ground motion

Time-history representations of earthquake motion may be applied, according to Eurocode 8 (2003), by using either recorded or simulated accelerograms generated through a physical simulation of source and travel path mechanisms, provided that the samples used are adequately qualified with regard to the seismogenetic features of the sources and to the soil conditions appropriate to the site. The duration of the accelerograms should be consistent with the magnitude and the other relevant features of the seismic event underlying the establishment of the peak acceleration and seismic coefficient for the zone under consideration.

The synthetic time series derived based on source models (Ólafsson et al. 2001; Ólafsson and Sigbjörnsson, 2004) for the above defined earthquake scenario for the Theistareykir site, is displayed in Figure 5.16 along with the corresponding response spectrum. The applied site condition is rock and the adopted critical damping ratio for the spectral calculations is 5%. Both horizontal and vertical components are shown. The frequency content of the vertical acceleration is slightly higher than found in the horizontal component. Furthermore, the vertical peak acceleration is significantly lower than that of the horizontal component in accordance with the above obtained results and Section 5.1.4.

Similar time series can be obtained for the sites located within the Krafla fissure swarm. The main differences are the smaller magnitude and shorter duration, which result in lower peak ground acceleration than found in the case of the Theistareykir site.

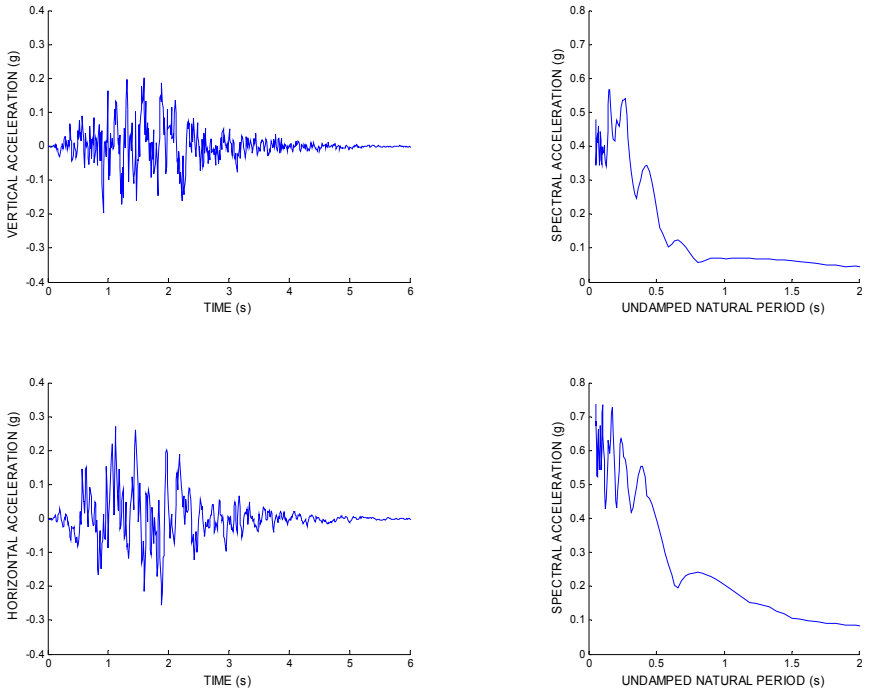

(a)

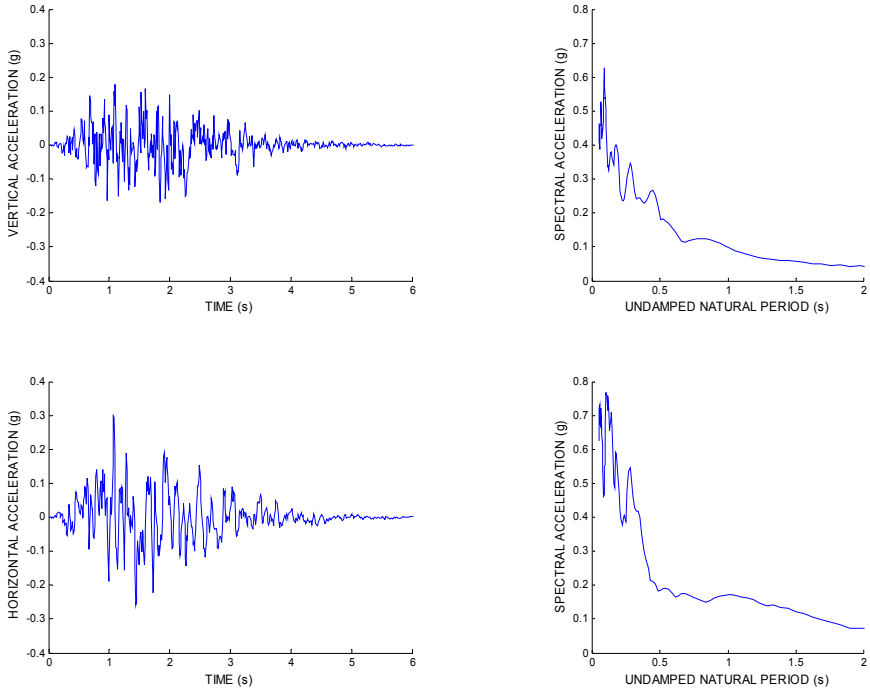

(b)

Figure 5.16 Two examples, (a) and (b), of simulated time series of ground acceleration and corresponding response spectra based on the result of a de-aggregation study for the Theistareykir site. Rock site conditions are assumed and the critical damping ratio is taken as equal to 5%.

5.4.4 Linear elastic response spectra

It should be recognized that the response spectra derived from the simulated synthetic time series deviates significantly from the uniform hazard spectra presented in Section 5.3.4. The reason is that the uniform hazard spectra are obtained as a 'weighted' sum of response spectra obtained from a (given) synthetic earthquake catalogue. This is seen in Figure 5.17 below for the Theistareykir site. The black curves are response spectra derived from synthetic time series based on the above defined scenario event, i.e. a magnitude 6 earthquake with very short epicentral distance. The red curve represents the uniform hazard spectrum for Theistareykir corresponding to the mean return period of 475 years. The deviation of the red and black curves is especially seen in the short period range and in the range around 1.5 seconds where the black curves tend to overshoot the uniform hazard spectrum. The reason for the deviation in the long periodic range is due to near fault effects included in the simulation model. It is found that a fair fit to the simulated spectra can be obtained using the spectral model by Ambraseys et al. (2005) represented by the blue curve. In this case zero epicentral distance has been applied which is not entirely consistent with the synthetic spectra. The fit can, however, only be regarded as reasonable for the short period range while the deviation in the range around 1.5 s is persisting. Hence, it is recommended to account for potential near-fault effects for the Theistareykir site, especially in the case, if nearby active faults are identified.

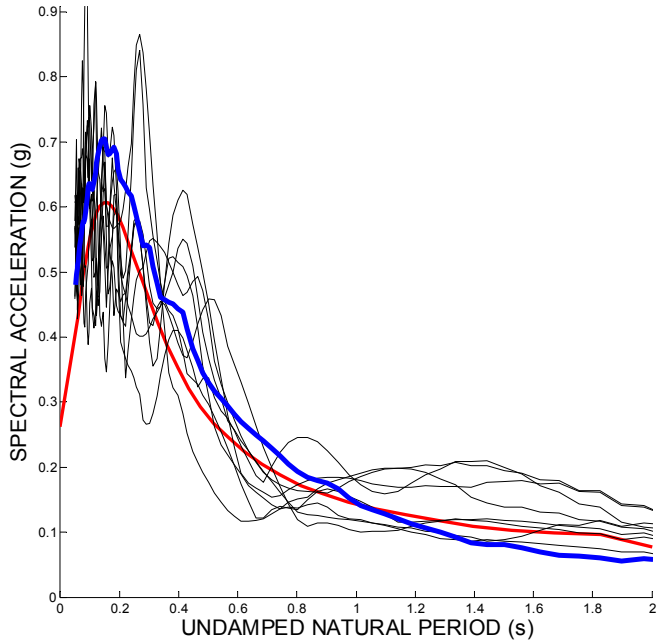

Figure 5.17 Horizontal, linear elastic response spectra based on simulated time series (black curves) compared with uniform hazard spectrum (red curve) with mean return period 475 year and a spectrum based on the model of Ambraseys et al. (2005) for magnitude equal to 6 and epicentral distance < 5 km. Location: Theistareykir. Site condition: rock. Critical damping ratio: 5%.

5.5 *Definition of earthquake action*

The earthquake action is described in terms of two parameters, i.e. the value of the reference peak ground acceleration on firm ground and the elastic response spectral acceleration as a function of undamped structural period.

The peak ground acceleration of horizontal and vertical motion are defined through the uniform hazard curves put forward in section 5.3 and values representing various mean return periods are listed in Tables 5.1 and 5.2.

5.5.1 Suggested design specifications

In Section 5.1, definitions of different design earthquakes were given. In view of the engineering hazard study presented, it is recommended that an event corresponding to mean return period equal to 95 year is defined as an operating base earthquake, an event defined for a 475 year mean return period as the maximum design earthquake and an event corresponding to a 3000 year mean return period as the maximum credible earthquake.

Based on probabilistic hazard analysis it is recommended that the PGA values summarised in Table 5.1 shall be used as the basic quantities for the definition of uniform hazard spectra for horizontal action and the PGA values summarised in Table 5.2 shall be used as the basic quantities for the definition of uniform hazard spectra for vertical action.

Uniform hazard spectra for horizontal action are shown in Figure 5.14 and the corresponding seismic coefficient in Figure 5.15. Spectral ordinates of the type commonly used in engineering design, that fit the uniform hazard spectra, are given in terms of the seismic coefficient by the following expression:

$$S_a = \begin{cases} PGA_{horizontal} \times \left(1 + \dfrac{T}{0.05} \times (2.5 - 1)\right) & 0\,s \le T < 0.05\,s \\ PGA_{horizontal} \times 2.5 & 0.05\,s \le T < 0.25\,s \\ PGA_{horizontal} \times 2.5 \left(\dfrac{0.25}{T}\right)^{7/8} & 0.25\,s \le T < 2.5\,s \end{cases} \tag{5.7}$$

Here, $PGA_{horizontal}$ is the horizontal peak ground acceleration (see Table 1), T is the undamped natural period in seconds (s) and the critical damping ratio is taken as 5%. This simplified expression for the uniform hazard spectrum is plotted in Figure 5.18.

The spectral form of Eq. (5.7) is compared with Eurocode 8 response spectra of Type 1 (high-seismicity context) and Type 2 (moderate-seismicity context). It can be seen that the Eurocode

Type 1 spectrum severely overestimates the action for periods below 2 s, whereas the Eurocode Type 2 spectrum underestimates the action for periods above ~1 s. The spectral form of Eq. (5.7) corresponds to the Eurocode 8 spectrum, Type 2, except for an introduction of a power of 7/8 for the last segment.

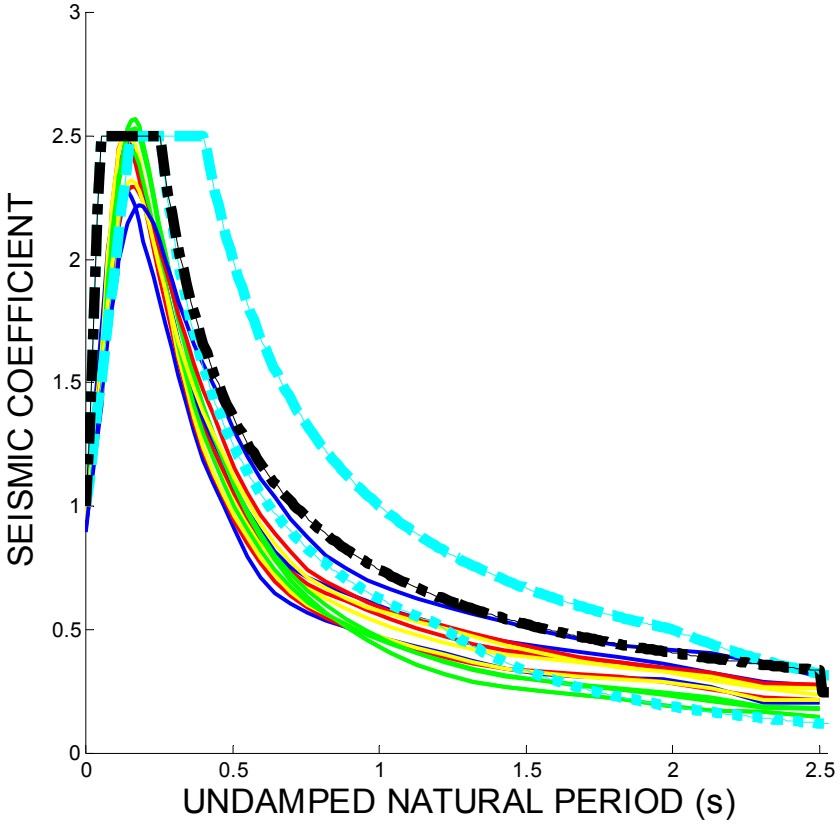

Figure 5.18 Suggested seismic coefficients (normalised spectral acceleration ordinates) for horizontal earthquake action (black dash-dotted curve) plotted along with simulated data (see Figures 5.13 and 5.14). Critical damping ratio is equal to 5%. Rock conditions are assumed. The Eurocode response spectra is also shown on the figure, type 1 is the cyan dashed line and type 2 is the cyan dotted line.

Uniform hazard spectra for vertical action are shown in Figure 5.14 and the corresponding seismic coefficient in Figure 5.15. Similar to the horizontal action specified above, spectral ordinates of the vertical action, in terms of the seismic coefficient, are given by the following expression:

$$S_a = \begin{cases} PGA_{vertical} \times \left(1 + \dfrac{T}{0.05}(2.5-1)\right) & 0\,s \le T < 0.05\,s \\ PGA_{vertical} \times 2.5 & 0.05\,s \le T < 0.15\,s \\ PGA_{vertical} \times 2.5\left(\dfrac{0.13}{T}\right)^{3/4} & 0.15\,s \le T < 2.5\,s \end{cases} \quad (5.8)$$

Here, $PGA_{vertical}$ is the vertical peak ground acceleration (see Table 2), T is the undamped natural period in seconds (s) and the critical damping ratio is taken as 5%. This simplified expression for the uniform hazard spectrum is plotted in Figure 5.19. Again, the Eurocode spectral form for vertical action is compared to the simulated data and the spectral form of Eq. (5.8). As can be seen the Eurocode spectrum, overestimates the expected action for periods between 0.05 s and 0.15 s, but underestimates the action for periods above ~1 s. The spectral form of Eq. (5.7) corrects these deficits by lowering the peak value and by introducing a power of 3/4 for the last segment.

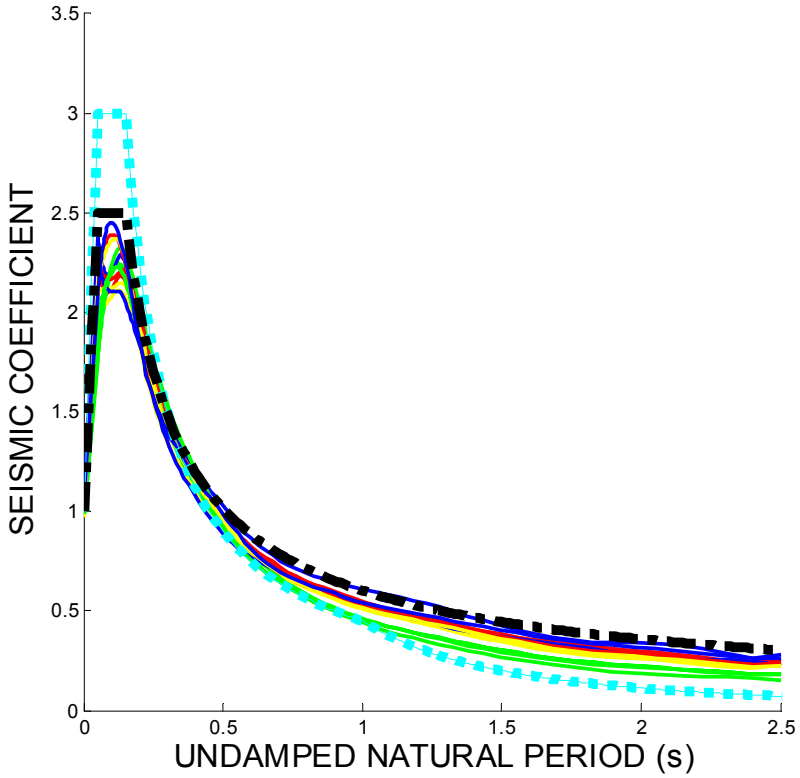

Figure 5.19 Suggested seismic coefficients (normalised spectral acceleration ordinates) for vertical earthquake action (black dash-dotted curve) plotted along with simulated data (see Figures 5.13 and 5.14). Critical damping ratio is equal to 5%. Rock conditions are assumed. The Eurocode response spectrum for vertical action is also shown on the figure (cyan dotted curve).

It can be observed that the derived linear elastic response spectrum has distinct features that are different from those seen in the case of the normalised standard spectrum in Eurocode 8[1]. However, the guideline table values defining the breakpoint values for the Type 2 (moderate-seismicity context) spectral form in Eurocode 8 have been selected here.

The reason for the differences between the Eurocode spectrum and the results from the seismic hazard analysis is primarily linked to the characteristics of the seismic environment in North Iceland. There are several source zones at different distances from the sites and different magnitude earthquakes. In general the earthquakes are small to moderately sized and therefore reasonable that the resulting spectral shape resembles the Type 2 Eurocode spectrum. On the other hand distant earthquakes may exceed magnitude 7, which influences the longer period response. This dependence on the local seismic environment is recognised in Eurocode 8, and individual countries can define their own type and shape of spectrum to fit their local conditions. It is also stated in Eurocode 8, that when the earthquakes affecting a site are generated by widely differing sources, the possibility of using more than one shape of spectra each with a different value of *PGA*, should be considered to adequately represent the seismic action. In the approach presented herein, the hazard simulation accounts simultaneously for the different sources involved and it is simpler and more reliable to apply a single spectral shape associated with one set of ground acceleration values.

The horizontal seismic action is described by two orthogonal components assumed as being independent and represented by the same response spectrum.

The horizontal and vertical action described above can be treated as statistically independent. Hence, the horizontal and vertical acceleration can be regarded as uncorrelated.

For structures with natural periods above 2.5 s it is recommended to use the respective S_a values for $T = 2.5$ s.

In this presentation so far, only linear elastic systems have been considered, which is not entirely satisfactory for design. The reason for this is that firstly, engineered structures usually do not behave strictly linearly and secondly, it is economically feasible to utilise the inelastic structural behaviour to dissipate the earthquake-induced wave energy. This is commonly achieved in codes by introducing a structural behaviour factor that is used to reduce the strength demand. The reduction of strength, on the other hand, increases the displacement demand and, at the same time, the ductility demand. Unfortunately, the structural behaviour factors do not depend only on the structural property but also on the properties of the earthquake action, such as the spectral composition of accelerograms and duration characteristics. These effects are primarily influenced by the source characteristics. As the earthquakes expected are small to moderately sized, the

[1] It is worth noting that the boxed guideline values in Eurocode 8 have not been calibrated for Icelandic environments.

inelastic response tends to be significantly smaller than anticipated from the experience of big earthquakes.

Comment on the application of the design response spectra

The response spectra for horizontal and vertical action have been defined for three natural period regimes. It is appropriate to point out, that spectral shapes for the first segment containing the lowest natural period regimes may be suitable for an OBE event. However, it is recommended that for an MDE or an MCE event the second spectral regime is applied for structures of low natural period. During MDE and MCE events substantial deterioration of structures is generally predicted and consequently the natural period may increase resulting in an un-conservative design if the first part of the response spectra is applied.

Comment on target reliabilities and importance factors

Target reliabilities for no-collapse or damage limitation requirements are generally established by the National Authorities for different types of buildings or civil engineering works on the basis of the consequences of failure. In Eurocode 8, reliability differentiation is implemented by classifying structures into four importance classes, depending on the consequences of collapse for human life, on their importance for public safety and civil protection in the immediate post-earthquake period, and on the social and economic consequences of collapse. An importance factor is assigned to each importance class. The importance factor $\gamma_I = 1.0$ is for importance class II buildings, i.e. ordinary buildings, and is associated with a seismic event having a reference return period of 475 years. Power plants fall within importance class IV, according to the code with an importance factor $\gamma_I = 1.4$.

It is stated in the code that wherever feasible this factor should be derived so as to correspond to a higher or lower value of the return period of the seismic event (with regard to the reference return period) as appropriate for the design of the specific category of structures. Effectively, this has been done herein. Referring back to Tables 5.1 and 5.2, and the defined PGA values for various mean return periods, it can be noticed that the resulting ratios, when normalized with the PGA value for a mean return period of 475 years, actually correspond quite well with the importance factor in Eurocode 8. Judging by this comparison, a design PGA value for a 3000 year mean return period (MCE) would correspond to an importance class IV.

5.5.2 On inelastic effects

The presentation so far has only dealt with linear elastic systems. For design purposes the inelastic structural behaviour must be considered. The reason for this is that engineered structures usually do not behave strictly linearly and it is economically feasible to utilise the inelastic structural behaviour to dissipate the earthquake-induced wave energy. This is commonly achieved in codes by introducing a structural behaviour factor which is used to reduce the strength demand. The reduction of strength, on the other hand, increases the displacement demand and at the same time the ductility demand. Unfortunately, the structural behaviour factor

does not depend only on the structural property as such but depends also on the properties of the earthquake action, such as the spectral composition and duration characteristics of the accelerograms.

For simplification it is suggested that the design spectrum can be derived from the suggested elastic response spectrum divided by an appropriate behaviour factor. The following relation is adopted to relate the global ductility factor and the structural behaviour factor:

$$q = \begin{cases} 1 + (\mu_\delta - 1)\dfrac{T}{T_C} & T < T_C \\ \mu_\delta & T_C \le T \end{cases} \tag{5.9}$$

Here, q is the structural behaviour factor, μ_δ is the global ductility factor, T_C is the transition period (see the above presented elastic response spectra in section 5.5.1) and T is the undamped natural period. It should be noted that the structural behaviour factor is dependant on the structural period, especially for stiff systems. For a given structural behaviour factor the following formula is obtained for the global ductility factor:

$$\mu_\delta = \begin{cases} 1 + (q - 1)\dfrac{T_C}{T} & T < T_C \\ q & T_C \le T \end{cases} \tag{5.10}$$

A corresponding relationship applicable for the local ductility is given as follows:

$$\mu_\phi = \begin{cases} 1 + 2(q - 1)\dfrac{T_C}{T} & T < T_C \\ 2q - 1 & T_C \le T \end{cases} \tag{5.11}$$

This is in accordance with the recommendation of Eurocode 8 in the case that more precise data and analysis are not available.

The design spectrum can be expressed in terms of the structural behaviour factor defined above. For the horizontal action, taking the critical damping ratio equal to 5%, the following expressions are obtained:

$$S_{design}(T) = \begin{cases} PGA_{horizontal} \cdot \left[1 + \frac{T}{T_B} \cdot \left(\frac{2.5}{q} - 1\right)\right] & 0 \le T < T_B \\ PGA_{horizontal} \cdot \frac{2.5}{q} & T_B \le T < T_C \\ PGA_{horizontal} \cdot \frac{2.5}{q} \cdot \left(\frac{T_C}{T}\right)^{7/8} & T_C \le T < 2.5s \end{cases} \quad (5.12)$$

Here, T is the undamped natural period, T_B = 0.05 *s* and T_C = 0.25 *s*. The behaviour factor q is obtained from Eq. (5.9) for a given ductility factor and the transition period T_C = 0.25 *s*. The vertical action for 5% damping ratio is given as:

$$S_{design}(T) = \begin{cases} PGA_{vertical} \cdot \left[1 + \frac{T}{T_B} \cdot \left(\frac{2.5}{q} - 1\right)\right] & 0 \le T < T_B \\ PGA_{vertical} \cdot \frac{2.5}{q} & T_B \le T < T_C \\ PGA_{vertical} \cdot \frac{2.5}{q} \cdot \left(\frac{T_C}{T}\right)^{3/4} & T_C \le T < 2.5s \end{cases} \quad (5.13)$$

where, T_B = 0.05 *s* and T_C = 0.15 *s* and the behaviour factor q is obtained from Eq. (5.9) for a given ductility factor and the transition period T_C = 0.15 *s*. The seismic coefficients in Figure 5.20 are obtained after normalisation with $PGA_{horizontal}$ and $PGA_{vertical}$, respectively.

It should be noted that the seismic coefficients defined in this way approach 1 as the undamped natural period goes towards 0. This is based on the assumption that an infinitely stiff structure is non-ductile. In Eurocode 8, on the other hand, the corresponding quantity approaches 2/3 conforming to the assumption of a minimum structural behaviour factor of 1.5 to be used in design.

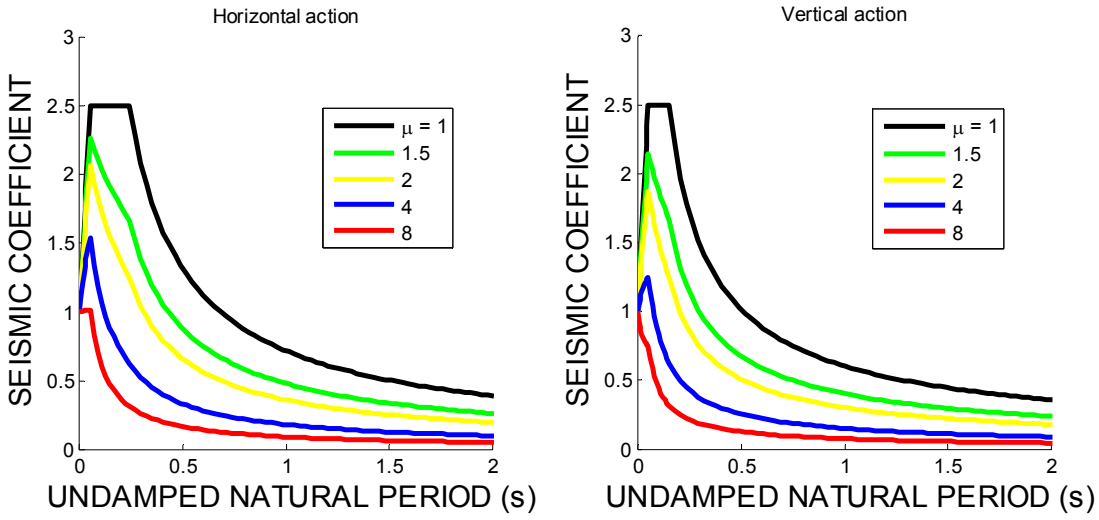

Figure 5.20 Normalised response spectral acceleration (seismic coefficient) for inelastic systems with different ductility factors. Critical damping ratio is equal to 5% and rock site conditions are assumed.

The overall response behaviour should be considered more or less elastic for acceleration levels that can be considered as relatively small. In such cases a global ductility ratio equal to 1.5 should be adopted for horizontal action. In other cases the global ductility ratio should be preferably not exceed 2.5 for elements defined as critical (horizontal action with 475 year mean return period). This implies a local ductility factor equal to 4 for flexible systems. For the vertical action global ductility ration should preferably not exceed 1.5.

Comment on displacement response

The relative global displacements corresponding to the inelastic response spectra defined above can be derived using the following displacement spectrum:

$$S_d\left(T\,|\,\mu_\delta\right) = \mu_\delta \left(\frac{T}{2\pi}\right)^2 S_{design}\left(T\,|\,\mu_\delta\right) \tag{5.14}$$

Here T is the undamped natural period, μ_δ is the global ductility factor and S_{design} is the design spectrum defined above in Eq. (5.12) and (5.13) after substitution of an appropriate structural behaviour factor.

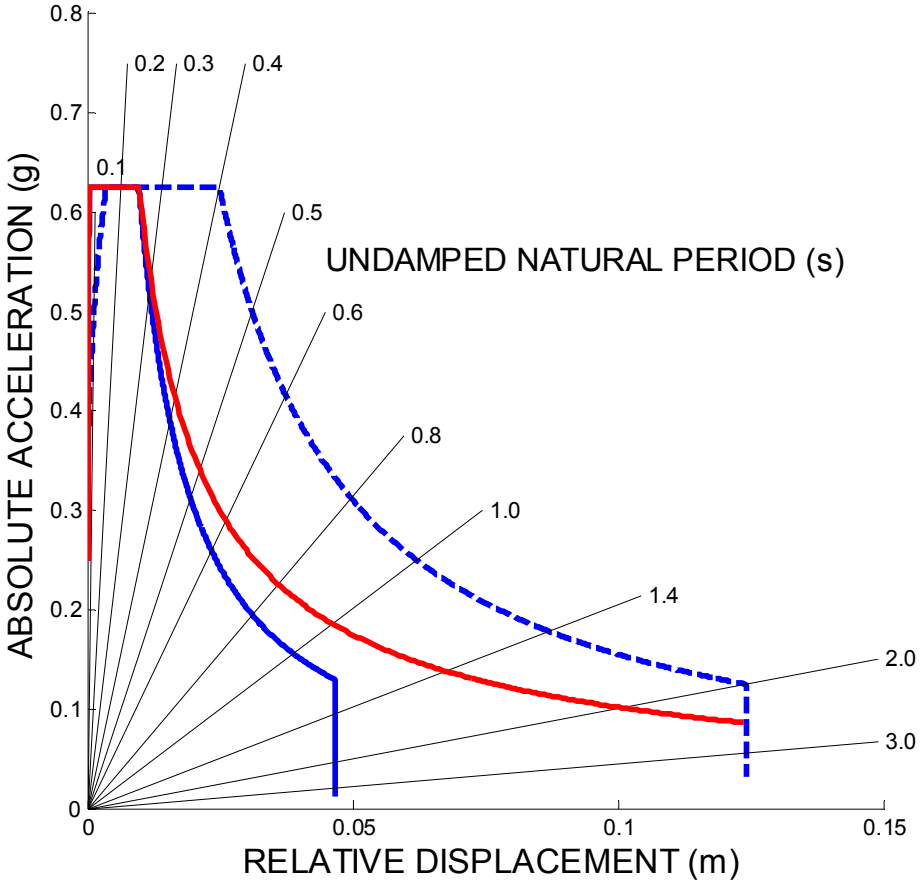

Figure 5.21 Relative displacements for linear elastic systems obtained by Eq.(5.14) for the horizontal action derived from the suggested design spectrum (the red curve) along with displacements corresponding to Eurocode 8 spectrum Type 2 (solid blue curve) and Eurocode 8 spectrum Type 1 (dashed blue curve). The peak ground acceleration (PGA) is taken as equal to 0.25 g which corresponds to the Theistareykir site. Critical damping ration is equal to 5% of the critical. Site conditions are rock.

The relative displacements obtained by Eq. (5.14) are displayed in Figure 5.21 for the horizontal action derived from the suggested design spectrum (the red curve) along with displacements corresponding to Eurocode 8 spectrum Type 2 (solid blue curve) and Eurocode 8 spectrum Type 1 (dashed blue curve). The radial lines in the figure correspond to different undamped natural periods. In all cases only linear elastic systems are considered, i.e. the global ductility factor, μ_δ, is equal to one. By inspecting the figure it is observed that the proposed design spectrum resembles the Type 2 Eurocode 8 spectrum for the stiff structures, while it approaches the Type 1 spectrum for the flexible structures. This behaviour is due to the fact that the uniform hazard spectrum (the red curve in Figure 5.21) is governed by small to moderate locally-induced earthquake action for the short period structure while moderate to big distant earthquakes tend to dominate the earthquake action induced by long period structures.

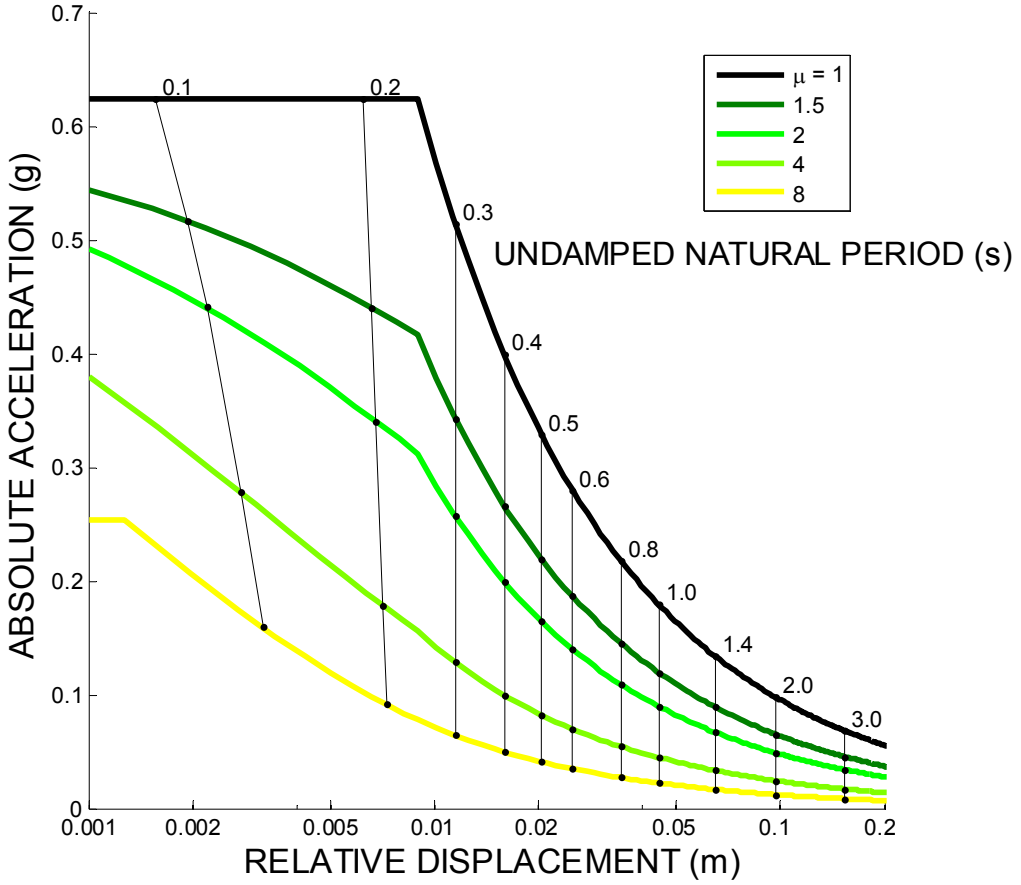

Figure 5.22 Relative displacements for inelastic systems obtained by Eq. (5.14) for the horizontal action derived from the suggested design spectrum. The peak ground acceleration (PGA) is taken as equal to 0.25 g which corresponds to the Theistareykir site. Critical damping ration is equal to 5% of the critical. Site conditions are rock. The black curve describes linear elastic systems and is included as a reference for the inelastic systems.

The relative displacements for inelastic systems are displayed in Figure 5.22 as derived from Eq.(5.14) representing the horizontal action. The peak ground acceleration used is equal to 0.25 g which corresponds to the Theistareykir site. The global ductility factors are in the range of 1 to 8. It is seen that the displacements are independent of the ductility factor for structures with an undamped natural period above 0.25 s. Conversely for structures with an undamped natural period shorter than 0.25 s the displacements increase with growing ductility factor. Hence, the lines describing the undamped natural period radiating from the point (0.0) in Figure 5.21 have been transformed into 'vertical' lines. This behaviour, which is characteristic for the inelastic displacements, is a result of the assumed relation between the global ductility and structural behaviour factor.

5.5.3 Recorded time series and derived data for general reference

As stated in Eurocode 8 and discussed in section 5.4, time-history representation of the earthquake motion may be used. In that context, it should be pointed out that time series as well as linear spectra from the South Iceland earthquakes in June 2000 are available online at the website: http://www.isesd.hi.is/. This information is also available on a CDROM, entitled *European Strong Motion Database*, Vol. 2, with non-linear response spectra added among other relevant data.

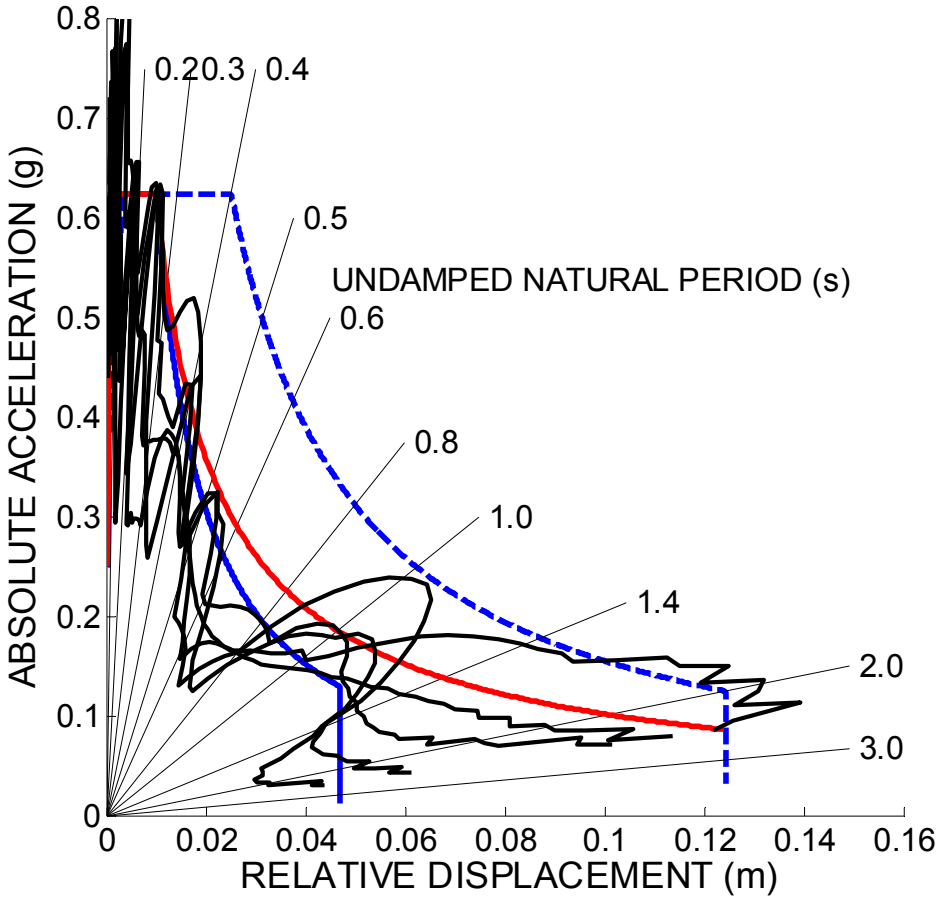

Figure 5.23 Relative displacements for linear elastic systems derived by simulations (black curves) compared to the proposed design spectrum (red curve) as well as Eurocode 8 Type 2 spectrum (solid blue curve) and Type 1 spectrum (dashed blue curve). The peak ground acceleration is taken equal to 0.25 g which corresponds to the Theistareykir site.

Figure 5.23 displays five response spectra obtained by simulation using a source model approach. These response spectra are compared to the recommended design spectra as well as Eurocode 8 spectra Type 1 and 2. In two cases the simulated spectra overshoots the displacements derived from the recommended design spectrum. This occurs for long period structures and is due to rupturing effects observed for sites in the direction of the causative fault. These fling effects can

even lead to overshooting of Eurocode Type 1 spectrum for structures with period exceeding 1.0 s. Hence, special consideration should be given to potentially active fault close to the Theistareykir site judged capable to produce a moderate sized earthquake, i.e. with magnitude exceeding 6.

5.5.4 Conceptual design consideration for damage tolerant structures

Experience from past strong earthquakes demonstrates that the aspect of seismic hazard needs to be taken into account in the early stages of the conceptual design of a building. The objective is to achieve a structural system which, within acceptable costs, satisfies the fundamental requirements specified and guarantees favourable structural behaviour during earthquakes. The following guiding principles governing the initial conceptual design are general considerations that designers should try to adhere to, however it should be noted that their applicability may vary depending on the type of structure and the conditions involved:

- Structures should have adequate foundation
- Structures should be simple
- Structure should be compact and regular in both plan and elevation. Avoid structures with elongated or irregular plans; that have substantial setbacks in elevation; or those that are unusually slender
- Avoid unnecessary mass and achieve a uniform distribution of mass
- Transmission of the seismic (inertia) forces to the ground should be direct and clear, i.e. complete load path
- Uniformity, symmetry and redundancy should be ensured
- Structures should be statically undetermined i.e. redundant. Use a backup structural system wherever possible
- Bi-directional resistance and stiffness should be ensured
- Torsion resistance and stiffness should be ensured and symmetry preserved (main structural elements should be placed symmetrically near to the periphery of the building)
- Structural elements should be appropriately connected with floor systems or diaphragms (which must have sufficient in-plane stiffness)
- Use a uniform and continuous distribution of stiffness and strength. Avoid non-structural components that unintentionally effect this distribution. Avoid sudden changes in member sizes or details
- Permit inelastic action (damage) only in inherently non-critical ductile elements (i.e., in beams rather than columns)
- Detail the members to avoid premature, brittle failure modes. Utilize capacity design principles to avoid undesired shear, axial or joint failures and to foster ductile flexural failure modes in the event of accidental overloads
- Avoid hammering (pounding) of adjacent structures
- Tie all structural components together. Anchor non-structural components to the structure to avoid falling hazards

- Avoid systems with low amounts of viscous damping. Absence of non-structural components tied to structure may be an indication of low damping in steel structures

The main principles mentioned in the above listing are discussed in Eurocode 8 and by Bachmann (2003). In this context it is worth mentioning that softening of the structural system may often be more beneficial than strengthening (Bachmann, 2003).

6. Summary and conclusions

Landsvirkjun, in cooperation with Theistareykir Ltd and Landsnet plans to build geothermal power plants at four sites in the volcanic zone in NE Iceland and transmission systems to an industrial site at Bakki near Húsavík. For location see Figure 1.1. The four geothermal areas considered for power production are at Krafla, Theistareykir, Gjástykki and Bjarnarflag. The goal is to produce 400 MWe. The first production phase of 200 MWe is expected to be finished in 2012 and the second production phase of 200 MWe in 2015.

This report presents a study of geo–hazards that may cause operational interruptions or damage to planned geothermal power plants in NE Iceland, transmission lines and substations. The hazard assessment for the area of concern can be limited to three types of geo-hazards. They are: a) volcanic activity with lava flows from nearby craters or fissures and ash fall from distal volcanoes, b) earthquakes originating in the Tjörnes Fracture Zone as well as local earthquakes within the volcanic zone, and c) tectonic movements of land associated with the plate movements, deformation due to rifting and intrusion of magma into the crust. A second objective of the report is to determine the likely impacts of hazardous events in the area, on the planned power plants and transmission systems and mitigate risk through suggestions of protective measures and location of structures along with structural design recommendations based on a predefined probability of occurrence.

A most important measure to mitigate risk is the decision to build the four planned power plants and drill the production wells at four different locations in an area of some 10 x 30 km within the volcano-tectonic zone. Simultaneous eruptive activity and fracturing in all of the four considered geothermal fields at any time is very unlikely. In the case that one field or a part of a geothermal field becomes un-exploitable it should be possible to increase the production in the other fields or obtain reserve power from the regional grid. There will be two independent transmission lines running from the power plants to the industrial lot at Bakki. Each power line will be able to carry the total energy needed i.e. 400 MWe. One of the transmission lines will be running in a geo-logically stable zone to the west of the hazardous volcano-tectonic zone, except for a short distance west of the Krafla power plant and hence its vulnarability to geo-risk is considered low. This further increases the overall reliability of power transmission.

6.1 Volcanic hazard

The northern volcanic zone (NVZ) is segmented into discrete volcanic systems consisting of a central volcano and a fissure swam. A large strain release affected the northern part of the NVZ in 1975-1984. Regarding local volcanic hazard for the next 100-200 years it may be considered the safest of the spreading zones in Iceland for harnessing geothermal energy. Ash-fall from distal volcanoes can not be excluded as a potential hazard, however, large plinian eruptions are rare. Phreatic eruptions from sub-glacial eruptions are more common, but few have caused heavy ash-fall in NE-Iceland. Furthermore, the substations will be indoor facilities and are, hence, not at

risk from ash-fall from local or distal volcanoes. Ash-fall on power-lines could cause temporary disturbances but is not considered as a major risk factor.

During Postglacial time volcanic eruptions of the Theistareykir volcanic system have been of the lava shield type only, most of them occurring in early Postglacial time, i.e. more than 10,000 years ago. Only one later eruption has occurred in the area. It produced Theistareykjahraun about 2500 years ago. The early Postglacial lavas of the Theistareykir area are extensively broken up by normal faults and tension gashes. Faulting during the last 2500 years has been limited to the western part of the swarm. The eastern part, where the future production area is located is considered suitable and fairly safe as a building site for the planned power plant. This part is also well suited as a drilling area from the point of view of well siting and reservoir characteristics. Theistareykjahraun is one of only two lava shields in Iceland younger than 3000 years. Renewed volcanic activity of the Theistareykir system in the near future must be considered unlikely in view of the distribution of eruptions in time and rare occurrences of late Holocene shields in Iceland. The possibility of a recurrent dyke injection underneath the western or central part of the fissure swarm is a more likely scenario in future.

The geothermal fields at Krafla, Bjarnarflag and Gjástykki are all located in the Krafla volcanic system. It has been the main center of rifting in this part of the NVZ during the past 3000 years. There have been 6 fissure eruptions in the Krafla volcanic system in the last 3000 years. Three occurred between 2000 and 3000 years ago, the other three in historical time, i.e. after ~870 AD. The last eruption occurred in 1975-1984. It was accompanied by dike intrusions and up to 9 m widening of the fissure swarm. The strain release associated with this episode would require centuries for build up of stress to prepare for a new rifting episode. During this volcanic episode only the central part of the fissure swarm split up and subsided. In this context it should be noted, that the existing power plant at Krafla is sited outside this critical central zone and the planned power plants will also be sited outside the central zone. Volcanic gas fluxes rendered a part of the Krafla geothermal system unexploitable for over two decades. However, Bjarnarflag (~8 km to the south) was not affected. Hydrothermal and hydrovolcanic eruptions have accompanied some of the fissure eruptions at Krafla. From the minimum recurrence intervals of earlier episodes of about 250 years, and the fact that it takes time to build up sufficient tensional stress for a new episode, the Krafla system is considered comparatively safe for utilization during this century at least. Inter rifting volcanic eruptions due to overpressure in Kraflas magma chamber may have occurred in early Postglacial Time during excessive volcanic production following rapid isostatic rebound.

As mentioned above the production area and power station of Krafla are and will be located east of the main activity of the fissure swarm. Similarly, the surface constructions planned for future development of Bjarnarflag will be on relatively safe ground, east of the zone that rifted in the 18th and 20th centuries. Boreholes, however, are planned both in this area and partly sidetracked into the rifted segment to the west. The prospect area of Gjástykki is located on the margin of the central depression. A power house can be built outside it on the western flank, in an area where

faults and ground fissures are clearly visible and can thus be avoided. In case of pipelines, appropriate measures can be taken where faults need to be crossed.

It is concluded, that a rifting episode in the NVZ as a whole can be expected roughly once every century. The rifting episodes may be accompanied by a volcanic eruption in the case of the Krafla and Askja systems but volcanic eruption is less likely in the Theistareykir volcanic system. It should be noted that dyke and sheet intrusions are beneficial to the geothermal system in the long run. They form a dense complex at 1–3 km depth and act as a heat source which maintains and drives the circulation of the geothermal system.

6.2 Tectonic movements

Plate movements cause gradual stretching across the rift zone in Northern Iceland, which accommodates the full spreading rate of about 2 cm/yr over a plate boundary deformation zone some 20 – 60 km wide. The average strain accumulation is 0.3 - 1 μstrain/yr, and the associated tectonic stress build-up is on the order of 0.04 – 0.12 MPa /yr. This strain accumulation causes rifting episodes, but their timing is modulated by availability of magma in the rift. Episodic flow of magma from the mantle towards shallow depth causes irregularity in timing of rifting episodes, but they are the main geologic hazard along the plate boundary. The probability of a new rifting episode in any of the four northernmost volcanic systems in the Northern Volcanic Zone is considered to be low, with the most probable rifting site being the Askja volcanic system, which is more than 50 km outside the area of interest in this study. During a future rifting episode in the Krafla volcanic system a similar behaviour is expected as in the18th century and in the Krafla fires with major diking events, and fracturing focused in a narrow strip of land above an intruded complex of dikes. The dikes are expected to extend only through a fraction of the crust, with plate motion being accommodated in the lower crust by ductile processes. Deformation is expected at Krafla, Gjástykki and Theistareykir during inter-rifting periods. Local magmatic and geothermal pressure sources are known to have contributed continuously to deformation processes at Krafla in past decades, but not at Þeistareykir which appears more stable. Deformation due to pressure variations in a shallow magma chamber at the Krafla volcanic system may be expected, as well as deformation due to exploitation and other processes in geothermal fields. They can cause deformation at a rate of up to few centimeters per year. Furthermore, a deep-seated pressure increase appears to take place under Gjástykki at the present and is interpreted as magma accumulation near the crust-mantle boundary. The evolution of this source is being monitored with a geodetic monitoring program in the area.

6.3 Seismic hazard

Seismic hazard in the region is due primarily to large earthquakes on the Húsavík-Flatey fault (HFF). This northwest-striking system of faults adjoins the Theistareykir fissure swarm in the east and the Kolbeinsey Ridge in the west. Before 1755 only one damaging earthquake is known on the HFF; it occurred in 1260 and is described as a "great earthquake in Flatey" in medieval annals from the region. In 1755 an earthquake took place on the HFF, with an epicentre somewhere between Flatey and Húsavík. Its magnitude has been estimated as 7 on the Richter scale. At Theistareykir, the intensity of the 1755 earthquake would have been ~7, with a corresponding ground acceleration of 7% g. In 1872 two large earthquakes occurred in the Skjalfandaflói bay; both earthquakes were approximated at magnitude 6.5 on the Richter scale. Since 1927, 9 earthquakes ≥4 on the Richter scale have been detected within the HFF region

It is possible that, following the 1975 – 1984 rifting episode in the Krafla area, aseismic movements on the HFF might have released accumulated stresses in the region. Assuming that the HFF is locked, the accumulated moment since 1872 is estimated 3.1×10^{19} Nm. If this energy were released in one earthquake, the corresponding moment magnitude (M_w) would be 6.9. It is therefore plausible to assume a future earthquake magnitude of 6.5 in the eastern part of the fault with an epicentre near to Höskuldsvatn.

In the area around the vicinity of the planned power plants, a significant change between the periods before and after 1975 is observed, from $b \approx 0.9 \pm 0.2$ to $b \approx 1.2 \pm 0.2$. The most common explanation for high b-values is a week crust, incapable of sustaining high strain and heterogeneous stress system. The lower b-value before the last rifting episode indicates that the crust had stabilized during the 200 years since the 1724 – 1746 rifting episode. For an individual year within the region the a-value is 2.5.

6.4 Earthquake action design criteria

The seismic hazard is described in terms of the peak ground acceleration on firm ground and the normalized response acceleration (seismic coefficient) as a function of un-damped natural period of the structure. The critical damping ratio is taken equal to 5% in accordance with Eurocode 8. The probabilistic seismic hazard model for the study area reflects the different zones of seismic activity. On one hand, there are the seismic zones defined in terms of the fissure swarms in the North Volcanic Zone, where the earthquakes are small to moderate sized, and, on the other hand, the seismic delineations that belong to the Tjörnes Fracture Zone, largely located off-shore, where the earthquakes are expected to be moderate sized to big. In this context the selected upper bounds for earthquake magnitude is a key parameter. The adopted upper bounds are in all cases judged to be conservative in view of the available geological information and data. This applies especially to the on-land part of the Flatey-Husavik seismic delineation where limited data are at hand. The result is conservative PGA-values leading to potential earthquake action that can be treated as upper bounds.The result of this is that the earthquake action is highest closest to the Húsavík-Flatey seismic delineation but lowest at the southernmost sites where it is only

moderate. For a uniform hazard event with 475 year mean return period the peak ground acceleration is not expected to exceed 20% g for the Krafla volcanic system, while for Theistareykir it is expected to be around 25% g. For comparison this value is about 45% g at the industrial lot at Bakki. This dependence of earthquake action on geographic location has bearings on the design of overhead transmission lines going from the power plants in the south to Bakki in north.

Based on the probabilistic hazard analysis three different earthquakes have been defined to facilitate the design. They are, an Operating Base Earthquake (~100 year return period) for no damage and undisturbed plant operation, a Maximum Design Earthquake (~457 year return period) for life safety and limited damage and a Maximum Credible Earthquake (~3000 year return period) for collapse prevention checking. Estimated horizontal peak ground acceleration (PGA) for each of the defined earthquakes is derived from the hazard curves.

Duration of ground motion has an effect on both the spectral acceleration ordinates and the structural behavior factors. A model of duration of ground motion is presented in terms of the relative significant duration. It should be noted that the duration of strong shaking is relatively short for the study sites. The dynamic amplification of earthquake induced response tends to be higher for events with long duration, than for those with shorter durations. The rapid attenuation of spectral acceleration ordinates with increasing source distance is also worth noting.

The effects of the spatial variation of earthquake motion should be considered for structures with large horizontal dimensions, e.g. pipelines. A simplified model, judged to be applicable for the current study area, has been presented.

Deterministic seismic hazard analysis based earthquake scenarios derived from de-aggregation of the PSHA results was introduced. In that context time-history representation of the earthquake motion was demonstrated through examples of simulated time-series and evaluated elastic response spectra for the Theistareykir site. Earthquake response spectra for linear elastic systems under uniform hazard were evaluated. Based on those, seismic coefficients (normalised spectral acceleration ordinates) for horizontal and vertical earthquake action to be applied in design were suggested in-line with the spectral shapes Type 1 (high-seismicity context) and Type2 (moderate-seismicity context) from Eurocode 8.

To facilitate the structural design and to take into consideration inelastic effects seismic coefficients representing different ductility factors have been included. The design data presented should be sufficient for an initial design phase, more detailed design data will be provided upon request as the project evolves. The recommended design spectra and the prescriptions presented are conservative and can be used with confidence.

6.5 Main conclusions

- Time between major volcano-tectonic rifting episodes in the Krafla volcanic system is several 100s of years. The last episode, called the Krafla fires, lasted 1975-1984. Another similar episode took place 250 years ago in the early 18th century and before that, about 1000 years ago, the area was volcanically active.
- The last eruption in the Theistareykir field occurred about 2500 years ago. Since then no tectonic movements have occurred in the eastern part of the field where the present drilling area is located and where the planned power-plant will be built.
- During the 18th and 20th century rifting episodes a major stress release took place in the northern part of the North Volcanic Zone. Therefore, the probability of new rifting during the next 100-200 years is low.
- Probability of earthquakes with $M > 5$ within or close to the geothermal fields is low. However, earthquakes up to $M = 6.5$ within the southern part of the Húsavík fault are considered.
- Risk can be mitigated by locating structures outside the central zone of the fissure swarms. Risk is further mitigated and reliability of energy delivery increased by building four power plants at four different locations in the volcano-tectonic zone. It is extremely unlikely that all four geothermal areas will be affected simultaneously during a rifting episode or seismic event.
- Two separate transmission lines will be running from the power plants to the industrial lot to enhance the reliability of energy delivery. Each power line will be able to carry the total energy needed. One of the transmission lines will be running through a geologically stable area west of the fissure swarms of the volcano-tectonic zone, except for a short distance west of Krafla. This further increases the overall reliability of power transmission.
- Probabilistic seismic hazard analysis reveals low to moderate earthquake hazard for the proposed powerplant sites. This result is obtained using conservative estimates for upper bounds of earthquake magnitudes.
- De-aggregation of the seismic hazard curves indicates that small to moderate sized near-fault earthquakes with short duration contribute most to the suggested design values for the proposed power plant sites. In the case of long periodic structures a big distant earthquakes may be a contributing event.
- The results of the de-aggregation are used in deterministic hazard analysis resulting in simulated time series applicable for design considerations.
- The main findings of the probabilistic and deterministic hazard analysis are synthesized into suggested design provisions for earthquake action conforming to Eurocode 8. This includes presentation of inelastic effects.

References

Aki, K., 1965. The maximum-likelihood estimate of b in the formula log N = a - bM and its confidence limits. Bull. Earthquake Res. Inst., 43, 237−239.

Ambraseys, N.N., Sigbjörnsson, R., 2000. Re-appraisal of the seismicity of Iceland, Earthquake Engineering Research Centre, Selfoss, June 2000, ISBN 9797-989-91-4X, 196 pages.

Ambraseys, N.N., Smit, P., Sigbjörnsson, R., Suhadolc, P., and Margaris, B., 2002. Internet-Site for European Strong-Motion Data. (http://www.ISESD.hi.is), European Commission, Research-Directorate General, Environment and Climate Programme.

Ambraseys, N., Douglas, J., Sigbjörnsson, R., Berge-Thierry, C., Suhadolc, P., Costa, G., et al., 2004. European Strong-Motion Database (Vol. 2). London, Imperial College.

Ambraseys, N.N. et al., 2005. Equations for the Estimation of Strong Ground Motions from Shallow Crustal Earthquakes Using Data from Europe and the Middle East: Horizontal Peak Ground Acceleration and Spectral Acceleration. Bull. Earthquake Eng., 3 (1): 1-53.

Águstsson, K., Flóvenz, O.G., 2005. The thickness of the seismogenic crust in Iceland and its implications for geothermal systems. In: Proceedings World Geothermal Congress 2005, Antalya, Turkey, 24-29 April. pp. 9, International Geothermal Association.

Ármannsson H., Benjamínsson J. and Jeffrey A. W. A., 1989. Gas changes in the Krafla geothermal system, Iceland. Chem. Geol., 76, 175-196.

Árnadóttir, Th., Sigmundsson, F., and Delaney, P. T., 1998. Sources of crustal deformation associated with the Krafla, Iceland, eruption of September 1984, Geophys. Res. Lett., 25, 1043-1046.

Bachmann, H., 2003. Seismic Conceptual Design of Buildings – Basic principles for engineers, architects, building owners, and authorities, © BWG, Biel, 2003, www.bwg.admin.ch, 84 pages.

Bazzurro, P., Cornell, C.A., 1994. Seismic Hazard Analysis of Nonlinear Structures, 2. Applications. Journal of Structural Engineering-Asce, 120 (11): 3345-3365.

Bazzurro, P., Cornell, C.A., 1999. De-aggregation of seismic hazard. Bull. Seismol. Soc. Am., 89 (2): 501-520.

Beblo, M., and A. Björnsson, 1980. A model of electrical resistivity beneath NE-Iceland, correlation with temperature. J. Geophys., 47, 184-190, 1980.

Bjarnason, I.Th., Menke, W., Flóvenz, Ó., Caress, D., 1993. Tomographic Image of the Mid-Atlantic plate boundary in Southwest Iceland. Journal of Geophysical Research, 98, 6607-6622.

Bjarnason, I.Th., Menke, W., Flóvenz, Ó.G., 1994. Tomographic Image of the Mid-Atlantic plate boundary in Southwest Iceland: Reply. Journal of Geophysical Research 99, 17915-17917.

Björnsson, A., 1976. Jardhraeringar vid Kröflu (Rifting and volcanism in the Krafla area 1975-1977), in Icelandic with English summary. Náttúrufraedingurinn, 46, 177-198.

Björnsson, A., K. Saemundsson, P. Einarsson, E. Tryggvason, and K. Grönvold, 1977. Current rifting episode in North Iceland, Nature, 266, 318-323.

Björnsson, A. and Sigurdsson, O., 1978. Hraungos úr borholu í Bjarnarflagi (Volcanic eruption through a deep drillhole in Bjarnarflag), Náttúrufraedingurinn, 48, 19-23. (In Icelandic with English summary)

Björnsson, A., Johnsen, G., Sigurdsson, S.,. Thorbergsson, G. and Tryggvason, E., 1979. Rifting of the plate boundary in North Iceland 1975-1978, J. Geophys. Res., 84, 3029-3038.

Björnsson, A., 1985. Dynamics of crustal rifting in NE Iceland. Journal of Geophys. Research, 90, 10151-10161.

Björnsson, A. and Eysteinsson, H., 1998. Breytingar á landhæð við Kröflu 1974-1995 – Samantekt á landhæðar-mælingum (Elevation changes in the Krafla area 1974-1995 – compilation of all existing data). Scientific report Orkustofnun and Nordic Volc. Institute, OS-98002, pp. 161. (In Icelandic with English summary).

Björnsson, A., Eysteinsson, H., Beblo, M., 2005. Crustal formation and magma genesis beneath Iceland: Magneto-telluric constraints. In: Foulger, G.R., Natland, J.H., Presnall, D.C., Anderson, D.L. (Eds.), Plates, Plumes and Paradigms, Geological Society of America, Spec. Pap., 388, pp. 665-686.

Björnsson, A., 2007. Temperature of the Icelandic crust: Inferred from electrical conductivity, temperature surface gradient, and maximum depth of earthquake. Tectonophysics (accepted).

Boore, D.M., 2003. Simulation of Ground Motion Using the Stochastic Method, Journal Pure and Applied Geophysics, 160 (3-4), 635-676.

Brandsdóttir, B., Menke, W., Einarsson, P., White, S. and Staples, R. K., 1997. Faroe-Iceland ridge experiment 2. Crustal structure of the Krafla central volcano. J. Geophys. Res., 102, 7867-7886.

Breddam, K., 2002. Kistufell: Primitive melt from the Iceland mantle plume. Journal of Petrology, 44, 2081-2112.

Brune, J.N., 1970. Tectonic stress and the spectra of seismic shear waves from earthquakes. Journal of Geophysical Research, **75** (26), 4997–5009.
Brune, J.N., 1971. Correction. Journal of Geophysical Research, **76**(20): 5002.
Buerger, S., Jacoby, W.R., Hagedoorn, J., and Wolf, D., 2002. Zeitliche Schwereenderungen und glazio-isostatische Ausgleichsbewegungen am Vatnajökull, Suedost-Island: Mitteilungen, Deutsche Geophysikalische Gesellschaft, Nr. 1/2002, p. 2-10.
Chapman, M.C., 1995. A Probabilistic Approach to Ground-Motion Selection for Engineering Design, Bull. Seismol. Soc. Am., 85, 937-942.
Chen W.-F., Scawthorn C., (editors), 2003. Earthquake Engineering Handbook, CRC Press, ISBN: 0849300681, 1512 p.
Convertito, V. and Herrero, A., 2004. Influence of focal mechanism in probabilistic seismic hazard analysis. Bull. Seismol. Soc. Am., 94 (6), 2124-2136.
Cornell, C.A., 1968. Engineering seismic risk analysis. Bull. Seismol. Soc. Am., 58, 1583-1606.
Cornell, C.A., Winterstein, S.R., 1988. Temporal and Magnitude Dependence in Earthquake Recurrence Models. Bull. Seismol. Soc. Am., 78, 1522-1537.
de Zeeuw-van Dalfsen, E., Pedersen, R., Sigmundsson, F. and Pagli, C., 2004. Deep accumulation of magma near crust-mantle boundary at the Krafla volcanic system, Iceland: Evidence from satellite radar interferometry 1993-1999. Gephys. Res. Lett., 31, L13611, doi:10.1029/2004GL020059.
de Zeeuw-van Dalfsen, E., Rymer, H., Williams-Jones, Sturkell, E. and Sigmundsson, F., 2006. The integration of micro-gravity and geodetic data at Krafla volcano, N Iceland. Bull. Volc., 68, 420-431.
DeMets, C., Gordon, R. G., Argus, D. F. and Stein, S., 1994. Effect of recent revisions to the geomagnetic reversal time scale on estimates of current plate motions. Geophys. Res. Lett., 21, 2191-2194.
Douglas, J., 2003. Earthquake ground motion estimation using strong-motion records: A review of equations for the estimation of peak ground acceleration and response spectral ordinates. Earth-Science Reviews, 61 (1–2), 43–104.
Einarsson P., 1978. S-wave shadows in the Krafla caldera in NE-Iceland, evidence for a magma chamber in the crust. Bull. Volcanol., 41, 1–9.
Einarsson P. and Saemundsson K., 1987. Earthquake epicenters 1982–1985 and volcanic systems in Iceland. Map in scale 1:750,000. Menningarsjódur.
Einarsson, P., 1991. The 1975-89 activity at Krafla (in Icelandic). In Náttúra Mývatns, Gardarson, A. and Einarsson, Á. (eds.). Hid Íslenska Náttúrufraedifélag, Reykjavík, Iceland, 97-139.
Einarsson, P. and Brandsdottir, B., 1980. Seismological evidence for lateral magma intrusion during the July 1978 deflation of the Krafla volcano in NE-Iceland. J. Geophys., 47, 160-165.
European Committee for Standardization, 2003. Eurocode 8: Design of structures for earthquake resistance – Part 1: General rules, seismic actions and rules for buildings, EUROPEAN STANDARD, FINAL DRAFT prEN 1998-1 December 2003 ICS 91.120.20, English version.
Fardis, M., Carvalho, E., Elnashai, A., Faccioli, E., Pinto, P., 2005. Designers' Guide to EM 1998-1 and EN 1998-5 Eurocode 8: Design of structures for earthquake resistance, Gulvanessian H. (series editor), Thomas Teleford, 279 pages.
Foulger, G. R., Jahn, C.-H., Seeber, G., Einarsson, P., Julian, B. R. and Heki, K., 1992. Post-rifting stress relaxation at the divergent plate boundary in Northeast Iceland. Nature, 358, 488-490.
Foulger, G. R., Hofton, M. A., Julian, B. R., Jahn, C.-H. and Heki, K., 1994. Regional post-diking deformation in Northeast Iceland: A third epoch of GPS measurements in 1992. Proceedings of the CRCM 1993, Kobe, December 6-11, 1993, pp. 99-105.
Foulger, G., 1995. The Hengill geothermal area, Iceland: Variation of temperature gradients deduced from maximum depth of seismogenesis: Journal of Volcanology and Geothermal Research, 65, 119-133.
Gebrande, H., Miller, H., and Einarsson, P., 1980. Seismic profile of Iceland along the RRISP profile. J. Geophys., 47, 239-249.
Geirsson, H., Árnadóttir, Th., Völksen, C, Jiang, W, Sturkell, E, Villemin, T., Einarsson, P., Sigmundsson, F., Stefansson, R., 2006. Current plate movement across the Mid-Atlantic Ridge determined from 5 years of continuous GPS measurements in Iceland. J. Geophys. Res., 111, No. B9
Giardini, D., Ed., 1999. The Global Seismic Hazard Assessment Program (GSHAP) 1992-1999. Ann. Geofis., 42 (6), 957-1230.
Grapenthin, R., Sigmundsson, F., Geirsson, H., Árnadóttir, T., Pinel, V., 2006. Icelandic rhythmics: Annual modulation of land elevation and plate spreading by snow load, Geophys. Res. Lett., 33, L24305.

Grönvold, K., 1984. Mývatn fiers 1724-1729 - Chemical composition of the lava. Nordic Volcanol. Inst. Report 8401.
Gudmundsson, A., 1983. Form and dimensions of dykes in Eastern Iceland. Tectonophysics, 95, 295-307.
Haimson and Rummel, 1982. Hydrofracturing stress measurements in the Iceland Research Drilling Project drill hole at Reydarfjordur, Iceland. J. Geophys. Res., 87, 6631-6649.
Halldórsson, B. and Papageorgio, A.S., 2005. Calibration of the specific barrier model to earthquakes of different tectonic regions. Bull. Seism. Soc. Am., 95 (4), 1276-1300.
Halldórsson, P., 2005. Earthquake activity in North Iceland (Jardskjálftavirkni á Nordurlandi), Icelandic Meteorological Office (Vedurstofa Íslands), Report, 05021, VÍ-ES-10, 39 p.
Hartzell, S.H., 1978. Earthquake Aftershocks as Green's Functions. Geophys. Res. Lett., 5, 1-4.
Heki, K., Foulger, G. R., Julian, B. R. and Jahn, C.-H., 1993. Plate dynamics near divergent boundaries. Geophysical implications of postrifting crustal deformation in NE Iceland. J. Geophys. Res., 98, 14279-14297.
Hermance, J.F., 1981. Crustal genesis in Iceland. Geophysical constraints on crustal thickening with age. Geophys. Res. Letters, 8, 203-206.
Hofton, M.A. and Foulger, G.R., 1996a. Postrifting anelastic deformation around the spreading plate boundary, north Iceland 1. Modelling of the 1987–1992 deformation field using a viscoelastic Earth structure. Journal of Geophysical Research., 101 (B11), 25403–25421.
Hofton, M.A. and Foulger, G.R., 1996b. Postrifting anelastic deformation around the spreading plate boundary, north Iceland 2. Implications of the model derived from the 1987–1992 deformation field. Journal of Geophysical Research., 101 (B11), 25423–25436.
Iwatsubo T., 1998. Damage to industrial equipment in the 1995 Hyogoken-Nanbu Earthquake. Nuclear Engineering and Design, 181 (1-3), 41-53.
Jaeger, J. C., Cook, N. G., and Zimmerman, R. W., 2007. Fundamentals of Rock Mechanics, 4th edition, Blackwell Publishing, USA.
Jahn, C.-H., 1992. Untersuchungen über den Einsatz des Global Positioning Systems (GPS) zum Nachweis recenter Erdkrustenbewegungen im Spaltengebiet Nordost-Islands. Ph. D. thesis, Wissenschaftliche Arbeit der Fachrichtung Vermessungswesen der Universität Hannover, Nr. 182.
Jakobsson, S.P., 1979. Outline of the pertology of Iceland. Jökull, 29, 57-73.
Johannesson, H. and Saemundsson, K., 1998. Geological map of Iceland, 1:500,000, Tectonics. Icelandic Institute of Natural History, Iceland.
Jouanne, F., Villemin, T., Berger, A. and Henriot, O., 2006. Rift-transform junction in North Iceland: rigid blocks and narrow accommodation zones revealed by GPS 1997-1999-2002. Geophys. J. Int., 167, 1439-1446.
Kaban, M.K., Flóvenz, O.G., and Pálmason, G., 2002. Nature of the crust-mantle transition zone and the thermal state of the upper mantle beneath Iceland from gravity modelling. Geophysical Journal International, 149, 281-299.
Kameda, H., 1994. Probabilistic Seismic Hazard and Stochastic Ground Motions, Engineering Structures, 16 (7), 547-557.
Kanngieser, E., 1983. Vertical component of ground deformation in north Iceland. Annales Geophysical, 1, 321-328.
Kristmannsdóttir, H., 1984. Chemical Evidence from Icelandic Geothermal Systems as Compared to Submarine Geothermal Systems. In: Hydrothermal Processes at Seafloor Spreading Centers (Ed. Rona P.A. et al.), NATO Conference Series, Series IV: Marine Science, 291-320.
Kristmannsdóttir, H. and Swantesson, J., 1978. Greining á útfellingum úr borholum KJ-7, KG-10 og KJ-9 í Kröflu. (Precipitation in geothermal wells at Krafla). OS-JHD-7820, Orkustofnun, Oct. 1978, 31 p.
Larsen G., 2000. Holocene eruptions within the Katla volcanic system, South Iceland: Characteristics and environmental impact. Jökull, 49, 1-28.
Larsen, G., Vilmundardóttir E. G. and Thorkelsson B., 1992. The Hekla eruption of 1991. The tephra fall. Náttúrufraedingurinn, 61, 159–176.
Lee, C.H., Hsieh, S.C., 2002. Lessons learned from the power outages on 29 July and 21 September 1999 in Taiwan, IEE Proceedings Generation, Transmission and Distribution, 149 (5): 543-549.
Maclennan, J., McKenzie, D., Gronvold, K., Slater, L., 2001. Crustal accretion under Northern Iceland. Earth and Planetary Science Letters 191, 295-310.
Massonnet, D. and Sigmundsson, F., 2000. Remote sensing of volcano deformation by radar interferometry from various satellites. In: Remote sensing of volcanoes, Am. Geophys. Union Geophysical Monograph, vol. 116, 207-221.
Mayer, P.S., Sigurdsson, H., Schilling, J.G., 1985. Petrological and geochemical variations along Iceland's neovolcanic zones. Journal of Geophysical Research, 90, 10043-10072.

McGuire, R. K., 1995. Probabilistic Seismic Hazard Analysis and Design Earthquakes – Closing the Loop. Bull. Seismol. Soc. Am., 85 (5), 1275-1284.
McGuire, R. K., 2001. Deterministic vs probabilistic earthquake hazards and risks, Soil Dynamics and Earthquake Engineering, 21, 377-84.
McGuire, R. K., 2004. Seismic Hazard and Risk Analysis. Earthquake Engineering Research Institute. MNO-10.
McTigue, D. F. (1987) Elastic stress and deformation near a finite spherical magma body: Resolution of the point source paradox, J. Geophys. Res., 92, 12391-12940.
Melchers R.E., 1999. Structural Reliability. Analysis and Prediction. J Wiley & Sons, N.Y., 2nd ed, 436pp.
Menke, W. and V. Levin, V., 1994. Cold crust in a hot spot. Geophysical Research Letters, 21, 1967-1970.
Menke, W., Brandsdóttir, B., Einarsson, P. and Bjarnason, I. Th., 1996. Reinterpretation of the RRISP-77 Iceland shear-wave profiles, Geohys. J. Int., **126**, 166-172
Mogi, K., 1958. Relations between the eruptions of various volcanoes and the deformation of the ground around them. Bull. Earthquake Res. Inst., 36, 99-134.
Möller, D., and B. Ritter, 1980. Geodetic measurements and horizontal crustal movements in the rift zone in NE-Iceland. J. Geophys., 47, 110-119.
Möller, D., B.Ritter, and K. Wendt, 1982. Geodetic measurement of horizontal deformations in Northeast Iceland. Earth Evolution Sciences, 2, 149-154.
Ólafsson, S., Remseth, S. and Sigbjörnsson, R., 2001. Stochastic models for simulation of strong ground motion in Iceland. Earthquake Engineering and Structural Dynamics, 30, 27.
Ólafsson, S. and Sigbjörnsson, R., 1999. A theoretical attenuation model for earthquake-induced ground motion, Journal of Earthquake Engineering, 3 (3), 287-315.
Ólafsson, S. and Sigbjörnsson, R., 2004. Attenuation of strong ground motion in shallow earthquakes, Proc. of the 13th World Conf. on Earthquake Eng., Vancouver, Mira.
Pagli, C., Sigmundsson, F., Lund, B., Sturkell, E., Geirsson, H., Einarsson, P., Árnadóttir, Th. and Hreinsdóttir, S., 2007. Glacioisostatic deformation around the Vatnajökull ice cap, Iceland, induced by recent climate warming: GPS observations and finite element modeling. J. Geophys. Res., 112, in press.
Palmason, G., 1980. Continuum model of crustal generation in Iceland, kinematics aspects. Journal of Geophysics, 47, 7-18.
Papageorgiou A.S., 2003. The barrier model and strong ground motion. Pure and Applied Geophysics, 160. 603–634.
Pedersen, R., F. Sigmundsson, Hooper, A. J. and Feigl, K. L., 2007. Extending the temporal coverage of Icelandic crustal deformation measurements through ENVISAT InSAR images. Paper ESA SP-636, 2007, Proc. of the 2007 ENVISAT Symposium, Montreux, Switzerland, 23-27 April, 2007.
Pinel, V. and Jaupart, C., 2003. Magma chamber behaviour beneath a volcanic edifice. J. Geophys. Res., 108, 2072, doi:10.1029/2002JB001751.
Pires J.A., Ang A.H.S., Villaverde R., 1996. Seismic reliability of electrical power transmission systems, Nuclear Engineering and Design, 160 (3), 427-439.
Reiter, L., 1990. Earthquake Hazard Analysis: Issues and Insights. Columbia University Press, New York.
Ross, S. M., 2003. Introduction to Probability Models, eight edition, Academic Press, UK, 755 pp.
Saemundsson, K., 1974. Evolution of the axial rift zone in northern Iceland and the Tjörnes Fracture Zone. Geological Society of America Bulletin, 85, 495- 504.
Saemundsson K., 1977. Geological map of Iceland 1:250.000. Sheet 7 North East Iceland. Museum of Natural History and Iceland Geodetic Survey.
Saemundsson K., 1978. Fissure swarms and central volcanoes of the neovolcanic zones of Iceland. In: D.R. Bowes and B.E. Leake (editors), Crustal evolution of northwestern Britain and adjacent regions. Geol. J. Spec. Issue, No 10, 415–432.
Saemundsson, K., 1979. Outline of the geology of Iceland, Jökull, 29, 7-28.
Saemundsson K., 1991. Jardfraedi Kröflukerfisins (Geology of the Krafla volcanic system). In: Árni Einarsson and Arnthór Gardarsson (editors). Náttúra Mývatns, 26–95. Hid íslenska náttúrufraedifélag. (In Icelandic).
Saemundsson, K., Jóhannesson, H., Flóvenz, Ó.G., 2003. Surface temperature gradient map of Iceland. ISOR, Annual Report 2003.
Sanford, A.R., and Einarsson, P., 1982. Magma chambers in rifts. Continents and Oceanic Rifts, Geodynamics Series. Volume **8,** 147-168.

Schillerup, H., 1995. Generation and equilibration of olivine tholeiites in the northern riff zone of Iceland. A petrogenetic study of the Bláfjall table mountain. Journal of Volcanology and Geothermal Research, 65, 161-179.
Sella, G. F., Dixon, T., Mao, A., 2002. REVEL: A model for recent plate velocities from space geodesy, J. Geophys. Res., 107, doi: 10.1029/2000JB00033.
Shaw, H.R., 1980. The fracture mechanism of magma transport from the mantle to the surface. In: Physics of magmatic processes, ed. R.B. Hargraves. Princeton Univ. Press, pp. 201-264.
Shinozuka M., Dong X., Chen T.C., Jin, X., 2007. Seismic performance of electric transmission network under component failures, Earthquake Engineering & Structural Dynamics, 36 (2), 227-244.
Sigbjörnsson R., and Ólafsson S., 2004. On the South Iceland earthquakes in June 2000: Strong-motion effects and damage. Bollettino di Geofisica Teorica ed Applicata, 45 (3): 131-152.
Sigmundsson, F., 1991. Post-glacial rebound and asthenospheric viscosity in Iceland. Geophysical Research Letters, **18**, 1131-1134.
Sigmundsson, F. and Einarsson, P., 1992. Glacio-isostatic crustal movements caused by historical volume change of the Vatnajökull ice cap, Iceland. Geophysical Research Letters, 21, 2123-2126.
Sigmundsson, F., 2006a. Iceland Geodynamics, Crustal Deformation and Divergent Plate Tectonics. Praxis Publishing, Springer Verlag, Chichester, UK, 209 pp.
Sigmundsson, F., 2006b. Plate tectonics: Magma does the splits. Nature, 442, 251-252.
Sigurdsson, H. and Sparks R.S.J., 1978. Rifting episode in North Iceland in 1874–1875 and the eruptions of Askja and Sveinagjá. Bull. Volcanol. 41 (3), 1–19.
Sigurdsson, O., 1977. Náttðúruhamfarir í Þingeyjarþingi (II) 1976-1978 (report of the rifting episode in NE-Iveland 1976-1978). Týli, 7, 41-56.
Sigurdsson, O., 1980. Surface deformation of the Krafla fissure swarm in two rifting events. J. of Geophys., 47, 154-159.
Sigvaldason G. E. 2002: Volcanic and tectonic processes coinciding with glaciation and crustal rebound. Bull. Volcanol., 64, 192–205.
Sjöberg, L.E., Pan, M., Asenjo, E. and Erlingsson, S., 2000, Glacial rebound near Vatnajökull, Iceland, studied by GPS campaigns in 1992 and 1996. Journal of Geodynamics, 29, 63-70.
Snaebjörnsson J.T., Sigbjörnsson R., Olafsson S., 2006. Kárahnjúkar hydroelectric project – Hálslón Area: Assessment of Earthquake Action, Report LV 2006/001; p. 168.
Snaebjörnsson, J.T., Sigbjörnsson, R., and Ólafsson, S., 2004. Modelling of earthquake response spectra for strike-slip earthquakes in the near- and far-field. In: Proceedings of the 13th World Conference on Earthquake Engineering, (pp. 10). Vancouver: Mira.
Sólnes, J., Sigbjörnsson, R., and Elíasson, J., 2004. Probabilistic seismic hazard mapping of Iceland: Proposed seismic zoning and de-aggregation mapping for EUROCODE 8. In Proceedings of the 13th World Conference on Earthquake on Earthquake Engineering, (pp. 14). Vancouver, Mira.
Stefánsson, R., 1976. Seismic activity in the Krafla area. Icelandic Meteorological Office, unpublished memo, July 10th 1976.
Stefánsson, R., Bödvarsson, R, Slunga, R., Einarsson, P., Jakobsdóttir S., Bungum, H., Gregersen, S., Havskov, J., Hjelme, J., Korhonen, H., 1993. Earthquake prediction research in the South Iceland seismic zone and the SIL project. Bull. Seism. Soc. Am., 696−716.
Sturkell, E., Sigmundsson, F. Geirsson, H., Ólafsson, H. and Th. Theodórsson, (submitted). Post-rifting deformation processes 1989–2005 at Krafla volcano, Iceland: Constraints from local levelling, tilt and GPS observations. J. Volc. Geotherm. Res.
Tenhaus, P.C. and Campbell, K.W., 2003. Seismic Hazard Analysis. In: Earthquake Engineering Handbook, W-F Chen and C. Scawthorn (ed.). CRC Press.
Thayer, R.E., Björnsson, A., Alvarez, L. and Hermance, J.F., 1981. Magma genesis and crustal spreading in the northern neovolcanic zone of Iceland. Telluric-magnetotelluric constraints. Geophys. J., 65, 423-442.
Thórarinsson S., 1971. The age of the light Hekla tephra layers according to corrected C14-datings. Náttúrufraedingurinn, 41, 99–106.
Tryggvason, E., 1980. Subsidence events in the Krafla area North Iceland, 1975-1979. J. Geophys., 47, 141-153.
Tryggvason E., 1984. Widening of the Krafla fissure swarm during the 1975–1981 volcano-tectonic episode. Bull. Volcanol., 47, 47–69.
Tryggvason, E., 1986. Multiple magma reservoirs in a rift-zone volcano – Ground deformation and magma transport during the September 1984 eruption of Krafla, Iceland, J. Volcanol. Geotherm. Res., 28, 1-44.

Tryggvason E,. 1994. Surface deformation at the Krafla volcano, North Iceland, 1982–1992. Bull. Volcanol., 56**,** 98–107.
Tsai, C.C.P., 1998. Engineering ground motion modelling in the near-source regime using the specific barrier model for probabilistic seismic hazard analysis. Pure and Applied Geophysics, 152 (1), 107-123.
Turcotte, D. and Schubert, G., 2002. Geodynamics, Second edition, Cambridge University Press.
Udias, A., 1999. Principles of seismology. Cambridge University Press, Cambridge: 475 p.
Vadon H., and Sigmundsson, F., 1997. Crustal deformation from 1992-1995 at the Mid-Atlantic Ridge, SW Iceland, mapped by satellite radar interferometry. Science, 275, 193-197.
Vidic, T., Fajfar, P. and Fischinger, M., 1994. Consistent inelastic design spectra: Strength and displacement. Earthquake Engineering and Structural Dynamics, 31, 1967-1991.
Völksen, C., 2000. Die Nutzung von GPS für die Deformationsanalyse in regionalen Netzen am Beispiel Island. Ph. D. Thesis, Wissenschaftliche Arbeiten der Fachrichtung Vermessungswesen der Universität Hannover, Nr. 237, Univ. Hannover, 2000.
Völksen, C. and Seeber, G., 1998. Nachweis von rezenten Krustendeformationen in Nordisland mit GPS. Zeitschrift für Vermessungsvesen, 2/1998, 68-75.
Walker G.P.L., 1989. Gravitational (density) controls on volcanism, magma chambers and intrusions. Australia Journal of Earth Sciences, 36, 149-165.
Wells, D.L. and Coppersmith, K.J., 1994. New empirical relationships among magnitude, rupture length, rupture width, rupture area, and surface displacement. Bull. Seismol. Soc. Am., 84, 974-1002.
Woo, G., 1996. Kernel estimation methods for seismic hazard area source modeling. Bull. Seismol. Soc. Am., 86 (2): 353-362.

List of Figures

center of the inflation bowl (see Fig. 2.2). Figure modified from Björnsson et al., (1979).

Figure 1.10 Land elevation changes during the Krafla fires at benchmark FM5596 0,8 km SSE of the apex of the inflation-deflation bowl. The first 9 years are characterized by continuous inflow of magma of about 1-5 m^3/s into a shallow magma chamber at 3 km depth, and drainage of magma into the fissure swarm in short rifting events, releasing the pressure in the magma chamber. In 9 of 24 total rifting events magma came up to the surface, indicated by red stars. Most of the rifting took place during the first 5 years (1976-1980) when the magma was flowing into the fissure swarm. During the next 4 years (1981-1984) most of the magma came up to the surface. During the following 2 years1985-1986 the elevation was stable, which indicates that the inflow of magma had stopped. In 1987 the land started to rise again, indicating increasing pressure in the magma chamber or intrusions into the roots of the central volcano without rifting. In March 1989 the inflow of magma from below suddenly stopped and since then slow, exponentially decaying deflation has been observed. Blue dots are elevation values based on extensive dry tilt surveys with a distal reference point. Open triangles during the first year show elevation calculated from tilt measurements at the Krafla power house, and the open squares are based on tilt measurements at a station south of the power hose. The curve itself is calculated from daily tilt measurements within the power house. The smallest subsidence events (< 4cm) shown in Table 1.1 are too small to be seen in this diagram. Redrawn from Björnsson and Eysteinsson (1998).

Figure 1.11 Fissure - eruption in the Krafla area in September 1977. The fissure is about 800 m long. The magma erupted at the beginning of the Krafla eruptions has a low viscoscity, contains high amount of gas and is flowing like water.

Figure 1.12 Activated areas of the Krafla fissure swarm from 1975 to 1978. Only one section is activated during each subsidence / rifting event. Redrawn from Einarsson and Brandsdóttir (1980), who delineated the active areas by locating earthquake epicenters. Mapping of ground fissures delivered in some instances a more detailed picture, for example during the initial rifting phase in December 1975 where the whole central part of the fissure swarm was activated (Sigurdsson, 1977, 1980), and not only the western part as indicated by the earthquake locations.

Figure 1.13 Total accumulated widening along the Krafla fissure swarm during the 1975-1984 volcanic episode. The maximum extension of 9 m took place close to the northern rim of the caldera. Redrawn from Tryggvason (1984) with additional data for September 1984 from E. Tryggvason and F. Sigmundsson.

Figure 1.14 Horizontal migration of earthquakes with time from the Krafla caldera to the north along the fissure swarm during a subsidence-rifting event in July 1978. The horizontal distance is measured from the center of the caldera. In the Snagi area some 10 km north of the caldera most of the earthquakes were at 2-4 km depth, but one occurred at 7 km and another at 14 km depth. The highest magnitude was around 4 but the majority of the earthquakes had a magnitude between 2.5 and 3.5. The b-value was 1.7 ± 0.2 Figure from Einarsson and Brandsdóttir, 1980).

Figure 1.15 Vertical movements across the Krafla fissure swarm at Bjarnarflag /Námafjall some 10 km south of the center of the caldera. The first profile (1974-1976) shows subsidence along the whole profile which might be part of the initial subsidence bowl, as well as regional pre-rifting subsidence. The second profile includes the rifting event of April 27.-28. 1977, as the magma was flowing to the south. The center part of the fissure swarm subsided about 80 cm and the flanks to the east and west were uplifted some 20 cm. The fourth profile includes the rifting event of 8.-10. September 1977 when the magma was also flowing to the south and some 6.5 $m^3$of scoria were erupted through one of the geothermal wells in Bjarnarflag. The last profile (1977-1979) shows some subsidence in the center part and uplift of the flanks.

Figure 1.16 Widening and elevation changes across the Krafla fissure swarm in Kelduhverfi, some 40 km north of the caldera, during a rifting event in January 1978. Figure redrawn from Sigurdsson (1980).

Figure 1.17 The upper part shows the tilt variations of the power house (in micro-radians) caused by land elevation changes, for the period August 1976 to January 1978. The middle part shows variation in width of a fissure located close to the apex of the inflation-deflation bowl. The fissure width correlates with the elevation (tilt). The lower part shows the width of a fissure in the central fissure swarm at Bjarnarflag, south of the caldera. The width is nearly constant except during two rifting deflation-events when the magma moved to the south, i.e. in April and September 1977. The widening of the fissure is around 20 cm in both cases. Figure from Björnsson et al., (1979).

Figure 1.18 The upper part shows horizontal movements from 1971 to 1980 in the Krafla area. The measurements were made by Möller et al. (1982) in co-operation with Orkustofnun. Horizontal widening of up to 8 m was observed across the active fissure swarm but contraction of the flanks. The lower part shows elevation changes from 1975 to 1980 on an E-W profile crossing the Krafla fissure swarm by Bjarnarflag. The measurements were made by Kanngieser (1983) in co-operation with Orkustofnun. Here the elevation data have been projected onto latitude 16°40′. The flank zones of the fissure swarm were uplifted around 0.6 m and uplift was observed out to a distance of 30 km from the rift zone. Figure from Björnsson (1985).

Figure 1.19 Variation in CO_2 content in two geothermal wells at Krafla from 1975 to 1984, measured in weight % of the total flow. Redrawn from Ármannsson et al., (1989).

Figure 1.20 A simplified model of episodic rifting in NE Iceland. Tension is gradually built up in the axial rift zone and is released every few years in a rifting episode.

Figure 2.1 The Northern Volcanic Zone (NVZ) is segmented into discrete volcanic systems. They include a central volcano and a fissure swarm with proximal eruptive fissures and distal non-eruptive faults and ground fissures. The two northernmost systems, those of Theistareykir and Krafla, host geothermal reservoirs to be harnessed, three of which are already exploited or proven. Dots show earthquake epicenters of magnitude 1-5 over a 4 years period (1982-1985). Map by Einarsson and Saemundsson (1987).

Figure 2.2 Central part of the Krafla volcanic system showing the caldera and the fissure swarm which traverses it. An inner segment of the fissure swarm was active during the last two volcanic episodes of 1724–1729 and 1975–1984. The geothermal areas of Krafla and Bjarnarflag are shown. Krafla has a magma chamber (S-wave shadow, Einarsson, 1978) at 3-7 km depth. Map from Saemundsson 1991.

Figure 2.3 Spread of hydrovolcanic mud erupted at Krafla in 1724 and basaltic lava of 1728-1729. The mud eruption started as a mixed rhyolite/basalt volcanic eruption which developed into a hydrovolcanic eruption due to ingression and explosive boiling of geothermal water. It lasted half a day. Two years of intermittent rifting events and another two years of also intermittent fissure eruptions followed. Map from Saemundsson 1991.

Figure 2.4 The Krafla volcano-tectonic episode of 1975-1984 produced basaltic lava about 35 km^2 in area. The eruptive phase of 1980–1984, which included five eruptive events that lasted 5–14 days each, was preceded by 5 years of intermittent rifting events. The main lava producing craters were in Gjástykki, well north of the Krafla caldera. Southern Gjástykki is being explored for geothermal utilization. Map from Saemundsson (1991).

Figure 2.5 Soil sections from the area between Bjarnarflag and Húsavík. Whitish ashes, H3 (3100 years old) and H4 (4500 years old), provide straigarphic markers. The age and provenance of the more prominent ashes has been determined by C-14 and by their chemical composition which is characteristic for each volcano. Fall-out of basaltic ash was relatively frequent during the first millenia of the postglacial, i.e. during the time of and following glacier melting. Ages are given for the most prominent ash layers. The year of fall-out is given for two historical ashes.

Figure 2.6 Isopach map of the 1991 Hekla ash fresh fallen. Thickness is in cm. The arrow points at the area affected by shortcuts. Figure from Larsen et al. (1992).

Figure 3.1 Seismic study of the Northern Volcanic Zone and the Krafla central volcano. (A) The seismic array of the FIRE 1994 project. (B) P-wave velocity cross section along the profile with a low-velocity anomaly under Krafla interpreted as a magma chamber. Modified from Brandsdóttir et al. (1997). Courtesy of Bryndís Brandsdóttir.

Figure 3.2 Schematic rheological structure of the oceanic crust and a riting event dominated by magna intrusion. The uppermost 5-10 km of the crust behave in an elastic manner over long time scales, but at greater depth viscoelastic effects are important and stresses relax in a ductile manner. Reproduced from Sigmundsson (2006a) with permission of Nature, London.

Figure 3.3a Geodetic network used to constrain deformation during the 1984 eruption of Krafla volcano consisting of electronic distance measurement stations (EDM), optical levelling tilt stations, and levelling bench

marks). Shading shows the extent of a lava flow formed in 1984, with the broken line on top outlining the eruptive fissure.

Figure 3.3.b Observed and model tilt and horizontal displacements (inferred from EDM) associated with the 1984 Krafla eruption. Eruptive fissure and extent of the modelled dike are indicated by broken and thick shaded line, respectively. Inversion of the geodedetict data gives a model dike extending to 7 km depth. Green rectangle denotes the location of a Mogi pressure source, located at 3 km depth. After Árnadóttir et al. (1998). Copyright by the American Geophysical Union.

Figure 3.4 Map view of horizontal displacements in the Krafla area March 1978 – March 1989, based on electronic distance measurements. Reproduced from Tryggvason (1994), Sigmundsson (2006a). The main deformation occurs along the central axis of the Krafla fissure swarm, with large cumulative horizontal displacements on both sides of the dike complex emplaced.

Figure 3.5 Spreading plate boundary – model for post-rifting deformation.

Figure 3.6 Horizontal crustal displacements inferred from continuous GPS-measurements in Northern Iceland (Geirsson et al., 2006 and later work). Black arrows are observations, the inferred velocity vectors relative to a stationary plate boundary. The white arrows are predictions of the REVEL plate motion model. See also http://www.vedur.is. Data from stations indicated by name (RHOF, ARHO, AKUR, REYK) displayed in Figure 3.7.

Figure 3.7 GPS time series at selected sites relative to the REYK reference station (Geirsson et al., 2006 and later work). See Figure 3.7 for locations of the RHOF, ARHO and AKUR sites.

Figure 3.8 Regional average plate velocities 1993-2004 in northern Iceland (ISNET suveys by the Land Survey of Iceland – data processing Thóra Árnadóttir). The results are displayed in a reference system relative to a stationary plate boundary.

Figure 3.9 Regional crustal velocities 1999-2002 at the rift-transform junction in N-Iceland displayed relative to stable Eurasian plate. After Jouanne et al., (2006).

Figure 3.10 Local GPS and tilt network at Krafla from Sturkell et al. (submitted).

Figure 3.11 The shallow magma chamer at Krafla – Stars indicate inferred locations of Mogi sources from different studies. After Sturkell et al. (submitted).

Figure 3.12 Vertical displacements inferred from levelling in the Krafla area 1989-2005. a) Vertical changes 1989-2005, b) vertical changes 1995-2000, c) vertical changes 2000-2005, and d) vertical changes 1989-2005. After Sturkell et al. (submitted).

Figure 3.13a Location of an InSAR study of the Krafla area showing the town of Húsavík (H), Lake Mývatn (L), the Krafla fissure swarm (dotted), the outline of the Krafla caldera central volcano (solid white line), and the Krafla caldera (white dashed line). M_2 and M_1 indicate the location of the Krafla magna chamber and the site of deep pressure increase in Gjástykki respectively. Reproduced from de Zeeuw-van Dalfsen et al., (2004).

Figrue 3.13b InSAR study of Krafla area. Interferograms (left column), models (center column), and residuals (right column). Each full color cycle (fringe) corresponds to a change in range from ground to satellite of 28 mm. See text for discussion. Reproduced from de Zeeuw-van Dalfsen et al., (2004).

Figure 3.14 Interferometric data covering the Northern Volcanic Zone. Black lines outline the fissure swarms in the area, circular outlines show the location of central volcanoes and the black stippled outline shows the location of the Krafla caldera. A) ERS data spanning 1993-1995. B) ENVISAT data spanning 2003-2005. Subsidence above shallow magma chamber has declined but deep inflation under Gjástykki continues. After Pedersen et al. (2007).

Figure 4.1 Logarithm of the number of earthquakes since 1994 in a 25 km^2 area having a magnitude ≥ 1.5 on the Richter scale. Number of earthquakes is counted in confined 25 km^2 areas.

Figure 4.2 Historical earthquakes (M = ≥ 6) since 1700 and earthquakes ≥ 1.5 since 1994.

Figure 4.3 Measured earthquakes (M ≥ 3) in the region from 1930 to 2000.

List of Tables

List of Maps

List of Abbreviations

MAR	Mid Atlantic Ridge
NVZ	North Volcanic Zone
EVZ	East Volcanic Zone
WVZ	West Volcanic Zone
TFZ	Tjörnes Fracture Zone
SISZ	South Iceland Seismic Zone
HFF	Húsavik Flatey Fault
GPS	Global Positioning System
CGPS	Continuous GPS
EDM	Electronic Distance Measurements
DSHA	Deterministic Hazard Analysis
PSHA	Probabilistic Hazard Analysis
PGA	Peak Ground Acceleration
OBE	Operating Base Earthquake
MDE	Maximum Design Earthquake
MCE	Maximum Credible earthquake
SIL	Originally used for South Iceland Lowland seismic network, now used for similar type of seismic network.